University of Leeds
School of Mathematics
Ph.D. Pure Mathematics

Paul Leask

Skyrmion Crystals

Finite Atomic Nuclei to Compact Stars

Thesis submitted in accordance with the requirements for the degree of
Doctor of Philosophy in Pure Mathematics at the University of Leeds

UK – Leeds
March 2024

Joint publications/preprints reproduced in this thesis

Title: Skyrme crystals with massive pions
Authors: Derek Harland, Paul Leask and Martin Speight
Journal: Journal of Mathematical Physics **Publisher**: American Institute of Physics (AIP) Publishing **Date of publication**: 4 October 2023 **DOI**: 10.1063/5.0159674
Author contributions: **Derek Harland**: Conceptualization (equal); Formal analysis (equal); Methodology (equal); Supervision (equal); Writing – original draft (supporting); Writing – review & editing (equal) **Paul Leask**: Conceptualization (equal); Formal analysis (equal); Methodology (equal); Software (lead); Visualization (lead); Writing – original draft (supporting); Writing – review & editing (equal) **Martin Speight**: Conceptualization (equal); Formal analysis (equal); Methodology (equal); Supervision (equal); Writing – original draft (lead); Writing – review & editing (equal)
Permissions: The results from this article are reproduced in Chapter 3, with the standard author permissions from the American Institute of Physics

Title: Generalized skyrmion crystals with applications to neutron stars
Authors: Paul Leask, Miguel Huidobro and Andrzej Wereszczynski
Journal: Physical Review D **Publisher**: American Physical Society **Date of publication**: 11 March 2024 **DOI**: 10.1103/PhysRevD.109.056013
Author contributions: **Paul Leask**: Conceptualization (equal); Formal analysis (equal); Methodology (lead); Software (lead); Visualization (lead); Writing – original draft (lead); Writing – review & editing (equal) **Miguel Huidobro**: Conceptualization (equal); Formal analysis (equal); Methodology (supporting); Writing – original draft (supporting); Writing – review & editing (supporting) **Andrzej Wereszczynski**: Conceptualization (equal); Formal analysis (equal); Methodology (supporting); Writing – original draft (supporting); Writing – review & editing (equal)
Permissions: The results from this article are reproduced in Chapter 4, with the standard author permissions from the American Physical Society

Title: Skyrmion crystals stabilized by ω-mesons
Authors: Derek Harland, Paul Leask and Martin Speight
arXiv ref.: arXiv:2404.11287 **Date of submission**: 17 April 2024 **DOI**: 10.48550/arXiv.2404.11287
Author contributions: **Derek Harland**: Conceptualization (equal); Formal analysis (equal); Methodology (equal); Supervision (equal); Writing – original draft (equal) **Paul Leask**: Conceptualization (equal); Formal analysis (equal); Methodology (equal); Software (lead); Visualization (lead); Writing – original draft (equal); **Martin Speight**: Conceptualization (equal); Formal analysis (equal); Methodology (equal); Supervision (equal); Writing – original draft (equal);
Permissions: The results from this preprint are reproduced in Chapter 5, with author permissions

Paul Leask

Skyrmion Crystals

Finite Atomic Nuclei to Compact Stars

Thesis submitted in accordance with the requirements for the degree of Doctor of Philosophy in Pure Mathematics at the University of Leeds.

Supervisor 1: Dr. Derek Harland

Supervisor 2: Prof. Martin Speight

UK – Leeds
March 2024

This copy was revised and altered with respect to the original version, according with the observations raised by the examining committee on the defense day, under the author's sole responsibility and with the consent of the supervisors.

This study was supported by a Ph.D. studentship from UKRI, Grant No. EP/V520081/1.

To my mum, my granny and my partner, Ellie.

Abstract

In this thesis we study the properties of nuclear matter in the massive $\mathscr{L}_{024}$ and generalized $\mathscr{L}_{0246}$ Skyrme models, and also the ω-meson variant of the Skyrme model. A semi-analytic method is developed to determine local minima of the static energy functional with respect to variations of both the field and the period lattice of the crystal. In general, four distinct skyrmion crystals are found. Two of these were already known – the cubic lattice of half-skyrmions and the α-particle crystal – but two are new. In the Skyrme model with no vector mesons, these new solutions have lower energy per baryon number and less symmetry, being periodic with respect to trigonal but *not* cubic period lattices. Minimal energy crystals are also constructed under the constraint of constant baryon density, and it is shown that the two new non-cubic crystals tend to chain and multi-wall solutions at low densities.

Isospin asymmetric nuclear matter is investigated in the generalized $\mathscr{L}_{0246}$-Skyrme mode by canonically quantizing the isospin collective degrees of freedom of the multi-wall crystal. We obtain, for the first time, an equation of state from the Skyrme model which interpolates between infinite isospin asymmetric nuclear matter and finite isospin symmetric atomic nuclei. This enables us to describe neutron stars with crusts within the Skyrme framework. Furthermore, we observe that the symmetry energy tends to a constant value at zero density, which can be identified with the asymmetry coefficient in the semi-empirical mass formula for atomic nuclei. The symmetry energy also reveals a cusp in its structure below the nuclear saturation point n_0 at $n_* \sim 3n_0/4$. This cusp density point n_* can be interpreted as the nuclear density whereby the infinite crystalline multi-wall configuration undergoes a phase transition to a finite isolated multi-wall configuration. Both of these observations are observed to be generic features of skyrmion crystals that tend asymptotically to somewhat isolated skyrmion configurations in the zero density limit. We find that the resulting neutron stars from our study agree quite well with recent NICER/LIGO observational data.

In the ω-meson variant of the Skyrme model, the solitonic crystals are stable with respect to variations of the Skyrme φ and ω-meson fields, and also the period lattice Λ of the crystal. In the conventional massive Skyrme model the ground state is a multi-wall solution, whereas the ground state in this theory is dependent upon the choice of free parameters. Further, we predict coefficients in the Bethe–Weizsäcker semi empirical mass formula using ω-skyrmion crystals and the α-particle approximation. Finally, we attempt to address the compression modulus problem and determine a more acceptable value of the nuclear matter incompressibility coefficient.

Keywords: Topological Solitons, Skyrmion Crystals, Dense Nuclear Matter, Neutron Stars, Vector Mesons.

Acknowledgments

I would like to thank my Ph.D. supervisors, Dr. Derek Harland and Prof. Martin Speight, for their guidance and continued support throughout my doctoral studies. I am grateful for their time, patience, and many insightful discussions. In particular, I am thankful for them allowing me the freedom to steer the direction of the project and explore what interests me.

Throughout my research I have been lucky to have the opportunity to collaborate and visit other researchers within the skyrmion community. In particular, I would like to thank Prof. Andrzej Wereszczynski for integrating me into the Solitons at Work community. We have shared many great moments together, during numerous stays at the Jagiellonian University in Krakow. I am sure this collaboration with my friend will remain fruitful and I look forward to returning to Krakow! I am also grateful to Carlos Naya and Kasia Oles for their hospitality during these visits, and the daily coffee break discussions.

During my third year I visited IGFAE at the University of Santiago de Compostela and was graciously hosted by Prof. Christoph Adam. While there I spent most of my time with Miguel Huidobro and Alberto Martín-Caro, which resulted in a continued collaboration. I am particularly grateful for their hospitality and the many shared cañas (with Jorge Castelo also)! I have many fond memories of my time there.

Nearing the end of my studies I was fortunate to be able to visit Tokyo and Hiroshima. In Tokyo I was hosted by Prof. Muneto Nitta and Dr. Yuki Amari at Keio University. While there I had many interesting discussions with Muneto and Yuki, and I am thankful for their kind hospitality. I am particularly thankful to Yuki for meeting me upon arrival and also taking time to show me around Tokyo. In Hiroshima I was hosted by SKCM^2 at Hiroshima University. I met many people there and had many insightful discussions. To mention a few, I am thankful to Dr. Andrey Leonov and Dr. Allison Teixeira for their time and company. I am also grateful to SKCM^2 for arranging everything and the hospitality they provided.

In addition to these, from the solitons community, I also thank Tat Ghosh, Gautam Chaudhuri, Tom Galvin, Chris Halcrow, Tom Winyard, Nick Manton, and Bjarke Gudnason for stimulating discussions. I am also grateful to the friends I have gained from the climbing community.

Finally, I thank my mum, Brendan, and Murray for their continued love and support. Most of all I am grateful to my partner, Ellie, for whom none of this would have been possible.

Contents

List of Figures

List of Tables

One

Introduction

It is well known that the phase structure of nuclear matter is rich and highly non-trivial. At high densities, the hadrons have considerably different properties than in the lower density regimes. In order to understand what happens to nuclear matter under extreme conditions, the underlying theory must be consistent with quantum chromodynamics (QCD). It was initially believed by many nuclear theorists that descriptions of the low energy regime of QCD must contain explicit quarks. However, this was shown not to be the case by 't Hooft [1], wherein he considered the number of quark colors N_c as a free parameter. Then a detailed analysis showed that, in the large N_c-limit, low-energy QCD can be reduced to an effective chiral field theory of mesons. Witten [2] took this further and conjectured that baryons arise as solitons in this large-N_c theory. Rather, the quarks can be integrated away and the degrees of freedom are no longer quarks and gluons, they are hadrons, that is, the family of mesons and baryons.

Skyrme's original model [3] is one such description; it is an effective Lagrangian involving only the lightest of mesons, the pions, with the idea that baryons emerge as stable solitons with non-trivial topological charge. These baryons are realized as non-perturbative excitations of the pionic fields (π^+, π^-, π^0). The theory has $N_f = 2$ flavours of quarks: the up and down quarks (and their corresponding antiquarks). These make up the pion fields, which are encoded in the SU(N_f)-valued Skyrme field. Skyrmions are field configurations classified topologically by an integer-valued homotopy invariant B, which is interpreted physically as the baryon number of the configuration [4, 5]. They can be quantized as rigid-bodies acquiring spin and isospin [6], which has been reasonably successful for some light nuclei [7–9], and can be improved by considering quantized vibrational deformations [10–14].

Skyrmions are minimal energy field configurations within their homotopy class, that is, they are solutions of the Euler–Lagrange field equations corresponding to some static energy functional. There is a topological lower bound on this static energy of the form $E \geq E_{\text{top}}B$, where E_{top} is some positive constant, originally due to Faddeev [15] and subsequently improved by Harland [16]. (Improved in this context means that the constant E_{top} is increased.) Let $E(B)$ denote the minimum static energy among all fields of baryon number B. The energy bound $E(B) = E_{\text{top}}B$ is never attained, but numerical studies suggest that the ratio $E(B)/B$ decreases monotonically, and hence converges to some limit E_* as $B \to \infty$, which is bounded below. This suggests that, as B grows large, minimal energy Skyrme fields may tend to some regular, spatially periodic crystalline structure, with baryon number B_{cell} and energy E_*B_{cell} per unit cell.

One of the outstanding problems in the Skyrme model is the correct prediction of nuclear binding energies. One would like to be able to predict correct binding energies using the Bethe–

Weizsäcker semi empirical mass formula (SEMF), which is composed of five terms: the volume term, the surface term, the Coulomb term, the asymmetry term, and the pairing term. The coefficients in each term are normally determined empirically, and the problem at hand is: can the coefficients be estimated by using skyrmions? Baskerville [17] attempted to address the volume and surface terms using the standard massless $\mathscr{L}_{24}$-Skyrme model but was unsuccessful, overestimating the coefficients by an order of magnitude. Ma *et al.* [18] had more success with the Coulomb coefficient in the conventional massive $\mathscr{L}_{024}$-Skyrme model, predicting the coefficient within 3%. This proved promising, however, the other coefficients still remained out of grasp.

In the Skyrme model, the classical mass of a skyrmion roughly plays the same role as the volume and surface terms. To be able to address these first two terms, we need to understand the phases of nuclear matter in the Skyrme model. An important question arises when studying phases of nuclear matter regarding the nature of high-density and low-density phases, and the transition between these phases. At high densities the skyrmions form a crystal [19], whereas at low densities the skyrmions are localised to their corresponding lattice points and form clusters, chains, and other exotic shapes like graphene [20]. As the ground state of nuclear matter has a crystalline structure in the classical approximation, understanding the infinite crystalline structure is key.

In order to determine such crystalline structures, one must find local minimizers of the relevant static energy functional associated to some action, or Lagrangian. The generalized Skyrme Lagrangian consists of four terms and is given by

$$\mathscr{L}_{0246} = \mathscr{L}_0 + \mathscr{L}_2 + \mathscr{L}_4 + \mathscr{L}_6, \tag{1.0.1}$$

where the index i denotes the degree of each term as a polynomial in spatial derivatives. The four terms appearing in the generalized Lagrangian are the potential, Dirichlet, Skyrme and sextic terms, respectively, and are detailed later. It is conventional to label the models by terms used in the Lagrangian, e.g. the generalized model is labelled $\mathscr{L}_{0246}$, the standard massive model is denoted $\mathscr{L}_{024}$, the massless Skyrme model $\mathscr{L}_{24}$ and the BPS (Bogomol'nyi–Prasad–Sommerfield) model $\mathscr{L}_{06}$. We will formulate our studies in terms of the full $\mathscr{L}_{0246}$-model; however, we shall only consider the $\mathscr{L}_{024}$- and $\mathscr{L}_{24}$-models in our numerical studies in Chap. 3. The subsequent chapter (Chap. 4) will deal with $\mathscr{L}_{0246}$-crystals and their applications to cold dense nuclear matter. Chap. 5 deals with an ω-meson variant of the Skyrme model without the Skyrme term, related to the $\mathscr{L}_{026}$-model.

For $\mathscr{L}_{24}$-skyrmions with $B < 8$, solutions were found to be hollow fullerene structures [21, 22]. These are well approximated by the rational map approximation (RMA) [23]. In the RMA, the target manifold S^3 is decomposed into horizontal slices, with a radial profile function $f(r)$, and a angular direction described by a rational map $S^2 \to S^2$, where the domain S^2 is identified with concentric spheres in $\mathbb{R}^3$ and the target S^2 with spheres of latitude on S^3. This was extended to include all $B \leq 22$ [24] and then icosahedrally symmetric rational maps for $B = 37, 47, 67, 97$ were constructed [25]. These hollow fullerenes collapse into smaller clusters in the $\mathscr{L}_{024}$-model [26]. A multi-layer rational map approach was proposed by Manton and Piette [27] and later considered in the context of the Skyrme crystal by Manton [28]. Feist *et al.* [29] developed this further by using a cubic grid method to determine multi-layer rational maps for the construction of skyrmions as chunks of the Skyrme crystal.

Atiyah and Manton [30] showed that skyrmions could be generated from SU(2) instantons by computing the holonomy along lines parallel to the time direction. The Atiyah–Manton construction was extended by Sutcliffe [31] to a BPS Skyrme model where the Skyrme field is

coupled to a tower of vector mesons. Truncating this BPS Skyrme model to include only the first term produces the standard Skyrme model. Halcrow and Winyard [32] then conjectured that, by coupling the Skyrme field to at least one vector meson, the low energy modes of a skyrmion can be used to understand the moduli space of instantons. Skyrmions have also been derived from holographic QCD models such as the Sakai-Sugimoto model [33]. More recently, skyrmions have been approximated directly from ADHM (Atiyah–Drinfeld–Hitchin–Manin) data [34, 35], which has been particularly successful at describing clusters of skyrmions and highly-symmetric amalgamated skyrmions. Manton and Sutcliffe [36] have approximated the Skyrme crystal from the holonomy of a twisted instanton on a 4-torus, obtaining a Skyrme crystal whose energy is 2% above that of the known numerical solution.

The crystal structure of $\mathscr{L}_{24}$-skyrmions was first studied by Klebanov [19], wherein he found a crystal of $B = 1$ skyrmions arranged in attractive channel orientations in a simple cubic (SC) lattice. This was achieved by considering a $B = 1$ hedgehog in a cubic period lattice with twisted boundary conditions [37]. At higher densities, this SC lattice undergoes a phase transition to a body centered cubic (BCC) lattice of half-skyrmions, which Manton & Goldhaber [38] later formulated as an enhanced symmetry. Then, independently, Kugler & Shtrikman [39] and Castillejo *et al.* [40] determined a new lower E/B solution, whereby skyrmions are initially arranged in a face centered cubic (FCC) lattice and relax to a SC lattice of half-skyrmions. In all of these studies, the $\mathscr{L}_{24}$ energy functional has only been varied for cubic lattices, in which only the side length of the cube is varied. This was carried out at various cube side lengths and a curve fitted to the data.

The phase structure of the $\mathscr{L}_{24}$-Skyrme model has been studied by Jackson and Verbaarschot [41], and Perapechka and Shnir [42] investigated phase transitions in the generalized $\mathscr{L}_{0246}$-Skyrme model. Two candidates have been previously proposed as the minimal E/B crystal for $\mathscr{L}_{024}$-skyrmions, these are the cubic lattice of half-skyrmions [39, 40] and the α-particle lattice [29]. Many skyrmions can be constructed as chunks of the infinite crystal [17, 43] and many have been built from α-particles [44]. The phase transition between the α-particle and the α-particle lattice has been investigated in both the $\mathscr{L}_{24}$-model [45] and $\mathscr{L}_{0246}$-model [46]. This $B = 4$, or α-particle, cluster picture supports the α-particle model of nuclei in which medium to large skyrmions are composed of $B = 4$ skyrmions in many arrangements [43, 44]. This α-clustering model has been pretty successful in the predicting the energy spectrum of states of Carbon-12 [9, 13] and Oxygen-16 [11, 12].

One would expect that most skyrmions would be constructed from chunks of some infinite crystalline configuration, such as the α particle lattice or the SC lattice of half-skyrmions. However, Gudnason and Halcrow [20] show that only the global minimisers for $B = 4, 8, 12$ for $B \leq 16$ are constructed from chunks of the α-particle lattice. They find a plethora of skyrmions with many new solutions constructed from sheets of square and hexagonal layers, chains of 2- and 3-tori, and chains of loosely bound clusters of lower charge skyrmions. Some work has been done on Skyrme chains [47, 48], domain walls [49] and multi-walls [50]. However, a rigorous numerical investigation into Skyrme crystals minimized over all period lattices has hitherto not been performed.

Additionally, a quantization of the isospin degrees of freedom for the SC crystal of half-skyrmions, in the $\mathscr{L}_{24}$-model, has been carried out by Baskerville [51] and the state corresponding to a neutron crystal identified. This was taken further by Adam *et al.* [52], in the context of the generalized $\mathscr{L}_{0246}$-model, to model isospin asymmetric nuclear matter and determine the nuclear matter equation of state (EoS) at high densities [53]. A key part of these studies is the isotropy of the isospin inertia tensor, which is only the case for the SC half-skyrmion crystal. So treatment for

the isospin quantization of Skyrme crystals with non-isotropic inertia tensors is needed. Further, the EoS derived from the Skyrme crystal is only valid in the high density regime where nuclear matter is assumed to be homogeneous. Whereas, below the nuclear saturation density, nuclear matter is known to be rather inhomogeneous. So, previous studies using the Skyrme crystal to model compact stars have had to interpolate between the high density Skyrme EoS and some other EoS valid in the low density regime [54].

The equation of state of nuclear matter plays a key role in understanding a number of interesting phenomena such as the mass and radii of neutron stars, the neutron-skin thickness of heavy nuclei, and the collective behavior of nucleons. So, our main aim is to derive an EoS from pure skyrmion matter which describes matter over *all* density regimes, that is, it interpolates between infinite nuclear matter and finite atomic nuclei. Then, using the EoS, we can estimate coefficients in the Bethe–Weizsäcker SEMF and extract information regarding the nuclear matter incompressibility coefficient.

1.1 The Skyrme Model

The Skyrme model consists of a single scalar field $\phi : \Sigma \to \mathrm{SU}(2)$ where spacetime is given by the $(3+1)$-dimensional Lorentzian manifold $\Sigma = \mathbb{R} \times M$ with the pseudo-Riemannian product metric $\eta = -\mathrm{d}t^2 + g$, and (M, g) is an oriented 3-dimensional Riemannian manifold with Riemannian metric g. We equip $(\mathrm{SU}(2), h)$ with the canonical bi-invariant metric $h(X,Y) = \frac{1}{2}\,\mathrm{Tr}(X^\dagger Y)$ and denote the Lie algebra of $\mathrm{SU}(2)$ by $\mathfrak{su}(2)$. Let us introduce oriented local coordinates $x = (t, x^1, x^2, x^3)$ on the domain Σ and let $\{\partial_0, \partial_1, \partial_2, \partial_3\}$ be a local basis for the tangent space $T_x\Sigma$ at $x \in \Sigma$, where we have denoted $\partial_\mu \equiv \partial/\partial x^\mu$. Let $\omega \in \Omega^1(\mathrm{SU}(2)) \otimes \mathfrak{su}(2)$ be the left Maurer-Cartan form. Then, for any left invariant vector fields $X, Y \in T_{\phi(x)}\,\mathrm{SU}(2)$, where $x \in \Sigma$, we define $\Omega \in \Omega^2(\mathrm{SU}(2)) \otimes \mathfrak{su}(2)$ to be be an $\mathfrak{su}(2)$-valued two-form on $\mathrm{SU}(2)$ given by

$$\Omega(X,Y) = [\omega(X), \omega(Y)]\,, \tag{1.1.1}$$

where $[\cdot,\cdot] : \mathfrak{su}(2) \times \mathfrak{su}(2) \to \mathfrak{su}(2)$ is the usual Lie bracket. The pullback of the left Maurer-Cartan form ω defines the $\mathfrak{su}(2)$-valued *left current*

$$\phi^*\omega =: L_\mu \mathrm{d}x^\mu, \qquad L_\mu = \omega_\phi(\partial_\mu \phi) = \phi^\dagger \partial_\mu \phi. \tag{1.1.2}$$

Let us write the pullback of the curvature as $\Omega_{\mu\nu} = \phi^*\Omega(\partial_\mu, \partial_\nu)$. Then the curvature can be expressed in terms of the $\mathfrak{su}(2)$-valued left current as

$$\Omega_{\mu\nu} = \Omega\left(\mathrm{d}\phi(\partial_\mu), \mathrm{d}\phi(\partial_\nu)\right) = \left[\omega_\phi(\partial_\mu\phi), \omega_\phi(\partial_\nu\phi)\right] = \left[L_\mu, L_\nu\right]. \tag{1.1.3}$$

Skyrme's original $\mathscr{L}_{24}$-model [3] is composed of two terms: the Dirichlet (or kinetic) term, which is given by

$$\mathscr{L}_2 = \frac{F_\pi^2}{16\hbar}\eta^{\mu\nu}\,\mathrm{Tr}\big(L_\mu L_\nu\big), \tag{1.1.4}$$

and the Skyrme term, corresponding to the four pion interaction,

$$\mathscr{L}_4 = \frac{\hbar}{32e^2}\eta^{\mu\alpha}\eta^{\nu\beta}\,\mathrm{Tr}\left(\left[L_\mu, L_\nu\right]\left[L_\alpha, L_\beta\right]\right). \tag{1.1.5}$$

The $\mathscr{L}_{24}$-model is $(\mathrm{SU}(2)\times\mathrm{SU}(2))/\mathbb{Z}_2 \cong \mathrm{SO}(4)$ invariant and the pions are massless in this theory. If one studies static Skyrme fields $\phi : \mathbb{R}^3 \to \mathrm{SU}(2)$ and wants to obtain finite energy configurations, then they are required to impose the vacuum boundary conditions $\phi(\vec{x} \to \infty) = \mathrm{Id}_2$. This vacuum boundary condition spontaneously breaks the chiral $\mathrm{SO}(4)$ symmetry to an $\mathrm{SO}(3)$ isospin symmetry, which acts on the pion fields $\vec{\pi}$. So, the pion fields $\vec{\pi}$ are actually the Goldstone bosons associated with this spontaneous symmetry breaking. The massive $\mathscr{L}_{024}$-Skyrme model includes the pion mass term

$$\mathscr{L}_0 = -\frac{1}{8\hbar^3}F_\pi^2 V(\phi). \tag{1.1.6}$$

where, throughout, we will use the standard pion mass potential $V : \mathrm{SU}(2) \to [0,\infty)$ given by

$$V(\phi) = m_\pi^2 \operatorname{Tr}(\mathrm{Id}_2 - \phi). \tag{1.1.7}$$

This has the effect of giving the pions of the theory (small amplitude waves about the vacuum $\phi = \mathrm{Id}_2$) mass m_π. Therefore, in the massive $\mathscr{L}_{024}$-model, the inclusion of the pion mass potential (1.1.6), first proposed by Adkins and Nappi [6], explicitly breaks the chiral $\mathrm{SO}(4)$ symmetry to an isospin $\mathrm{SO}(3) \cong \mathrm{SU}(2)$ isospin symmetry, given by the conjugation

$$\phi \mapsto A\phi A^\dagger, \quad A \in \mathrm{SU}(2). \tag{1.1.8}$$

Upon quantization, this gives rise to the quantity that distinguishes protons and neutrons: isospin.

In addition to the spontaneous symmetry breaking, the finite energy boundary condition $\phi(\vec{x} \to \infty) = \mathrm{Id}_2$ yields the one-point compactification of space $\mathbb{R}^3 \cup \{\infty\} \cong S^3$, such that the Skyrme field can be identified as a map $\phi : S^3 \to \mathrm{SU}(2) \cong S^3$. The disjoint homotopy classes of such maps are labelled by their topological degree $B \in \pi_3(S^3) = \mathbb{Z}$ and the fields are necessarily topologically stable configurations. In general, the topological degree is identified with the physical baryon number upon quantization, so we often to refer to B as the baryon number, which may be computed using

$$B = \deg(\phi) = \int_M \mathrm{d}^3x\sqrt{g}\,\mathscr{B}^0, \quad \mathscr{B}^\mu = \frac{1}{24\pi^2\sqrt{g}}\epsilon^{\mu\nu\rho\sigma}\operatorname{Tr}\big(L_\nu L_\rho L_\sigma\big), \tag{1.1.9}$$

where M is a connected, oriented, 3-dimensional manifold without boundary.

We will also consider the generalization of the massive $\mathscr{L}_{024}$-Skyrme Lagrangian which yields an ω-meson-like repulsion on short distances, while also allowing the quartic Skyrme term to describe scalar meson effects. This is achieved by including the sextic term, defined by [55]

$$\mathscr{L}_6 = -\pi^4\lambda^2\eta^{\mu\nu}\mathscr{B}_\mu\mathscr{B}_\nu, \tag{1.1.10}$$

where $\mathscr{B}^\mu$ is the topological current defined in (1.1.9). So, the free parameters of the model are the pion decay constant F_π, the pion mass m_π, the dimensionless Skyrme parameter e, and λ which is related to the ω-meson mass m_ω and the coupling constant β_ω of the ω meson via $\lambda^2 = \beta_\omega^2\hbar^3/(2\pi^4 m_\omega^2)$ [56], where $\hbar = 197.33$ MeV fm is the reduced Planck constant.

Our aim is normally to find *static* solutions and, so, we define $\phi = \varphi \circ \mathrm{pr}_2$ where $\varphi : M \to \mathrm{SU}(2)$ is a fixed map and $\mathrm{pr}_2 : \mathbb{R}\times M \to M$ is a projection. The map $\varphi : M \to \mathrm{SU}(2)$ will now be identified as the Skyrme field. Following convention, we adopt the usual Skyrme units of length and energy. The classical energy scale is $\tilde{E} = F_\pi/4e$ (MeV) and the length scale is $\tilde{L} = 2\hbar/eF_\pi$ (fm). Thus the

quantum energy scale is defined by $\tilde{\hbar} = 2e^2$. In these dimensionless Skyrme units, the Lagrangian is given by

$$\begin{aligned}\mathscr{L} &= \frac{\tilde{L}^3}{\tilde{E}}\mathscr{L}_0 + \frac{\tilde{L}}{\tilde{E}}\mathscr{L}_2 + \frac{1}{\tilde{L}\tilde{E}}\mathscr{L}_4 + \frac{1}{\tilde{L}^3\tilde{E}}\mathscr{L}_6 \\ &= -m^2 \operatorname{Tr}\left(\mathrm{Id}_2 - \phi\right) + \frac{1}{2}\eta^{\mu\nu}\operatorname{Tr}\left(L_\mu L_\nu\right) + \frac{1}{16}\eta^{\mu\alpha}\eta^{\nu\beta}\operatorname{Tr}\left(\left[L_\mu, L_\nu\right]\left[L_\alpha, L_\beta\right]\right) - c_6\eta^{\mu\nu}\mathscr{B}_\mu\mathscr{B}_\nu,\end{aligned} \tag{1.1.11}$$

where the rescaled pion mass for our studies is

$$m = \frac{2m_\pi}{F_\pi e} \tag{1.1.12}$$

and the dimensionless sextic coupling constant is

$$c_6 = \frac{\pi^4\lambda^2 e^4 F_\pi^2}{2\hbar^3}. \tag{1.1.13}$$

It will prove useful throughout to introduce the Hilbert energy-momentum tensor (in dimensionless Skyrme units):

$$\begin{aligned}T_{\mu\nu} &= -\frac{2}{\sqrt{-\eta}}\frac{\partial(\sqrt{-\eta}\mathscr{L}_{0246})}{\partial\eta^{\mu\nu}} = -2\frac{\partial\mathscr{L}_{0246}}{\partial\eta^{\mu\nu}} + \eta_{\mu\nu}\mathscr{L}_{0246} \\ &= -\operatorname{Tr}\left(L_\mu L_\nu\right) - \frac{1}{4}\eta^{\alpha\beta}\operatorname{Tr}\left([L_\mu, L_\alpha][L_\nu, L_\beta]\right) + 2c_6\mathscr{B}_\mu\mathscr{B}_\nu + \eta_{\mu\nu}\mathscr{L}_{0246}.\end{aligned} \tag{1.1.14}$$

The static energy functional can be obtained from the timelike part of the energy-momentum tensor, $T_{00} = \mathscr{E}_{\text{stat}} + \mathscr{E}_{\text{kin}}$, and is given by

$$\begin{aligned}M_B(\varphi, g) &= \int_M \mathrm{d}^3x\sqrt{g}\,\mathscr{E}_{\text{stat}} \\ &= \int_M \mathrm{d}^3x\sqrt{g}\left\{m^2\operatorname{Tr}\left(\mathrm{Id}_2 - \varphi\right) - \frac{1}{2}g^{ij}\operatorname{Tr}\left(L_iL_j\right) - \frac{1}{16}g^{ia}g^{jb}\operatorname{Tr}\left([L_i, L_j][L_a, L_b]\right)\right. \\ &\quad \left. + c_6\frac{\epsilon^{ijk}\epsilon^{abc}}{(24\pi^2\sqrt{g})^2}\operatorname{Tr}\left(L_iL_jL_k\right)\operatorname{Tr}(L_aL_bL_c)\right\}.\end{aligned} \tag{1.1.15}$$

A field configuration φ which minimizes the static energy functional (1.1.15), for some choice of domain metric g, is referred to as a *skyrmion* and the static energy M_B is often interpreted as the classical mass of the skyrmion.

Throughout, it will be convenient to utilize the non-linear σ-model (NLσM) formulation of the model, that is, we write $\varphi = \sigma\,\mathrm{Id}_2 + i\vec{\tau}\cdot\vec{\pi}$ where τ^i are the usual Pauli spin matrices. Then, exploiting the isometry between $(\mathrm{SU}(2), h)$ and S^3 with its round metric of unit radius, we can identify

$$\mathrm{SU}(2) \ni \begin{pmatrix}\sigma + i\pi^3 & i\pi^1 + \pi^2 \\ i\pi^1 - \pi^2 & \sigma - i\pi^3\end{pmatrix} \leftrightarrow (\sigma, \pi^1, \pi^2, \pi^3) \in S^3, \tag{1.1.16}$$

with the unitary condition $\sigma^2 + \vec{\pi}\cdot\vec{\pi} = 1$, where $\vec{\pi} = (\pi^1, \pi^2, \pi^3)$ is normally identified with the triplet of pion fields and σ with the non-linear σ-field. For numerical purposes, we will write φ^μ

where it is understood that $\varphi^0 = \sigma$ and $\varphi^i = \pi^i$. Then we can write the energy functional in NLσM notation as

$$\begin{aligned} M_B(\varphi, g) = \int_M \mathrm{d}^3x\sqrt{g}\Big\{&2m^2(1-\sigma) + g^{ij}\partial_i\varphi^\mu\partial_j\varphi^\mu + \frac{1}{2}g^{ik}g^{jl}\left(\partial_i\varphi^\mu\partial_k\varphi^\mu\partial_j\varphi^\nu\partial_l\varphi^\nu - \partial_i\varphi^\mu\partial_l\varphi^\mu\partial_j\varphi^\nu\partial_k\varphi^\nu\right) \\ &+ \frac{c_6\epsilon^{ijk}\epsilon^{lmn}}{(12\pi^2\sqrt{g})^2}\epsilon_{\mu\nu\rho\sigma}\epsilon_{\alpha\beta\gamma\delta}\varphi^\mu\varphi^\alpha\partial_i\varphi^\nu\partial_j\varphi^\rho\partial_k\varphi^\sigma\partial_l\varphi^\beta\partial_m\varphi^\gamma\partial_n\varphi^\delta\Big\}. \end{aligned} \tag{1.1.17}$$

After a lengthy but straightforward calculation, the corresponding Euler–Lagrange field equations (for a flat metric) are found to be

$$\begin{aligned} \frac{\delta\mathscr{E}_{\mathrm{stat}}}{\delta\varphi^\mu} &= \frac{\partial\mathscr{E}_{\mathrm{stat}}}{\partial\varphi^\mu} - \partial_i\left(\frac{\partial\mathscr{E}_{\mathrm{stat}}}{\partial(\partial_i\varphi^\mu)}\right) \\ &= \frac{\partial V}{\partial\varphi^\mu} - 2g^{pa}\Big\{\partial_{pa}\varphi^\mu + g^{qb}\Big[\Big(\partial_{pa}\varphi^\mu\partial_q\varphi^\alpha\partial_b\varphi^\alpha + \partial_p\varphi^\mu\partial_{qa}\varphi^\alpha\partial_b\varphi^\alpha + \partial_p\varphi^\mu\partial_q\varphi^\alpha\partial_{ba}\varphi^\alpha\Big) \\ &\quad - \Big(\partial_{qa}\varphi^\mu\partial_p\varphi^\alpha\partial_b\varphi^\alpha + \partial_q\varphi^\mu\partial_{pa}\varphi^\alpha\partial_b\varphi^\alpha + \partial_q\varphi^\mu\partial_p\varphi^\alpha\partial_{ba}\varphi^\alpha\Big)\Big]\Big\} + \frac{2c_6\epsilon^{pqr}\epsilon^{abc}}{(12\pi^2\sqrt{g})^2}\epsilon_{\alpha\beta\gamma\delta}\epsilon_{\mu\nu\rho\sigma} \\ &\quad \times\Big\{\varphi^\alpha\partial_p\varphi^\nu\partial_a\varphi^\beta\partial_q\varphi^\rho\partial_b\varphi^\gamma\partial_r\varphi^\sigma\partial_c\varphi^\delta + 3\Big[\partial_p\varphi^\nu\varphi^\alpha\partial_a\varphi^\beta\partial_q\varphi^\rho\partial_b\varphi^\gamma\partial_r\varphi^\sigma\partial_c\varphi^\delta \\ &\quad + \varphi^\nu\partial_p\varphi^\alpha\partial_a\varphi^\beta\partial_q\varphi^\rho\partial_b\varphi^\gamma\partial_r\varphi^\sigma\partial_c\varphi^\delta + \varphi^\nu\varphi^\alpha\Big(\partial_{pa}\varphi^\beta\partial_q\varphi^\rho\partial_b\varphi^\gamma\partial_r\varphi^\sigma\partial_c\varphi^\delta \\ &\quad + \partial_a\varphi^\beta\partial_{pq}\varphi^\rho\partial_b\varphi^\gamma\partial_r\varphi^\sigma\partial_c\varphi^\delta + \partial_a\varphi^\beta\partial_q\varphi^\rho\partial_{pb}\varphi^\gamma\partial_r\varphi^\sigma\partial_c\varphi^\delta \\ &\quad + \partial_a\varphi^\beta\partial_q\varphi^\rho\partial_b\varphi^\gamma\partial_{pr}\varphi^\sigma\partial_c\varphi^\delta + \partial_a\varphi^\beta\partial_q\varphi^\rho\partial_b\varphi^\gamma\partial_r\varphi^\sigma\partial_{pc}\varphi^\delta\Big)\Big]\Big\}. \end{aligned} \tag{1.1.18}$$

Arrested Newton Flow

The Euler–Lagrange field equations (1.1.18) associated to (1.1.15) can be approximately solved by discretizing the static energy (1.1.15) and employing a 4th order central finite-difference method. This is carried out using the NLσM formulation detailed above. The first order and second order spatial derivatives with respect to the local coordinate x^1 are, respectively, given by

$$\frac{\partial\varphi^\mu_{i,j,k}}{\partial x^1} = \frac{\frac{1}{12}\varphi^\mu_{i-2,j,k} - \frac{2}{3}\varphi^\mu_{i-1,j,k} + \frac{2}{3}\varphi^\mu_{i+1,j,k} - \frac{1}{12}\varphi^\mu_{i+2,j,k}}{\Delta x^1} \tag{1.1.19}$$

$$\frac{\partial^2\varphi^\mu_{i,j,k}}{\partial(x^1)^2} = \frac{-\frac{1}{12}\varphi^\mu_{i-2,j,k} + \frac{4}{3}\varphi^\mu_{i-1,j,k} - \frac{5}{2}\varphi^\mu_{i,j,k} + \frac{4}{3}\varphi^\mu_{i+1,j,k} - \frac{1}{12}\varphi^\mu_{i+2,j,k}}{(\Delta x^1)^2}, \tag{1.1.20}$$

with the x^2, x^3 derivatives defined analogously. We can then regard the static energy as a function $M_B : \mathscr{C} \to \mathbb{R}$, where the discretised configuration space is the manifold $\mathscr{C} = (S^3)^{N_1N_2N_3} \subset \mathbb{R}^{4N_1N_2N_3}$. To solve the Euler–Lagrange field equations (1.1.18) we use arrested Newton flow: an accelerated gradient descent method with flow arresting, with some appropriate initial configuration. That is, we are solving the system of 2nd order ODEs

$$\ddot{\varphi} = -\frac{\delta\mathscr{E}_{\mathrm{stat}}}{\delta\varphi}, \qquad \varphi(0) = \varphi_0, \tag{1.1.21}$$

with initial velocity $\dot{\varphi}(0) = 0$. Setting $\psi := \dot{\varphi}$ as the velocity with $\psi(0) = \dot{\varphi}(0) = 0$ reduces the problem to a coupled system of 1st order ODEs. We implement a 4th order Runge–Kutta method

to solve this coupled system. In general, the initial configuration φ_0 is not a minimizer and so it swaps its potential energy for kinetic energy as it evolves. During the evolution we check to see if the potential energy is increasing. If the energy is indeed increasing, we take out all the kinetic energy in the system by setting $\psi(t) = \dot{\varphi}(t) = 0$ and restart the flow (this is the arresting criteria). Naturally the field will relax to a local, or global, minimum in some potential well. The evolution then terminates when every component of the energy gradient $\frac{\partial M_B}{\partial \varphi}$ is zero within some specified tolerance, e.g. tol $= 10^{-5}$.

It is essential that we ensure our Skyrme field lies on the target 3-sphere. Numerically we pull our target space back onto S^3. This is done by normalizing the Skyrme field φ each loop,

$$\varphi^\mu \to \frac{\varphi^\mu}{\varphi \cdot \varphi}. \tag{1.1.22}$$

We also need to project out the component of the energy gradient, and velocity, in the direction of Skyrme field, that is

$$\frac{\partial \mathscr{E}}{\partial \varphi^\mu} \to \frac{\partial \mathscr{E}}{\partial \varphi^\mu} - \left(\frac{\partial \mathscr{E}}{\partial \varphi} \cdot \varphi\right) \frac{\varphi^\mu}{\varphi \cdot \varphi} \quad \text{and} \quad \psi^\mu \to \psi^\mu - (\psi \cdot \varphi) \frac{\varphi^\mu}{\varphi \cdot \varphi}. \tag{1.1.23}$$

1.2 The $B = 1$ 🦔 Skyrmion

In Skyrme's original $\mathscr{L}_{24}$-model he presented the spherically symmetric $B = 1$ hedgehog skyrmion [3]. The existence of a minimizer in the charge 1 sector with spherical symmetry was proven by Kapitanski and Ladyzenskaia [57], and Esteban [58] proved existence of a $B = 1$ minimizer in general. The hedgehog ansatz takes the form

$$\varphi_H(\vec{x}) = \exp\left(i f(r) \hat{\vec{x}} \cdot \vec{\tau}\right), \tag{1.2.1}$$

where $f : [0, \infty) \to \mathbb{R}$ is some radial profile function. This ansatz is known as the hedgehog ansatz because the pion fields point radially outwards from the origin at all points in space. This can be easily seen by considering the ansatz in terms of the pion fields,

$$\sigma = \cos f(r), \qquad \vec{\pi} = \sin f(r) \hat{\vec{x}}. \tag{1.2.2}$$

In order to ensure the boundary condition $\varphi(\vec{x} \to \infty) = \mathrm{Id}_2$, the profile function $f(r)$ must satisfy the boundary conditions $f(0) = \pi$ and $f(\infty) = 0$. The hedgehog solution does indeed have baryon number $B = 1$ since, upon substitution of (1.2.1) into (1.1.9), one finds that

$$B = -\frac{1}{2\pi^2} \int_0^\infty \frac{\sin^2 f}{r^2} \frac{\mathrm{d}f}{\mathrm{d}r} 4\pi r^2 \mathrm{d}r = \frac{1}{\pi} f(0) = 1. \tag{1.2.3}$$

To determine the $B = 1$ skyrmion, we have to solve the Euler–Lagrange field equations corresponding to the static energy functional associated to the hedgehog ansatz (1.2.1). The associated energy functional is found to be (upon substituting (1.2.1) into (1.1.15) with $V(\varphi) = 0 = c_6$)

$$M_1 = 4\pi \int_0^\infty \left[r^2 \left(\frac{\mathrm{d}f}{\mathrm{d}r}\right)^2 + 2 \sin^2 f \left(1 + \left(\frac{\mathrm{d}f}{\mathrm{d}r}\right)^2\right) + \frac{\sin^4 f}{r^2} \right] \mathrm{d}r \tag{1.2.4}$$

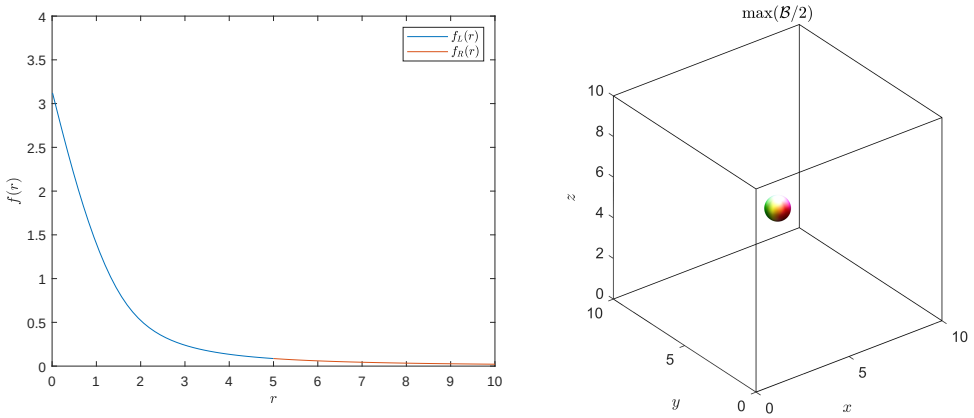

(a) (b)

Figure 1.1: The profile function (a) and isosurface plot of the baryon density (b) of the $B = 1$ hedgehog skyrmion.

and the corresponding Euler–Lagrange field equations reduce to a second order non-linear ODE that can only be solved numerically, which are given by

$$\left(r^2 + 2\sin^2 f\right)\frac{\mathrm{d}^2 f}{\mathrm{d}r^2} + 2r\frac{\mathrm{d}f}{\mathrm{d}r} + \sin 2f\left[\left(\frac{\mathrm{d}f}{\mathrm{d}r}\right)^2 - 1 - \frac{\sin^2 f}{r^2}\right] = 0. \tag{1.2.5}$$

Using a shooting method, the resulting profile function $f(r)$ is shown in Fig. 1.1a. We observe that the massless $B = 1$ hedgehog skyrmion has energy per baryon $E/(12\pi^2) = 1.232$. As a fidelity check on our numerics we also obtain the $B = 1$ skyrmion using arrested Newton flow, and we find that both results are in agreement. Also shown in Fig. 1.1 is an isosurface plot of the baryon density $\mathcal{B}^0(\vec{x})$, which is colored using the Runge color sphere detailed in Sec. A.2.

The asymptotic behavior of the profile function $f(r)$ can be determined by linearizing the field equations (1.2.5) for large r, revealing that $f(r) \to c/r^2$, for some constant c. This shows that, to leading order, the pion fields behave asymptotically as a triplet of scalar orthogonal dipoles, $\vec{\pi} \to (c/r^2)\hat{\vec{x}}$. We employ a multiple shooting method to numerically determine the asymptotic constant c, where we define two profile functions: the left $f_L(r)$ and right $f_R(r)$ profiles. These profiles must satisfy the boundary conditions $f_L(0) = \pi$ and $f_R(\infty) = 0$. At some $r_* \in [0, \infty)$, we require the profiles and their derivatives to match, that is, $f_L(r_*) = f_R(r_*)$ and $f_L'(r_*) = f_R'(r_*)$. Setting $f_R(r) = c/r^2$ and shooting from both sides, we find that $c = 2.157$ which is in agreement with [59]. This enables one to determine the dipole strength $E_D = 4\pi c$ and also calculate the asymptotic forces between well-separated skyrmions. Jackson *et al.* [60] investigated the asymptotic interactions of two well-separated $B = 1$ skyrmions. Therein, they observed that two $B = 1$ skyrmions with one rotated by an angle of π about a line perpendicular to the line joining them produces the lowest interaction energy. This is known as the *attractive channel* orientation.

1.3 Skyrmion Crystals

So far, we have only detailed the $B = 1$ skyrmion solution on $\mathbb{R}^3$. However, as we have previously motivated, we wish to study static Skyrme fields $\varphi : \mathbb{R}^3 \to \mathrm{SU}(2)$ that are periodic with respect to some 3-dimensional period lattice

$$\Lambda = \left\{ n_1 \vec{X}_1 + n_2 \vec{X}_2 + n_3 \vec{X}_3 : n_i \in \mathbb{Z} \right\}, \tag{1.3.1}$$

i.e. we impose the condition $\varphi(x + X) = \varphi(x)$ for all $x \in \mathbb{R}^3$ and $X \in \Lambda$. We can equivalently interpret the domain of the Skyrme field as $\mathbb{R}^3/\Lambda$, where $(\mathbb{R}^3/\Lambda, d)$ is a 3-torus equipped with the standard Euclidean metric d. Now, let us denote the unit 3-torus by $\mathbb{T}^3 \equiv S^1 \times S^1 \times S^1 = \mathbb{R}^3/\mathbb{Z}^3$ and equip it with a flat Riemannian metric g. Let (x^1, x^2, x^3) be oriented local coordinates on $\mathbb{T}^3$ and $\{\partial_1, \partial_2, \partial_3\}$ be a local frame for the tangent space $T_x\mathbb{T}^3$ at $x \in \mathbb{T}^3$. Then every 3-torus $(\mathbb{R}^3/\Lambda, d)$ can be identified with this unit 3-torus $(\mathbb{T}^3, g)$ via the diffeomorphism

$$F : \mathbb{T}^3 \to \mathbb{R}^3/\Lambda, \quad (x^1, x^2, x^3) \mapsto x^1 \vec{X}_1 + x^2 \vec{X}_2 + x^3 \vec{X}_3. \tag{1.3.2}$$

The associated metric g on $\mathbb{T}^3$ is the pullback of the metric d by F, i.e.

$$g = F^* d = g_{ij} \mathrm{d}x^i \mathrm{d}x^j, \quad g_{ij} = \vec{X}_i \cdot \vec{X}_j. \tag{1.3.3}$$

Note that the matrix (g_{ij}) is a symmetric positive definite real 3×3 matrix. We denote the set of such matrices SPD_3 and note that every such matrix arises as the metric on $\mathbb{T}^3$ corresponding to some lattice Λ, with lattices producing the same matrix related by an oriented isometry of $\mathbb{R}^3$. So, we can now consider variations of the period lattice Λ_s, with $\Lambda_0 = \Lambda$, by equivalently varying the metric g_s on $\mathbb{T}^3$ with $g_0 = F^* d$.

Definition 1. *An energy minimizing map $\varphi : (\mathbb{T}^3, g_*) \to S^3$, where g_* is some fixed metric, is a skyrmion lattice. A* skyrmion crystal *is a skyrmion lattice such that the field φ is also critical with respect to variations of the metric g about g_*.*

Theorem 2 (Hopf Degree Theorem)**.** *If M is a connected, oriented, n-dimensional manifold without boundary, then two maps $M \to S^n$ are smoothly homotopic if and only if they have the same degree.*

For a proof of this theorem see, e.g., [61, p. 50]. Hopf's degree theorem ensures that such mappings $\varphi : \mathbb{T}^3 \to S^3$ are also characterized by a homotopy invariant: the topological degree $B \in H_3(\mathbb{T}^3) = \mathbb{Z}$, since $\mathbb{T}^3$ is compact and without boundary. That is, the unit cell of a skyrmion crystal has an associated topological charge, which we will denote by B_{cell}, and can be computed using (1.1.9). Further, the energy per unit cell E_{cell} is finite and well-defined. So, one can compute the energy per baryon of the infinitely extended crystal via

$$\frac{E_{\mathrm{crystal}}}{B_{\mathrm{crystal}}} = \frac{N_{\mathrm{cell}} E_{\mathrm{cell}}}{N_{\mathrm{cell}} B_{\mathrm{cell}}} = \frac{E_{\mathrm{cell}}}{B_{\mathrm{cell}}}. \tag{1.3.4}$$

For the remainder of this section, we focus mainly on the $\mathscr{L}_{24}$-Skyrme model on $\mathbb{T}^3$. The configuration space of skyrmion crystals is

$$\mathscr{M} = C^\infty(\mathbb{T}^3, S^3) \times \mathrm{SPD}_3, \tag{1.3.5}$$

and the massless $\mathscr{L}_{24}$-Skyrme energy functional is denoted $E_{24} : \mathscr{M} \to \mathbb{R}$ for $\varphi : \mathbb{T}^3 \to S^3$, $g \in \mathrm{SPD}_3$. Denote by O the subgroup of SO(3) consisting of orientation preserving symmetries of the cube (a finite group of order $|O| = 24$). Define $\mathrm{Aut}(\mathbb{T}^3)$ as the set of transformations on $\mathbb{T}^3$ of the form

$$S : \vec{x} \mapsto A\vec{x} + \vec{v}, \quad A \in O, \quad \vec{v} \in \mathbb{R}^3. \tag{1.3.6}$$

Then we observe that the massless Skyrme energy E_{24} is invariant under the left action of the group

$$G = \mathrm{SO}(4) \times \mathrm{Aut}(\mathbb{T}^3). \tag{1.3.7}$$

The natural action of this group G on the configuration space $\mathscr{M}$ is

$$\begin{aligned}(R, S) \cdot \left(\varphi(\vec{x}), g\right) &= \left(R \circ \varphi \circ S^{-1}(\vec{x}), (S^{-1})^* g\right) \\ &= \left(R\varphi\left(A^{-1}(\vec{x} - \vec{v})\right), (A^{-1})^T g A^{-1}\right).\end{aligned} \tag{1.3.8}$$

We now present a review of crystalline solutions in the Skyrme model, with the main focus on the $\mathscr{L}_{24}$-model. For a more general review see, e.g., [42, 46, 53, 62].

Klebanov [19] was the first to study the crystalline structure of skyrmion matter in the $\mathscr{L}_{24}$-model. Therein, he obtained a skyrmion lattice in the low density regime by arranging $B = 1$ hedgehog skyrmions in the attractive channel on a SC lattice. In practice, this was carried out by considering a $B = 1$ hedgehog in a cubic period lattice with twisted boundary conditions. We will label this simple cubic lattice of $B = 1$ hedgehogs as SC_1. The resulting unit cell is cubic with period lattice $\Lambda = L\mathbb{Z}^3$, for some constant unit cell side length L, and has charge $B_{\mathrm{cell}} = 8$ per unit cell. The corresponding metric on $\mathbb{T}^3$ is thus $g_{ij} = L^2\delta_{ij}$. The initial crystalline configuration Klebanov used is invariant under the following transformations

$$\mathrm{A}_1 : R(\varphi) = (\sigma, -\pi^1, \pi^2, \pi^3), \quad S(\vec{x}) = (-x^1, x^2, x^3), \tag{1.3.9}$$

$$\mathrm{A}_2 : R(\varphi) = (\sigma, \pi^2, \pi^3, \pi^1), \quad S(\vec{x}) = (x^2, x^3, x^1), \tag{1.3.10}$$

and an additional periodic symmetry,

$$\mathrm{A}_3 : R(\varphi) = (\sigma, -\pi^1, \pi^2, -\pi^3), \quad S(\vec{x}) = (x^1 + 1/2, x^2, x^3), \tag{1.3.11}$$

where we have opted to use the crystal notation of Kugler and Shtrikman [62]. These transformations act via (1.3.8) and we denote the symmetries of the SC_1 skyrmion lattice by $(\mathrm{A}_1, \mathrm{A}_2, \mathrm{A}_3)$.

The symmetries $(\mathrm{A}_1, \mathrm{A}_2, \mathrm{A}_3)$ of the Klebanov lattice SC_1 are detailed as follows. Relation A_1 (1.3.9) is a reflection in a face of the cube, coupled with a reflection on the field φ. Symmetry A_2 (1.3.10) is a simultaneous rotation around a three-fold axis in both spaces. Finally, A_3 (1.3.11) is a translation by $1/2$ along an axis coupled with a mutual isorotation into the attractive channel between nearest neighbours.

We remark that the Skyrme field of the SC_1 Klebanov lattice is invariant under translations by L in $\mathbb{R}^3/(L\mathbb{Z}^3)$; however, using symmetry A_3 (1.3.11), we see that the energy and baryon densities are invariant under translations by $L/2$. That is, the unit cell in $\mathbb{R}^3/(L\mathbb{Z}^3)$ of the baryon and energy densities is of periodicity $L/2$, whereas the unit cell for the Skyrme field is of periodicity L.

It was later observed by Goldhaber and Manton [38] that, at higher densities, the SC_1 skyrmion lattice of Klebanov undergoes a phase transition to a BCC skyrmion crystal of $1/2$-skyrmions. This $\mathrm{BCC}_{1/2}$ crystal shares the simple cubic symmetries $(\mathrm{A}_1, \mathrm{A}_2, \mathrm{A}_3)$ plus a further symmetry,

$$\mathrm{B}_4 : R(\varphi) = (-\sigma, \pi^2, \pi^1, \pi^3), \quad S(\vec{x}) = (1/4 - x^3, 1/4 - x^2, 1/4 - x^1). \tag{1.3.12}$$

This corresponds to a rotation of π around an axis going through the points $(0, 1/8, 1/4)$ and $(1/4, 1/8, 0)$ and an $O(4)$ transformation. Like Klebanov's SC skyrmion lattice, the energy and baryon densities of the BCC skyrmion crystal are periodic in $L/2$ but the field periodic in L, and the unit cell has topological charge $B_{\text{cell}} = 8$.

Kugler and Shtrikman [62] then proposed a FCC lattice of $B = 1$ skyrmions with the symmetries $(\mathrm{A}_1, \mathrm{A}_2, \mathrm{C}_3, \mathrm{C}_4)$, where

$$\mathrm{C}_3 : R(\varphi) = (\sigma, -\pi^1, \pi^3, -\pi^2), \quad S(\vec{x}) = (x^1, x^3, -x^2) \tag{1.3.13}$$

$$\mathrm{C}_4 : R(\varphi) = (\sigma, -\pi^1, -\pi^2, \pi^3), \quad S(\vec{x}) = (x^1 + 1/2, x^2 + 1/2, x^3). \tag{1.3.14}$$

The resulting unit cell is cubic with charge $B_{\text{cell}} = 4$. However, in contrast to the SC_1 lattice and $\mathrm{BCC}_{1/2}$ crystal, the FCC_1 lattice has energy and baryon densities periodic in L. Kugler & Shtrikman [39] and Castillejo *et al.* [40] independently found, by allowing this FCC_1 lattice to vary by homothety, a SC crystal of 1/2-skyrmions that shares the C_3 symmetry and an additional chiral SO(4) symmetry [62],

$$\mathrm{D}_4 : R(\varphi) = (-\sigma, -\pi^1, \pi^2, \pi^3), \quad S(\vec{x}) = (x^1 + 1/2, x^2, x^3). \tag{1.3.15}$$

The enhanced symmetry D_4 (1.3.15) means that the energy and baryon densities are now periodic in $L/2$, with the field remaining period in L. This $\mathrm{SC}_{1/2}$ skyrmion crystal has charge $B_{\text{cell}} = 4$ and is believed to be the lowest energy (per baryon) crystalline configuration in the massless $\mathscr{L}_{24}$-Skyrme model. As it has been believed to be the ground state crystalline configuration for many decades, the $\mathrm{SC}_{1/2}$ crystal has been coined *the Skyrme crystal*.

Before detailing the construction of these skyrmion lattices/crystals, we briefly summarize them. In the low density regime there exists a SC_1 lattice that undergoes a phase transition to a $\mathrm{BCC}_{1/2}$ crystal in the higher density region. Likewise, there also exists a FCC_1 lattice at low densities that phase transitions to a $\mathrm{SC}_{1/2}$ crystal at high density. At low densities, the FCC_1 lattice generally has lower energy than the SC_1 lattice. However, at densities higher than that of the saturation density*, the $\mathrm{SC}_{1/2}$ lattice exhibits a phase transition to the $\mathrm{BCC}_{1/2}$ lattice [42, 46].

The starting point in the construction of the above skyrmion lattices and crystals is the Fourier series-like expansion of the Skyrme fields as an initial configuration [62],

$$\sigma = \sum_{a,b,c}^{\infty} \beta_{abc} \cos\left(\frac{2a\pi x^1}{L}\right) \cos\left(\frac{2b\pi x^2}{L}\right) \cos\left(\frac{2c\pi x^3}{L}\right), \tag{1.3.16a}$$

$$\pi^1 = \sum_{h,k,l}^{\infty} \alpha_{hkl} \sin\left(\frac{2h\pi x^1}{L}\right) \cos\left(\frac{2k\pi x^2}{L}\right) \cos\left(\frac{2l\pi x^3}{L}\right), \tag{1.3.16b}$$

$$\pi^2 = \sum_{h,k,l}^{\infty} \alpha_{hkl} \cos\left(\frac{2l\pi x^1}{L}\right) \sin\left(\frac{2h\pi x^2}{L}\right) \cos\left(\frac{2k\pi x^3}{L}\right), \tag{1.3.16c}$$

$$\pi^3 = \sum_{h,k,l}^{\infty} \alpha_{hkl} \cos\left(\frac{2k\pi x^1}{L}\right) \cos\left(\frac{2l\pi x^2}{L}\right) \sin\left(\frac{2h\pi x^3}{L}\right), \tag{1.3.16d}$$

with initial metric $g = L^3 \,\mathrm{Id}_3$ on $\mathbb{T}^3$. This is a valid expansion as all of the lattice/crystal symmetries above have the two common cubic transformations A_1 (1.3.9) and A_2 (1.3.10). The additional

*The saturation density is the density, or volume, for which the lattice is minimal energy, i.e. it is the density at which the skyrmion lattice becomes a skyrmion crystal.

symmetries (A_3, B_4, C_3, C_4, D_4) impose some conditions on the Skyrme field which, in turn, are translated into constraints on the expansion coefficients β_{abc} and α_{bkl}. Varying a finite truncation of these expansion coefficients enables the calculation of the lowest energy configuration at fixed unit cell size L, i.e. it determines a skyrmion lattice. Carrying this out for various side lengths L and fitting a curve to the data produces an energy against length curve $E_{24}(L)$, yielding the lowest energy lattice configuration (a skyrmion crystal) at some unit cell size L_*. This is the general methodology employed when investigating the Skyrme crystal and its applications. However, the method is rather cumbersome and highly restrictive on the geometry. In particular, it only really allows for the consideration of cubic crystals on fixed period lattices, with many simulations required in order to determine the minimal energy crystalline configuration and the corresponding energy minimizing cubic lattice size L_*.

A more appealing method was presented and implemented by Baskerville [17]. This method does also rely on the period lattice being cubic and uses a Derrick scaling argument to determine the optimal unit cell size L_*. We now detail this method and use it to obtain the $SC_{1/2}$ and $BCC_{1/2}$ crystals. Consider the massless $\mathscr{L}_{24}$-model for an arbitrary field configuration $\varphi : \mathbb{T}^3 \to S^3$ with metric $g_{ij} = L^2\delta_{ij}$ on $\mathbb{T}^3$, associated to the cubic lattice $\Lambda = L\mathbb{Z}^3$. The resulting energy functional is found to be

$$\begin{aligned} E_{24}(\varphi; L) &= \int_{\mathbb{T}^3} \mathrm{d}^3x\, L^3 \left\{ \frac{1}{L^2}\delta^{ij}\partial_i\varphi^\mu\partial_j\varphi^\mu + \frac{1}{2L^4}\delta^{ik}\delta^{jl}\left(\partial_i\varphi^\mu\partial_k\varphi^\mu\partial_j\varphi^\nu\partial_l\varphi^\nu - \partial_i\varphi^\mu\partial_l\varphi^\mu\partial_k\varphi^\nu\partial_j\varphi^\nu\right)\right\} \\ &= L\int_{\mathbb{T}^3} \mathrm{d}^3x\, \left(\partial_i\varphi\cdot\partial_i\varphi\right) + \frac{1}{L}\int_{\mathbb{T}^3} \mathrm{d}^3x\, \frac{1}{2}\left[\left(\partial_i\varphi\cdot\partial_i\varphi\right)\left(\partial_j\varphi\cdot\partial_j\varphi\right) - \left(\partial_i\varphi\cdot\partial_j\varphi\right)^2\right] \\ &= LE_2^{\mathbb{T}^3} + \frac{1}{L}E_4^{\mathbb{T}^3}. \end{aligned} \tag{1.3.17}$$

Then the optimal unit cell size L_* can be computed simply as

$$\left.\frac{\mathrm{d}}{\mathrm{d}L}\right|_{L=L_*} E_{24}(\varphi; L) = 0 \quad \Rightarrow \quad L_* = \sqrt{\frac{E_4^{\mathbb{T}^3}}{E_2^{\mathbb{T}^3}}}. \tag{1.3.18}$$

The energy (1.3.17) needs to be minimized with respect to variations of the field φ, using, e.g., arrested Newton flow. During each iteration of the algorithm, the unit cell size L needs to be updated using (1.3.18). Once the algorithm finds the local minimizer, Derrick's scaling argument (or the virial constraint) will be satisfied, $E_2 = E_4$. Thus, the energy for the minimizer can be computed independently of L_* as

$$E_{24}(\varphi; L_*) = 2\sqrt{E_2^{\mathbb{T}^3}E_4^{\mathbb{T}^3}}, \tag{1.3.19}$$

provided the virial constraint is satisfied.

Now, we need initial configurations φ_0 for the algorithm. As we are finding the $SC_{1/2}$ and $BCC_{1/2}$ crystals numerically, only an approximation is needed for the initial configuration. The resulting baryon and energy density plots of the $BCC_{1/2}$ and $SC_{1/2}$ crystals are shown in Fig. 1.2 and Fig. 1.3, respectively, alongside isosurface plots of the associated Skyrme fields.

For the $BCC_{1/2}$ crystal, the Fourier coefficients β_{abc} and α_{bkl} must satisfy the conditions: h is odd, k and l are even, and a, b, c are all even [62]. For the initial configuration, we truncate the Fourier series expansion of the fields (1.3.16) to include only the first few terms, and then normalize the field, $\varphi^\mu \to \varphi^\mu/(\varphi\cdot\varphi)$. After relaxation, this yields the $BCC_{1/2}$ crystal with unit cell charge $B_{\text{cell}} = 8$ and

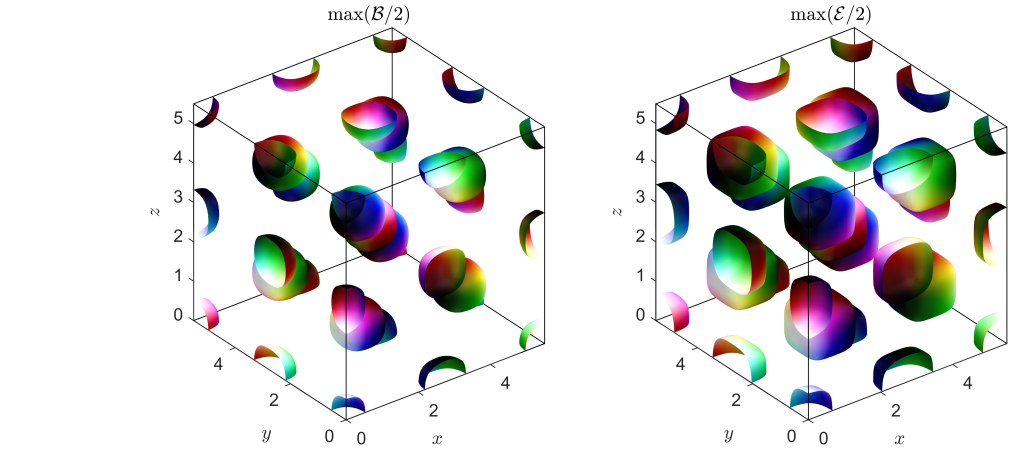

(a) Isosurface plots of the baryon density $\mathscr{B}^0$ and energy density $\mathscr{E}$.

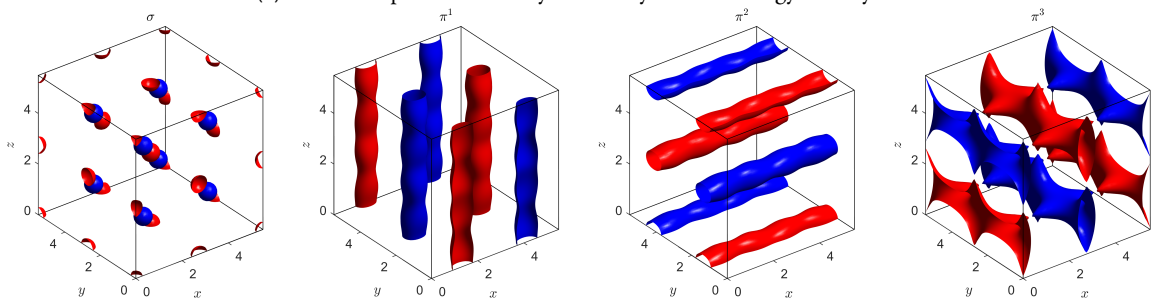

(b) Plots of the Skyrme fields $\varphi = (\sigma, \pi^1, \pi^2, \pi^3)$.

Figure 1.2: Plots of the (a) baryon density $\mathscr{B}^0$ and energy density $\mathscr{E}$ and (b) the Skyrme fields $\varphi = (\sigma, \pi^1, \pi^2, \pi^3)$ for the $\mathrm{BCC}_{1/2}$ Skyrme crystal, with unit cell charge $B_{\mathrm{cell}} = 8$.

optimal cell size $L_* = 5.50$. The crystal is also found to have energy per baryon $E/(12\pi^2 B) = 1.0856$, which is in reasonable agreement with Goldhaber and Manton's estimation of $E/(12\pi^2 B) = 1.08$ at $L_* = 5.54$ [38], and also Klebanov's calculation of $E/(12\pi^2 B) = 1.0807$.

For the $\mathrm{SC}_{1/2}$ crystal, the Fourier coefficients β_{abc} and α_{bkl} must satisfy the conditions: h and k are odd, and l is even, and a, b, c are all odd [53]. Then, truncating the Fourier series (1.3.16) to only include the first terms in the expansions yields the approximation of Castillejo *et al.* [40],

$$\sigma = -\cos\left(\frac{2\pi x^1}{L}\right)\cos\left(\frac{2\pi x^2}{L}\right)\cos\left(\frac{2\pi x^3}{L}\right), \tag{1.3.20a}$$

$$\pi^1 = \sin\left(\frac{2\pi x^1}{L}\right)\sqrt{1 - \frac{1}{2}\sin^2\left(\frac{2\pi x^2}{L}\right) - \frac{1}{2}\sin^2\left(\frac{2\pi x^3}{L}\right) + \frac{1}{3}\sin^2\left(\frac{2\pi x^2}{L}\right)\sin^2\left(\frac{2\pi x^3}{L}\right)}, \tag{1.3.20b}$$

and cyclic [63]. The optimal unit cell size is found to be $L_* = 4.61$ and has normalized energy $E/(12\pi^2 B) = 1.0378$. Kugler and Shtrikmann [39] approximated the $\mathrm{SC}_{1/2}$ crystal to have an energy excess of 3.8% above the topological energy bound, and Battye and Sutcliffe [22] compute the energy excess to be 3.6%, which are both in good agreement with our result. Baskerville [51] determined the lattice parameter to be $L_* = 4.70$ and, so, our findings are thus consistent.

Recall that the $\mathscr{L}_{24}$-Skyrme energy is invariant under the natural action of SO(4) on the target S^3, that is $E_{24}(R\varphi, g) = E_{24}(\varphi, g)$ for all $R \in \mathrm{SO}(4)$. So, the $\mathrm{SC}_{1/2}$ crystal is just one critical point of

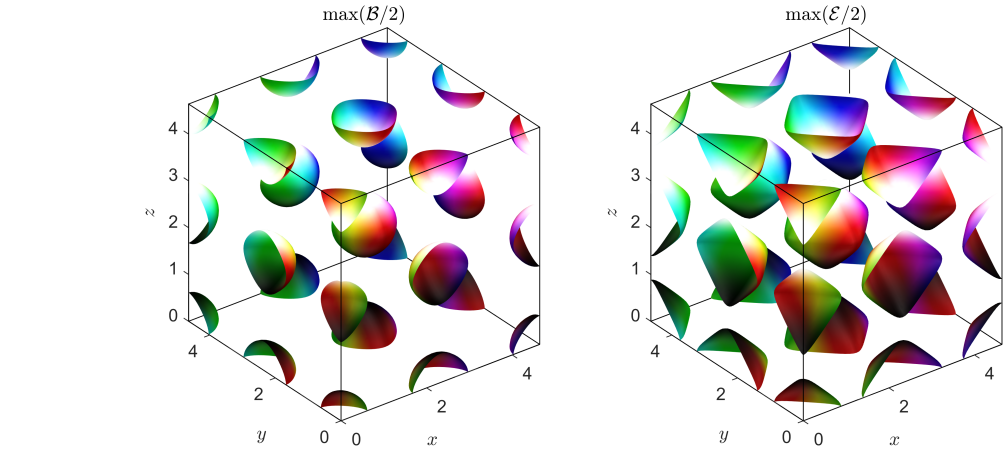

(a) Isosurface plots of the baryon density $\mathscr{B}^0$ and energy density $\mathscr{E}$.

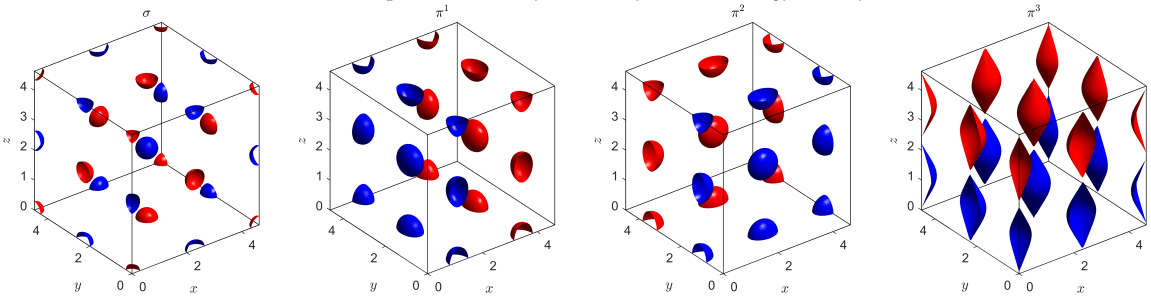

(b) Plots of the Skyrme fields $\varphi = (\sigma, \pi^1, \pi^2, \pi^3)$.

Figure 1.3: Plots of the (a) baryon density $\mathscr{B}^0$ and energy density $\mathscr{E}$ and (b) the Skyrme fields $\varphi = (\sigma, \pi^1, \pi^2, \pi^3)$ for the $SC_{1/2}$ Skyrme crystal, with unit cell charge $B_{\text{cell}} = 4$.

E_{24}, with other critical points lying on the SO(4) orbit of the $SC_{1/2}$ crystal. Speight [64] showed that the $SC_{1/2}$ crystal is indeed a skyrmion crystal, that is, it is stable with respect to variations of the metric g on $\mathbb{T}^3$. The interesting question is: what happens to the $SC_{1/2}$ crystal, and the family of crystals under the SO(4) orbit, when the pion mass is switched on? The pion mass potential (1.1.7) explicitly breaks the SO(4) symmetry to an SO(3) isospin symmetry. So, the $SC_{1/2}$ crystal will no longer enjoy the enhanced SO(4) symmetry D_4 (1.3.15), as the vacuum $\sigma = 1$ will now be penalized by the pion mass potential. Will it, and any other crystals, survive the perturbation? However, before we proceed with investigating massive (3 + 1)-dimensional skyrmion crystals, we turn our focus initially to a simpler toy model to start with: the (2 + 1)-dimensional *baby Skyrme model*.

Two

Baby Skyrmion Crystals

This chapter is based on the work in the single author paper [65].

2.1 Introduction

The baby Skyrme model [66] is a (2 + 1)-dimensional analogue of the (3 + 1)-dimensional Skyrme model, where interest in the baby Skyrme model has peaked again with the apparent prevalence of baby skyrmions in condensed matter systems [67], quantum hall systems [68, 69], chiral magnetic systems [70] and nematic liquid crystals [71]. We investigate the crystalline structure for baby skyrmions and formulate our method in terms of an arbitrary potential term. The choice of potential is crucial for baby skyrmions as it determines the behaviour of the solitons and, thus, the underlying skyrmion crystalline structure. For the first time, we propose a method to determine the surface energy contribution of a crystal chunk, once the minimal energy infinite crystal structure is determined. In order to predict the minimal energy of a charge-B crystal chunk with a fixed area, we then study isoperimetric problems for particular crystal symmetries.

For the standard baby Skyrme model [66] we find that the solitons form a hexagonal crystal structure with D_6 symmetry, which was first proposed by Hen and Karliner [72, 73]. This hexagonal crystal structure is not unique to the baby Skyrme model; it also arises in quantum hall systems [69], chiral magnetic skyrmion systems [74, 75], Ginzburg-Landau vortices [76] and (3 + 1)-dimensional skyrmions in analogy with fullerene shells in carbon chemistry [49, 50]. However, in the easy plane model [77–79] the optimal crystal structure is found to be a square lattice of half solitons, similar to that of the $SC_{1/2}$ crystal in the $\mathscr{L}_{24}$-Skyrme model. This square crystal structure also arises in chiral magnets with easy plane anisotropy [80].

This chapter is laid out as follows. We begin by discussing the general baby Skyrme model. From here, we define the initial configurations that we use to initialize our numerical minimization algorithm. Then static multi-soliton solutions are considered on the plane and a discussion of the possible global minima is presented. In Sec 2.4 we investigate the lattice structure of baby skyrmions and formulate a method to determine the minimum energy baby skyrmion crystal. Once these minimal energy infinite crystals are known, we construct a crystal slab model to numerically determine the surface energy of a crystal chunk. Finally, we study chunks of the infinite crystal in a bid to predict the classical energies of baby skyrmion crystals.

2.2 Baby Skyrme Model

The general static baby Skyrme model consists of a single scalar field $\varphi : \Sigma \to S^2$ where (Σ, g) is a 2-dimensional Riemannian manifold, and (S^2, h, ω) is the 2-sphere embedded in $\mathbb{R}^3$ with the induced flat Euclidean metric h and area 2-form ω. We will often write the baby Skyrme field as the 3-vector $\varphi = (\varphi^1, \varphi^2, \varphi^3)$. The static energy functional of this model on Σ is given by

$$E[\varphi] = \int_\Sigma \left\{ \frac{1}{2} |\mathrm{d}\varphi|^2 + \frac{\kappa^2}{2} |\varphi^* \omega|^2 + V(\varphi) \right\} \mathrm{vol}_g, \tag{2.2.1}$$

where $V : S^2 \to \mathbb{R}$ is the potential of the baby Skyrme model, $|\cdot|$ denotes the Hilbert-Schmidt norm and vol_g is the volume form on Σ associated with its metric g. The parameter κ is a standard coupling constant for which we will set $\kappa = 1$ for our numerical analysis. Note that the differential form $\mathrm{d}\varphi \in \varphi^{-1} TS^2$ is a linear map $\mathrm{d}\varphi_x : T_x\Sigma \to T_{\varphi(x)} S^2$ and so the Hilbert-Schmidt norm $|\mathrm{d}\varphi_x|$ depends on both the domain metric g and target metric h. However, the pullback of the area form $\omega \in \Omega^2(S^2)$ is $\varphi^* \omega \in \Omega^2(\Sigma)$ and so its norm only depends on the metric g.

We will follow the terminology of harmonic map theory, and Chap. 1, and refer to the first term in (2.2.1) as the Dirichlet energy, or the NLσM term. The second term is known as the Skyrme energy. It is conventional to label the three terms in (2.2.1) as E_2, E_4, and E_0 respectively, where, akin to the (3 + 1)-dimensional Skyrme model, each term is thought of as a polynomial in spatial derivatives with the subscript denoting the degree.

Let us introduce oriented local coordinates (x^1, x^2) on the domain Σ and let $\{\partial_1, \partial_2\}$ be a local basis for the tangent space $T_x\Sigma$ at $x \in \Sigma$. Then the Dirichlet energy in local coordinates is given by [81]

$$E_2 = \frac{1}{2} \int_\Sigma |\mathrm{d}\varphi|_g^2 \, \mathrm{vol}_g = \frac{1}{2} \int_\Sigma \mathrm{d}^2x \sqrt{g}\, g^{ij} \partial_j \varphi^a \partial_j \varphi^b h_{ab}, \tag{2.2.2}$$

where, as before, $\partial_i \equiv \partial/\partial x^i$. The Skyrme energy in local coordinates is

$$E_4 = \frac{\kappa^2}{2} \int_\Sigma |\varphi^* \omega|_g^2 \, \mathrm{vol}_g = \frac{\kappa^2}{4} \int_\Sigma \mathrm{d}^2x \sqrt{g}\, g^{ij} g^{kl} (\varphi^* \omega)_{ik} (\varphi^* \omega)_{jl}. \tag{2.2.3}$$

We can compute the pullback $\varphi^* \omega$ explicitly for the local frame $\{\partial_1, \partial_2\}$, that is

$$\varphi_x^* \omega(\partial_i, \partial_j) = \omega_{\varphi(x)} \left(\varphi_*(\partial_i|_x), \varphi_*(\partial_j|_x) \right) = \langle \varphi(x), \partial_i \varphi \times \partial_j \varphi \rangle_h = \varphi(x) \cdot (\partial_i \varphi \times \partial_j \varphi). \tag{2.2.4}$$

It is easy to see that $\varphi_x^* \omega(\partial_i, \partial_i) = 0$ and $\varphi_x^* \omega(\partial_i, \partial_j) = 0$ is antisymmetric, therefore, the pullback of the area 2-form ω on the 2-sphere to Σ is

$$\varphi^* \omega = \varphi \cdot \left(\partial_1 \varphi \times \partial_2 \varphi \right) \mathrm{d}x^1 \wedge \mathrm{d}x^2 \in \Omega^2(\Sigma). \tag{2.2.5}$$

If the domain Σ is compact, then the baby Skyrme map $\varphi : \Sigma \to S^2$ has an associated topological degree given by the pullback of the normalised area 2-form of the target space S^2,

$$B[\varphi] = \frac{1}{4\pi} \int_\Sigma \varphi^* \omega \in \mathbb{Z}. \tag{2.2.6}$$

In terms of the local coordinates (x^1, x^2) on Σ, the topological degree is explicitly

$$B[\varphi] = \frac{1}{4\pi}\int_\Sigma \varphi\cdot\left(\partial_1\varphi\times\partial_2\varphi\right)\,\mathrm{d}x^1\mathrm{d}x^2. \tag{2.2.7}$$

We refer to minimizers of the static energy functional E for fixed degree B as baby skyrmions. The topological degree B is also referred to as the topological charge, or just charge, which we adopt throughout. Finding baby skyrmions involves numerically solving partial differential equations. We do this using an accelerated gradient descent algorithm for second order dynamics, detailed in Sec 2.2.

In order for static (multi)soliton solutions to exist in the baby Skyrme system, we must evade Derrick's non-existence Theorem. Consider a variation $\varphi_\lambda : \Sigma\times\mathbb{R}\to S^2$ of the baby Skyrme field φ such that $\varphi_{\lambda=0}=\varphi$. This has infinitesimal generator $\partial_\lambda\varphi_\lambda|_{\lambda=0}\in\Gamma(\varphi^{-1}TS^2)$, where $\varphi^{-1}TS^2$ is the vector bundle over Σ with fibre $T_{\varphi(x)}S^2$ over $x\in\Sigma$. Explicitly, if we consider the spatial rescaling $x\mapsto e^\lambda x$, then we have a one-parameter family of maps $\varphi_\lambda=\varphi(e^\lambda x)$ such that $\varphi_{\lambda=0}=\varphi$. The rescaled static energy functional is then

$$E_\lambda = E[\varphi_\lambda] = E_2 + e^{-2\lambda}E_4 + e^{2\lambda}E_0. \tag{2.2.8}$$

If the baby Skyrme field configuration φ is a minimizer of the energy E, then we require

$$\frac{\mathrm{d}}{\mathrm{d}\lambda}\bigg|_{\lambda=0} E[\varphi_\lambda] = E_0 - E_4 = 0, \tag{2.2.9}$$

which yields the familiar virial constraint $E_4=E_0$. Unlike the $(3+1)$-dimensional Skyrme model, the potential $E_0=\int_\Sigma V(\varphi)\mathrm{vol}_g$ is necessary in the baby Skyrme model otherwise the energy $E[\varphi]$ can be lowered by spatial rescaling and thus cannot have minima. So the baby skyrmions have a preferred size determined by the ratio $\sqrt{\kappa/m}$, where m is the mass normally appearing in the potential $V(\varphi)$. There also exists a lower topological Bogomol'nyi bound on the (static) energy given by [82]

$$E \geq \pm\left(1+\kappa\langle V\rangle\right)\int_\Sigma \varphi^*\omega = 4\pi|B|\left(1+\kappa\langle V\rangle\right), \tag{2.2.10}$$

where $\langle V\rangle$ is the average value of $V:S^2\to\mathbb{R}$ on S^2.

In comparison to the NLσM, the addition of the Skyrme term stabilizes the NLσM to spatial rescalings. The addition of any term that is cubic, or more, in spatial derivatives would stabilise the model (for example, the $O(3)$ NLσM coupled to a massive vector meson [83]), however the Skyrme term is the lowest order expression that retains the second order nature of the equations of motion in terms of time derivatives.

Throughout this paper, there are three choices of the physical space Σ that we will consider. The first physical space we will consider is the plane $\Sigma=\mathbb{R}^2$. For the solitons to have finite energy, it is necessary to impose the boundary conditions

$$\lim_{|x|\to\infty}\varphi(x)\equiv\varphi_\infty = \text{constant}, \tag{2.2.11}$$

and select φ_∞ from the vacuum manifold of the model, i.e. such that $V(\varphi_\infty)=0$. Without loss of generality, we choose the vacuum $\varphi_\infty=(0,0,1)$ throughout. This gives us the one-point compactification of space $\mathbb{R}^2\cup\{\infty\}\cong S^2$. The baby Skyrme field can then be viewed as the map $\varphi:S^2\to S^2$,

which has a conserved topological charge $B \in \pi_2(S^2) = \mathbb{Z}$, characterized as the topological degree of the map and given explicitly by (2.2.7).

The second physical space we will consider is that of the 2-torus $\Sigma = \mathbb{R}^2/\Lambda$, in which our field satisfies the doubly-periodic boundary conditions $\varphi(x) = \varphi(x + n_1 X^1 + n_2 X^2)$. Here $n_1, n_2 \in \mathbb{Z}$ and $X^1, X^2 \in \mathbb{R}^2$ are a fundamental pair of periods that generate the lattice Λ. The maps $\varphi : \mathbb{R}^2/\Lambda \to S^2$ have an associated integer degree, and so admit topological solitons.

Finally, the third physical space we consider is the infinite cylinder $\Sigma = S^1 \times \mathbb{R}$. This corresponds to a Dirichlet boundary condition in the x^2-direction, $\lim_{|x^2|\to\infty} = \varphi_\infty$, and a periodic boundary condition in the x^1-direction, $\varphi(x) = \varphi(x + n_1 X^1)$, where $n_1 \in \mathbb{Z}$ and $X^1 \in \mathbb{R}^2$ is a vector in the x^1-direction. The maps $\varphi : S^1 \times \mathbb{R} \to S^2$ also have a conserved integer topological degree and admit topological solitons.

Initial Configurations

To initialize the numerical minimization procedure, the gradient descent algorithm requires an initial configuration, or approximation to the static soliton. This is carried out using polar coordinates on $\Sigma = \mathbb{R}^2$ or $\Sigma = \mathbb{R}^2/\Lambda$. Consider the axially symmetric field configuration

$$\varphi = \big(\sin f(r)\cos B\theta, \sin f(r)\sin B\theta, \cos f(r)\big), \tag{2.2.12}$$

with the monotonically decreasing radial profile function $f(r)$ satisfying $f(0) = \pi$ and $f(\infty) = 0$. Equivalently, the profile function f vanishes at the boundary of the grid. Here, r and θ are polar coordinates in the plane and there exists an internal phase that has been set to zero by applying the global symmetry that rotates the φ^1, φ^2 field components [84].

For our numerical minimization procedure, the profile function is taken to be [85]

$$f(r) = \pi \exp(-r). \tag{2.2.13}$$

The initial field configuration is a linear superposition of axially symmetric configurations; typically we use a set-up of N charge-1 skyrmions with a favourable relative phase-shift between each other (for maximal attraction). This is known as the attractive channel, and is dependent upon the choice of potential. The superposition is justified because the profile function decays exponentially. The superposition is done in the complex field formalism, i.e. where $W : S^2 \to \mathbb{C}P^1$ is the stereographic projection of the φ field of S^2. We use the profile function of a static solution (typically of topological charge one) to obtain

$$W[\varphi] = \frac{\varphi^1 + i\,\varphi^2}{1 - \varphi^3}. \tag{2.2.14}$$

Using the radial ansatz (2.2.12), this is

$$W = \tan\left(\frac{f(r)}{2}\right) e^{iB\theta}. \tag{2.2.15}$$

We can then assume that if the solitons are well separated in relation to their size, then we can approximate the resulting solution as $W = \sum_i^N W_i$, where N is the total number of solitons in the system, and $B = \sum_i^N B_i$ is the total baryon number of the system. In terms of the stereographic coordinate W, the baby Skyrme field is

$$\varphi = \left(\frac{W + \bar{W}}{1 + |W|^2}, -i\frac{(W - \bar{W})}{1 + |W|^2}, \frac{1 - |W|^2}{1 + |W|^2}\right). \tag{2.2.16}$$

Numerical Minimization Procedure

In order to find local minima of the static energy, we must numerically relax the baby Skyrme field. The numerical methods are carried out on a $N_1 \times N_2$ grid with lattice spacings $\Delta x^1, \Delta x^2$. The baby Skyrme energy is then discretised using a 4th order central finite-difference scheme. This yields a discrete approximation $E_{\text{dis}}[\varphi]$ to the static energy functional $E[\varphi]$, which we can regard as a function $E_{\text{dis}} : \mathscr{C} \to \mathbb{R}$, where the discretised configuration space is the manifold $\mathscr{C} = (S^2)^{N_1 N_2} \subset \mathbb{R}^{3 N_1 N_2}$ [86, 87].

To compute the minima of the discretised static energy, initially a gradient descent method was chosen. However, gradient descent can be particularly slow method when the Hessian is of poor condition. A more efficient way to is to simulate the time development using an accelerated gradient descent algorithm known as arrested Newton flow [88]. The essence of the algorithm is as follows: we solve Newton's equations of motion for a particle on the discretised configuration space $\mathscr{C}$ with potential energy E_{dis}. Explicitly, we are solving the system of 2nd order ODEs

$$\ddot{\varphi} = -\frac{\delta E_{\text{dis}}}{\delta \varphi}[\varphi], \quad \varphi(0) = \varphi_0, \tag{2.2.17}$$

with initial velocity $\dot{\varphi}(0) = 0$. Setting $\psi := \dot{\varphi}$ as the velocity with $\psi(0) = \dot{\varphi}(0) = 0$ reduces the problem to a coupled system of 1st order ODEs. We implement a 4th order Runge–Kutta method to solve this coupled system.

The main advantage in implementing the arrested Newton flow algorithm is that the field will naturally relax to a local minimum. After each time step $t \mapsto t + \delta t$, we check to see if the energy is increasing. If $E_{\text{dis}}(t + \delta t) > E_{\text{dis}}(t)$, we take out all the kinetic energy in the system by setting $\psi(t + \delta t) = 0$ and restart the flow. The flow then terminates when every component of the energy gradient $\frac{\delta E_{\text{dis}}}{\delta \varphi}$ is zero to within a given tolerance (we have used 10^{-4}). Unless stated otherwise, the plots shown throughout were simulated on a grid with 0.05 lattice spacings and grid sizes 1000×1000.

It is essential that we enforce the constraint $\varphi \cdot \varphi = 1$. This is normally done by including a Lagrange multiplier term into the Lagrangian, and the form for the Lagrange multiplier can be found taking the dot product of the field with the resulting Euler-Lagrange equations. However, to do this numerically we have to pull our target space back onto S^2. This is done by normalizing the Skyrme field φ each loop,

$$\varphi^a \to \frac{\varphi^a}{\sqrt{\varphi \cdot \varphi}}. \tag{2.2.18}$$

Then we need to project out the component of the energy gradient, and velocity, in the direction of Skyrme field, that is

$$\frac{\delta \mathscr{E}_{\text{dis}}}{\delta \varphi^a} \to \frac{\delta \mathscr{E}_{\text{dis}}}{\delta \varphi^a} - \left(\frac{\delta \mathscr{E}_{\text{dis}}}{\delta \varphi} \cdot \varphi \right) \frac{\varphi^a}{\varphi \cdot \varphi} \tag{2.2.19}$$

and

$$\psi^a \to \psi^a - (\psi \cdot \varphi) \frac{\varphi^a}{\varphi \cdot \varphi}. \tag{2.2.20}$$

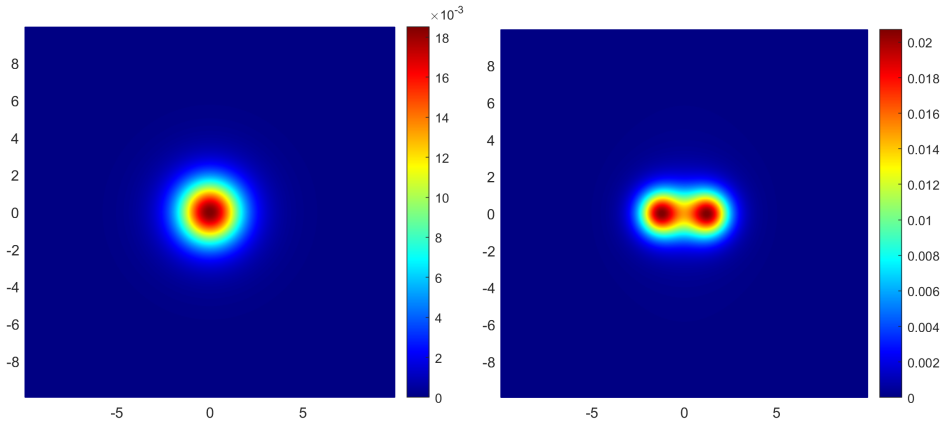

(a) Standard charge-1 energy density. (b) Easy plane charge-1 energy density.

Figure 2.1: Plots of the energy density of (a) the axially symmetric charge-1 baby skyrmion, for the standard potential $V(\varphi) = m^2(1-\varphi^3)$, and (b) the charge-1 baby skyrmion for the easy plane potential $V(\varphi) = \frac{1}{2}m^2(\varphi^1)^2$.

2.3 Baby Skyrmions on the Plane

Consider the real plane $\mathbb{R}^2$ with the usual flat Euclidean metric $g = d$, such that $g_{ij} = \delta_{ij}$. The static energy functional of the baby Skyrme model on $\mathbb{R}^2$ takes the familiar form

$$E[\varphi] = \int_{\mathbb{R}^2} \left\{ \frac{1}{2}(\partial_i\varphi)^2 + \frac{\kappa^2}{4}\left(\partial_i\varphi \times \partial_j\varphi\right)^2 + V(\varphi) \right\} \mathrm{d}^2x. \tag{2.3.1}$$

For numerical analysis, it proves convenient to express the static energy functional using Einstein's summation notation, that is

$$E[\varphi] = \int_{\mathbb{R}^2} \left\{ \frac{1}{2}\left(\partial_i\varphi^a\right)^2 + \frac{\kappa^2}{4}\left((\partial_i\varphi^a\,\partial_j\varphi^b)^2 - \partial_i\varphi^a\,\partial_j\varphi^a\,\partial_j\varphi^b\,\partial_i\varphi^b\right) + V(\varphi) \right\} \mathrm{d}^2x, \tag{2.3.2}$$

where $i, j \in \{1,2\}$ and $a, b \in \{1,2,3\}$. The energy functional has a continuous $O(3)$ symmetry before the symmetry is broken by the choice of potential term $V(\varphi)$. To carry out arrested Newton flow, or a numerical relaxation method using the gradient of the energy, we need to calculate the energy gradient explicitly. We will do this in index notation for numerical convenience. The variation of the energy density with respect to field φ^a is

$$\frac{\partial\mathscr{E}}{\partial\varphi^a} = \frac{\partial V}{\delta\varphi^a} - \left\{ \partial_{ii}\varphi^a + \kappa^2\left[\partial_{ii}\varphi^a\left(\partial_j\varphi^b\right)^2 + \partial_i\varphi^a\left(\partial_{ij}\varphi^b\,\partial_j\varphi^b - \partial_{jj}\varphi^b\,\partial_i\varphi^b\right) - \partial_{ij}\varphi^a\left(\partial_i\varphi^b\,\partial_j\varphi^b\right)\right]\right\}.$$

Standard Baby Skyrmions

Numerous potentials have been proposed [66, 77, 84, 89–93] and studied extensively in the literature. However, there are two choices of potential that we are particularly interested in: the standard potential and the easy plane potential. These two theories are quite distinct and, as we will describe below, we should expect different phenomena. In the standard baby Skyrme model

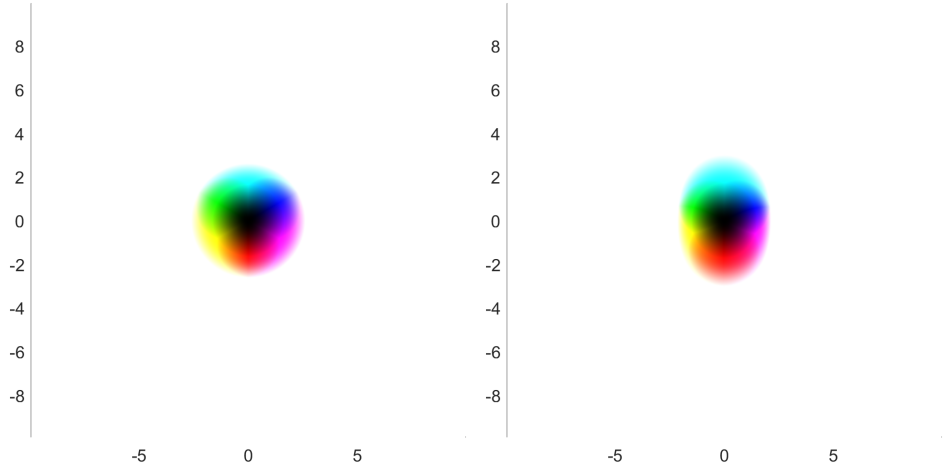

(a) Standard charge-1 coloring. (b) Easy plane charge-1 coloring.

Figure 2.2: Plots of the coloring scheme detailed in the text for (a) the axially symmetric charge-1 baby skyrmion, for the standard potential, and (b) the charge-1 baby skyrmion for the easy plane potential.

[66], the standard potential is an analogue of the pion mass term in the Skyrme model, and takes the form

$$V = m^2(1 - \varphi^3). \tag{2.3.3}$$

If we consider excitations around our unique choice of vacuum $\varphi_\infty = (0, 0, 1)$, then the fields φ^1 and φ^2 acquire a mass m. The standard potential (2.3.3) spontaneously breaks the $O(3)$ symmetry to an $O(2)$ symmetry that acts on the field components φ^1, φ^2. For this potential, the charge-1 baby skyrmion is axially symmetric and exponentially localised, see Fig. 2.1a. Piette *et al.* [66] studied the asymptotic interactions of standard baby skyrmions and found that two well-separated charge-1 solitons have an interaction energy that can be calculated using a dipole approximation, such that

$$E_{\text{standard}} \propto \cos(\chi_1 - \chi_2), \tag{2.3.4}$$

where $\chi_1 - \chi_2$ is the relative phase. The attraction between these two well-separated baby skyrmions is greatest when $\chi_1 - \chi_2 = \pi$. This is also known as the attractive channel orientation.

There is a rather nice way to graphically represent the phase of a baby skyrmion [94] using a HSV color model, which is almost analogous to the Runge color sphere coloring in the Skyrme model. We begin by plotting the energy density and color it using the stereographic coordinate W, given in (2.2.14). The phase of W, $\arg(\phi^1 + i\phi^2)$, gives the hue of the color and is defined such that $\arg(\phi^1 + i\phi^2) = 0$ is red, $\arg(\phi^1 + i\phi^2) = 2\pi/3$ is green and $\arg(\phi^1 + i\phi^2) = 4\pi/3$ is blue. We use the value of ϕ^3 to determine the lightness, such that $\phi^3 = +1$ is white and $\phi^3 = -1$ is black [95]. The coloring scheme detailed above is shown in Fig. 2.2.

For both potentials, multi-charged baby skyrmion solutions have an underlying modular structure. One such structure of interest for the standard potential (2.3.3) is that of chains of solitons. This was first investigated by Harland [96], in the context of baby skyrmions, and then later by Foster [97] and also Shnir [48]. Each chain has its ends capped by charge-2 solutions and the chain links are built from either charge-1 baby skyrmions, with a relative phase of π with each

neighbour, or charge-2 solitons. Shnir [48] showed that a chain with charge-1 links has a lower energy than a chain with charge-2 links within each homotopy class. For low charge solutions, chains appear to be good candidates for the global minima. A typical chain configuration for the standard potential (2.3.3) is displayed in Fig. 2.3a.

Foster [97] also investigated baby skyrmions on a cylinder $\mathbb{R} \times S^1$, and calculated the minimum energy per charge of an infinite chain to be $\mathscr{E}_{\text{chain}} = 1.4549$. We have carried out the same calculation using the lattice variation method detailed in Sec 2.4. This is done by imposing a Dirichlet boundary condition in the x^2-direction, $\lim_{|x^2|\to\infty} = \varphi_\infty$, and a periodic boundary condition in the x^1-direction, $\varphi(x^1, x^2) = \varphi(x^1 + n_1 L, x^2)$, where $n_1 \in \mathbb{Z}$. The periodic cell length L is then varied to minimize the energy, and a minimum energy of $\mathscr{E}_{\text{chain}} = 1.4548$ was found for a periodic cell length of $L = 8.53$. Thus, our results provide excellent fidelity.

Later, it was realised by Winyard [98] that the energy density peaks at the ends of the chains could be reduced by joining the two ends into a ring-like solution with an added energy correction for the curvature of the ring. Using a least squares fitting, they were able to obtain values for the energy contributions from the chain caps and the ring curvature. They showed that ring solutions are a better candidate for the global minima for $B > B_{\text{ring}} \in \mathbb{Z}$. For the mass $m^2 = 0.1$, this transition from chains to rings is numerically found to occur at $B_{\text{ring}} = 15$. A typical ring configuration is displayed in Fig. 2.3c.

Skyrmion crystals in the standard baby Skyrme model, with the standard potential (2.3.3), were studied by Hen and Karliner [72, 73]. Through their work they observed that the minimal energy skyrmion crystal was almost hexagonal by use of simulated annealing. So one would expect chunks of the infinite hexagonal crystal to be global minima for some $B > B_{\text{crystal}} \in \mathbb{Z}$. This prompts the basis of this chapter: at what charge do chunks of the infinite skyrmion crystal become the global minima?

Easy Plane Baby Skyrmions

The second potential of particular interest is the easy plane potential,

$$V(\varphi) = \frac{1}{2} m^2 (\varphi^1)^2, \tag{2.3.5}$$

proposed by Jäykkä and Speight [77]. As with the standard potential, the easy plane potential leaves an unbroken $O(2)$ symmetry. However, the canonical choice of vacuum $\varphi_\infty = (0, 0, 1)$ distinguishes a point on the $O(2)$ orbit and breaks the symmetry further to a discrete D_2 symmetry. Unlike the standard model, the charge-1 baby skyrmion is not axially symmetric but rather is composed of two charge-1/2 baby skyrmions. This is shown in Fig. 2.1b. As we did before, let us consider elementary excitations around our canonical choice of vacuum $\varphi_\infty = (0, 0, 1)$, then the field φ^1 acquires a mass m and the φ^2 field is massless. Adapting the dipole approximation proposed by Piette *et al.* [66], and assuming that φ^2 mediates the dominant interaction asymptotically [77], gives us an interaction energy

$$E_{\text{easy-plane}} \propto \cos(\chi_1 + \chi_2). \tag{2.3.6}$$

This shows that the interaction energy depends only on the average phase of the dipoles, which is exactly opposite of the situation in the standard model.

While the phase coloring is particularly useful for the standard potential, it is actually more instructive to use the field structure of the field component φ^1 for the easy plane model. The red

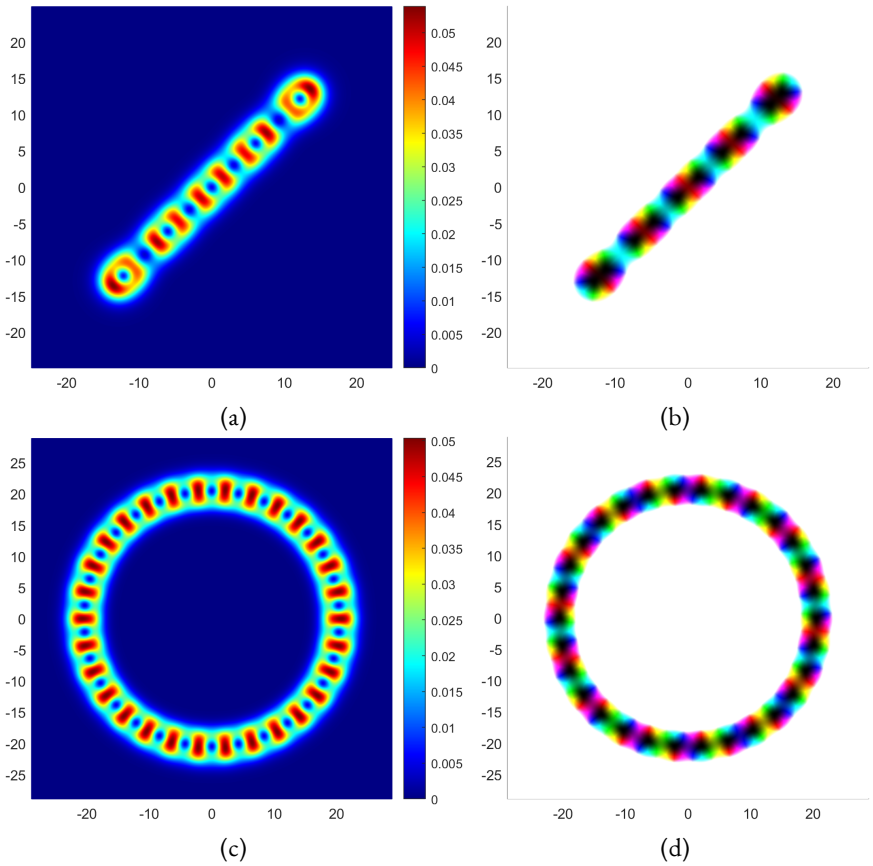

Figure 2.3: Energy density plots of (a) the charge-10 chain solution, and (c) the charge-30 ring solution. On the right hand side are the corresponding plots using the color scheme detailed in the text.

peaks and blues peaks are attracted to one another, but peaks of the same color are repelled by each other. As each individual peak in the energy density resembles a $\mathbb{C}P^1$ model lump, then we refer to each lump as a half charge lump. Each of these half lumps are located at the red and blue peaks of φ^1 and come in pairs. So more information can be gained by studying plots of the φ^1 density than the energy density itself.

In contrast to the standard model, chains do not appear to be the global minima for low charges in the easy plane model. For charges $B \leq 6$ with mass $m^2 = 1$, the global minima are $2B$-gons or ring-like solutions. Chunks of an infinite crystal with a square/rectangular crystalline structure seem to be the global minima for *almost* all charges $B > 6$. An example of such a global minimum for $B = 8$ can be seen in Fig. 2.4c. The easy plane model also exhibits a modular structure with some more exotic local minima consisting of square and polygonal building blocks. One such solution is the $B = 10$ easy plane baby skyrmion built from square and hexagonal units in Fig. 2.4e.

Although chunks of the assumed infinite crystal are prevalent, ring-like solutions and chain solutions do exist as other local minima. Jäykkä and Speight [77] showed that $2B$-gon rings are the global minima for low charges, that is a single ring of $2B$ half lumps. For higher charges, it is energetically favourable for the ring solutions to form a double ring structure with some discrete symmetry. Example solutions for the easy plane model are shown in Fig. 2.4. The charge-5 chain

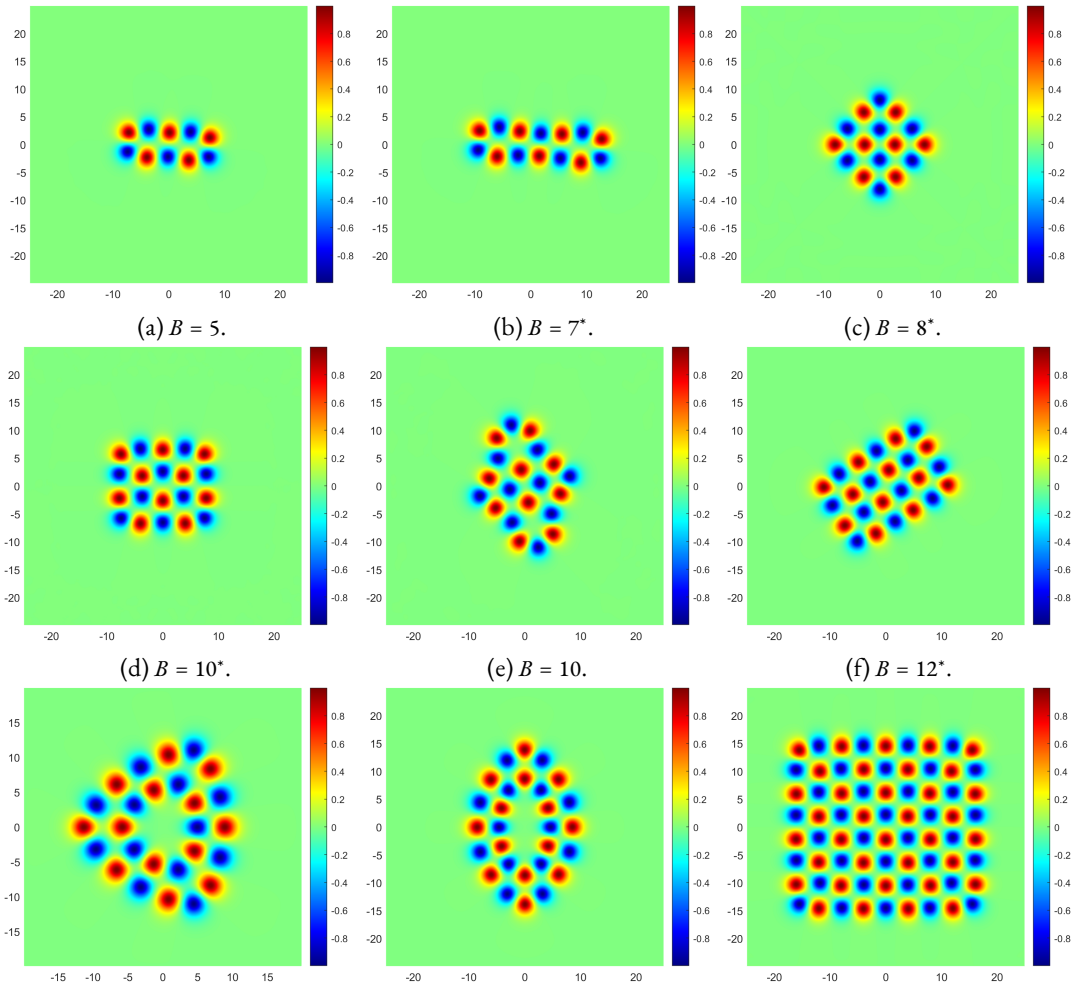

(a) $B = 5$. (b) $B = 7^*$. (c) $B = 8^*$.

(d) $B = 10^*$. (e) $B = 10$. (f) $B = 12^*$.

(g) $B = 13$. (h) $B = 14$. (i) $B = 36^*$.

Figure 2.4: φ^1 density plots of various local and global (*) energy minimizers.

in Fig. 2.4a is coincidentally a chunk of the assumed infinite skyrmion crystal and is only a local minimizer for $B = 5$, rather a 10-gon of half lumps is the global minimizer. The particularly interesting aspect of the charge-5 chain is that its shape is closer to that of a square skyrmion crystal chain than that of a double hexagon. This suggests that the square skyrmion crystal is a lower energy crystalline structure than the hexagonal skyrmion crystal.

2.4 Lattice Structure of Baby Skyrmions

In a series of papers by Hen and Karliner [72, 73], they determine the minimal energy skyrmion crystal for the standard model to be hexagonal. They scanned the parallelogram parameter space at a constant skyrmion density to find the parallelogram that minimizes the static energy. Once they found the optimal parallelogram, they then varied the skyrmion density to find the minimal energy skyrmion structure. In what follows, we refer to the shape of the lattice Λ as the lattice structure

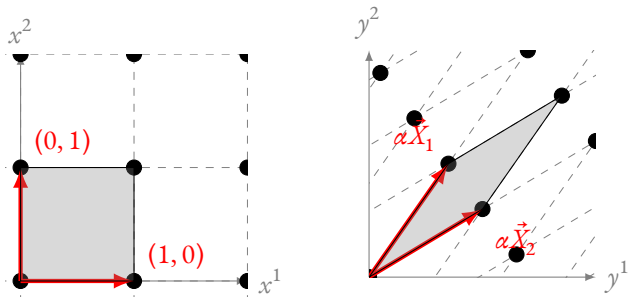

(a) $\mathbb{T}^2 = \mathbb{R}^2/\mathbb{Z}^2$ (b) $\mathbb{R}^2/\Lambda$

Figure 2.5: The (a) domain 2-torus $\mathbb{T}^2$ and (b) target 2-torus $\mathbb{R}^2/\Lambda$ for the diffeomorphism $F : \mathbb{T}^2 \to \mathbb{R}^2/\Lambda$.

and the energy minimizing skyrmion as the skyrmion crystal. Note that for an energy minimizer φ to be a skyrmion crystal it has to satisfy the extended virial constraints detailed below. We use a more robust method based on the work done by Speight [64] and propose a semi-analytic method to determine the optimal lattice structure for an arbitrary potential. We then apply this method to study skyrmion crystals in the standard model and in the easy plane model.

The physical space of interest is the 2-torus $\mathbb{R}^2/\Lambda$, where Λ is the set of all 2-dimensional period lattices

$$\Lambda = \left\{ \sum_{i=1}^{2} n_i(\alpha\vec{X}_i) \;\middle|\; n_i \in \mathbb{Z}, \alpha \in \mathbb{R}^* \right\}, \tag{2.4.1}$$

where α is a scaling parameter and $\{\vec{X}_1, \vec{X}_2\}$ is a basis for $\mathbb{R}^2$. We have written the fundamental pair of periods in the form $\vec{Y}_i = \alpha\vec{X}_i \in \mathbb{R}^2$ for later convenience, where we will introduce a constraint such that the area of the period lattice is α^2. The crystallographic restriction theorem states that there are 5 Bravais lattice types in 2-dimensions [99]. In each of these lattice types the fundamental unit cell is a certain type of a parallelogram. To find skyrmion crystals we minimize the static energy functional over all period lattices. Equivalently, we fix our domain of φ to be the unit 2-torus $\mathbb{R}^2/\mathbb{Z}^2$ and identify every other torus $\mathbb{R}^2/\Lambda$ with $\mathbb{R}^2/\mathbb{Z}^2$, but with a non-standard Riemannian metric g. This metric g on $\mathbb{R}^2/\mathbb{Z}^2$ is the pullback of the flat Euclidean metric d on $\mathbb{R}^2/\Lambda$ via the diffeomorphism $\mathbb{R}^2/\mathbb{Z}^2 \to \mathbb{R}^2/\Lambda$. As we vary the period lattice Λ then the metric g varies [64].

Now, let $F : \mathbb{T}^2 \to \mathbb{R}^2/\Lambda$ be a diffeomorphism with $F \in \mathrm{GL}^+(2,\mathbb{R})$ and $\mathbb{T}^2 = \mathbb{R}^2/\mathbb{Z}^2$, as shown in Fig. 2.5. Using the identification $\mathrm{GL}^+(2,\mathbb{R}) = \mathrm{SL}(2,\mathbb{R}) \times \mathbb{R}^*/\mathbb{Z}_2$, let $\mathscr{A} = [\vec{X}_1\ \vec{X}_2] \in \mathrm{SL}(2,\mathbb{R})$ and $\alpha \in \mathbb{R}^*$ such that $F = \alpha\mathscr{A} \in \mathrm{GL}^+(2,\mathbb{R})$. We will now identify the domain of φ as $\Sigma = \mathbb{T}^2$, so that the Skyrme field is a map $\varphi : \mathbb{T}^2 \to S^2$. The metric on $\mathbb{T}^2$ is the pullback $g = F^*d$ of the flat Euclidean metric d on $\mathbb{R}^2/\Lambda$, that is

$$g = F^*d = g_{ij}\mathrm{d}x^i\,\mathrm{d}x^j, \quad g_{ij} = \alpha^2\vec{X}_i \cdot \vec{X}_j. \tag{2.4.2}$$

The corresponding matrix representation of the inverse metric is given by

$$g^{-1} = \frac{1}{\alpha^2}\begin{bmatrix} \vec{X}_2 \cdot \vec{X}_2 & -\vec{X}_1 \cdot \vec{X}_2 \\ -\vec{X}_1 \cdot \vec{X}_2 & \vec{X}_1 \cdot \vec{X}_1 \end{bmatrix}, \tag{2.4.3}$$

and the Riemannian volume form is simply $\mathrm{vol}_g = \sqrt{\det g}\,\mathrm{d}x^1 \wedge \mathrm{d}x^2 = \alpha^2\,\mathrm{d}x^1 \wedge \mathrm{d}x^2$.

Then, using the local form for the Dirichlet term (2.2.2) and the inverse metric (2.4.3), we can compute the Dirichlet energy on $\mathbb{T}^2$ to be

$$E_2 = \frac{1}{2}\int_{\mathbb{T}^2} \mathrm{d}^2x \left\{(\vec{X}_2\cdot\vec{X}_2)(\partial_1\varphi)^2 - 2(\vec{X}_2\cdot\vec{X}_1)(\partial_1\varphi\cdot\partial_2\varphi) + (\vec{X}_1\cdot\vec{X}_1)(\partial_2\varphi)^2\right\}. \tag{2.4.4}$$

Since the Dirichlet energy is conformally invariant, it does not have a dependence on the scaling parameter α. Likewise, using the local form for the Skyrme term (2.2.3), the inverse metric (2.4.3) and the pullback of the area 2-form (2.2.5), the Skyrme energy on $\mathbb{T}^2$ is

$$E_4 = \frac{\kappa^2}{2\alpha^2}\int_{\mathbb{T}^2} \mathrm{d}^2x \left(\partial_1\varphi\times\partial_2\varphi\right)\cdot\left(\partial_1\varphi\times\partial_2\varphi\right), \tag{2.4.5}$$

and the potential energy is simply

$$E_0 = \alpha^2\int_{\mathbb{T}^2} \mathrm{d}^2x\, V(\varphi). \tag{2.4.6}$$

Putting this together, we see that the static energy functional for baby skyrmions on the unit area 2-torus $\mathbb{T}^2$ with the non-standard Riemannian metric g is

$$\begin{aligned} E = \frac{1}{2}\int_{\mathbb{T}^2} \mathrm{d}^2x \left\{\vec{X}_2^2(\partial_1\varphi)^2 - 2(\vec{X}_2\cdot\vec{X}_1)(\partial_1\varphi\cdot\partial_2\varphi) + \vec{X}_1^2(\partial_2\varphi)^2\right\} + \frac{\kappa^2}{2\alpha^2}\int_{\mathbb{T}^2} \mathrm{d}^2x \left(\partial_1\varphi\times\partial_2\varphi\right)^2 \\ + \alpha^2\int_{\mathbb{T}^2} \mathrm{d}^2x\, V(\varphi). \end{aligned} \tag{2.4.7}$$

As before, we need an explicit description of the energy gradient for our numerical analysis. The variation of the energy density with respect to field φ^a can be obtained from the Euler–Lagrange field equations, that is

$$\frac{\delta\mathscr{E}}{\delta\varphi^a} = \alpha^2\frac{\partial V}{\partial\varphi^a} - \left\{\alpha^2 g^{ij}\partial_{ij}\varphi^a + \frac{\kappa^2}{\alpha^2}\left[\partial_{ii}\varphi^a\left(\partial_j\varphi^b\right)^2 + \partial_i\varphi^a\left(\partial_{ij}\varphi^b\,\partial_j\varphi^b - \partial_{jj}\varphi^b\,\partial_i\varphi^b\right) - \partial_{ij}\varphi^a\left(\partial_i\varphi^b\,\partial_j\varphi^b\right)\right]\right\},$$

where $i,j\in\{1,2\}$ and $a,b\in\{1,2,3\}$.

To find the optimal lattice structure, we must vary the static energy functional (2.4.7) with respect to the period lattice parameters $\vec{X}_1, \vec{X}_2$ and α. Firstly, taking the variation of the static energy functional (2.4.7) with respect to the scaling parameter α,

$$\frac{\partial E}{\partial\alpha} = \int_{\mathbb{T}^2} \mathrm{d}^2x \left\{-\frac{\kappa^2}{\alpha^3}\left(\partial_1\varphi\times\partial_2\varphi\right)^2 + 2\alpha V(\varphi)\right\} = 0,$$

yields the following relation for the scaling parameter:

$$\alpha^2 = \sqrt{\frac{\frac{\kappa^2}{2}\int_{\mathbb{T}^2}\mathrm{d}^2x\left(\partial_1\varphi\times\partial_2\varphi\right)^2}{\int_{\mathbb{T}^2}\mathrm{d}^2x\,V(\varphi)}} = \sqrt{\frac{E_4^{\mathbb{T}^2}}{E_0^{\mathbb{T}^2}}}. \tag{2.4.8}$$

Thus, the area of the period lattice is determined by the ratio of the flat Skyrme term to the flat potential term. Determining the fundamental pair of periods $\vec{X}_1, \vec{X}_2$ which minimize the

Dirichlet energy E_2 is a constrained quadratic optimization problem with the nonlinear constraint $\det\left([\vec{X}_1\ \vec{X}_2]\right) = 1$. For notational convenience, let us write

$$\mathscr{E}_{ij} = \int_{\mathbb{T}^2} \mathrm{d}^2x\ \left(\partial_i\varphi \cdot \partial_j\varphi\right). \tag{2.4.9}$$

Then the Dirichlet energy (2.4.4) can be expressed in the quadratic form

$$E_2 = \frac{1}{2}x^T\mathcal{Q}x, \quad \mathcal{Q} = \begin{bmatrix} \mathscr{E}_{22} & 0 & -\mathscr{E}_{12} & 0 \\ 0 & \mathscr{E}_{22} & 0 & -\mathscr{E}_{12} \\ -\mathscr{E}_{12} & 0 & \mathscr{E}_{11} & 0 \\ 0 & -\mathscr{E}_{12} & 0 & \mathscr{E}_{11} \end{bmatrix}, \tag{2.4.10}$$

where $x = \begin{bmatrix} \vec{X}_1 \\ \vec{X}_2 \end{bmatrix}$ is a 4-vector and $\mathcal{Q}$ is a 4×4-symmetric matrix. This constrained quadratic optimization problem can be solved by including the Lagrange term $\gamma(\det\left([\vec{X}_1\ \vec{X}_2]\right) - 1)$ into (2.4.10), where $\gamma \in \mathbb{R}^*$ is a Lagrange multiplier. This reduces the problem to an eigenvalue problem

$$\mathscr{B}x = \gamma x, \quad \mathscr{B} = \begin{bmatrix} 0 & \mathscr{E}_{12} & 0 & -\mathscr{E}_{11} \\ -\mathscr{E}_{12} & 0 & \mathscr{E}_{11} & 0 \\ 0 & \mathscr{E}_{22} & 0 & -\mathscr{E}_{12} \\ -\mathscr{E}_{22} & 0 & \mathscr{E}_{12} & 0 \end{bmatrix}. \tag{2.4.11}$$

Now, we focus on the stress tensor S of the field φ and its relation to baby skyrmion crystals. In this chapter we only briefly cover the stress tensor formulation for completeness, but in subsequent chapters we will delve more into it and exploit it in the $(3+1)$-dimensional models. By definition, for an energy minimizer $\varphi : \mathbb{R}^2/\Lambda \to S^2$ to be a skyrmion lattice, its stress tensor $S[\varphi]$ must be L^2 orthogonal to the space of parallel symmetric bilinear forms $\mathbb{E}$ (a 3-dimensional subspace of the space of sections of the rank 3 vector bundle $T^*\mathbb{R}^2/\Lambda \odot T^*\mathbb{R}^2/\Lambda$). Furthermore, if the Hessian of the skyrmion lattice is positive definite then it is a skyrmion crystal. In fact, Speight [64] showed that *every* baby Skyrme lattice is a skyrmion crystal. The stress tensor of φ is given by [90]

$$S[\varphi] = \left(\frac{1}{2}|\mathrm{d}\varphi|_d^2 - \frac{1}{2}|\varphi^*\omega|_d^2 + V(\varphi)\right)d - \varphi^*h. \tag{2.4.12}$$

Let $\mathbb{E}_0$ be the 2-dimensional space of traceless parallel symmetric bilinear forms. Then the Skyrme field φ is a skyrmion lattice if and only if $S[\varphi]$ is L^2 orthogonal to d and $\mathbb{E}_0$. This gives us the familiar virial constraint

$$\int_{\mathbb{R}^2/\Lambda}\left(-\frac{1}{2}|\varphi^*\omega|_d^2 + V(\varphi)\right)\mathrm{vol}_d = E_0 - E_4 = 0. \tag{2.4.13}$$

Let (y^1, y^2) be local orthonormal coordinates on $\mathbb{R}^2/\Lambda$ and $\varepsilon \in \mathbb{E}_0$. Then for S to be L^2 orthogonal to $\mathbb{E}_0$, we require

$$\langle S, \varepsilon\rangle_{L^2} = -\frac{1}{2}\langle\varphi^*h, \varepsilon\rangle_{L^2} = 0.$$

As $\mathbb{E}_0$ is spanned by $\varepsilon_1 = (\mathrm{d}y^1)^2 - (\mathrm{d}y^2)^2$ and $\varepsilon_2 = 2\mathrm{d}y^1\mathrm{d}y^2$, we get the following additional virial constraints

$$\int_{\mathbb{R}^2/\Lambda}\left(\left|\frac{\partial\varphi}{\partial y^1}\right|^2 - \left|\frac{\partial\varphi}{\partial y^2}\right|^2\right)\mathrm{d}y^1\mathrm{d}y^2 = 0 \tag{2.4.14}$$

and

$$\int_{\mathbb{R}^2/\Lambda} \frac{\partial \varphi}{\partial y^1} \cdot \frac{\partial \varphi}{\partial y^2} \, \mathrm{d}y^1 \mathrm{d}y^2 = 0. \tag{2.4.15}$$

These additional virial constraints state that the Skyrme map φ must be conformal on average. We have shown above that for the skyrmion lattice φ to be critical with respect to variations of the period lattice Λ, it must satisfy the extended virial constraints in each lattice cell.

The extended Derrick virial constraints (2.4.13)–(2.4.15) can be imposed as a consistency check when implementing the lattice optimisation method detailed above. For numerics, the domain manifold of interest is the 2-torus $\mathbb{T}^2 = \mathbb{R}^2/\mathbb{Z}^2$ with metric $g = F^* d$, where we previously introduced the diffeomorphism $F : \mathbb{T}^2 \to \mathbb{R}^2/\Lambda$. Recall that we used the identification $F = \alpha \mathscr{A} \in \mathrm{GL}^+(2, \mathbb{R})$ for $\alpha \in \mathbb{R}^*$ and $\mathscr{A} = [\vec{X}_1 \, \vec{X}_2] \in \mathrm{SL}(2, \mathbb{R})$. Thus, using the compact notation (2.4.9), the generalised virial constraints (2.4.14) and (2.4.15) on $\mathbb{T}^2$ are given, respectively, by

$$(\mathscr{A}_{22}^2 - \mathscr{A}_{12}^2)\mathscr{E}_{11} + (\mathscr{A}_{21}^2 - \mathscr{A}_{11}^2)\mathscr{E}_{22} + 2(\mathscr{A}_{11}\mathscr{A}_{12} - \mathscr{A}_{21}\mathscr{A}_{22})\mathscr{E}_{12} = 0 \tag{2.4.16}$$

and

$$-\mathscr{A}_{12}\mathscr{A}_{22}\mathscr{E}_{11} - \mathscr{A}_{11}\mathscr{A}_{21}\mathscr{E}_{22} + (\mathscr{A}_{11}\mathscr{A}_{22} + \mathscr{A}_{12}\mathscr{A}_{21})\mathscr{E}_{12} = 0, \tag{2.4.17}$$

where $\mathscr{A}_{ij} = (\vec{X}_j)_i$, the i^{th} component of $\vec{X}_j$, and $(\mathscr{A}_{ij}) = \mathscr{A}$.

In this section, we have shown that the problem of determining the optimal lattice structure that minimizes the baby Skyrme energy (2.4.7) amounts to solving an eigenvalue problem (2.4.11). During each iteration of our numerical minimization algorithm, we perform an accelerated gradient descent then we compute the scaling parameter α via (2.4.8) and solve the eigenvalue problem (2.4.11) to give us the pair of periods $\vec{X}_1, \vec{X}_2$. We also check that the generalised virial constraints (2.4.13), (2.4.16) and (2.4.17) are satisfied each iteration, showing that the energy minimizer $\varphi : \mathbb{R}^2/\Lambda \to S^2$ is indeed a skyrmion lattice and thus a skyrmion crystal. This determines the lattice Λ and the algorithm in turn determines the skyrmion crystal. The numerics detailed throughout this section were carried out initially on a 200×200-grid with lattice spacing $\Delta x = 0.005$, with a final higher accuracy simulation carried out on a 500×500-grid with lattice spacing $\Delta x = 0.002$. Finer meshes were tried but there were no considerable changes in the final energy. Note that the coarser 200×200-grid would be sufficient as this gives approximately the same accuracy as the numerics for the baby skyrmions on $\mathbb{R}^2$. It is also worth noting that the lattice spacings are fixed sizes on the discretised unit area 2-torus $\mathbb{T}^2$, whereas the equivalent lattice spacings on the discretised 2-torus $\mathbb{R}^2/\Lambda$ vary as the lattice Λ varies.

Standard Baby Skyrmion Crystals

Employing the lattice optimisation method detailed in Sec 2.4 for the standard potential (2.3.3) with $m^2 = 0.1$ (and κ^2=1), the optimal lattice is found to be an equianharmonic lattice with the baby skyrmions forming a hexagonal skyrmion crystal with D_6 symmetry. This is found for almost all $B = 2$ initial configurations on random initial lattice geometry (with the exception of relaxing to the infinite chain solution occasionally). Each unit cell contains a charge of $B = 2$ and has sides of equal length $L_{\text{crystal}} = 9.60$ with the angle between the two periods $\vec{X}_1, \vec{X}_2$ being $\theta = \frac{2\pi}{3}$, giving a unit cell area of $\mathcal{A} = 79.84$. We find that the skyrmion crystal has energy $\mathscr{E}_{\text{crystal}} = 1.4543$, which is lower than the infinite chain energy $\mathscr{E}_{\text{chain}} = 1.4548$. Note that when we refer to energy values, we have normalised them by the Bogomolny bound, i.e. $\mathscr{E} := E/(4\pi B)$. The hexagonal skyrmion crystal

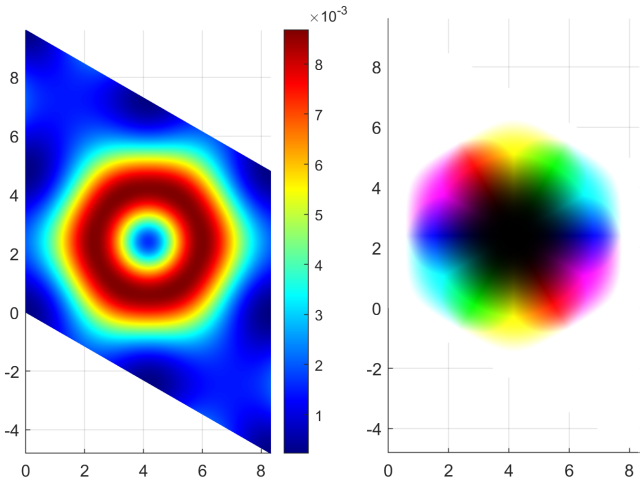

(a) Energy density. (b) Phase coloring.

Figure 2.6: Hexagonal crystalline structure of the infinite crystal in the standard model.

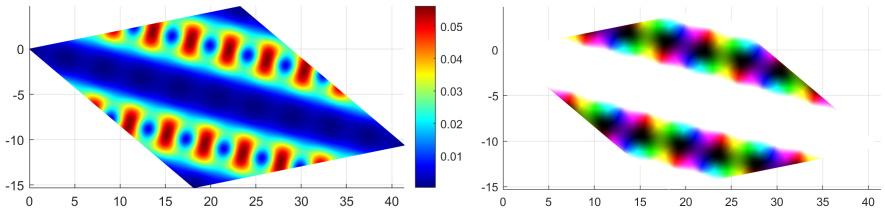

(a) Energy density. (b) Phase coloring.

Figure 2.7: Plots of the adjacent infinite chains in the attractive channel, yielding an energy lower than the infinite chain but higher than the hexagonal infinite crystal.

can be seen in Fig. 2.6. As a fidelity check with Hen and Karliner's work, we also determined the optimal lattice to be equianharmonic with a hexagonal skyrmion crystal for $m^2 = 0.1$ and $\kappa^2 = 0.03$. The energy for this crystal is found to be $\mathscr{E}_{\text{crystal}} = 1.0799$, which is in excellent agreement with their numerically determined value of $\mathscr{E}_{\text{crystal}} = 1.08$.

Other skyrmion crystals were searched for at numerous topological charges for various initial configurations and initial lattice geometry. However, they all had a tendency to relax into a chain or rows of separate chains with the infinite chain energy $\mathscr{E}_{\text{chain}} = 1.4548$. A slightly lower energy configuration was found for rows of adjacent chains with all the charge-1 links rotated by π in one chain relative to the other. This attractive chains configuration has an energy of $\mathscr{E}_{\text{2-chains}} = 1.4545$ and is shown in Fig. 2.7.

Easy Plane Baby Skyrmion Crystals

As previously proposed in Sec 2.3, it seems likely that there may possibly be a few skyrmion crystals for the easy plane model. This prompts the search for skyrmion crystals for a range of charges with various initial configurations. The lowest energy skyrmion crystal is a square of half lumps with D_4 symmetry in a square lattice for $B = 2$, with energy $\mathscr{E}_{B=2} = 1.5152$. The square lattice has sides of equal length $L_{\text{crystal}} = 8.20$, giving a unit cell area of $A = 67.24$. Two other skyrmion crystals were

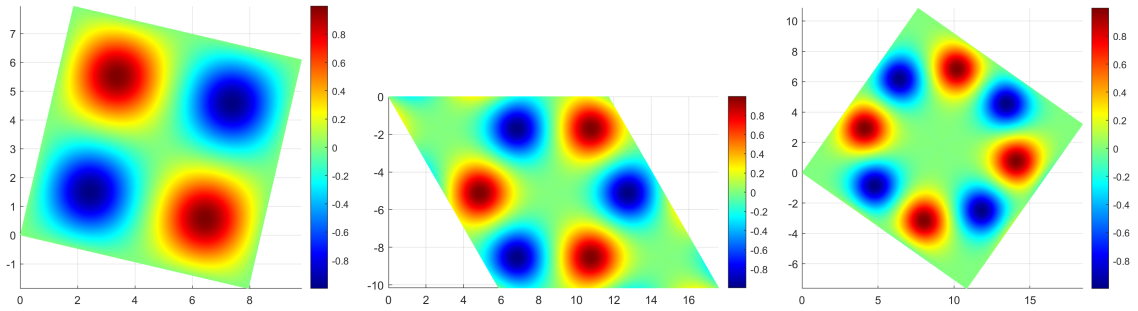

(a) $B = 2$. (b) $B = 3$. (c) $B = 4$.

Figure 2.8: φ^1 density plots of the optimal crystalline structures and their corresponding lattices. The lowest energy crystal structure is the $B = 2$ and the highest is $B = 4$.

found with slightly higher energies: a hexagonal skyrmion crystal in an equianharmonic lattice for $B = 3$ with D_6 symmetry and energy $\mathscr{E}_{B=3} = 1.5207$, and an octagonal skyrmion crystal in a square lattice with D_4 symmetry and energy $\mathscr{E}_{B=4} = 1.5228$. These three skyrmion crystals are shown in Fig. 2.8.

2.5 Baby Skyrmion Crystal Chunks

The skyrmion crystal is the ground state crystalline configuration, so one would expect chunks of the skyrmion crystal to be the global minima for charges past a critical charge B_{crystal}. A starting point would be to split the crystal chunk energy into a bulk volume, or area, term and a surface term. For a given charge B, we know the minimal energy skyrmion crystal, the corresponding lattice Λ and the lattice area. So, the bulk area term is easy to calculate. However, the problem lies in minimizing the surface energy contribution for a fixed area, which corresponds to minimizing the crystal perimeter for a fixed area. This is known as an isoperimetric problem. Even once the minimal energy crystal chunk shape has been found, we still require an estimate of the surface energy (per unit length) to determine the surface energy of the crystal chunk.

Surface Energy of a Baby Skyrmion Crystal Chunk

The surface energy per unit length of a skyrmion crystal chunk can be predicted by using a crystal slab model. Skyrmion crystals are layered on an infinite cylinder $\Sigma = \mathbb{R} \times S^1$ of width $L = L_{\text{crystal}}$, and the number of layers $n \in \mathbb{N}$ are increased to estimate the surface energy contribution. As stated in Sec 2.2, this corresponds to a Dirichlet boundary condition in the x^2-direction, $\lim_{|x^2|\to\infty} = \varphi_\infty$, and a periodic boundary condition in the x^1-direction, $\varphi(x) = \varphi(x + n_1 X^1)$. Each layer contributes a charge of 2 in this model, giving an n-layer crystal slab a total charge of $B = 2n$. The crystal slab layering can be seen in Fig. 2.9.

For the standard potential, each hexagonal baby skyrmion has 6 *bonding* sides (or nearest neighbours) and each crystal slab edge has 2 unbonded sides. Similarly, for easy plane crystal chunks, each baby skyrmion has 4 bonding sides and each crystal slab edge has 2 unbonded sides. We can express the crystal slab energy as

$$E_{\text{slab}} = E_{\text{crystal}} + N_{\text{free}} E_{\text{bond}}, \tag{2.5.1}$$

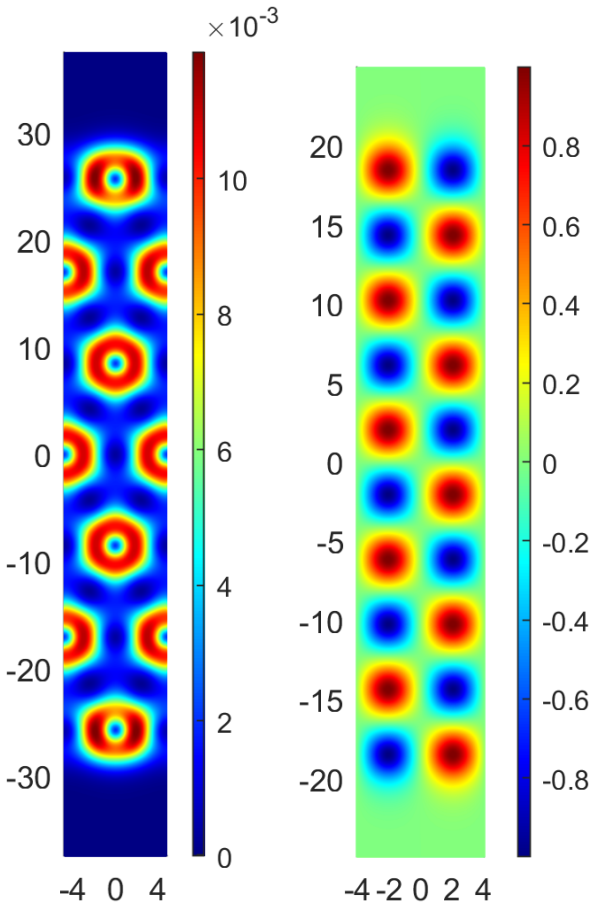

Figure 2.9: Energy density and φ^1 density plots showing a (a) 7-layer standard hexagonal crystal slab and (b) a 5-layer easy plane square crystal slab.

where N_{free} is the number of free bonds (or unbonded sides) and E_{bond} is the energy of each free bond. For the standard and easy plane crystal slabs in Fig. 2.9 we have $N_{\text{free}} = 4$. We can approximate the surface energy contribution by applying a least squares fitting to the crystal slab energy normalised by the Bogomolny bound,

$$\mathscr{E}_{\text{slab}} = \mathscr{E}_{\text{crystal}} + \frac{N_{\text{free}}}{2n}\mathscr{E}_{\text{bond}}, \tag{2.5.2}$$

where $\mathscr{E}_{\text{bond}}$ is the normalised free bond energy such that $E_{\text{bond}} = 4\pi\mathscr{E}_{\text{bond}}$. For approximating the surface energy, we computed the energies of various n-layer crystal slabs with $n \in \{3, \dots, 11\}$. Using a trust region reflective algorithm, and the crystal slab approximation (2.5.2), we find that for the standard potential $\mathscr{E}_{\text{bond}} = 0.0031$ (with $m^2 = 0.1$) and for the easy plane potential $\mathscr{E}_{\text{bond}} = 0.0103$ (with $m^2 = 1$).

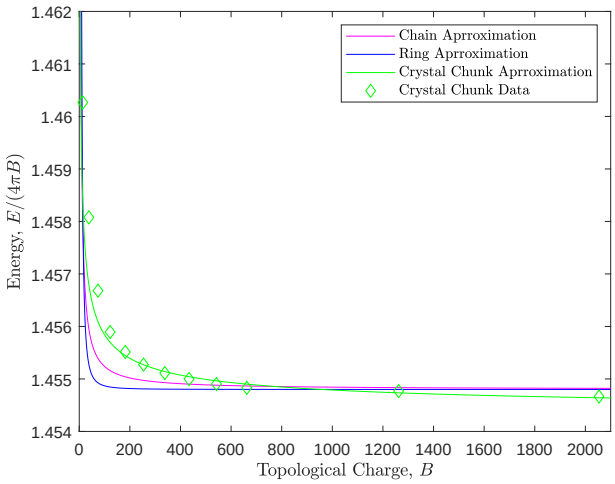

Figure 2.10: Comparison of ring, chain and crystal chunk approximations in the standard model.

Standard Crystal Chunks

To model a skyrmion crystal chunk, we split the crystal chunk energy into a bulk volume term and a surface term, $E_{\text{chunk}} = E_{\text{bulk}} + E_{\text{surface}}$. The surface energy contribution of a baby Skyrme crystal is determined by the number of unbonded sides. As stated before, for the standard potential, each hexagonal baby skyrmion has 6 *bonding* sides (or nearest neighbours) which means there are many possible arrangements for crystal chunks for a given charge B. For easy plane crystal chunks, the square lattice is the minimal energy crystal configuration so we only consider each easy plane baby skyrmion to have 4 bonding sides. Our aim is to determine the shape of an equilibrium crystal by minimizing the total surface energy associated to the crystal-vacuum interface. In crystallography one normally employs the Wulff construction method to determine the equilibrium shape of a crystal chunk. However, we take a simpler approach and only consider the perimeter of the crystal chunk boundary, not its shape. Equivalently, we are considering the number of free bonds in a given crystal chunk. This enables us to write the energy in the form

$$E_{\text{chunk}} = E_{\text{bulk}} + N_{\text{free}} E_{\text{bond}}. \tag{2.5.3}$$

Therefore, we want to find the crystal chunk that minimizes the number of free bonds, and hence its surface energy contribution, for a fixed charge B and crystal area A.

The infinite standard crystal has a discrete D_6 symmetry, so we propose that minimal energy chunks of the infinite crystal take the form of layered hexagonal solitons, as can be seen in Fig. 2.11. The number of charge-2 units in each layer is precisely $6n$. As we consider each charge-2 baby Skyrme unit to have 6 bonding sides, we can determine the number of free bonds in an n-layer crystal chunk to be $N_{\text{free}} = (12n + 6)$. This accounts for the 2 free bonds on each outer charge-2 soliton plus the additional free bond at each vertex of the crystal chunk. The total charge of a crystal chunk is $B = 2(3(n + 1)n + 1)$, such that

$$n = \frac{1}{6}\left(\sqrt{6B - 3} - 3\right). \tag{2.5.4}$$

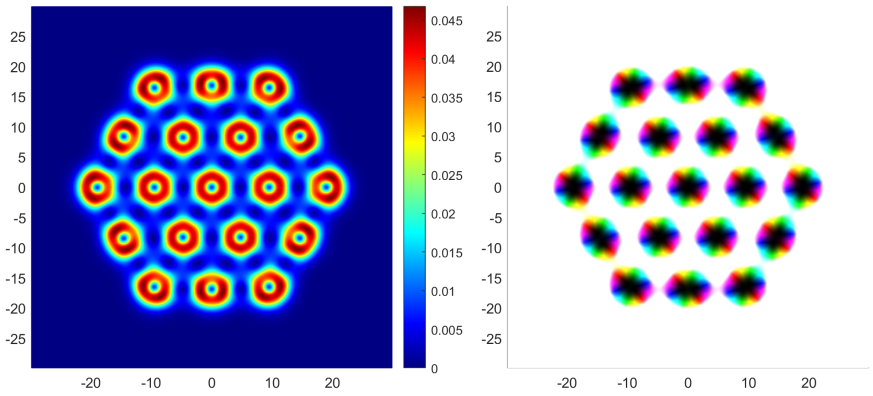

(a) $n = 2, B = 38$. (b) $B = 38$ coloring.

Figure 2.11: Energy density plot of a crystal chunk solution in the standard model and its corresponding coloring on the right hand side.

Thus, we can approximate the normalised energy of a hexagonal standard baby skyrmion crystal chunk to be given by

$$\mathscr{E}_{\text{chunk}} = \mathscr{E}_{\text{crystal}} + \frac{N_{\text{free}}}{B}\mathscr{E}_{\text{bond}} = \mathscr{E}_{\text{crystal}} + \frac{2\sqrt{6B-3}}{B}\mathscr{E}_{\text{bond}}. \tag{2.5.5}$$

To determine the transition charge B_{crystal} where chunks of the infinite skyrmion crystal become the global minima, we need to compare the crystal chunk model (2.5.5) to chain and ring models. Using the models proposed by Winyard [98], and our numerically determined value for the infinite chain, we are able to approximate ring and chain solutions. The results are plotted in Fig. 2.10, which includes data points from crystal chunk solutions for numerous charges B up to $B = 2054$. It can be observed that the crystal chunk approximation (2.5.5) fits the data very well. We find that crystal chunk solutions become global minima for charges $B > B_{\text{crystal}} = 954$. An energy density plot of the $B = 38$ skyrmion crystal chunk solution is shown in Fig. 2.11. Most of the crystal chunks were found numerically on grids with lattice spacing 0.05, with grid sizes ranging from 800×800 to 2400×2400. Crystal chunk solutions for $B = 1262$ and $B = 2054$ were obtained on grids with lattice spacing 0.1 and grid sizes 3000×3000 and 3800×3800, respectively.

Easy Plane Crystal Chunks

To predict the energy of an easy plane crystal chunk is somewhat more challenging. There exists three skyrmion crystals, all relatively close in energy with one other. For charges B such that $\sqrt{2B} \in \mathbb{Z}$, the minimal energy crystal chunk is the minimal perimeter $\sqrt{2B} \times \sqrt{2B}$-square of half lumps. For non-square $2B$, it becomes exceedingly difficult to predict the global minima. This is because there exists a smörgåsbord of local minima for a given charge, which increases with the charge number.

Nevertheless, some progress can be made if we consider rectangular crystal chunks built from the square skyrmion crystal. In the first instance, if $2B$ has factors other than 2 and B, say $a \in \mathbb{Z}$ and $2B/a \in \mathbb{Z}$, then the (local) minimal energy crystal chunk will be an $a \times 2B/a$-rectangle of half lumps such that the sum $a + 2B/a$ is minimal with respect to the other pairs of possible factors. We ignore the trivial factors $2B$ and 1 as the $2B \times 1$-chain is most likely *not* a local minimizer for the easy plane

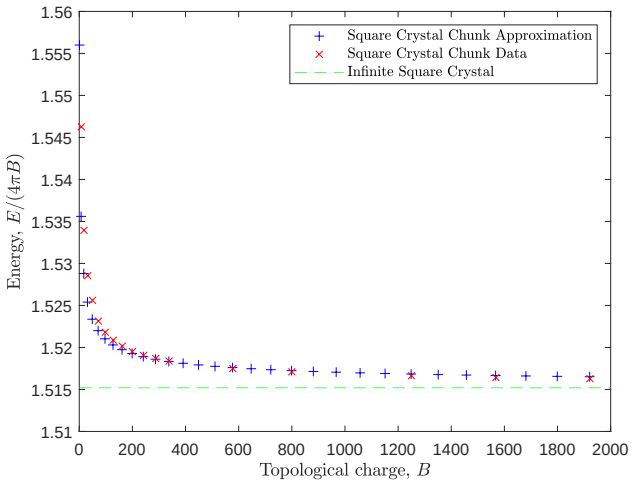

Figure 2.12: Comparison of approximate and true square crystal chunks in the easy plane model.

model. Random initial configurations do not relax to a single linear chain, unlike the standard model. Even starting with a single chain initial configuration in attractive channel orientations does not result in a relaxed final state of a single chain, it normally relaxes to the double chain. To find the pair of factors with minimum sum, one would find the factor $a \in \mathbb{Z}$ of $2B$ that minimizes the perimeter function $f(a) = 2(a + 2B/a)$.

Using the above information, we are able estimate the energy of a crystal chunk for a given charge B. Similar to the standard model, we split the crystal chunk energy into a bulk term and a surface term. For charges B, we need to determine the pair $(a, 2B/a)$ of minimal sum factors of $2B$. Then we can calculate the surface energy and determining the bulk energy is straightforward. Explicitly, the normalised energy for a charge-B crystal chunk is given by

$$\mathscr{E}_{\text{chunk}} = \mathscr{E}_{B=2} + \frac{N_{\text{free}}}{B}\mathscr{E}_{\text{bond}} = \mathscr{E}_{B=2} + 2\left(a + \frac{2B}{a}\right)\frac{\mathscr{E}_{\text{bond}}}{B}. \tag{2.5.6}$$

This approximation for square crystal chunks ($2B = a^2$) is plotted in Fig. 2.12, alongside the corresponding true numerically determined (normalised) energies.

Clearly, the further a deviates from $\sqrt{2B}$ the higher the surface energy contribution. So one would expect there to be normalised energy bands at high charges for this rectangular approximation. These bands can be determined in the limit $B \to \infty$, and for such highly rectangular pairs $(a, 2B/a)$ the bands in the limit $B \to \infty$ are given by

$$\mathscr{E}_{\text{bands}} = \mathscr{E}_{B=2} + \frac{4}{a}\mathscr{E}_{\text{bond}}. \tag{2.5.7}$$

Since there are three skyrmion crystals, there are obviously better crystal chunk solutions for highly rectangular factors (a, b). As an example, lets consider local minima for the charge-13 easy plane soliton. There are three solutions that one might expect to be contenders for the crystal chunk for this charge. Firstly, the natural choice is the minimal perimeter rectangle, which will be a double chain, or simply a 2×13-rectangle of half lumps. This is depicted in Fig. 2.13a. The next

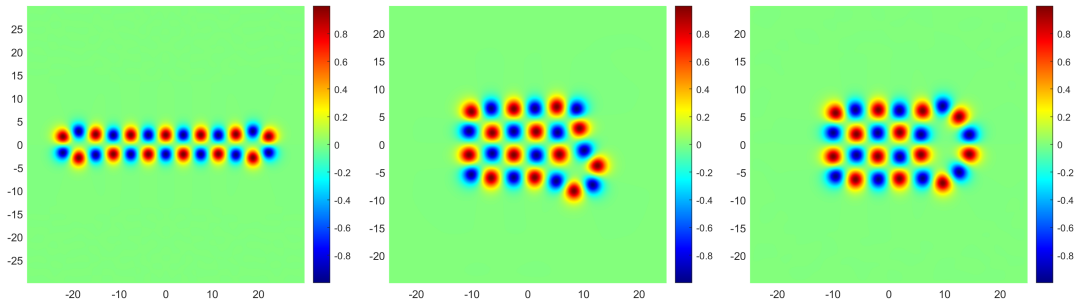

(a) $\mathscr{E} = 1.5411$. (b) $\mathscr{E} = 1.5395^*$. (c) $\mathscr{E} = 1.5407$.

Figure 2.13: φ^1 density plots of the three candidates for the crystal chunk solution for a $B = 13$ easy plane baby skyrmion. The asterisk (*) indicates the global minimum.

idea is to consider the minimal perimeter rectangle of half lumps for a $B-1 = 12$ crystal chunk, then add a half lump pair to one of its corners to create a defect. This results in a 6×4-rectangular crystal chunk with one distorted hexagonal corner, as shown in Fig. 2.13b. The third contender is akin to the corner cutting method used in the Skyrme model [28, 43], in which we try to remove half lumps (one blue and one red) from two corners of the minimal perimeter 7×4-rectangular $B = 14$ crystal chunk. This does not have the intended effect of missing half lumps on corners, rather it pulls the rest of the row, and the adjacent row, away from the chunk to form an arc with two half lumps more than the half lump height of the rectangular chunk. This can be seen in Fig. 2.13c. Out of these three most likely crystal chunk candidates for a charge-13 soliton, the rectangular crystal chunk with one distorted hexagonal corner is the minimal energy solution.

So for a charge-13 baby skyrmion the minimal perimeter rectangle model fails as a candidate for the global minimal energy crystal chunk in the easy plane model. So even at charge-13 we have already found a lower energy crystal arrangement than the rectangular crystal chunk. One would expect that adding hexagonal/octagonal defects to nearly square crystal chunks would result in lower energy solutions than rectangular crystal chunks. However, for square crystal chunks, such that $B \in \sqrt{2B}$, the rectangular crystal chunk model (2.5.6) is an excellent approximation.

In brief, we conjecture that the prevalent minimal energy crystal chunks for the easy plane model are squares of half lumps if $\sqrt{2B} \in \mathbb{Z}$, otherwise they are minimal perimeter rectangles of half lumps, with some crystal chunks having distorted hexagonal defects. We have also proposed an empirical model to determine the energy for a given square/rectangular crystal chunk.

2.6 Concluding Remarks

In this chapter, we have presented a method to determine skyrmion crystals on an optimised lattice for arbitrary potentials in the baby Skyrme model. Once the minimal energy skyrmion crystal is known, the solitons can be layered by use of a crystal slab model and the surface energy per unit length obtained numerically. Using insight obtained from the skyrmion crystal and the surface energy, chunks of the skyrmion crystal can be constructed and their corresponding energies determined.

For the standard potential, we have demonstrated that the global minimum energy skyrmion crystal exhibits a clear hexagonal D_6 symmetry. This hexagonal skyrmion crystal has a lower nor-

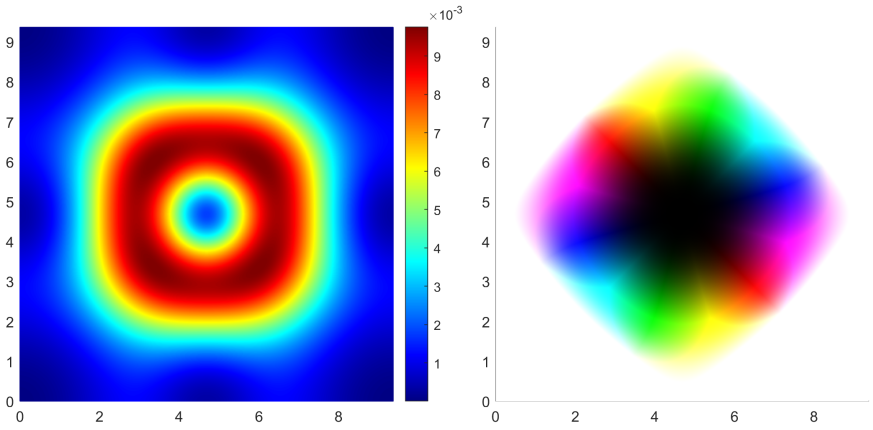

(a) Energy density. (b) Phase coloring.

Figure 2.14: Plots of the (a) energy density and (b) phase coloring for the (2 + 1)-dimensional square lattice

malised energy than the infinite chain solution proposed by Foster [97]. We propose that the global minima are layered hexagonal crystals for $B > 954$ with $m^2 = 0.1$.

We determined that rows of adjacent infinite chains in attractive orientations have normalised energies close to that of the the infinite hexagonal crystal. So it is quite possible that concentric ring solutions in attractive orientations could be the global minima for charges B with $B_{\text{ring}} < B < B_{\text{crystal}}$, this would need to be investigated. Likewise, Winyward [98] showed that chain solutions could also intersect to form junctions, and proposed that networks of standard baby skyrmions could be the global minima between rings and crystal chunks. This too would need to be studied.

Solitons in the easy plane model take the form of configurations of half lumps. This model has three skyrmion crystals all relatively close in energy: square, hexagonal and octagonal. Of these, the square skyrmion crystal of half lumps is the global minimum. This is more reminiscent of the three dimensional Skyrme system and, in a manner of respect, a better analogue. The easy plane model exhibits a plethora of local minima with various different types of symmetries. We conjecture that, when $2B$ is a perfect square, square crystal chunks are the global minima. For rectangular $2B$, the minimal energy crystal chunks are, as close to square as possible, rectangular crystal chunks of half lumps with some chunks having hexagonal surface defects. The study of internal anomalies has not been carried out, so it is possible that the inclusion of a defect into the bulk is more energetically favourable over a surface defect.

The obvious extension of the work detailed in this chapter is to the (3 + 1)-dimensional Skyrme model. However, there is no direct natural extension of the semi-analytic method developed here, as the NLσM term is not conformally invariant in three dimensions. So, perhaps an alternative numerical method is required. In the (3 + 1)-dimensional model, the crystal structure has been studied extensively in the literature and a review is detailed in the previous chapter, Chap. 1. Recall that all the lattice variations that have been studied were for a cubic lattice of side length L, in which only L is varied. In this case, the conjectured ground state skyrmion crystal is the cubic arrangement of half skyrmions, that is, the $\text{SC}_{1/2}$ crystal [39].

Now consider the standard pion mass analogue potential (2.3.3), if we allow our two dimensional baby skyrmion lattice to only vary over all *square* lattices then we get the analogue structure of the three dimensional cubic $\text{SC}_{1/2}$ crystal. The resulting square skyrmion lattice of half baby

skyrmions is shown in Fig. 2.14. Considering only scalings of cubic lattices is highly restrictive in three dimensions as there exists fourteen types of Bravais lattices, in each of which the fundamental unit cell is a certain type of parallelepiped. So one would need to vary over all 3-tori, or equivalently vary the metric on the fixed unit 3-torus $\mathbb{T}^3$. It is believed that the $\mathrm{SC}_{1/2}$ skyrmion crystal is indeed the ground state skyrmion crystal. However, if the $(3+1)$-dimensional Skyrme model and the $(2+1)$-dimensional baby Skyrme model truly are analogous, it is possible that a hexagonal skyrmion configuration could prevail (or even an entirely different crystalline structure).

Three

Skyrmion Crystals with Massive Pions

This chapter is an extension of the work presented in the joint paper with D. Harland and M. Speight [100].

3.1 Introduction

In this chapter, we study $\mathscr{L}_{024}$-Skyrme crystals and minimize the energy with respect to variations of *both* the Skyrme field $\varphi : \mathbb{R}^3/\Lambda \to \mathrm{SU}(2)$ and the period lattice Λ. This is achieved through the correspondence between all 3-tori $\mathbb{R}^3/\Lambda$ and the fixed 3-torus $\mathbb{T}^3 = S^1 \times S^1 \times S^1 = \mathbb{R}^3/\mathbb{Z}^3$, where $\mathbb{R}^3/\Lambda$ is equipped with the standard Euclidean metric d and the metric g on $\mathbb{T}^3$ is the pullback of d via the diffeomorphism $\mathbb{T}^3 \to \mathbb{R}^3/\Lambda$. Varying over all period lattices Λ is then equivalent to varying over all flat metrics g on the fixed torus $\mathbb{T}^3$. This approach was introduced by Speight [64], in which the interpretation of the gradient of the energy with respect to the metric g as the stress tensor of the field was repeatedly exploited. We will utilize this exploitation but also identify g with the constant symmetric positive definite matrix (g_{ij}) representing it with respect to the canonical coordinate system on $\mathbb{T}^3$.

So, the numerical task we set ourselves is, for fixed topological degree $B = B_{\mathrm{cell}}$ per unit cell, to minimize $E(\varphi, g)$ among all degree B maps $\varphi : \mathbb{T}^3 \to \mathrm{SU}(2)$ and flat metrics g on $\mathbb{T}^3$. It is known that, for fixed g, the function $\varphi \mapsto E(\varphi, g)$ attains a minimum (in a function space of rather low regularity) [101]. The complementary problem of minimizing in g for fixed φ was first studied in [64] and numerically implemented in [65, 102]. In [64] it was shown that in the baby Skyrme model, any critical metric g is automatically a local minimum of E. The problem of extending this result to the Skyrme model was discussed, but unfortunately the proof used in two dimensions did not generalise. Further, the existence of critical metrics was not addressed in [64].

We define Skyrme lattices and Skyrme crystals using the definitions laid out by Speight [64] and determine the necessary requirements for an energy minimizer to be a crystal and/or lattice. In the context of the baby Skyrme model, Speight [64] showed that all Skyrme lattices are Skyrme crystals. We take this further and do so in the full generalized $\mathscr{L}_{0246}$-Skyrme model.

In the present chapter we obtain a much stronger result. We show in Corollary 13 that, for fixed φ satisfying very mild assumptions, there is a unique flat metric with respect to which $E(\varphi, g)$ is minimal, and hence a unique period lattice Λ (up to automorphism) with respect to which φ has minimal energy per unit cell. In the $\mathscr{L}_{24}$-model, we can even write down this metric explicitly. In the (more interesting) massive $\mathscr{L}_{024}$- and $\mathscr{L}_{0246}$-models, we can resort to a gradient based numerical minimization scheme to find g. Applying a similar scheme to minimize over $\varphi : \mathbb{T}^3 \to \mathrm{SU}(2)$ in

tandem, we can find the energetically optimal field and period lattice for a given B, without ever imposing any symmetry assumptions on the lattice.

The results reveal that, for $m_\pi > 0$, the energetically optimal lattice (with $B = 4$ per unit cell) does *not* have cubic symmetry. In fact there are two crystal solutions with trigonal period lattices (orthorhombic with side lengths $L_1 = L_2 \neq L_3$) which have lower energy than the lowest strictly cubic lattice. This fact persists if, instead of minimizing over all flat g, we minimize only over the subset of metrics with fixed total volume. This is equivalent to minimizing under the constraint of fixed average baryon density, a problem of phenomenological interest in determining equations of state for neutron stars [46]. We will explore this application in the next chapter. As might be expected, the energy difference between the trigonal and cubic lattices becomes negligible as baryon density grows very large, but is significant at lower densities.

This chapter is structured as follows. In section 3.2, we formulate the model mathematically, considering in detail how its energy functional depends on the metric on physical space. In particular, we consider the first variation of the static energy functional with respect to the metric. This allows us to introduce the stress-energy tensor, which lies at the core of our numerical method. In section 3.3, we prove existence and uniqueness of an energy minimizing metric g for any given fixed field. In section 3.4 we describe our numerical scheme in detail, while section 3.5 presents the results of this scheme. In section 3.6 we determine minimal energy crystals under the constraint of fixed baryon density. Finally, section 3.7 presents some concluding remarks.

The main mathematical problem that this chapter addresses is to minimize $E(\varphi, g)$, with respect to both φ and g, among all fields of fixed degree B and all metrics $g \in \mathrm{SPD}_3$.

3.2 Mathematical Formulation of the Generalized Skyrme Model

Recall that the general static $\mathscr{L}_{0246}$-Skyrme model we are interested in consists of a single scalar field $\varphi : \mathbb{T}^3 \to \mathrm{SU}(2)$ where $\mathbb{T}^3$ is the unit 3-torus $\mathbb{T}^3 = \mathbb{R}^3/\mathbb{Z}^3$ with Riemannian metric g, and $(\mathrm{SU}(2), h)$ a compact simple Lie group with the canonical bi-invariant metric $h(X, Y) = \frac{1}{2}\operatorname{Tr}(X^\dagger Y)$. We denote the Lie algebra of SU(2) by $\mathfrak{su}(2)$. Let us introduce oriented local coordinates (x^1, x^2, x^3) on the domain $\mathbb{T}^3$ and let $\{\partial_1, \partial_2, \partial_3\}$ be a local basis for the tangent space $T_x\mathbb{T}^3$ at $x \in \mathbb{T}^3$.

Let

$$\varphi^{-1}T\,\mathrm{SU}(2) = \{(x, v) \in \mathbb{T}^3 \times T\,\mathrm{SU}(2) : \varphi(x) = \pi(v)\} \tag{3.2.1}$$

be the vector bundle with base space $\mathbb{T}^3$ induced by the field φ from the tangent bundle $\pi : T\,\mathrm{SU}(2) \to \mathrm{SU}(2)$. We have a vector bundle morphism with the commutative diagram

$$\begin{array}{ccc} \varphi^{-1}T\,\mathrm{SU}(2) & \xrightarrow{p_2} & T\,\mathrm{SU}(2) \\ {\scriptstyle p_1}\downarrow & & \downarrow{\scriptstyle \pi} \\ \mathbb{T}^3 & \xrightarrow[\varphi]{} & \mathrm{SU}(2) \end{array} . \tag{3.2.2}$$

Let $\mathrm{d} : \Omega^p(\mathbb{T}^3) \to \Omega^{p+1}(\mathbb{T}^3)$ be the exterior derivative. Then the differential $\mathrm{d}\varphi_x : T_x\mathbb{T}^3 \to T_{\varphi(x)}\,\mathrm{SU}(2)$ is a linear map for each $x \in \mathbb{T}^3$, and can be interpreted as an element of the vector space $T_x^*\mathbb{T}^3 \otimes T_{\varphi(x)}\,\mathrm{SU}(2)$. Thus we obtain a section $\mathrm{d}\varphi$ of the bundle $\bigwedge^1(\varphi^{-1}T\,\mathrm{SU}(2)) = T^*\mathbb{T}^3 \otimes T\,\mathrm{SU}(2) \to \mathbb{T}^3$. The Hilbert–Schmidt norm $|\cdot|$ on $T_x^*\mathbb{T}^3 \otimes T_{\varphi(x)}\,\mathrm{SU}(2)$ of the differential $\mathrm{d}\varphi_x : T_x\mathbb{T}^3 \to T_{\varphi(x)}\,\mathrm{SU}(2)$

at $x \in \mathbb{T}^3$ is defined by [81]

$$|\mathrm{d}\varphi_x|_g^2 = \mathrm{Tr}_g(\varphi^* h) = g^{ij} h_\varphi \left(\mathrm{d}\varphi_x(\partial_i), \mathrm{d}\varphi_x(\partial_j)\right), \tag{3.2.3}$$

where $\varphi^* h$ is known as the first fundamental form of φ on $\mathbb{T}^3$ [103]. The trace of a bilinear form X on $\mathbb{T}^3$ with respect to a metric g on $\mathbb{T}^3$ is defined by $\mathrm{Tr}_g(X) = \mathrm{Tr}\left(\sharp_g X\right) = g^{ij} X_{ij}$, where we define the sharp musical isomorphism on $\mathbb{T}^3$ induced by the metric g by $\sharp_g : \Omega^1(\mathbb{T}^3) \to T\mathbb{T}^3$.

As before, let $\Omega \in \Omega^2(\mathrm{SU}(2)) \otimes \mathfrak{su}(2)$ be an $\mathfrak{su}(2)$-valued two-form on $\mathrm{SU}(2)$, defined below, and $\omega \in \Omega^1(\mathrm{SU}(2)) \otimes \mathfrak{su}(2)$ be the left Maurer-Cartan form (an $\mathfrak{su}(2)$-valued one-form on $\mathrm{SU}(2)$). Then, for any left invariant vector fields $X, Y \in T_{\varphi(x)}\,\mathrm{SU}(2)$, where $x \in \mathbb{T}^3$, we define

$$\Omega(X, Y) = [\omega(X), \omega(Y)]\,. \tag{3.2.4}$$

We have the $\mathrm{Ad}(\mathrm{SU}(2))$ invariant inner product on the Lie algebra $\mathfrak{su}(2)$ given by

$$h_{\mathrm{Id}_2}(X, Y) = \frac{1}{2}\,\mathrm{Tr}\left(X^\dagger Y\right), \quad X, Y \in \mathfrak{su}(2). \tag{3.2.5}$$

For notational convenience we will write $h(X, Y) = h_{\mathrm{Id}_2}(X, Y)$. Consider the action of $\mathrm{SU}(2)$ on itself by left translation,

$$\begin{aligned} L : \mathrm{SU}(2) \times \mathrm{SU}(2) &\to \mathrm{SU}(2) \\ (\varphi, \mu) &\mapsto L_\varphi(\mu) = \varphi\mu. \end{aligned} \tag{3.2.6}$$

This induces a map of the tangent bundle to itself $(L_\varphi)_* : T_\mu\,\mathrm{SU}(2) \to T_{\varphi\mu}\,\mathrm{SU}(2)$. The left Maurer-Cartan form ω is defined on vectors $X \in T_\varphi\,\mathrm{SU}(2)$ by

$$\omega_\varphi(X) = (L_{\varphi^{-1}})_* X \in \mathfrak{su}(2). \tag{3.2.7}$$

Consider a curve $\gamma : (-\epsilon, \epsilon) \to \mathrm{SU}(2)$ through $\varphi \in \mathrm{SU}(2)$ with tangent vector $X \in T_\varphi\,\mathrm{SU}(2)$ defined by $\gamma(t) = \varphi + tX + O(t^2)$. Then $L_{\varphi^{-1}}(\gamma)$ is a curve through Id_2 with tangent vector $\varphi^{-1}X$. Thus, for $\mathrm{SU}(2)$, L_φ is a linear operation so $(L_\varphi)_* = L_\varphi$ and hence

$$\omega_\varphi(X) = L_{\varphi^{-1}}(X) = \varphi^{-1}X. \tag{3.2.8}$$

Now we can use this action to identify the inner product at $\varphi \in \mathrm{SU}(2)$ with the inner product at the identity Id_2,

$$h_\varphi(X, Y) = h_{L_{\varphi^{-1}}(\varphi)}\left((L_{\varphi^{-1}})_* X, (L_{\varphi^{-1}})_* Y\right) = h_{\mathrm{Id}_2}(\varphi^{-1}X, \varphi^{-1}Y), \quad X, Y \in T_\varphi\,\mathrm{SU}(2). \tag{3.2.9}$$

Then the Dirichlet energy in local coordinates is given by

$$E_2(\varphi, g) = \int_{\mathbb{T}^3} |\mathrm{d}\varphi|_g^2\,\mathrm{vol}_g = \int_{\mathbb{T}^3} g^{ij} h(L_i, L_j)\,\mathrm{vol}_g, \tag{3.2.10}$$

where $L_i = \varphi^{-1}\partial_i\varphi$ is the previously defined $\mathfrak{su}(2)$-valued left current.

In Sec 3.3 we want to reduce the underlying metric variational problem to a non-linear matrix equation. To do this, we appeal to an isomorphism peculiar to 3-dimensions. We define a vector

field $X_{\varphi,g}$ that is metrically dual to the Hodge dual of $\varphi^*\Omega$ with respect to the metric g. Then, we construct an isomorphism $\Omega^2(\mathcal{M}) \otimes \mathfrak{su}(2) \cong T\mathbb{T}^3 \otimes \mathfrak{su}(2)$ via the mapping

$$\varphi^*\Omega \mapsto \sharp_g\left(\star_g \varphi^*\Omega\right) = X_{\varphi,g}, \tag{3.2.11}$$

where $\star_g : \Omega^p(\mathbb{T}^3) \to \Omega^{3-p}(\mathbb{T}^3)$ is the Hodge star operator. An alternative interpretation is is given by considering the inverse isomorphism

$$\begin{aligned} T\mathbb{T}^3 \otimes \mathfrak{su}(2) &\cong \Omega^2(\mathbb{T}^3) \otimes \mathfrak{su}(2) \\ X_{\varphi,g} &\mapsto \iota_{X_{\varphi,g}} \mathrm{vol}_g = \varphi^*\Omega, \end{aligned} \tag{3.2.12}$$

where $\iota_{X_{\varphi,g}} : \Omega^p(\mathbb{T}^3) \to \Omega^{p-1}(\mathbb{T}^3)$ is the interior product. Now, let us write $X_{\varphi,g} = X^i_\varphi \partial_i/\sqrt{g}$, where $X^i_\varphi \in \mathfrak{su}(2)$ and we have introduced the $1/\sqrt{g}$ factor for later convenience. As before, the pullback $\varphi^*\Omega$ can be written as $\Omega_{ij} = \varphi^*\Omega(\partial_i, \partial_j)$, such that

$$\Omega_{ij} = \Omega\left(\mathrm{d}\varphi(\partial_i), \mathrm{d}\varphi(\partial_j)\right) = \left[\omega_\varphi(\partial_i\varphi), \omega_\varphi(\partial_j\varphi)\right] = \left[L_i, L_j\right]. \tag{3.2.13}$$

Then, the metric isomorphism is computed to be given by

$$\sharp_g\left(\star_g \varphi^*\Omega\right) = \frac{1}{2}\frac{1}{\sqrt{g}}\varepsilon^{ijk}\Omega_{jk}\partial_i \in T\mathbb{T}^3 \otimes \mathfrak{su}(2). \tag{3.2.14}$$

Hence, the corresponding $\mathfrak{su}(2)$-valued vector field on $\mathbb{T}^3$ is given by

$$X_{\varphi,g} = \frac{1}{\sqrt{g}} X^i_\varphi \partial_i, \quad X^i_\varphi = \frac{1}{2}\epsilon^{ijk}\Omega_{jk} \in \mathfrak{su}(2). \tag{3.2.15}$$

The $\mathfrak{su}(2)$-valued 2-form $\varphi^*\Omega$ on $\mathbb{T}^3$ can be expressed in terms of the $\mathfrak{su}(2)$-valued vector field $X_{\varphi,g}$ on $\mathbb{T}^3$ via the relation

$$\Omega_{jk} = X^i \varepsilon_{ijk} \in \mathfrak{su}(2). \tag{3.2.16}$$

We can write $|\varphi^*\Omega|^2_g = |\star_g \varphi^*\Omega|^2_g = |\sharp_g(\star_g\varphi^*\Omega)|^2_g$, such that the Skyrme energy E_4 can be expressed as

$$E_4(\varphi, g) = \frac{1}{4}\int_{\mathbb{T}^3} |\sharp_g(\star_g\varphi^*\Omega)|^2_g \,\mathrm{vol}_g = \frac{1}{4}\int_{\mathbb{T}^3} \frac{1}{\sqrt{g^2}} g_{ij} h\left(X^i_\varphi, X^j_\varphi\right) \mathrm{vol}_g. \tag{3.2.17}$$

For completeness, we have included the sextic term [104] and define the natural three-form $\Xi \in \Omega^3(\mathrm{SU}(2))$ by

$$\Xi(X, Y, Z) = \frac{1}{24\pi^2} h\left(\omega(X), \Omega(Y, Z)\right). \tag{3.2.18}$$

Note that this three-form Ξ coincides with the normalized volume form on SU(2), where

$$\mathrm{vol}_{\mathrm{SU}(2)} = \frac{1}{24\pi^2}\,\mathrm{Tr}\left(\varphi^{-1}\mathrm{d}\varphi \wedge \varphi^{-1}\mathrm{d}\varphi \wedge \varphi^{-1}\mathrm{d}\varphi\right). \tag{3.2.19}$$

Terms of this kind are of phenomenological interest since they arise in so-called near BPS variants of the Skyrme model [105]. We can also explicitly write the pullback $\varphi^*\Xi$ in terms of the local frame $\{\partial_1, \partial_2, \partial_3\}$ as $\Xi_{ijk} = \varphi^*\Xi(\partial_i, \partial_j, \partial_k)$ with

$$\Xi_{ijk} = \frac{1}{24\pi^2} h\left(\omega_\varphi(\partial_i\varphi), \Omega\left(\partial_j\varphi, \partial_k\varphi\right)\right) = \frac{1}{24\pi^2} h\left(L_i, \Omega_{jk}\right) = \frac{1}{48\pi^2}\,\mathrm{Tr}\left(L_i, [L_j, L_k]\right). \tag{3.2.20}$$

Then we can compute the norm of the sextic term of $\varphi^*\Xi$, which reads

$$E_6(\varphi, g) = c_6 \int_{\mathbb{T}^3} |\varphi^*\Xi|_g^2 \operatorname{vol}_g = c_6 \int_{\mathbb{T}^3} \left(\frac{1}{\sqrt{g}}\epsilon^{ijk}\Xi_{ijk}\right)\left(\frac{1}{\sqrt{g}}\epsilon^{abc}\Xi_{abc}\right) \operatorname{vol}_g. \tag{3.2.21}$$

Throughout, we will use the standard pion mass potential $V : \mathrm{SU}(2) \to [0, \infty)$ given by

$$V(\varphi) = m^2 \operatorname{Tr}(\mathrm{Id}_2 - \varphi), \tag{3.2.22}$$

with m the rescaled pion mass defined by (1.1.12).

Definition 3. *The static energy functional of the generalized $\mathscr{L}_{0246}$-Skyrme model on $\mathbb{T}^3$, in Skyrme units, is given by*

$$M_B(\varphi, g) = \int_{\mathbb{T}^3} \left\{ |\mathrm{d}\varphi|_g^2 + \frac{1}{4}|\sharp_g(\star_g \varphi^*\Omega)|_g^2 + V \circ \varphi + c_6 |\varphi^*\Xi|_g^2 \right\} \operatorname{vol}_g, \tag{3.2.23}$$

where c_6 is defined by (1.1.13).

Variation of the Field

Consider the more general case $\varphi : M \to \mathrm{SU}(2)$, where M is a connected, oriented, 3-dimensional Riemannian manifold. The metric g on M induces a point-wise metric $\langle \cdot, \cdot \rangle_g$ on the bundle $\bigwedge^p T^*M \to M$ of p-forms $\zeta \in \Omega^p(M) = \Gamma(\bigwedge^p T^*M)$ on M. In terms of the local frame $\{\partial_1, \partial_2, \partial_3\}$ on M, this metric is defined by

$$\langle \eta, \zeta \rangle_g = \frac{1}{p!} \sum_{i_1, \dots, i_p = 1}^{3} g^{i_1 j_1} \dots g^{i_p j_p} \eta(\partial_{i_1}, \dots, \partial_{i_p}) \zeta(\partial_{j_1}, \dots, \partial_{j_p}). \tag{3.2.24}$$

Using the Hodge star operator, we define the Hodge dual of $\zeta \in \Omega^p(M)$ as $\star_g \zeta \in \Omega^{3-p}(M)$ satisfying the relation

$$\eta \wedge \star_g \zeta = \langle \eta, \zeta \rangle_g \operatorname{vol}_g. \tag{3.2.25}$$

This gives a global L^2-inner product,

$$\langle \eta, \zeta \rangle_{L^2} = \int_M \langle \eta, \zeta \rangle_g \operatorname{vol}_g = \int_M \eta \wedge \star_g \zeta \quad \left(\eta, \zeta \in \Omega^p(M)\right), \tag{3.2.26}$$

with corresponding norm $\|\eta\|_{L^2}^2 = \langle \eta, \eta \rangle_{L^2}$. Let the operator adjoint to d with respect to the L^2-inner product be the codifferential

$$\delta : \Omega^p(M) \to \Omega^{p-1}(M), \quad \delta = (-1)^{3(p+1)-1} \star \mathrm{d} \star . \tag{3.2.27}$$

We will also need the flat musical isomorphism on M, defined by

$$\flat_g : TM \to \Omega^1(M), \quad \flat_g X = g(X, \cdot), \quad \flat = \sharp^{-1}. \tag{3.2.28}$$

Let $X \in \Gamma(TM)$ be a vector field and its flow at time t be φ_t. Then we can define the Lie derivative $\mathscr{L}_X \eta$ of $\eta \in \Omega^p(M)$ along X by

$$\mathscr{L}_X \eta = \left.\frac{\mathrm{d}}{\mathrm{d}t}\right|_{t=0} \varphi_t^* \eta. \tag{3.2.29}$$

Denote the contraction of a vector field X and a differential form η by $\iota_X \eta$, where $\iota_X : \Omega^p(M) \to \Omega^{p-1}(M)$ is the interior product. Vector fields along φ, or (infinitesimal) variations of φ, are sections $\Gamma(\varphi^{-1} T\,\mathrm{SU}(2))$ of the bundle induced by φ [103].

Lemma 4 (Homotopy Lemma)**.** *Let η be a closed p-form on* SU(2) *(i.e.* $\mathrm{d}\eta = 0$*) and*

$$\varphi_t : M \to \mathrm{SU}(2) \tag{3.2.30}$$

be a smooth one-parameter family of maps with variational vector field $X = \partial_t \varphi_t|_{t=0} \in \Gamma(\varphi^{-1} T\,\mathrm{SU}(2))$. Then

$$\mathscr{L}_X \eta = \left.\frac{\mathrm{d}}{\mathrm{d}t}\right|_{t=0} \varphi_t^* \eta = \mathrm{d}\left(\varphi^* \iota_X \eta\right). \tag{3.2.31}$$

For a proof of the homotopy lemma see, e.g., [106, p. 49].

Definition 5. *A critical point (or an extremum) of the energy functional $M_B(\varphi, g)$ is a map $\varphi : M \to$* SU(2) *such that*

$$\left.\frac{\mathrm{d}M_B(\varphi_t, g)}{\mathrm{d}t}\right|_{t=0} = 0 \tag{3.2.32}$$

for all deformations $(\varphi_t)_{t\in\mathbb{R}}$ of the field $\varphi = \varphi_0$.

Proposition 6. *Let φ_t be a smooth one-parameter variation of the field $\varphi : M \to$* SU(2)*, with infinitesimal generator $X = \partial_t \varphi_t|_{t=0} \in \Gamma(\varphi^{-1} T\,\mathrm{SU}(2))$. Then*

$$\left.\frac{\mathrm{d}M_B(\varphi_t, g)}{\mathrm{d}t}\right|_{t=0} = -\int_M \langle X, \tau(\varphi)\rangle_g \,\mathrm{vol}_g, \tag{3.2.33}$$

where $\tau(\varphi) \in \Gamma(\varphi^{-1} T\,\mathrm{SU}(2))$ is the tension field of φ given by

$$\tau(\varphi) = -2\,\delta\mathrm{d}\varphi - \mathrm{grad}(V) \circ \varphi - 2\left(\frac{1}{4}\sharp_b \mu_\Omega(\varphi) + c_6 \sharp_b \mu_\Xi(\varphi)\right) \tag{3.2.34}$$

and $\mu_\eta(\varphi) \in \Gamma(\varphi^{-1} T^*\,\mathrm{SU}(2))$ maps elements $A \in T_{\varphi(x)}\,\mathrm{SU}(2)$ to

$$\mu_\eta(\varphi)(A) = \langle \delta\varphi^*\eta, \iota_A \varphi^* \eta\rangle_g. \tag{3.2.35}$$

Proof. The tension field of the Dirichlet term is well known, and the variation of the Dirichlet energy with respect to the smooth variation φ_t is given by (e.g. [88])

$$\left.\frac{\mathrm{d}E_2(\varphi_t, g)}{\mathrm{d}t}\right|_{t=0} = 2\int_M \langle X, -\star\,\mathrm{d}\star\,\mathrm{d}\varphi\rangle_g \,\mathrm{vol}_g = 2\,\langle X, \delta\mathrm{d}\varphi\rangle_{L^2}. \tag{3.2.36}$$

The potential and sextic term variations haven been computed by Adam *et al.* [107], they are

$$\left.\frac{\mathrm{d}E_0(\varphi_t, g)}{\mathrm{d}t}\right|_{t=0} = \langle X, \mathrm{grad}(V) \circ \varphi\rangle_{L^2} \tag{3.2.37}$$

and

$$\left.\frac{\mathrm{d}E_6(\varphi_t, g)}{\mathrm{d}t}\right|_{t=0} = 2c_6 \int_M \langle \delta\varphi^*\Xi, \varphi^*\iota_X \Xi\rangle_g \,\mathrm{vol}_g = 2c_6\,\langle X, \sharp_b \mu_\Xi(\varphi)\rangle_{L^2}, \tag{3.2.38}$$

where we have used Stokes' Theorem and the homotopy lemma, $\partial_t|_{t=0}\varphi_t^*\Xi = \mathrm{d}(\iota_X \varphi^*\Xi)$. Similarly, for the Skyrme term we have

$$\left.\frac{\mathrm{d}E_4(\varphi_t, g)}{\mathrm{d}t}\right|_{t=0} = \frac{1}{2}\int_M \langle \delta\varphi^*\Omega, \varphi^*\iota_X \Omega\rangle_g \,\mathrm{vol}_g = \frac{1}{2}\,\langle X, \sharp_b \mu_\Omega(\varphi)\rangle_{L^2}, \tag{3.2.39}$$

which completes the proof. □

Definition 7. *A skyrmion is a critical point φ of the energy functional M_B such that $\tau(\varphi) \equiv 0$ for all variations $(\varphi_t)_{t\in\mathbb{R}}$, i.e. the tension field $\tau(\varphi)$ corresponds to the Euler–Lagrange operator associated to the energy functional M_B.*

Variation of the Metric

In order to find skyrmion crystals, we have to consider variations of the metric g on $\mathbb{T}^3$. For now, let us remain in the general setting $\varphi : M \to \mathrm{SU}(2)$ and let g_s be a smooth one-parameter family of metrics on M with initial metric $g_0 = g$. Set $\dot{g} = \partial_s g_s|_{s=0} \in \Gamma(\odot^2 T^*M)$, a symmetric 2-covariant tensor field on M. Denote the inner product on the space of 2-covariant tensor fields of the tangent space T_xM to M at $x \in M$ by $\langle\cdot,\cdot\rangle$. Then for any pair of symmetric bilinear forms A, B we have [108]

$$\langle A, B\rangle_g = A_{ij} g^{jk} B_{kl} g^{li}. \tag{3.2.40}$$

In particular, we have the following result:

$$\mathrm{Tr}_g(A) = \langle A, g\rangle_g. \tag{3.2.41}$$

Let us consider the rate of change of the energy of the Skyrme field φ with respect to varying the domain metric g. This enables us to define the stress-energy tensor, which is the key component of our numerical algorithm.

Proposition 8. *The first variation of the energy* (3.2.23) *with respect to the smooth one-parameter family of variations g_s of the metric on M is given by*

$$\left.\frac{\mathrm{d}M_B(\varphi, g_s)}{\mathrm{d}s}\right|_{s=0} = \int_M \langle S(\varphi, g), \dot{g}\rangle_g \,\mathrm{vol}_g, \tag{3.2.42}$$

where $S(\varphi, g) = S_{ij}\mathrm{d}x^i\mathrm{d}x^j \in \Gamma(\odot^2 T^*M)$ is a symmetric 2-covariant tensor field on M, known as the stress-energy tensor, *given by*

$$S(\varphi, g) = \frac{1}{2}\left(|\mathrm{d}\varphi|_g^2 - \frac{1}{4}|\#_g(\star_g\varphi^*\Omega)|_g^2 + V\circ\varphi - c_6|\varphi^*\Xi|_g^2\right)g - \left(\varphi^*h - \frac{1}{4\sqrt{g}^2}ghXg\right). \tag{3.2.43}$$

Proof. The variation of the volume form vol_{g_s} with respect to the metric g_s is well known and is given by [109, p. 82]

$$\left.\frac{\mathrm{d}}{\mathrm{d}s}\right|_{s=0}\mathrm{vol}_{g_s} = \left.\frac{\mathrm{d}}{\mathrm{d}s}\right|_{s=0}\sqrt{g_s}\,\mathrm{d}^m x = \frac{1}{2}\sqrt{g}\,\mathrm{Tr}_g(\dot{g})\,\mathrm{d}^m x = \frac{1}{2}\,\mathrm{Tr}_g(\dot{g})\,\mathrm{vol}_g = \frac{1}{2}\,\langle g, \dot{g}\rangle_g\,\mathrm{vol}_g. \tag{3.2.44}$$

The first variation of the Dirichlet energy with respect to the metric g is given by, e.g., [110, p. 19]

$$\begin{aligned}
\left.\frac{\mathrm{d}E_2(\varphi,g_s)}{\mathrm{d}s}\right|_{s=0} &= \left.\frac{\mathrm{d}}{\mathrm{d}s}\right|_{s=0}\left(\int_M |\mathrm{d}\varphi|^2_{g_s}\mathrm{vol}_{g_s}\right)\\
&= \left.\frac{\mathrm{d}}{\mathrm{d}s}\right|_{s=0}\left(\int_M g^{ij}(s)h(L_i,L_j)\,\mathrm{vol}_{g_s}\right)\\
&= \int_M \left.\frac{\mathrm{d}g^{ij}(s)}{\mathrm{d}s}\right|_{s=0} h(L_i,L_j)\,\mathrm{vol}_g + \int_M g^{ij}h(L_i,L_j)\left.\frac{\mathrm{dvol}_{g_s}}{\mathrm{d}s}\right|_{s=0}\\
&= -\int_M g^{il}\dot{g}_{lk}g^{kj}h(L_i,L_j)\,\mathrm{vol}_g + \frac{1}{2}\int_M g^{ij}h(L_i,L_j)\,\mathrm{Tr}_g(\dot{g})\,\mathrm{vol}_g\\
&= \int_M \dot{g}_{nm}\left(-g^{in}g^{mj}+\frac{1}{2}g^{ij}g^{mn}\right)h(L_i,L_j)\,\mathrm{vol}_g\\
&= \int_M \langle\frac{1}{2}|\mathrm{d}\varphi|^2_g g-\varphi^*h,\dot{g}\rangle_g\,\mathrm{vol}_g,
\end{aligned}\tag{3.2.45}$$

where we have used the identity $g^{ij}(s)g_{jk}(s)=\delta^i_k$, for all s, to deduce that

$$\left.\frac{\mathrm{d}}{\mathrm{d}s}\right|_{s=0} g^{ij}(s) = -g^{il}\dot{g}_{lk}g^{kj}.\tag{3.2.46}$$

Then the corresponding variation of the Skyrme energy with respect to the metric is

$$\begin{aligned}
\left.\frac{\mathrm{d}E_4(\varphi,g_s)}{\mathrm{d}s}\right|_{s=0} &= \left.\frac{\mathrm{d}}{\mathrm{d}s}\right|_{s=0}\left(\frac{1}{4}\int_M |\#_{g_s}(\star_{g_s}\varphi^*\Omega)|^2_{g_s}\,\mathrm{vol}_{g_s}\right)\\
&= \left.\frac{\mathrm{d}}{\mathrm{d}s}\right|_{s=0}\left(\frac{1}{4}\int_M \frac{1}{\sqrt{g_s}^2}g_{ij}(s)h\left(X^i_\varphi,X^j_\varphi\right)\,\mathrm{vol}_{g_s}\right)\\
&= \frac{1}{4}\int_M \frac{1}{\sqrt{g}^2}\dot{g}_{ij}h\left(X^i_\varphi,X^j_\varphi\right)\,\mathrm{vol}_g - \int_M \langle\frac{1}{4\sqrt{g}^2}g_{ij}h\left(X^i_\varphi,X^j_\varphi\right)g,\dot{g}\rangle_g\,\mathrm{vol}_g\\
&\quad + \frac{1}{2}\int_M \langle\frac{1}{4\sqrt{g}^2}g_{ij}h\left(X^i_\varphi,X^j_\varphi\right)g,\dot{g}\rangle_g\,\mathrm{vol}_g\\
&= \int_M \langle\frac{1}{4\sqrt{g}^2}gh_Xg-\frac{1}{8}|(\star_g\varphi^*\Omega)|^2_g g,\dot{g}\rangle_g\,\mathrm{vol}_g,
\end{aligned}\tag{3.2.47}$$

where $h_X=\left(h(X^i_\varphi,X^j_\varphi)\right)$ and we have used the fact that

$$\langle gh_Xg,\dot{g}\rangle_g = \left(gh_Xg\right)_{ij}g^{jk}\dot{g}_{kl}g^{li} = g_{im}h(X^m_\varphi,X^n_\varphi)g_{nj}g^{jk}\dot{g}_{kl}g^{li} = h(X^m_\varphi,X^n_\varphi)\dot{g}_{nm}.\tag{3.2.48}$$

The potential function V has no dependence on the metric and so the potential term has variation

$$\left.\frac{\mathrm{d}E_0(\varphi,g_s)}{\mathrm{d}s}\right|_{s=0} = \int_M (V\circ\varphi)\left.\frac{\mathrm{dvol}_{g_s}}{\mathrm{d}s}\right|_{s=0} = \int_M \langle\frac{1}{2}(V\circ\varphi)g,\dot{g}\rangle_g\,\mathrm{vol}_g.\tag{3.2.49}$$

However, the sextic term E_6 is inversely proportional to the metric determinant $E_6\sim 1/\sqrt{g}$ and, thus,

$$\left.\frac{\mathrm{d}E_6(\varphi,g_s)}{\mathrm{d}s}\right|_{s=0} = \int_M \langle-\frac{c_6}{2}|\varphi^*\Xi|^2_g g,\dot{g}\rangle_g\,\mathrm{vol}_g.\tag{3.2.50}$$

This establishes the stress tensor (3.2.43), as required. □

The space of allowed variations $\mathscr{E}$ is a 6-dimensional subspace of the space of sections of the rank 6 vector bundle $\odot^2 T^*M$,

$$\mathscr{E} = \left\{ \dot{g}_{ij} \mathrm{d}x^i \mathrm{d}x^j \in \Gamma(\odot^2 T^*M) : \dot{g}_{ij} \text{ constant}, \dot{g}_{ji} = \dot{g}_{ij} \right\}. \tag{3.2.51}$$

By definition, the energy $\mathcal{M}_B$ is critical with respect to variations g_s of the metric if and only if

$$\left. \frac{\mathrm{d}\mathcal{M}_B(\varphi, g_s)}{\mathrm{d}s} \right|_{s=0} = \int_M \langle S(\varphi, g), \dot{g} \rangle_g \, \mathrm{vol}_g = 0, \tag{3.2.52}$$

that is, if and only if $S \perp_{L^2} \mathscr{E}$. Now let the orthogonal complement of g in $\mathscr{E}$, the space of traceless parallel symmetric bilinear forms, given by

$$\mathscr{E}_0 = \left\{ \theta \in \mathscr{E} : \mathrm{Tr}_g(\theta) = \langle \theta, g \rangle_g = 0 \right\}. \tag{3.2.53}$$

Then the criticality condition $S \perp_{L^2} \mathscr{E}$ can be reformulated as [64]

$$\int_M \langle S(\varphi, g), g \rangle_g \, \mathrm{vol}_g = 0 \quad \text{and} \quad S \perp_{L^2} \mathscr{E}_0. \tag{3.2.54}$$

The first condition $S \perp_{L^2} g$ is analogous to a virial constraint and the second condition $S \perp_{L^2} \mathscr{E}_0$ coincides with the extended virial constraints derived by Manton [111]. We can determine the virial constraint by evaluating

$$\begin{aligned}
\int_M \langle S(\varphi, g), g \rangle_g \, \mathrm{vol}_g &= \int_M \mathrm{Tr}_g(S) \, \mathrm{vol}_g \\
&= \int_M \mathrm{Tr}_g \left\{ \left(\frac{1}{2} |\mathrm{d}\varphi|_g^2 - \frac{1}{8} |(\star_g \varphi^* \Omega)|_g^2 + \frac{1}{2} V \circ \varphi - \frac{c_6}{2} |\varphi^* \Xi|_g^2 \right) g - \left(\varphi^* h - \frac{1}{4} g h_X g \right) \right\} \mathrm{vol}_g \\
&= \int_M \left\{ \frac{3}{2} \left(|\mathrm{d}\varphi|_g^2 - \frac{1}{4} |(\star_g \varphi^* \Omega)|_g^2 + V \circ \varphi - c_6 |\varphi^* \Xi|_g^2 \right) - |\mathrm{d}\varphi|_g^2 + \frac{1}{4} |(\star_g \varphi^* \Omega)|_g^2 \right\} \mathrm{vol}_g \\
&= \frac{1}{2} \int_M \left(|\mathrm{d}\varphi|_g^2 - \frac{1}{4} |(\star_g \varphi^* \Omega)|_g^2 + 3(V \circ \varphi - c_6 |\varphi^* \Xi|_g^2) \right) \mathrm{vol}_g \\
&= \frac{1}{2} \left(E_2 - E_4 + 3(E_0 - E_6) \right),
\end{aligned} \tag{3.2.55}$$

where we have used the identities (3.2.3) and

$$\mathrm{Tr}_g \left(g h_X g \right) = \left(g h_X g \right)_{ij} g^{jk} g_{kl} g^{li} = g_{im} h(X_\varphi^m, X_\varphi^n) g_{nj} g^{jk} g_{kl} g^{li} = g_{nm} h(X_\varphi^m, X_\varphi^n) = |(\star_g \varphi^* \Omega)|_g^2. \tag{3.2.56}$$

Hence, the condition $S \perp_{L^2} g$ establishes the familiar virial constraint

$$E_2 - E_4 + 3(E_0 - E_6) = 0. \tag{3.2.57}$$

To determine the extended virial constraint corresponding to the condition $S \perp_{L^2} \mathscr{E}_0$, we define a symmetric bilinear form

$$\Delta : T_x M \times T_x M \to \mathbb{R}, \quad \Delta(X, Y) = \int_M \left(\varphi^* h(X, Y) - \frac{1}{4\sqrt{g^2}} (g h_X g)(X, Y) \right) \mathrm{vol}_g. \tag{3.2.58}$$

Then $S \perp_{L^2} \mathscr{E}_0$ if and only if Δ is orthogonal to $\mathscr{E}_0$ with respect to the inner product $\langle \cdot, \cdot \rangle_{\mathscr{E}}$. Therefore, for $\lambda \in \mathbb{R}$ we must have

$$\Delta = \lambda g. \tag{3.2.59}$$

Taking the trace of both sides yields

$$3\lambda = \int_M \left(|\mathrm{d}\varphi|_g^2 - \frac{1}{4} |\#_g(\star_g \varphi^* \Omega)|_g^2 \right) \mathrm{vol}_g = E_2 - E_4. \tag{3.2.60}$$

Thus, the condition $S \perp_{L^2} \mathscr{E}_0$ produces the extended virial constraint

$$\Delta = \frac{1}{3} (E_2 - E_4)\, g. \tag{3.2.61}$$

So, we see that $\varphi : M \to \mathrm{SU}(2)$ is a critical point with respect to variations of the metric if and only if the extended virial constraints hold

$$E_2 - E_4 = 3(E_6 - E_0), \tag{3.2.62a}$$

$$\Delta = \frac{1}{3} (E_2 - E_4)\, g. \tag{3.2.62b}$$

We will verify numerically that the extended virial constraints are being satisfied within some tolerance, e.g. $\mathrm{tol} = 10^{-5}$. This is done by checking that

$$\left| \frac{E_4}{E_2 + 3(E_0 - E_6)} - 1 \right| < \mathrm{tol} \quad \text{and} \quad \left| \frac{\Delta_{ij}}{(E_6 - E_0) g_{ij}} - 1 \right| < \mathrm{tol}. \tag{3.2.63}$$

Now we need to show that not only is it a critical point but it is in fact a minimum.

3.3 Existence, Uniqueness and Criticality of the Metric

For fixed $g \in \mathrm{SPD}_3$, $(\mathbb{T}^3, g)$ is a fixed, compact oriented Riemannian 3-manifold, and it follows from a direct application of the calculus of variations that the functional $\varphi \mapsto E(\varphi, g)$ attains a minimum in each degree class in the space of finite energy maps in the Sobolev space $W^{1,2}(\mathbb{T}^3, \mathrm{SU}(2))$ [101]. In this section we address the complementary variational problem: we fix a map $\varphi : \mathbb{T}^3 \to \mathrm{SU}(2)$ and establish existence, and uniqueness, of a minimizer of the function $\mathrm{SPD}_3 \to \mathbb{R}, g \mapsto M_B(\varphi, g)$ which, for brevity, we will denote $M_B(g)$.

We begin by analyzing in more detail the g dependence of the terms in M_B. We first note that

$$E_2(\varphi, g) = \int_{\mathbb{T}^3} |\mathrm{d}\varphi|_g^2 \,\mathrm{vol}_g = \sqrt{g} g^{ij} \int_{\mathbb{T}^3} \mathrm{d}^3x\, h(L_i, L_j) = \sqrt{g} g^{ij} H_{ij} \tag{3.3.1}$$

where

$$H_{ij}(\varphi) = \int_{\mathbb{T}^3} \mathrm{d}^3x\, h(L_i, L_j) = \int_{\mathbb{T}^3} \mathrm{d}^3x\, \partial_i \varphi^\mu \partial_j \varphi^\mu \tag{3.3.2}$$

is a symmetric positive semi-definite matrix depending on φ but independent of g. Then we can express the Dirichlet energy in terms of the trace of a matrix product, that is

$$E_2(\varphi, g) = \sqrt{\det g}\, \mathrm{Tr}(H g^{-1}). \tag{3.3.3}$$

Let us assume that φ is C^1 (so that this matrix is well-defined) and is immersive somewhere, meaning that there is some point $p \in \mathbb{T}^3$ at which $\mathrm{d}\varphi_p$ is invertible. Note that this follows immediately for all maps with $B \neq 0$. By continuous differentiability, it follows that φ is immersive on some neighbourhood of p. Then the matrix H is actually positive definite, for if not, there exists $\vec{v} \in \mathbb{R}^3$ with $\vec{v} \cdot H\vec{v} = 0$, whence

$$\int_{\mathbb{T}^3} |\vec{v} \cdot \vec{L}|^2_{\mathfrak{su}(2)} \mathrm{vol}_0 = 0 \tag{3.3.4}$$

and hence $\mathrm{d}\varphi(v_i \partial/\partial x_i) = 0$ almost everywhere. This contradicts immersivity of φ on a neighbourhood of p. We conclude that $H \in \mathrm{SPD}_3$.

Now, we turn our attention to the Skyrme energy, E_4. This is given by

$$E_4(\varphi, g) = \frac{1}{4}\int_{\mathbb{T}^3} |\sharp_g(*_g\varphi^*\Omega)|^2_g \,\mathrm{vol}_g = \frac{1}{\sqrt{g}} g_{ij} \int_{\mathbb{T}^3} \mathrm{d}^3x \,\frac{1}{4} h(X^i_\varphi, X^j_\varphi) = \frac{1}{\sqrt{\det g}} g_{ij} F_{ij}, \tag{3.3.5}$$

where we use relation (3.2.15) to express the matrix F in terms of the Skyrme fields as

$$\begin{aligned} F_{ij}(\varphi) &= \frac{1}{16}\varepsilon^{iab}\varepsilon^{jcd}\int_{\mathbb{T}^3} \mathrm{d}^3x \, h(\Omega_{ab}, \Omega_{cd}) \\ &= \frac{1}{4}\varepsilon^{iab}\varepsilon^{jcd}\int_{\mathbb{T}^3} \mathrm{d}^3x \, \left\{ \left(\partial_a\varphi^\mu \partial_c\varphi^\mu\right)\left(\partial_b\varphi^\nu\partial_d\varphi^\nu\right) - \left(\partial_a\varphi^\mu\partial_d\varphi^\mu\right)\left(\partial_b\varphi^\nu\partial_c\varphi^\nu\right)\right\}. \end{aligned} \tag{3.3.6}$$

Once again, our non-degeneracy assumption on φ (that it is C^1 and somewhere immersive) implies that F is positive definite. For if not, there exists $\vec{v} \in \mathbb{R}^3$ such that $\vec{v} \cdot F\vec{v} = 0$, whence $\vec{v} \cdot X_\varphi = 0$ and so $*_g\varphi^*\Omega(v_i\partial/\partial x_i) = 0$. But then $\varphi^*\Omega$ vanishes on every plane in $T\mathbb{T}^3$ g-orthogonal to $\vec{v}$, which contradicts non-degeneracy of Ω and immersivity of φ.

The remaining terms of $\mathcal{M}_B$ are more straightforward.

$$E_0(\varphi, g) = \int_{\mathbb{T}^3} V(\varphi)\mathrm{vol}_g = C_0\sqrt{\det g}, \tag{3.3.7}$$

where

$$C_0(\varphi) = 2m^2 \int_{\mathbb{T}^3} \mathrm{d}^3x \,(1 - \sigma) \geq 0 \tag{3.3.8}$$

is a constant. Finally, we note that $\varphi^*\Xi = f_\Xi \mathrm{vol}_0$ for some real function $f_\Xi : \mathbb{T}^3 \to \mathbb{R}$ independent of g. Then it is easy to see that $*_g\varphi^*\Xi = f_\Xi/\sqrt{g}$ and, hence,

$$E_6(\varphi, g) = \int_{\mathbb{T}^3} \varphi^*\Xi \wedge *_g\varphi^*\Xi = \frac{C_6}{\sqrt{\det g}}, \tag{3.3.9}$$

where

$$C_6(\varphi) = \int_{\mathbb{T}^3} \mathrm{d}^3x \, f_\Xi^2 = \frac{c_6\epsilon^{ijk}\epsilon^{lmn}}{(12\pi^2)^2}\epsilon_{\mu\nu\rho\sigma}\epsilon_{\alpha\beta\gamma\delta}\int_M \mathrm{d}^3x \,\varphi^\mu\varphi^\alpha\partial_i\varphi^\nu\partial_j\varphi^\rho\partial_k\varphi^\sigma\partial_l\varphi^\beta\partial_m\varphi^\gamma\partial_n\varphi^\delta \geq 0 \tag{3.3.10}$$

is a constant. Note that we allow the possibility that C_0 or C_6 is 0, to accommodate versions of the model with no potential or sextic term.

In summary, for a fixed C^1 map $\varphi : \mathbb{T}^3 \to \mathrm{SU}(2)$ which is immersive somewhere, the total Skyrme energy as a function of the metric g on $\mathbb{T}^3$ is

$$\mathcal{M}_B(g) := \mathcal{M}_B(\varphi|_{\text{fixed}}, g) = \sqrt{\det g}\,\mathrm{Tr}(Hg^{-1}) + \frac{1}{\sqrt{\det g}}\,\mathrm{Tr}(Fg) + C_0\sqrt{\det g} + \frac{C_6}{\sqrt{\det g}}, \tag{3.3.11}$$

where $H, F \in \mathrm{SPD}_3$ and $C_0, C_6 \in [0,\infty)$ are constants. We wish to prove that the function $M_B : \mathrm{SPD}_3 \to \mathbb{R}$ attains a unique global minimum, and has no other critical points. Before doing so, we note that $M_B = \widetilde{E} \circ \sigma$ where

$$\widetilde{E} : \mathrm{SPD}_3 \to \mathbb{R}, \qquad \widetilde{E}(\Sigma) = \mathrm{Tr}\left(H\Sigma^{-1}\right) + \mathrm{Tr}(F\Sigma) + \frac{C_0}{\det \Sigma} + C_6 \det \Sigma \tag{3.3.12}$$

and σ is the map

$$\sigma : \mathrm{SPD}_3 \to \mathrm{SPD}_3, \qquad g \mapsto \Sigma = \frac{g}{\sqrt{\det g}}. \tag{3.3.13}$$

Since σ is a diffeomorphism, we may equivalently prove that $\widetilde{E} : \mathrm{SPD}_3 \to \mathbb{R}$ attains a unique global minimum and has no other critical points. We do this in two stages.

Theorem 9 (Bolzano–Weierstrass Theorem)**.** *Every bounded sequence $\{\vec{x}_n\}_{n=1}^{\infty}$ in $\mathbb{R}^m$ has a convergent subsequence.*

Proposition 10. *The function $\widetilde{E} : \mathrm{SPD}_3 \to \mathbb{R}$ of equation (3.3.12) attains a global minimum.*

Proof. We want to show that there exists a critical point of the energy functional $\widetilde{E} : \mathrm{SPD}_3 \to \mathbb{R}^3$. Clearly $\widetilde{E}$ is bounded below (by 0). Let $f : \mathscr{D} \to \mathrm{SPD}_3$, with $\mathscr{D} = (0,\infty)^3 \times O(3)$, be a surjection given by the mapping

$$f\left(\vec{\lambda}, \mathcal{O}\right) = \mathcal{O}^T D_{\vec{\lambda}} \mathcal{O}, \qquad D_{\vec{\lambda}} = \begin{pmatrix} \lambda_1 & 0 & 0 \\ 0 & \lambda_2 & 0 \\ 0 & 0 & \lambda_3 \end{pmatrix}. \tag{3.3.14}$$

Then the composition $\widetilde{E} \circ f : \mathscr{D} \to \mathbb{R}$ is non-negative and so we define

$$E_* = \inf_{(\vec{\lambda}, Q) \in \mathscr{D}} (\widetilde{E} \circ f) \geq 0. \tag{3.3.15}$$

We must show that there exists $\Sigma_* \in \mathrm{SPD}_3$ with $\widetilde{E}(\Sigma_*) = E_*$.

The map $f : \mathscr{D} \to \mathrm{SPD}_3$ is indeed surjective: given any $\Sigma \in \mathrm{SPD}_3$ we may take λ_i to be its eigenvalues and $\mathcal{O}$ to be an orthogonal matrix whose columns are its corresponding eigenvectors. Hence, it suffices to prove that

$$(\widetilde{E} \circ f)(\vec{\lambda}, \mathcal{O}) = \mathrm{Tr}\left(\mathcal{O}^T H \mathcal{O} D_{\vec{\lambda}}^{-1}\right) + \mathrm{Tr}\left(\mathcal{O}^T F \mathcal{O} D_{\vec{\lambda}}\right) + \frac{C_0}{\lambda_1\lambda_2\lambda_3} + C_6\lambda_1\lambda_2\lambda_3 \tag{3.3.16}$$

attains the value E_*. We do this by showing that there exists a sequence $\{(\vec{\lambda}_n, \mathcal{O}_n)\}_{n=1}^{\infty}$ such that

$$\lim_{n\to\infty} (\widetilde{E} \circ f)(\vec{\lambda}_n, \mathcal{O}_n) = E_*. \tag{3.3.17}$$

Firstly, we note that SPD_3 can be smoothly embedded in $\mathbb{R}^6$ via the map $p : \mathrm{SPD}_3 \to \mathbb{R}^6$ defined by

$$\Sigma = \begin{pmatrix} v_1 & v_4 & v_5 \\ v_4 & v_2 & v_6 \\ v_5 & v_6 & v_3 \end{pmatrix} \mapsto p(\Sigma) = (v_1, v_2, v_3, v_4, v_5, v_6) = \vec{v}. \tag{3.3.18}$$

We will show that the sequence $\{(\vec{\lambda}_n, \mathcal{O}_n)\}_{n=1}^{\infty}$, corresponding to the sequence $\{\vec{v}_n\}_{n=1}^{\infty}$ in $\mathbb{R}^6$ with $\vec{v}_n = (p \circ f)(\vec{\lambda}_n, \mathcal{O}_n)$, is bounded and thus has a convergent subsequence.

Let $\Sigma = f(\vec{\lambda}, \mathcal{O}) = \mathcal{O}^T D_{\vec{\lambda}} \mathcal{O}$. Denote the eigenvalues of F and H by $\mu_i, \nu_i \in \mathbb{R}_{>0}$, respectively. Since F and H are both symmetric and positive definite, we can diagonalize them: $F = P_1 D_1 P_1^T$ and $H = P_2 D_2 P_2^T$, where $D_1 = \mathrm{diag}(\mu_1, \mu_2, \mu_3)$ and $D_2 = \mathrm{diag}(\nu_1, \nu_2, \nu_3)$.

Let us first consider the Skyrme term,

$$\begin{aligned} \mathrm{Tr}(\Sigma F) &= \mathrm{Tr}\left(\mathcal{O}^T D_{\vec{\lambda}} \mathcal{O} P_1 D_1 P_1^T\right) \\ &= \mathrm{Tr}\left(D_{\vec{\lambda}} R D_1 R^T\right) \\ &= \lambda_i \left((R_{ij})^2 \mu_j\right) = \lambda_i \alpha_i > 0, \end{aligned} \tag{3.3.19}$$

where we have defined $R = \mathcal{O} P_1$ and $\alpha_i = (R_{ij})^2 \mu_j$. If we take $\alpha := \min\{\alpha_1, \alpha_2, \alpha_3\}$, then it is easy to see that

$$(E_4 \circ f)(\vec{\lambda}, \mathcal{O}) \geq \alpha \sum_{i=1}^{3} \lambda_i. \tag{3.3.20}$$

Analogously, we can determine a $\beta > 0$ such that

$$(E_2 \circ f)(\vec{\lambda}, \mathcal{O}) \geq \beta \sum_{i=1}^{3} \frac{1}{\lambda_i}. \tag{3.3.21}$$

The bounds coming from the potential and sextic terms are trivial, they are

$$(E_0 \circ f)(\vec{\lambda}, \mathcal{O}) = \frac{C_0}{\lambda_1 \lambda_2 \lambda_3} > 0 \tag{3.3.22}$$

and

$$(E_6 \circ f)(\vec{\lambda}, \mathcal{O}) = C_6 \lambda_1 \lambda_2 \lambda_3 > 0. \tag{3.3.23}$$

Therefore we can always determine a pair $\alpha, \beta > 0$ such that

$$(E \circ f)(\vec{\lambda}, \mathcal{O}) \geq \sum_{i=1}^{3} \left(\alpha \lambda_i + \frac{\beta}{\lambda_i}\right). \tag{3.3.24}$$

Then there exists a $K > 0$ such that $0 < \lambda_i, \frac{1}{\lambda_i} \leq K$ for all $i \in \{1, 2, 3\}$. Set $K = E_* / \min\{\alpha, \beta, \frac{1}{2}\}$, then the sequence $\{(\vec{\lambda}_n, \mathcal{O}_n)\}_{n=1}^{\infty}$ is confined to $\left[\frac{1}{K}, K\right]^3 \times O(3)$, which is compact and bounded. Hence, by the Bolzano–Weierstrass Theorem, there exists a convergent subsequence $\{(\vec{\lambda}_n|_K, \mathcal{O}_n|_K)\}_{n=1}^{\infty}$, converging to $(\vec{\lambda}_*, \mathcal{O}_*)$. We may assume, without loss of generality, that $(\vec{\lambda}_n, \mathcal{O}_n)$ itself converges to $(\vec{\lambda}_*, \mathcal{O}_*)$. So $(\widetilde{E} \circ f)(\vec{\lambda}_n, \mathcal{O}_n) \to E_*$ and $(\vec{\lambda}_n, \mathcal{O}_n) \to (\vec{\lambda}_*, \mathcal{O}_*)$. But $(\widetilde{E} \circ f)$ is continuous, so $(\widetilde{E} \circ f)(\lambda_*, \mathcal{O}_*) = E_*$.

It follows that $\widetilde{E}(\Sigma_*) = E_*$ where

$$\Sigma_* = \mathcal{O}_* D_{\vec{\lambda}_*} \mathcal{O}_*^T, \tag{3.3.25}$$

which completes the proof. □

We note in passing that the minimizing *metric* whose existence follows from Proposition 10 is

$$g_* = \sigma^{-1}(\Sigma_*) = \frac{\Sigma_*}{\det \Sigma_*}. \tag{3.3.26}$$

It remains to prove that $\widetilde{E}$ has no other critical points. We achieve this by proving that $\widetilde{E}$ is *strictly convex*, in the following sense:

Definition 11. *A function $f : M \to \mathbb{R}$ on a Riemannian manifold M is **convex** if, for all non-constant geodesics $\gamma(t)$ in M, $(f\circ\gamma)''(t) \geq 0$, and **strictly convex** if, for all such geodesics, $(f\circ\gamma)''(t) > 0$.*

To apply this definition to $\widetilde{E}$, we must equip SPD_3 with a Riemannian metric, G. As a manifold, SPD_n is an open subset of Sym_n where Sym_n is the real vector space of symmetric $n\times n$-matrices. There exists a canonical immersion $\mathrm{Id} : \mathrm{SPD}_n \hookrightarrow \mathrm{Sym}_n$ which gives an identification between $T_\Sigma \mathrm{SPD}_n$ and Sym_n at any point $\Sigma \in \mathrm{SPD}_n$ via the map $(\mathrm{Id}_\Sigma)_* : T_\Sigma \mathrm{SPD}_n \xrightarrow{\sim} \mathrm{Sym}_n$. Therefore, we can consider any tangent vector $\xi \in T_\Sigma \mathrm{SPD}_n$ to be a symmetric matrix with $\xi \equiv (\mathrm{Id}_\Sigma)_*(\xi) \in \mathrm{Sym}_n$.

Let us consider the action of general linear group $\mathrm{GL}(n,\mathbb{R})$ on the space of symmetric positive-definite $n\times n$-matrices SPD_n given by

$$\begin{aligned} \mathrm{GL}(n,\mathbb{R})\times \mathrm{SPD}_n &\to \mathrm{SPD}_n \\ (A,\Sigma) &\mapsto A*\Sigma = A\Sigma A^T. \end{aligned} \tag{3.3.27}$$

There is a natural extension of this action to the tangent vectors: let $\Gamma : (-\epsilon,\epsilon) \to \mathrm{SPD}_n$ defined by $\Gamma_{(\Sigma,\xi)}(t) = \Sigma + t\xi + \mathcal{O}(t^2)$ be a curve through Σ with tangent vector $\xi = \frac{\mathrm{d}\gamma}{\mathrm{d}t}|_{t=0}$, then $A*\Gamma_{(\Sigma,\xi)}(t) = A\Sigma A^T + tA\xi A^T + \mathcal{O}(t^2)$ is a curve through $A\Sigma A^T$ with tangent vector $A*\xi = A\xi A^T$. Let $\langle\cdot,\cdot\rangle_{\mathrm{Id}_n} : \mathrm{Sym}_n \times \mathrm{Sym}_n \to \mathbb{R}$ be an inner product on $T_{\mathrm{Id}_n}\mathrm{SPD}_n = \mathrm{Sym}_n$. In particular, we choose the standard left $O(n)$-invariant inner product

$$\langle \xi_1,\xi_2\rangle_{\mathrm{Id}} = \mathrm{Tr}\big(\xi_1\xi_2^T\big), \qquad \xi_1,\xi_2 \in \mathrm{Sym}_n. \tag{3.3.28}$$

Then we can equip SPD_n with an affine invariant inner product $\langle\cdot,\cdot\rangle_\Sigma : T_\Sigma\mathrm{SPD}_n \times T_\Sigma\mathrm{SPD}_n \to \mathbb{R}$ at $\Sigma \in \mathrm{SPD}_n$, defined below.

For symmetric positive-definite matrices, we define the matrix square root as

$$\Sigma^{1/2} = \{S \in \mathrm{SPD}_n \mid S^2 = \Sigma\}. \tag{3.3.29}$$

For two arbitrary tangent vectors $\xi_1,\xi_2 \in T_\Sigma\mathrm{SPD}_n \cong \mathrm{Sym}_n$, we require the metric $\langle\cdot,\cdot\rangle_\Sigma$ to be invariant under the action (3.3.27), that is: $\langle\xi_1,\xi_2\rangle_\Sigma = \langle A*\xi_1, A*\xi_2\rangle_{A*\Sigma}$ for $A \in \mathrm{GL}(n,\mathbb{R})$. In particular, this should be true for $A = \Sigma^{-1/2}$ since $\Sigma^{-1/2}*\Sigma = \mathrm{Id}_n$. This allows us to identify the inner product at any point $\Sigma \in \mathrm{SPD}_n$ with the inner product at the identity [112]:

$$\langle\xi_1,\xi_2\rangle_\Sigma = \langle \Sigma^{-1/2}\xi_1\Sigma^{-1/2}, \Sigma^{-1/2}\xi_2\Sigma^{-1/2}\rangle_{\mathrm{Id}_n} = \mathrm{Tr}\big(\Sigma^{-1}\xi_1\Sigma^{-1}\xi_2\big), \tag{3.3.30}$$

where $\Sigma \in \mathrm{SPD}_n$ and $\xi_1,\xi_2 \in T_\Sigma\mathrm{SPD}_n$. It is easy to show that this metric is indeed invariant under the action of $\mathrm{GL}(n,\mathbb{R})$ on SPD_n, i.e.

$$\langle P\xi_1P^T, P\xi_2P^T\rangle_{P\Sigma P^T} = \langle\xi_1,\xi_2\rangle_\Sigma, \tag{3.3.31}$$

where $P \in \mathrm{GL}(n,\mathbb{R})$. Thus, the correct choice of metric for our purposes is

$$G_\Sigma : T_\Sigma\mathrm{SPD}_3 \times T_\Sigma\mathrm{SPD}_3 \to \mathbb{R}, \qquad G_\Sigma(\xi_1,\xi_2) = \langle\xi_1,\xi_2\rangle_\Sigma = \mathrm{Tr}\big(\Sigma^{-1}\xi_1\Sigma^{-1}\xi_2\big). \tag{3.3.32}$$

This metric is indeed affine invariant, which means that the mapping $\rho(A) : \mathrm{SPD}_n \to \mathrm{SPD}_n$ defined by $\rho(A)(\Sigma) = A\Sigma A^T$ for all $\Sigma \in \mathrm{SPD}_n$ is an isometry [113]. It is also inversion invariant, that is,

$$\iota : \mathrm{SPD}_n \to \mathrm{SPD}_n, \qquad \iota(\Sigma) = \Sigma^{-1} \tag{3.3.33}$$

is an isometry [113].

Since the metric (3.3.32), and hence the geodesics, is invariant under the group action (3.3.27), we can use this group action to relate geodesics starting at any point Σ with geodesics through the identity Id_n. Hence, a general non-constant geodesic through $\Sigma \in \mathrm{SPD}_n$, with tangent vector $\vartheta \in T_\Sigma \mathrm{SPD}_n$, is

$$\gamma_{(\Sigma,\vartheta)}(t) = \Sigma^{1/2} * \gamma_{(\mathrm{Id}_n, \Sigma^{-1/2}*\vartheta)}(t) = A \exp(t\xi) A^T, \tag{3.3.34}$$

where $A \in \mathrm{GL}(n,\mathbb{R})$ satisfies $AA^T = \Sigma$, and $\xi \in \mathrm{Sym}_n$ such that $\xi = \Sigma^{-1/2} * \vartheta \neq 0$. Finally, it is geodesically complete and between any pair of distinct points Σ_1, Σ_2, there is a geodesic, unique up to parametrization.

Proposition 12. *The function $\widetilde{E} : \mathrm{SPD}_3 \to \mathbb{R}$ of equation (3.3.12) is strictly convex with respect to the metric G.*

Proof. Given a constant $M \in \mathrm{SPD}_3$, consider the function

$$f_M : \mathrm{SPD}_3 \to \mathbb{R}, \qquad f_M(\Sigma) = \mathrm{Tr}(M\Sigma). \tag{3.3.35}$$

Let γ be an arbitrary non-constant geodesic, as in (3.3.34). Then

$$\begin{aligned} (f_M \circ \gamma)''(0) &= \frac{\mathrm{d}^2}{\mathrm{d}t^2}\Big|_{t=0} \mathrm{Tr}\big(MA\exp(t\xi)A^T\big) = \mathrm{Tr}\big(MA\xi^2A^T\big) \\ &= \mathrm{Tr}\big((A\xi)^T M(A\xi)\big) = \sum_{i=1}^{3} \vec{v}_i \cdot M\vec{v}_i \end{aligned} \tag{3.3.36}$$

where $\vec{v}_i$ are the columns of $A\xi$. Since M is positive definite, it follows that $(f_M \circ \gamma)''(0) \geq 0$, and equals 0 only if $\vec{v}_1 = \vec{v}_2 = \vec{v}_3 = 0$. But $\xi \neq 0$ (the geodesic is non-constant) so at least one $\vec{v}_i \neq 0$. Hence $(f_M \circ \gamma)''(0) > 0$ for all non-constant geodesics γ. It follows that $(f_M \circ \gamma)''(T) > 0$ for all non-constant geodesics and all $T \in \mathbb{R}$, since for all geodesics γ and constants T, $\tilde{\gamma}(t) = \gamma(t+T)$ is a geodesic.

Similarly, $\det : \mathrm{SPD}_3 \to \mathbb{R}$ is convex since, for all non-constant geodesics

$$\begin{aligned} (\det\circ\gamma)''(0) &= \frac{\mathrm{d}^2}{\mathrm{d}t^2}\Big|_{t=0} (\det A)^2 \det\exp(t\xi) = (\det A)^2 \frac{\mathrm{d}^2}{\mathrm{d}t^2}\Big|_{t=0} \exp\big(t\,\mathrm{Tr}\,\xi\big) \\ &= (\det A)^2 (\mathrm{Tr}\,\xi)^2 \geq 0 \end{aligned} \tag{3.3.37}$$

It follows that

$$\widetilde{E} = f_H \circ \iota + f_F + C_0 \det\circ\iota + C_6 \det \tag{3.3.38}$$

is strictly convex, since $H, F \in \mathrm{SPD}_3$, ι is an isometry, and $C_0, C_6 \geq 0$. □

Propositions 10 and 12 quickly yield the desired result.

Corollary 13. *Let $\varphi : \mathbb{T}^3 \to \mathrm{SU}(2)$ be a fixed C^1 map that is immersive somewhere. Then the function $\mathrm{SPD}_3 \to \mathbb{R}$ mapping a flat metric g on $\mathbb{T}^3$ to the Skyrme energy $M_B(\varphi, g)$ attains a unique global minimum, and has no other critical points.*

Proof. As previously established $M_B(\varphi, g) = \widetilde{E}(\sigma(g))$ where $\widetilde{E}$ is the function defined in (3.3.12) and σ is a diffeomorphism of SPD_3. By Proposition 10, $\widetilde{E}$ attains a minimum at some $\Sigma_* \in \mathrm{SPD}_3$, whence M_B attains a global minimum at $g_* = \sigma^{-1}(\Sigma_*)$. Assume, towards a contradiction, that M_B has a second critical point $g_{**} \neq g_*$. Then $\widetilde{E}$ has a second critical point at $\Sigma_{**} = \sigma(g_{**}) \neq \Sigma_*$. Let $\gamma : [0,1] \to \mathrm{SPD}_3$ be a geodesic (with respect to G) with $\gamma(0) = \Sigma_*$ and $\gamma(1) = \Sigma_{**}$. Then, by Rolle's Theorem applied to $(\widetilde{E} \circ \gamma)' : [0,1] \to \mathbb{R}$, there exists $t \in (0,1)$ at which $(\widetilde{E} \circ \gamma)''(t) = 0$. But this contradicts Proposition 12. □

Matrix Square Root Method for $\mathscr{L}_{24}$-Crystals

In the case of the standard massless $\mathscr{L}_{24}$-Skyrme model ($C_0 = 0$ and $C_6 = 0$), we can find the minimizing metric g_* explicitly. We note that, in this case

$$\widetilde{E}(\Sigma) = \mathrm{Tr}\big(H\Sigma^{-1} + F\Sigma\big), \tag{3.3.39}$$

whence

$$\mathrm{d}\widetilde{E}_\Sigma(\xi) = \mathrm{Tr}\big(-H\Sigma^{-1}\xi\Sigma^{-1} + F\xi\big) = \mathrm{Tr}\big((F - \Sigma^{-1}H\Sigma^{-1})\xi\big). \tag{3.3.40}$$

Hence, the unique critical point Σ_* of $\widetilde{E}$ satisfies the matrix equation

$$F = \Sigma_*^{-1}H\Sigma_*^{-1}, \tag{3.3.41}$$

which reduces nicely to a matrix square root problem

$$(F\Sigma_*)^2 = (\Sigma_*^{-1}H)^2 = FH \quad \Longrightarrow \quad \Sigma_* = (F^{1/2})^{-1}H^{1/2}. \tag{3.3.42}$$

Then, from the diffeomorphism (3.3.13), we have that $\det g_* = 1/(\det \Sigma_*)^2$ and, therefore, the $\mathscr{L}_{24}$-energy minimizing metric is determined to be

$$g_* = \frac{\Sigma_*}{\det \Sigma_*} = \left(\frac{\det F}{\det H}\right)^{1/2} F^{-1/2}H^{1/2}. \tag{3.3.43}$$

As a consistency check, we apply this matrix square root method to both the $\mathrm{S}_{1/2}$ and $\mathrm{BCC}_{1/2}$ crystals and obtain the same results as in Sec. 1.3.

We henceforth set $C_6 = 0$. In the case $C_0 \neq 0$, which is of primary interest in this chapter, we have not been able to solve for the minimum of $M_B(g)$ explicitly. Instead, we resort to a numerical method described in the next section.

3.4 The Numerical Method

We now return to the problem of primary interest: to minimize $E(\varphi, g)$ among all smooth maps $\mathbb{T}^3 \to \mathrm{SU}(2)$ of fixed degree B, and all flat metrics $g \in \mathrm{SPD}_3$. Our numerical scheme is similar to ones introduced in [65, 114] and based on the idea of arrested Newton flow. For fixed φ, we interpret M_B as a potential energy on the manifold SPD_3 and solve Newton's law of motion

$$\ddot{g} = -\mathrm{grad}_g M_B(\varphi, g) \tag{3.4.1}$$

with initial data $g(0) = g_0$. This solution begins to run "downhill" in SPD_3. We monitor $\mathcal{M}_B(\varphi, g(t))$ and, at any time t_* where $\frac{\mathrm{d}}{\mathrm{d}t}\mathcal{M}_B(\varphi, g(t)) > 0$ we arrest the flow, that is, stop and restart it at the current position but with velocity 0. The flow converges to the unique minimizing metric g_φ. We minimize over φ by a similar technique, solving

$$\ddot{\varphi} = -\mathrm{grad}_\varphi \mathcal{M}_B(\varphi, g_\varphi) \tag{3.4.2}$$

with initial data $\varphi(0) = \varphi_0$ (here $\mathrm{grad}_\varphi \mathcal{M}_B$ is the derivative in the first argument, φ, with g treated as constant). Again, we arrest the flow if $\mathcal{M}_B$ starts to increase.

In practice, we discretize space, placing φ on a cubic grid of N^3 points with lattice spacing $h = 1/N$ and periodic boundary conditions. We replace the spatial derivatives of φ occurring in E by finite difference approximations. This reduces the (3.4.2) to a system of ODEs in $\mathbb{R}^{4N^3}$, which we then solve using a 4th order Runge-Kutta scheme with fixed time step δt. The arresting criterion is that $\mathcal{M}_B(t + \delta t) > \mathcal{M}_B(t)$. After each iteration of the Runge-Kutta scheme, the metric g_φ is recalculated in a similar way by solving the ODE (3.4.1), using the metric g_φ from the previous iteration as initial datum. Once the flow for g has converged, the next iteration of φ is calculated, and so on. Each flow is deemed to have converged to a static solution if the sup norm of $\mathrm{grad}\mathcal{M}_B$ falls below some tolerance. The numerical results presented hereafter were obtained with $N = 201$. The time steps δ used were 0.0017 for the flow in φ and 0.1 for the flow in g. The tolerances were 10^{-5} for the flow in φ and 10^{-7} for the flow in g.

Implementing the method also entails choosing (formal) Riemannian metrics on SPD_3 and $C^\infty(\mathbb{T}^3, SU(2))$. These are required to make sense of both $\mathrm{grad}(\mathcal{M}_B)$ and the connexions ∇ occurring implicitly in (3.4.1) and (3.4.2). On SPD_3 we choose the Euclidean metric induced by identifying SPD_3 as a subset of $\mathbb{R}^9$ in the obvious way, that is

$$(\xi_1, \xi_2)_{\mathrm{SPD}_3} = \mathrm{Tr}\left(\xi_1^T \xi_2\right). \tag{3.4.3}$$

Note that this differs from the metric G used in section 3.3; it is simpler for the current purpose. On $C^\infty(\mathbb{T}^3, SU(2))$ we choose the L^2 metric defined by the volume form vol_0,

$$\left\langle \eta_1, \eta_2 \middle| \eta_1, \eta_2 \right\rangle_{L^2} = \int_{\mathbb{T}^3} h(\eta_1, \eta_2)\mathrm{vol}_0, \tag{3.4.4}$$

which is independent of g.

The gradient of $\mathcal{M}_B = E_2 + E_4 + E_0$ with respect to the field φ, regarded as a function on $C^\infty(\mathbb{T}^3, S^3)$, is

$$\begin{aligned}\frac{\delta \mathcal{M}_B}{\delta \varphi^\mu} = \sqrt{g}\frac{\partial V}{\partial \varphi^\mu} - 2\sqrt{g}g^{pa}\Big\{\partial_{pa}\varphi^\mu + g^{qb}\Big[\left(\partial_{pa}\varphi^\mu \partial_q\varphi^\alpha \partial_b\varphi^\alpha + \partial_p\varphi^\mu \partial_{qa}\varphi^\alpha \partial_b\varphi^\alpha + \partial_p\varphi^\mu \partial_q\varphi^\alpha \partial_{ba}\varphi^\alpha\right) \\ - \left(\partial_{qa}\varphi^\mu \partial_p\varphi^\alpha \partial_b\varphi^\alpha + \partial_q\varphi^\mu \partial_{pa}\varphi^\alpha \partial_b\varphi^\alpha + \partial_q\varphi^\mu \partial_p\varphi^\alpha \partial_{ba}\varphi^\alpha\right)\Big]\Big\}.\end{aligned} \tag{3.4.5}$$

Now, let us fix the field $\varphi : \mathbb{T}^3 \to S^3$ and think of the energy $\mathcal{M}_B$ as a function of the metric g on $\mathbb{T}^3$. That is, we define a map $E_\varphi : \mathrm{SPD}_3 \to \mathbb{R}$ such that $E_\varphi := \mathcal{M}_B(\varphi|_{\mathrm{fixed}}, g)$, where SPD_3 is the space of symmetric positive-definite 3×3-matrices. To minimize the energy functional E_φ with respect to variations of the metric g_s, we use arrested Newton flow on SPD_3 as detailed above. Now let g_s be a

smooth one-parameter curve in SPD_3 with $g_0 = F^* d$. Explicitly, we are solving the system of 2nd order ODEs

$$\frac{\mathrm{d}^2}{\mathrm{d}s^2}\bigg|_{s=0} (g_{ij})_s = -\frac{\partial E_\varphi}{\partial g_{ij}} = -\int_{\mathbb{T}^3} \mathrm{d}^3x \sqrt{g}\, S_\varphi^{ij}, \tag{3.4.6}$$

with initial condition $(g_{ij})_0 = \vec{X}_i \cdot \vec{X}_j$, and where $S_\varphi = S(g)$ is the stress-energy tensor for fixed field configuration φ. Setting $\dot{g}_s = \partial_s g_s$ as the velocity with initial velocity $\dot{g}_0 = \partial_s g_s\big|_{s=0} = 0$ reduces the problem to a coupled system of 1st order ODEs. We implement a 4th order Runge–Kutta method to solve this coupled system. The components of the stress-energy tensor for fixed field φ, given in the metric independent integral formulation, reads

$$\int_{\mathbb{T}^3} \mathrm{d}^3x \sqrt{g}\, S_\varphi^{ij} = \frac{1}{2} g^{ij} \left(\sqrt{g}\, C_6 - \frac{C_0}{\sqrt{g}} \right) + \sqrt{g} \left(\frac{1}{2} g^{kl} g^{ij} - g^{ik} g^{jl} \right) H_{kl} + \frac{1}{\sqrt{g}} \left(\partial^{ik} \partial^{jl} - \frac{1}{2} g_{kl} g^{ij} \right) F_{kl}. \tag{3.4.7}$$

3.5 $\mathscr{L}_{024}$-Skyrmion Crystals

This section presents the results of the numerical scheme just described in the charge $B_{\mathrm{cell}} = 4$ sector, concentrating on the model with normalized pion mass $m = 1$. Our approach is to treat the pion mass as a continuous variable parameter $m^2 = t \geq 0$: we minimize the energy

$$E_{(t)}(\varphi, g) = E_2(\varphi, g) + E_4(\varphi, g) + 2t \int_{\mathbb{T}^3} (1 - \sigma) \mathrm{vol}_g \tag{3.5.1}$$

starting in the massless case $t = 0$, and then increasing t gradually to 1.

We begin by recalling the lowest energy solution known in the massless $\mathscr{L}_{24}$-case, $t = 0$, that is, the $\mathrm{SC}_{1/2}$ crystal. This crystal is obtained using the matrix square root method with initial field configuration (1.3.20) and initial metric $g = \mathrm{Id}_3$. This solution is depicted in figure 3.1. In this orientation, it represents best a simple cubic lattice of half-skyrmions. That is, φ maps each of the eight sub-cubes of side length $L/2$ to either the upper ($\varphi_0 \geq 0$) or lower ($\varphi_0 \leq 0$) hemisphere of S^3, contributing charge $B = 1/2$ to the total topological charge of the unit cell. For this reason, we denote the $\mathrm{SC}_{1/2}$ crystal by $(\varphi_{1/2}, g_{1/2})$.

As we stressed in Sec. 1.3, it is important to note that the massless energy functional $E_{(0)} = E_2 + E_4$ is invariant under the natural action of SO(4) on the target three-sphere. That is, for all $(\varphi, g) \in \mathscr{M}$ and all $R \in \mathrm{SO}(4)$, $E_{(0)}(R\varphi, g) = E_{(0)}(\varphi, g)$, where $\mathscr{M} = C^\infty(\mathbb{T}^3, S^3) \times \mathrm{SPD}_3$ is the configuration space of skyrmion crystals, as before. Hence the solution described above is just one critical point of $E_{(0)}$ lying in a 6-dimensional family of critical points, its orbit under SO(4). If we now switch on the pion mass, that is, consider $E_{(t)}$ for small $t > 0$, we may ask which (if any) of these critical points survive the perturbation. It is useful to switch perspective slightly: rather than fixing the perturbation and considering what happens to all points in the SO(4) orbit of the $\mathrm{SC}_{1/2}$ crystal, it is convenient to fix the field and metric to be the $\mathrm{SC}_{1/2}$ crystal, and consider what happens to this fixed configuration under the SO(4) orbit of the perturbation. That is, we ask for which $p \in S^3$, if any, does the $\mathrm{SC}_{1/2}$ crystal $(\varphi_{1/2}, g_{1/2})$ lie in a curve $(\varphi(t), g(t))$ of critical points of the t-parametrized family of functions

$$E^p_{(t)}(\varphi, g) = E_2(\varphi, g) + E_4(\varphi, g) + 2t \int_{\mathbb{T}^3} (1 - p \cdot \varphi) \mathrm{vol}_g. \tag{3.5.2}$$

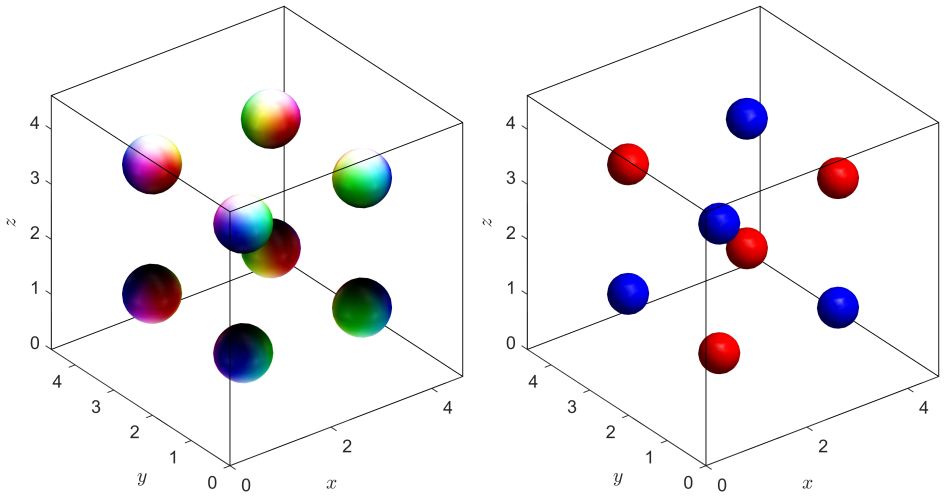

Figure 3.1: Plots of the (a) baryon density $\mathscr{B}^0$ and (b) the σ-field, where the vacuum ($\sigma = +0.9$) is colored red and the anti-vacuum ($\sigma = -0.9$) blue, for the $\mathrm{SC}_{1/2}$ skyrmion crystal with unit cell charge $B_{\mathrm{cell}} = 4$. Note that the solution has been translated by $x^i \mapsto x^i + L/4$.

(We recover the original function $E_{(t)}$ by choosing $p = (1, 0, 0, 0)$.) To answer this question, we will need to understand the symmetries of the $\mathrm{SC}_{1/2}$ crystal in some detail.

We recall that the energy of the massless $\mathscr{L}_{24}$-Skyrme model $E_{(0)} : \mathscr{M} \to \mathbb{R}$ is invariant under the left action of $G = \mathrm{SO}(4) \times \mathrm{Aut}(\mathbb{T}^3)$ on $\mathscr{M}$,

$$(R, S) \cdot (\varphi, g) = (R \circ \varphi \circ S^{-1}, (S^{-1})^* g). \tag{3.5.3}$$

The $\mathrm{SC}_{1/2}$ crystal $(\varphi_{1/2}, g_{1/2})$ is a critical point (in fact a minimum) of $E_{(0)}$. Its stabilizer Γ (the subgroup of $\mathrm{SO}(4) \times \mathrm{Aut}(\mathbb{T}^3)$ that leaves it fixed) is an order 192 group generated by

$$\begin{aligned} R(\varphi) &= (\varphi_0, \varphi_2, \varphi_3, \varphi_1), & S(\vec{x}) &= (x_2, x_3, x_1), \\ R(\varphi) &= (\varphi_0, \varphi_2, -\varphi_1, \varphi_3), & S(\vec{x}) &= (x_2, -x_1, x_3), \\ R(\varphi) &= (-\varphi_0, -\varphi_1, \varphi_2, \varphi_3), & S(\vec{x}) &= (x_1 + \tfrac{1}{2}, x_2, x_3). \end{aligned} \tag{3.5.4}$$

The image of the natural projection $\pi : \Gamma \to SO(4)$ is naturally isomorphic to the octahedral group O_h, and the kernel is isomorphic to $\mathbb{Z}_2 \times \mathbb{Z}_2$.

Once we turn on the perturbation, the symmetry group of the energy function $E^p_{(t)}$ is broken to $\mathrm{SO}(3)_p \times \mathrm{Aut}(\mathbb{T}^3)$ where

$$\mathrm{SO}(3)_p = \{R \in \mathrm{SO}(4) : Rp = p\}. \tag{3.5.5}$$

Let us define the reduced stabilizer of the $\mathrm{SC}_{1/2}$ crystal to be

$$\Gamma_p = \Gamma \cap (\mathrm{SO}(3)_p \times \mathrm{Aut}(\mathbb{T}^3)), \tag{3.5.6}$$

and the set of fixed points of Γ_p in $\mathscr{M}$ to be

$$\mathscr{M}^{\Gamma_p} = \{(\varphi, g) \in \mathscr{M} : \forall q \in \Gamma_p,\ q \cdot (\varphi, g) = (\varphi, g)\}. \tag{3.5.7}$$

Formally, this is a submanifold of $\mathscr{M}$, and it contains $(\varphi_{1/2}, g_{1/2})$ for all p, by construction. By the Principle of Symmetric criticality, a point $(\varphi, g) \in \mathscr{M}^{\Gamma_p}$ is a critical point of $E^p_{(t)}$ if (and only if) it is a critical point of its restriction $E^p_{(t)}| : \mathscr{M}^{\Gamma_p} \to \mathbb{R}$. For generic choices of $p \in S^3$ we expect Γ_p to be trivial, so that $\mathscr{M}^{\Gamma_p} = \mathscr{M}$, and this observation confers no advantage. The interesting case is when the intersection of $\mathscr{M}^{\Gamma_p}$ with the G orbit of $(\varphi_{1/2}, g_{1/2})$ is (locally) just $(\varphi_{1/2}, g_{1/2})$. Then $(\varphi_{1/2}, g_{1/2})$ is an *isolated* critical point of $E_{(0)}| : \mathscr{M}^{\Gamma_p} \to \mathbb{R}$. If, as seems likely, it is also a *nondegenerate* critical point of $E^p_{(0)}|$ (meaning that the Hessian of $E^p_{(0)}|$ at $(\varphi_{1/2}, g_{1/2})$ is nondegenerate), then the persistence of a critical point for $t > 0$ sufficiently small follows from the Inverse Function Theorem applied to $\mathrm{d}E^p_{(t)}|$. That is, there exists $\varepsilon > 0$ and a (unique) smooth curve $\gamma : (-\varepsilon, \varepsilon) \to \mathscr{M}^{\Gamma_p}$ such that $\gamma(0) = (\varphi_{1/2}, g_{1/2})$ and $\mathrm{d}E^p_{(t)}|_{\gamma(t)} = 0$ for all $t \in (-\varepsilon, \varepsilon)$.

To summarize, we expect $(\varphi_{1/2}, g_{1/2})$ to smoothly deform into a critical point of $E^p_{(t)}$ (as t increases from 0) if p is chosen so that a neighbourhood of $(\varphi_{1/2}, g_{1/2})$ in $\mathscr{M}^{\Gamma_p}$ intersects the G orbit of $(\varphi_{1/2}, g_{1/2})$ only at $(\varphi_{1/2}, g_{1/2})$. Let us call this condition the *isolation condition*. The next task is to understand this condition on p at an algebraic level.

Assume that p fails the isolation condition. Then there exists a regular curve $q : (-\varepsilon, \varepsilon) \to G$ with $q(0) = e$ such that, for all t, $q(t) \cdot (\varphi_{1/2}, g_{1/2}) \in \mathscr{M}^{\Gamma_p}$ or, more explicitly, for all $Q \in \Gamma_p$, and $t \in (-\varepsilon, \varepsilon)$

$$\begin{aligned} Q \cdot q(t) \cdot (\varphi_{1/2}, g_{1/2}) &= q(t) \cdot (\varphi_{1/2}, g_{1/2}) \\ \Rightarrow \quad [q(t)^{-1} Q q(t)] \cdot (\varphi_{1/2}, g_{1/2}) &= (\varphi_{1/2}, g_{1/2}). \end{aligned} \tag{3.5.8}$$

Hence, for all $Q \in \Gamma_p$ and t, $q(t)^{-1} Q q(t) \in \Gamma$. But Γ is discrete (in fact, finite), so for all t and Q,

$$q(t)^{-1} Q q(t) = q(0)^{-1} Q q(0) = Q \tag{3.5.9}$$

$$\Rightarrow \quad Q q(t) Q^{-1} = q(t). \tag{3.5.10}$$

The derivative of this equation at $t = 0$ implies that there exists some nonzero $\xi \in \mathfrak{g}$ (the Lie algebra of G), namely $\xi = \dot{q}(0)$, such that $Ad_Q \xi = \xi$. Conversely, given a nonzero $\xi \in \mathfrak{g}$ such that $Ad_Q \xi = \xi$ for all $Q \in \Gamma_p$, we can construct a curve $\gamma(t) = \exp(t\xi)$ such that $\gamma(t) \cdot (\varphi_{1/2}, g_{1/2})$ remains in $\mathscr{M}^{\Gamma_p}$. Hence, the isolation condition is that, for all $\xi \in \mathfrak{g} \setminus \{0\}$, there exists some $Q \in \Gamma_p$ such that $Ad_Q \xi \neq \xi$. More succinctly: p satisfies the isolation condition if and only if the adjoint representation of Γ_p on $\mathfrak{g}$ contains no copies of the trivial representation.

This reduces the problem to one in the representation theory of subgroups of O_h. Given a subgroup H of $O_h \subset \mathrm{SO}(4)$, we determine whether its action on $\mathbb{R}^4$ contains copies of the trivial representation. If not, it cannot arise as $\pi(\Gamma_p)$ for any choice of p. If it does, $\pi^{-1}(H)$ is a candidate for Γ_p for any p in a one-dimensional invariant subspace of the action. This produces a short list of candidate subgroups. For each of these we count copies of the trivial representation in the adjoint representation of $\pi^{-1}(H)$ on $\mathfrak{g}$. If there are none, this is a candidate for Γ_p for p satisfying the isolation condition.

The results are summarized in table 3.1. We find 28 points p for which $(\varphi_{1/2}, g_{1/2})$ is an isolated critical point of $E^p_{(0)}$ in $\mathscr{M}^{\Gamma_p}$, falling into 4 distinct classes. One class is $p \in \{(1,0,0,0), (-1,0,0,0)\}$. The other three classes all have $p_0 = 0$ and hence $(p_1, p_2, p_3) \in S^2 \subset \mathbb{R}^3$, pointing along some symmetry line of the unit cube: towards the centre of a face (e.g. $p = (0,0,0,1)$), the centre of an edge (e.g. $p = (0,1,1,0)/\sqrt{2}$) or a vertex (e.g. $p = (0,1,1,1)/\sqrt{3}$).

p	$\lvert\Gamma_p\rvert$	$\pi(\Gamma_p)$	Description as subgroup of O_h	g	label
$(1,0,0,0)$	96	O	Orientation preserving	$\mathrm{diag}(a,a,a)$	$\mathrm{SC}_{1/2}$ crystal
$(0,0,0,1)$	32	C_{4v}	Maps a face to itself	$\mathrm{diag}(a,a,b)$	multi-wall
$(0,0,1,1)/\sqrt{2}$	16	C_{2v}	Maps an edge to itself	$\mathrm{diag}(a,b,b)$	chain
$(0,1,1,1)/\sqrt{3}$	24	C_{3v}	Maps a vertex to itself	$\mathrm{diag}(a,a,a)$	α-crystal

Table 3.1: Points $p \in S^3$ for which the $\mathrm{SC}_{1/2}$ crystal is isolated in $\mathscr{M}^{\Gamma_p}$, and hence is expected to continue to a critical point of the massive Skyrme model. The leftmost column gives one representative point in each class. Subsequent columns record the order of the corresponding stabilizer $\Gamma_p \subset \Gamma$, the image of Γ_p in $\pi(\Gamma) = O_h$, its description as a subgroup of the group of symmetries of the cube, the most general metric consistent with the symmetry, and a descriptive label of the corresponding crystal.

To do numerics, we switch back to the viewpoint of internally rotating the field $\varphi_{1/2}$, rather than the energy functional, that is, we set $p = (1,0,0,0)$ in $E^p_{(t)}$ and start with the configuration

$$\varphi = Q\varphi_{1/2}, \qquad g = g_{1/2}, \tag{3.5.11}$$

where Q is any $\mathrm{SO}(4)$ matrix whose top row is p (the inverse of an $\mathrm{SO}(4)$ matrix mapping $(1,0,0,0) \mapsto p$). We then minimize $E_{(t)}$ using arrested Newton flow for a sequence of pion masses $m = t$ starting at $t = 0$ and ending at $t = 1$. As expected each of the 4 types of critical point smoothly continues. Somewhat unexpectedly, they are all, as far as we can determine, local minima of $E_{(t)}$; none are saddle points. We have checked this by perturbing the solutions with random perturbations breaking all symmetries, finding that they always relax back to the solutions presented.

The solutions at normalized pion mass $m = 1$ are depicted in figure 3.2, labelled as in the final column of table 3.1. Ordered by energy, we find multi-wall < chain < α-crystal < $\mathrm{SC}_{1/2}$ crystal, though the chain and α-crystals are so close in energy that their order is somewhat uncertain. The energies per baryon per unit cell are

$$\begin{aligned} \frac{E_{1/2}}{B} &= 1.2417 \times 12\pi^2 = 147.058, \\ \frac{E_\alpha}{B} &= 1.2368 \times 12\pi^2 = 146.479 \\ \frac{E_{\text{chain}}}{B} &= 1.2368 \times 12\pi^2 = 146.479 \\ \frac{E_{\text{multi-wall}}}{B} &= 1.2365 \times 12\pi^2 = 146.451. \end{aligned} \tag{3.5.12}$$

Neither the multi-wall crystal nor the chain crystal has an isotropic metric, meaning these crystals do *not* have a cubic period lattice. The α-crystal and the $\mathrm{SC}_{1/2}$ crystal do have cubic period lattices, as is consistent with our symmetry analysis (see column 5 of table 3.1). The minimal metrics are

$$\begin{aligned} g_{1/2} &= L^2\mathbb{I}_3, && L = 3.202, \\ g_\alpha &= L^2\mathbb{I}_3, && L = 3.278, \\ g_{\text{chain}} &= \mathrm{diag}(L_1^2, L_2^2, L_2^2), && L_1 = 3.221, \quad L_2 = 3.312, \\ g_{\text{multi-wall}} &= \mathrm{diag}(L_1^2, L_1^2, L_2^2), && L_1 = 3.222, \quad L_2 = 3.442 \end{aligned} \tag{3.5.13}$$

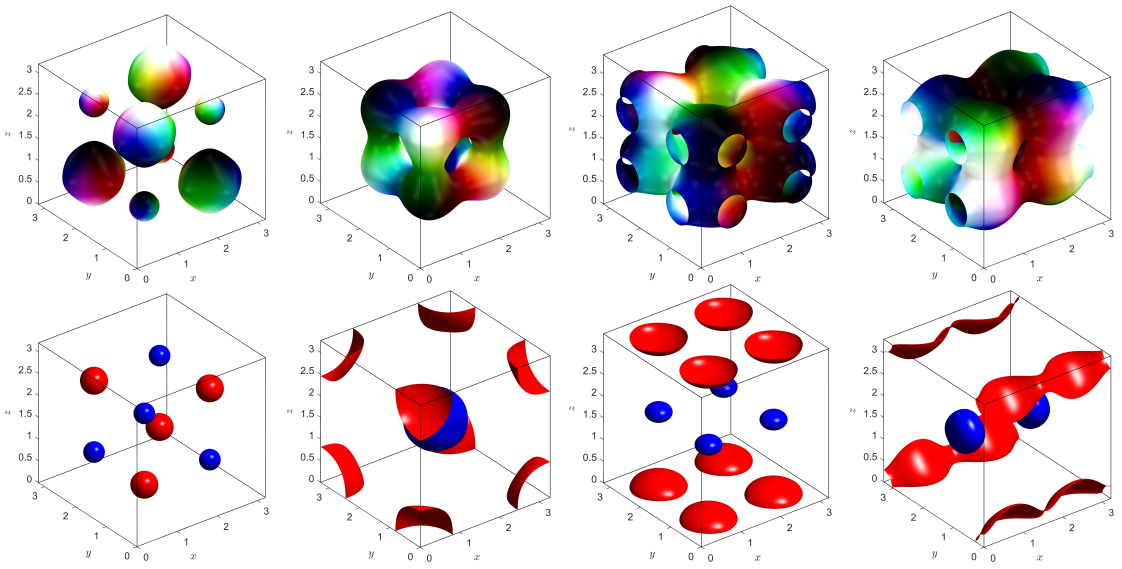

(a) $SC_{1/2}$ crystal (b) α-crystal (c) multi-wall crystal (d) chain crystal

Figure 3.2: $\mathscr{L}_{024}$-Skyrme crystals in the model with normalized pion mass $m = 1$. The top row is the isosurface plots of the baryon density. The bottom row is isosurface plots of the φ_0 field, where the vacuum ($\sigma = +0.9$) is colored red and the anti-vacuum ($\sigma = -0.9$) blue.

from which we deduce that the unit cells for the multi-wall and chain crystals are trigonal (cuboidal with one pair of periods equal), but with opposite types of distortion: the multi-wall's unit cell is a stretched cube, the chain's a squashed cube. Interestingly, the ordering of the volumes of the solutions' unit cells is the reverse of the ordering of their energies, with the multi-wall crystal occupying the greatest volume and the 1/2-crystal the least.

Restricting the kinetic energy functional of the model to the isospin orbit of a given static solution we obtain a left invariant metric on SO(3) called the isospin inertia tensor, which is of some significance in the method of rigid body quantization [51, 52]. The kinetic energy associated with the potential $\mathscr{L}_{024}$-energy, $M_B = E_2 + E_4 + E_0$, is

$$T(\varphi, \dot{\varphi}) = \int_{\mathbb{T}^3} \left[\dot{\varphi} \cdot \dot{\varphi} + g^{ij} \left\{ (\dot{\varphi} \cdot \dot{\varphi})\, (\partial_i \varphi \cdot \partial_j \varphi) - (\dot{\varphi} \cdot \partial_i \varphi)\, (\dot{\varphi} \cdot \partial_j \varphi) \right\} \right] \mathrm{vol}_g. \tag{3.5.14}$$

Writing $\dot{\varphi} = X^i J_i \varphi$, with J_i being the basis for $\mathfrak{so}(3)$ given by

$$J_1 = \begin{pmatrix} 0 & 0 & 0 & 0 \\ 0 & 0 & 0 & 0 \\ 0 & 0 & 0 & -1 \\ 0 & 0 & 1 & 0 \end{pmatrix}, \quad J_2 = \begin{pmatrix} 0 & 0 & 0 & 0 \\ 0 & 0 & 0 & 1 \\ 0 & 0 & 0 & 0 \\ 0 & -1 & 0 & 0 \end{pmatrix}, \quad J_3 = \begin{pmatrix} 0 & 0 & 0 & 0 \\ 0 & 0 & -1 & 0 \\ 0 & 1 & 0 & 0 \\ 0 & 0 & 0 & 0 \end{pmatrix}, \tag{3.5.15}$$

we find that $T(\varphi, \dot{\varphi}) = \frac{1}{2} X^i U_{ij} X^j$, where U is the symmetric matrix given by

$$U_{ij} = 2 \int_{\mathbb{T}^3} \mathrm{d}^3 x \sqrt{g} \left[\delta_{ij} \varphi_k \varphi_k - \varphi_i \varphi_j + g^{kl} (\delta_{ij} - \varphi_i \varphi_j) \partial_k \varphi_0 \partial_l \varphi_0 \right.$$
$$\left. + g^{kl} (\varphi_m \varphi_m \partial_k \varphi_i \partial_l \varphi_j + \varphi_0 \varphi_j \partial_k \varphi_0 \partial_l \varphi_i + \varphi_0 \varphi_i \partial_l \varphi_0 \partial_k \varphi_j) \right] \tag{3.5.16}$$

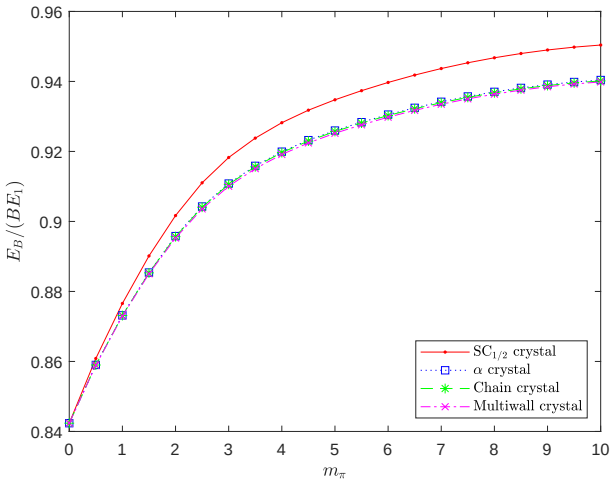

Figure 3.3: Comparison of the normalized energies per baryon per unit cell of the four Skyrme crystals for increasing pion mass m. Energies are presented in units of the energy of the $B = 1$ skyrmion at the relevant pion mass (which grows monotonically with m).

and repeated indices are summed from 1 to 3. We find that, except for the SC$_{1/2}$ crystal, this matrix is *not* isotropic:

$$\begin{aligned} U^{1/2} &= \begin{pmatrix} 165.2 & 0 & 0 \\ 0 & 165.2 & 0 \\ 0 & 0 & 165.2 \end{pmatrix}, \\ U^{\alpha} &= \begin{pmatrix} 135.5 & 0 & 0 \\ 0 & 135.5 & 0 \\ 0 & 0 & 167.3 \end{pmatrix} \\ U^{\text{chain}} &= \begin{pmatrix} 135.6 & 0 & 0 \\ 0 & 135.7 & 0 \\ 0 & 0 & 167.2 \end{pmatrix}, \\ U^{\text{multi-wall}} &= \begin{pmatrix} 135.8 & 0 & 0 \\ 0 & 135.8 & 0 \\ 0 & 0 & 166.8 \end{pmatrix}. \end{aligned} \tag{3.5.17}$$

As far as we are aware, in addition to the SC$_{1/2}$ crystal, only the α-crystal has been previously determined in the massive Skyrme model [29]. Neither of these is the minimal energy crystal.

It is interesting to track the energy as a function of pion mass, see figure 3.3. As m increases, all of the crystals' energies increase relative to that of the one-skyrmion. This is an indication that classical binding energies will be small (and hence close to experimental values) when m is large. Amongst the various crystal solutions, we find that the multi-wall, chain and α-crystals remain close in energy, with stable order, but the gap to the SC$_{1/2}$ crystal (which always has highest energy) grows with m.

3.6 $\mathscr{L}_{024}$-Skyrmion Crystals at Fixed Baryon Density

If we are to use Skyrme crystals as a model of dense nuclear matter (for example, in astrophysical contexts) it is important to understand the properties of the lowest energy configuration among all those with a fixed average baryon *density*, treating this density as a parameter of our system. This problem was first approached by Hen and Karliner [72] in the context of the baby Skyrme model. Therein they extremized the baby Skyrme energy functional with respect to variations of the period lattice at a constant skyrmion density. This method was carried out at various densities, producing an energy-density curve. However, they did not address the nature of the critical points they obtained, stating that they could in fact turn out to be maxima or saddle points. Our method is similar but it is more general and robust.

Let us fix B_{cell}, the baryon number per unit cell. Then the average baryon density of a configuration (φ, g) is

$$\rho_B = \frac{B_{\text{cell}}}{\int_{\mathbb{T}^3} \text{vol}_g} = \frac{B_{\text{cell}}}{\sqrt{\det g}}. \tag{3.6.1}$$

Hence, finding the minimal crystal with fixed baryon density (and baryon number B_{cell} per unit cell) amounts to minimizing $M_B : \mathscr{M} \to \mathbb{R}$ over a level set of $\det g$. Once again, we can address the partial minimization problem where we fix the field $\varphi : \mathbb{T}^3 \to SU(2)$ (assumed to be C^1 and somewhere immersive) and a density $\rho_B = B_{\text{cell}}/\nu$ then seek a minimum of $M_B(\varphi, \cdot) : \det^{-1}(\nu^2) \to \mathbb{R}$. It turns out that, like the unconstrained minimization problem studied in section 3.3, this problem has a unique global minimum and no other critical points.

Proposition 14. *Let $\varphi : \mathbb{T}^3 \to \text{SU}(2)$ be a fixed C^1 map that is immersive somewhere and $\nu > 0$ be a constant. Then the function $\text{SPD}_3 \supset \det^{-1}(\nu^2) \to \mathbb{R}$ mapping each flat metric g on $\mathbb{T}^3$ of volume ν to the Skyrme energy $M_B(\varphi, g)$ attains a unique global minimum, and has no other critical points.*

Proof. As before, it is equivalent to prove that the associated function

$$\widetilde{E} : \det^{-1}(\nu^{-1}) \to \mathbb{R}, \quad \widetilde{E} = M_B \circ \sigma^{-1} \tag{3.6.2}$$

attains a unique global minimum and has no other critical points, where $\sigma : \text{SPD}_3 \to \text{SPD}_3$ is the diffeomorphism $\sigma(g) = g/\sqrt{\det g}$. Now

$$\widetilde{E}(\Sigma) = \text{Tr}\big(H\Sigma^{-1}\big) + \text{Tr}(F\Sigma) + C_0\nu + C_6\nu^{-1} \tag{3.6.3}$$

where $H, F \in \text{SPD}_3$ and $C_0, C_6 \in [0, \infty)$ are the φ-dependent constants previously defined. Existence of a global minimum of $\widetilde{E}$ follows *mutatis mutandis* from Proposition 10, since the bound (3.3.24) still holds irrespective of the extra constraint $\lambda_1\lambda_2\lambda_3 = \nu^{-1}$ (equivalent to $\det \Sigma = \nu^{-1}$). This confines the minimizing sequence to a compact subset of the hypersurface $\lambda_1\lambda_2\lambda_3 = \nu^{-1}$ in $(0, \infty)^3 \times O(3)$, whence a convergent subsequence can be extracted, whose limit attains the infimum of $\widetilde{E}$ by continuity.

It remains to prove uniqueness. Assume towards a contradiction that $\widetilde{E} : \det^{-1}(\nu^{-1}) \to \mathbb{R}$ has two distinct critical points Σ_*, Σ_{**}. Then there exists a geodesic

$$\gamma(t) = A \exp(\xi t) A^T \tag{3.6.4}$$

in (SPD_3, G) with $\gamma(0) = \Sigma_*$ and $\gamma(1) = \Sigma_{**}$. Now

$$\det \gamma(t) = (\det A)^2 \det \exp(\xi t) = (\det A)^2 \exp\left(t \operatorname{Tr} \xi\right) \tag{3.6.5}$$

and $\det\big(\gamma(0)\big) = \det\big(\gamma(1)\big)$, so $\operatorname{Tr}\xi = 0$ and we conclude that $\det\big(\gamma(t)\big)$ is constant. Hence the geodesic γ remains on the level set $\det^{-1}(\nu^{-1})$. Since Σ_*, Σ_{**} are critical points of $\widetilde{E} : \det^{-1}(\nu^{-1}) \to \mathbb{R}$, and γ is tangent to the level set for all t, $(\widetilde{E} \circ \gamma)'(0) = 0 = (\widetilde{E} \circ \gamma)'(1)$, so by Rolle's Theorem $(\widetilde{E} \circ \gamma)''$ vanishes somewhere on $(0, 1)$, contradicting the convexity of $\widetilde{E}$ (Proposition 12). Hence no second critical point may exist. □

In the course of the proof above we established that all level sets of det are connected totally geodesic submanifolds of (SPD_3, G), and hence the restriction of $\widetilde{E}$ to any such level set is strictly convex. Note that, in general, the restriction of a convex function to a submanifold may fail to be convex, so total geodesicity of the level sets is crucial here.

We can again solve the minimization problem for $E : \det^{-1}(\nu^2) \to \mathbb{R}$ numerically by arrested Newton flow, but now we must take care to project the gradient of E tangent to the level set. Given a curve $g(t)$ in $\det^{-1}(\nu^2)$, we require

$$\left.\frac{\mathrm{d}}{\mathrm{d}t}\right|_{t=0} \det g(t) = \nu^2 \operatorname{Tr}\big(g(0)^{-1}\dot{g}(0)\big) = 0 \tag{3.6.6}$$

so $\dot{g}(0)$ is orthogonal to $g(0)^{-1}$ with respect to the Euclidean metric $\langle X, Y | X, Y\rangle = \operatorname{Tr}\big(X^T Y\big)$. That is, $\dot{g}(0)$ has to be an element of the space of traceless parallel symmetric bilinear forms $\mathscr{E}_0$. Hence $T_g \det^{-1}(\nu^2) = \big\langle g^{-1} \big| g^{-1}\big\rangle^{\perp}$. Now

$$E(g(t)) = \nu \operatorname{Tr}\big(Hg^{-1}\big) + \frac{\operatorname{Tr}(Fg)}{\nu} + C_0\nu + \frac{C_6}{\nu}, \tag{3.6.7}$$

and hence

$$\mathrm{d}E_g(v) = \frac{1}{\nu}\left\langle F - \nu^2 g^{-1}Hg^{-1}, v \middle| F - \nu^2 g^{-1}Hg^{-1}, v\right\rangle. \tag{3.6.8}$$

It follows that, with respect to the metric on $\det^{-1}(\nu^2)$ induced by the Euclidean metric,

$$(\mathrm{grad}E)(g) = \frac{1}{\nu}\left\{F - \nu^2 g^{-1}Hg^{-1} - \frac{\operatorname{Tr}\big((F - \nu^2 g^{-1}Hg^{-1})g^{-1}\big)}{\operatorname{Tr}\big(g^{-1}g^{-1}\big)}g^{-1}\right\}. \tag{3.6.9}$$

We solve the Newton flow $\ddot{g} = -(\mathrm{grad}E)(g)$ numerically, projecting g back onto $\det^{-1}(\nu^2)$ after each time step by radial dilation $\big(g \mapsto (\nu^2/\det g)^{1/3} g\big)$, arresting if $E(g(t + \delta t)) > E(g(t))$, and terminating if the sup norm of $\mathrm{grad}E$ falls below a prescribed tolerance. As for the unconstrained problem, we apply this algorithm after each iteration of the arrested Newton flow for the field $\varphi : \mathbb{T}^3 \to S^3$.

Applying this approach at various densities to the four crystals found in section 3.5 at pion mass $m = 1$, we observe that the three lower energy crystals tend to finite-energy solutions at low densities. The α-crystal tends to the $B = 4$ α-particle skyrmion on $\mathbb{R}^3$ [21], see figure 3.4. This phase transition has already been observed by Silva Lobo [45] in the massless model and by Adam *et al.* [46] in the massive model with sextic term. The multi-wall crystal tends to a double-layered square sheet on $\mathbb{T}^2 \times \mathbb{R}$, similar to the 2-wall massless solution found by Silva Lobo and Ward [50]. Finally, the chain crystal becomes a linear chain on $\mathbb{R}^2 \times S^1$, which appears to be a previously unknown solution.

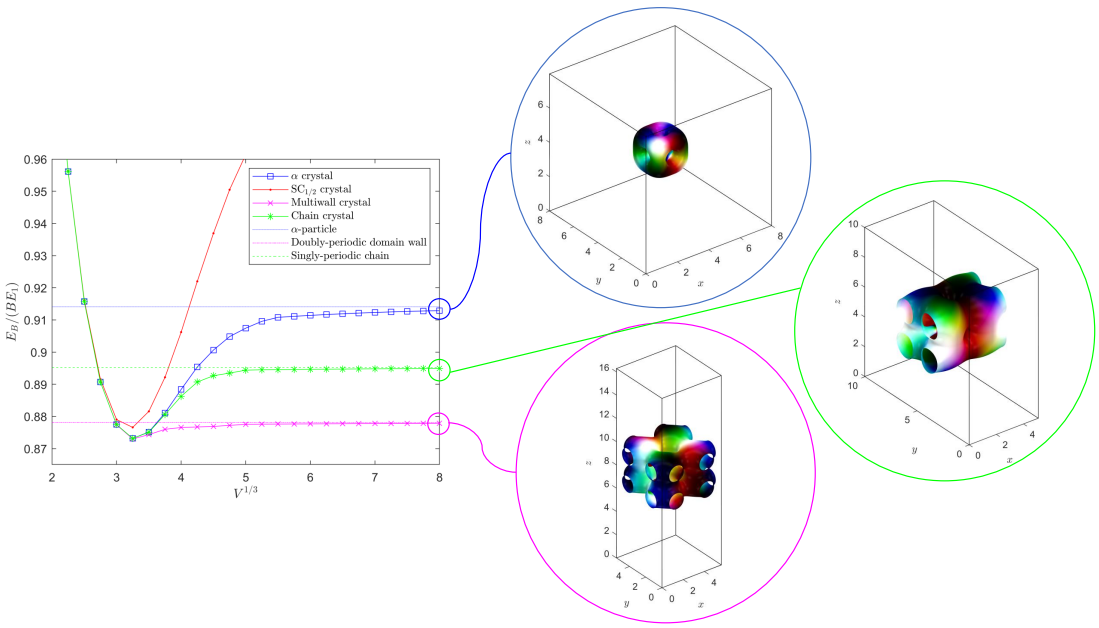

Figure 3.4: The energy per baryon per unit cell of the Skyrme crystals in the model with normalized pion mass $m = 1$ as a function of cell volume.

At low densities the multi-wall solution is clearly energetically preferred over other solutions. This qualitative result was predicted earlier in [115]. However, there are some important differences between between our result and [115]. Our result comes from a minimization over all Skyrme fields and lattice geometries, whereas [115] used the more restrictive Atiyah–Manton approximation for the Skyrme field and assumed symmetric lattice geometries. Second, our minimal-energy Skyrme multi-wall has a square geometry, whereas those constructed in [115] had a hexagonal geometry. Finally, our results are for the model with $m = 1$, whereas [115] considered $m = 0$.

As one might expect, the four crystals become energetically indistinguishable in the large density limit. As far as we can determine, the curves in figure 3.4 never cross, so we assume that the crystals maintain their energy ordering at all densities.

3.7 Concluding Remarks

In this chapter, we developed methods to obtain skyrmion crystals in a general class of Skyrme models, and presented a detailed numerical study of crystals in the standard Skyrme model with massive pions. To achieve this, we minimized the model's energy with respect to variations of both the field and its period lattice in $\mathbb{R}^3$. A key idea is to reformulate the latter variation as a variation over all flat metrics on the fixed unit torus $\mathbb{T}^3$. We obtained strong results on the partial minimization problem in which the field is fixed and only the metric varied: under a mild non-degeneracy assumption on the field, there exists a unique flat metric that globally minimizes the Skyrme energy, and no other critical metrics. This result holds also if we constrain the problem to vary only over metrics of fixed volume, a variant relevant to constructing skyrmion crystals of fixed

baryon density, i.e. determine an **equation of state**. Our methods impose no symmetry on the period lattice *a priori*, and hence go beyond previous studies which imposed a cubic unit cell.

We find that the minimal energy crystal (with baryon number $B_{\text{cell}} = 4$ per unit cell) has trigonal but not cubic periodicity. At low densities it tends to a double sheet solution. The next lowest energy crystal is also trigonal and not cubic, tending to a chain solution at low densities. Both these crystals are new. Above them in energy are two already known solutions, the α-crystal and the $\text{SC}_{1/2}$ crystal. All these crystals, except the most energetic, the $\text{SC}_{1/2}$ crystal, have anisotropic isospin inertia tensors. The existence of four distinct crystals can be understood semi-analytically by means of the Principle of Symmetric Criticality and the Inverse Function Theorem.

The methods detailed in this chapter can be applied to the study of isospin (a)symmetric nuclear matter within the Skyrme model. The next step would be to investigate neutron stars by considering the quantum corrections to the energy due to the quantization of the isospin degrees of freedom, and improve on the work done on neutron crystals in the massless $\mathscr{L}_{24}$-model by Baskerville [51]. In particular, one could determine "nuclear pasta" phases in neutron stars [116] by considering the quantization of generalized skyrmion crystals in the low density regime. The chain crystal we have found could correspond to the so-called "spaghetti" phase, and the multi-wall crystal the "nuclear lasagne". This is what we do in the succeeding chapter.

Four

Generalized Skyrmion Crystals with Applications to Neutron Stars

This chapter is based on the work in the joint paper with M. Huidobro and A. Wereszczynski [117].

4.1 Introduction

A natural field of application of the Skyrme model is to dense nuclear matter, particularly compact stars such as neutron stars [54, 118–125] and black holes [126–133]. In the present chapter we choose to focus on the former. The study of neutron stars can be approached by considering the crystalline structure of nuclear matter at finite densities, a problem of which we have resolved within the Skyrme framework in the preceding chapter. We showed that varying the density of the unit cell (while keeping the baryon number fixed) allows one to study nuclear matter at finite densities and, inter alia, to obtain an equation of state. Taking the advantage of the Tolman–Oppenheimer–Volkoff construction, one then obtains neutron stars by coupling the theory to gravity and considering the matter to be that of a perfect fluid [120].

Typically, there are five regions in a neutron star, all at different nuclear densities n_B. The accretion of material onto a neutron star can form a liquid ocean of ions with electron gases. At the bottom of this ocean material freezes and forms the denser outer crust, consisting of Coulomb crystals and degenerate electrons. Let us delve deeper into the star, with increasing density (still below saturation, $n_B < n_0$). At these densities, the electron Fermi energy is high and fuels electron capture reactions $e + p \to n + \nu_e$. Thus, nuclei in outer crust become more neutron rich with the increasing density, until they become so neutron rich that neutrons are forced out of these ions. This density is known as the neutron drip line and is the boundary separating the inner and outer crusts. So, the inner crust is composed of neutron rich Coulomb crystals, a relativistic and degenerate electron gas, and a gas of almost free neutrons. Below the inner crust, we are at densities approaching saturation $n_B \approx n_0$, where matter is dominated by the opposing interaction of the short range nuclear strong force and the long range Coulomb repulsion. This competition can cause the nearly spherical nuclei to form into more complex atomic structures such as nuclear pastas, e.g. tubes of spaghetti or sheets of lasagna [134, 135]. The most dense region is the core ($n_B > n_0$), where one expects to find a perfect fluid of neutron rich matter with electrons. For a more in-depth review of the structure of a neutron star see, e.g., Caplan and Horowitz [136].

Previous applications of the Skyrme model to the construction of neutron stars were based on the assumption of the $SC_{1/2}$ crystal being the ground state. That, coupled with the simple approximation of Kugler and Shtrikman [39], made it relatively straightforward to determine an

EoS by restricting the period lattice to be cubic at all densities. Even if one accepts this constrained approach, three important physical issues are still to be addressed:

i. $n_B > n_0$: the EoS is too soft, giving rise to neutron stars that are too light.

ii. $n_B < n_0$: the presence of a minimum at saturation in the EoS yields negative pressure, which represents a thermodynamically unstable phase at low density.

iii. $n_B = n_0$: nuclear binding energies are too large, which in turn means the compression modulus is too large.

The too softness of the standard $\mathscr{L}_{024}$-Skyrme model EoS was remedied by extension to the generalized $\mathscr{L}_{0246}$-Skyrme model. Indeed, the $\mathscr{L}_6$ term was essential not only to significantly increase the value of the maximal mass of neutron star (from $1.7\mathcal{M}_\odot$ [123] to above $2\mathcal{M}_\odot$ [54]), but also to render nuclear matter more like a perfect fluid, especially at higher densities, which corresponds very well to the standard picture of a (super-)fluid core of neutron star. These results are deeply anchored in the mathematical properties of the sextic term. Namely, if treated together with the (pion mass) potential term, the corresponding $\mathscr{L}_{06}$ energy-momentum tensor has a perfect fluid form [137]. In addition, it enjoys a volume preserving diffeomorphism symmetry which means that the energy of a solution is degenerate for all deformations which do not change its volume [104]. On the contrary, deformations that change the volume are strongly penalized as the corresponding EoS has a maximally stiff form [120, 121]. This agrees with a physical interpretation of the sextic term as a part of the action which effectively arises after integration of ω-mesons, a model of which will be the focus of the next chapter.

At low density the situation is much less clear due to the appearance of thermodynamically unstable regions. For a given classical crystal solution (which, in a natural way, is identified with symmetric nuclear matter), the energy per unit cell E_{cell} possesses a minimum for a certain volume V_*, which may be consistently identified with the nuclear saturation point, $n_0 = B/V_*$. Obviously, for $V > V_*$, the solution is thermodynamically unstable as it formally corresponds to negative pressure ($p = -\partial E/\partial V < 0$). However, taking into account the isospin quantum corrections and some further contributions, the classical minimum should hopefully disappear, thereby providing a thermodynamically stable description even in the low density regime. However, this is not always the case. For example, consider the α-crystal [53]. Although this configuration lowered the classical energy per cell, it did not cure the instability issue [52]. So, while the Skyrme model provided an equation of state, it did so only in the high density regime. In order to adequately model neutron stars, the resulting high density Skyrme EoS had to be interpolated with a low density EoS from another model, such as the BCPM EoS [54].

In any case, a thermodynamically stable phase at low density is the first necessary step in resolving nuclear pasta phases and the crust of a neutron star within the Skyrme model. Here, we apply the method developed in Chap. 3 to the generalized $\mathscr{L}_{0246}$-Skyrme model and obtain the lattice ground state of the generalized model at all densities, that is, above and below the nuclear saturation point n_0. In our model, the nuclear matter is not necessarily treated as being homogeneous. At saturation n_0, it appears as an almost homogeneous multi-wall configuration with near cubic symmetry. At low densities ($n < n_0$) then it is considered inhomogeneous, with distinct somewhat isolated multi-wall configurations present. Whereas, at high densities ($n > n_0$), e.g. in the core, it appears even more homogeneous and as a simple cubic crystal of fractional half-skyrmions, and should

be very well approximated by the $SC_{1/2}$ crystal. This allows us, for the first time, to obtain an EoS of the skyrmionic matter which interpolates between low and high density regimes. Further, the multi-wall crystalline configuration appears to appropriately model the different regions of the neutron star, unlike the homogeneous $SC_{1/2}$ crystal. We obtain an EoS, under the inclusion of the quantum corrections to the energy from the isospin d.o.f. and the assumption of β-equilibrium, and investigate its usefulness and consequences for nuclear physics.

4.2 $\mathscr{L}_{0246}$-Skyrmion Crystals at Fixed Baryon Density

The foundation for determining skyrmion crystals at finite density was laid out in the preceding chapter. In the present chapter, we consider the generalization of the massive $\mathscr{L}_{024}$-Skyrme Lagrangian which yields an ω-meson-like repulsion on short distances, while also allowing the quartic Skyrme term to describe scalar meson effects. Recall that the generalized static $\mathscr{L}_{0246}$-Skyrme Lagrangian, with metric signature $(-+++)$, is given by

$$\mathscr{L}_{0246} = -m^2 \operatorname{Tr}\left(\mathrm{Id}_2 - \varphi\right) + \frac{1}{2} g^{\mu\nu} \operatorname{Tr}\left(L_\mu L_\nu\right) + \frac{1}{16} g^{\mu\alpha} g^{\nu\beta} \operatorname{Tr}\left([L_\mu, L_\nu][L_\alpha, L_\beta]\right) - c_6 g^{\mu\nu} \mathscr{B}_\mu \mathscr{B}_\nu. \tag{4.2.1}$$

Likewise, the static energy (which can be identified with the classical mass of the skyrmion), for a fixed degree B map $\varphi : \mathbb{T}^3 \to S^3$, is defined by

$$M_B(\varphi, g) = \sqrt{g} g^{ij} H_{ij}(\varphi) + \frac{1}{\sqrt{g}} g_{ij} F_{ij}(\varphi) + \sqrt{g} C_0(\varphi) + \frac{C_6(\varphi)}{\sqrt{g}}, \tag{4.2.2}$$

where the metric independent integrals, in the NLσM formulation (1.1.16), are given by

$$H_{ij}(\varphi) = \int_{\mathbb{T}^3} \mathrm{d}^3x \, \partial_i \varphi^\mu \partial_j \varphi^\mu, \tag{4.2.3a}$$

$$F_{ij}(\varphi) = \frac{1}{4} \varepsilon^{iab} \varepsilon^{jcd} \int_{\mathbb{T}^3} \mathrm{d}^3x \, \left\{ \left(\partial_a \varphi^\mu \partial_c \varphi^\mu\right) \left(\partial_b \varphi^\nu \partial_d \varphi^\nu\right) - \left(\partial_a \varphi^\mu \partial_d \varphi^\mu\right) \left(\partial_b \varphi^\nu \partial_c \varphi^\nu\right) \right\}, \tag{4.2.3b}$$

$$C_0(\varphi) = 2m^2 \int_{\mathbb{T}^3} \mathrm{d}^3x \, (1 - \sigma), \tag{4.2.3c}$$

$$C_6(\varphi) = \frac{c_6 \varepsilon^{ijk} \varepsilon^{lmn}}{(12\pi^2)^2} \epsilon_{\mu\nu\rho\sigma} \epsilon_{\alpha\beta\gamma\delta} \int_M \mathrm{d}^3x \, \varphi^\mu \varphi^\alpha \partial_i \varphi^\nu \partial_j \varphi^\rho \partial_k \varphi^\sigma \partial_l \varphi^\beta \partial_m \varphi^\gamma \partial_n \varphi^\delta, \tag{4.2.3d}$$

with the pion mass and sextic coupling constant given by, respectively,

$$m = \frac{2m_\pi}{F_\pi e}, \qquad c_6 = \frac{\pi^4 \lambda^2 e^4 F_\pi^2}{2\hbar^3}. \tag{4.2.4}$$

We maintain the same classical energy scale of $\tilde{E} = F_\pi / 4e$ (MeV) and length scale of $\tilde{L} = 2\hbar / e F_\pi$ (fm). Throughout this chapter we will use the following values for the constants:

$$F_\pi = 122\,\mathrm{MeV}, \qquad e = 4.54, \qquad m_\pi = 140\,\mathrm{MeV}, \qquad \lambda^2 = 1\,\mathrm{MeV\,fm}^3. \tag{4.2.5}$$

Qualitatively, the parameters (4.2.5) don't have much affect on the ground state crystalline configuration. However, quantitatively this is not true. We fit the parameters of the model to give us approximately the binding energy at saturation and the nuclear density, while also allowing the

symmetry energy and the pion decay constant not to deviate too much from their experimental values. Other studies have done similar fittings to, e.g., the symmetry energy, but there is always a trade-off where if you fix one parameter accurately then other physical quantities will suffer in consequence. In other studies [52], the symmetry energy and saturation energy can be fitted correctly, but the saturation density can not also be simultaneously fitted correctly. That is the caveat of using the Skyrme model alone to model nuclear matter. For example, in our model, the symmetry energy at saturation is lower than expected but accurately predicts the asymmetry coefficient in the SEMF. If the model is tuned to give the correct symmetry energy value at saturation then the asymmetry coefficient would be off. For a more general review of the quantitative effects of the free parameters on a ground state configuration see [52, 53].

We now briefly review the findings of the previous chapter. Skyrmion crystals have been studied extensively in the literature, with it being previously accepted that the $\mathrm{SC}_{1/2}$ crystal found independently by Kugler & Shtrikmann [39] and Castillejo *et al.* [40] is the minimum energy skyrmion crystal. However, in the massless $\mathscr{L}_{24}$-Skyrme model, this $\mathrm{SC}_{1/2}$ crystal is just one point on an SO(4) orbit of solutions, i.e. it is not a unique critical point and all of these solutions are all energy degenerate. When the pion mass is turned on, there is no reason to expect these energy degenerate $\mathscr{L}_{24}$ critical points to extend to $\mathscr{L}_{0246}$ critical points upon perturbation. However, there are four critical points which survive perturbation. These are the $\mathrm{SC}_{1/2}$, α, chain and multi-wall crystals. Each crystal has baryon number $B_{\mathrm{cell}} = 4$ per unit cell, with three of the crystals having lower energy classically than the $\mathrm{SC}_{1/2}$ crystal for non-zero pion mass and non-cubic (trigonal) lattice geometry.

The $\mathrm{SC}_{1/2}$ crystal can be obtained from the Fourier series-like expansion of the fields as an initial configuration (1.3.20). From the $\mathrm{SC}_{1/2}$ crystal, the other three crystals can be constructed by applying a chiral SO(4) transformation $Q \in \mathrm{SO}(4)$, such that $\varphi = Q\varphi_{1/2}$, and minimizing the energy with respect to variations of the field and the lattice. These chiral transformations $Q \in \mathrm{SO}(4)$ can be determined by considering a deformed energy functional on the moduli space of critical points of the Skyrme energy functional, and are found to be

$$Q \in \left\{ \mathrm{Id}_4, \underbrace{\begin{pmatrix} (0,-1,1,1)/\sqrt{3} \\ * \end{pmatrix}}_{Q_\alpha}, \underbrace{\begin{pmatrix} (0,0,0,1) \\ * \end{pmatrix}}_{Q_{\text{multi-wall}}}, \underbrace{\begin{pmatrix} (0,0,1,1)/\sqrt{2} \\ * \end{pmatrix}}_{Q_{\text{chain}}} \right\}. \tag{4.2.6}$$

The other three rows of the chiral transformations Q_α, $Q_{\text{multi-wall}}$ and Q_{chain}, labelled by the asterisk, can be obtained by using the Gram–Schmidt process.

With the initial field configuration in place, we then minimize the static $\mathscr{L}_{0246}$-energy functional (4.2.2) with respect to variations of the metric g, for fixed field configuration $\varphi|_{\text{fixed}}$. This is achieved by considering the energy $\mathcal{M}_B$ as a function of the metric g on $\mathbb{T}^3$, and employing arrested Newton flow on SPD_3, which solves the system of 2nd order ODEs (3.4.6). The key component of the numerical algorithm is the computation of the stress-energy tensor, which is given by (3.4.7).

In general, the dimension of SPD_n is $\dim(\mathrm{SPD}_n) = n(n+1)/2$. In our case, we are working with SPD_3 and consider the energy as a function $E_\varphi : \mathrm{SPD}_3 \to \mathbb{R}$. So we are implementing arrested Newton flow on a 6 dimensional manifold. After each time step $t \mapsto t + \delta t$, we check to see if the energy is increasing. If $E_\varphi(t+\delta t) > E_\varphi(t)$, we take out all the kinetic energy in the system by setting $\dot{g}(t+\delta t) = 0$ and restart the flow. The flow then terminates when every component of the stress-energy tensor S_φ is zero to within a given tolerance (we have used 10^{-6}).

As the metric g_s on $\mathbb{T}^3$ varies so too does the lattice Λ_s, which we have labelled $\Lambda_s = \Lambda(g_s)$ where $\Lambda_0 = \Lambda$. Let $\vec{X}_1 = (x_1, y_1, z_1), \vec{X}_2 = (x_2, y_2, z_2)$ and $\vec{X}_3 = (x_3, y_3, z_3)$ be the period lattice vectors for Λ. In order to plot isosurfaces of the baryon density of the resulting skyrmion on $(\mathbb{R}^3/\Lambda, d)$, we need to reconstruct the lattice Λ from the metric g. To do this we need to solve the following under-determined system of equations

$$\begin{aligned}
\vec{X}_1 \cdot \vec{X}_1 &= x_1^2 + y_1^2 + z_1^2 = g_{11} \\
\vec{X}_1 \cdot \vec{X}_2 &= x_1x_2 + y_1y_2 + z_1z_2 = g_{12} \\
\vec{X}_1 \cdot \vec{X}_3 &= x_1x_3 + y_1y_3 + z_1z_3 = g_{13} \\
\vec{X}_2 \cdot \vec{X}_2 &= x_2^2 + y_2^2 + z_2^2 = g_{22} \\
\vec{X}_2 \cdot \vec{X}_3 &= x_2x_3 + y_2y_3 + z_2z_3 = g_{23} \\
\vec{X}_3 \cdot \vec{X}_3 &= x_3^2 + y_3^2 + z_3^2 = g_{33}
\end{aligned} \,. \tag{4.2.7}$$

This has infinitely many solutions which we can solve for by fixing a particular lattice vector, or by setting $y_1 = z_1 = z_2 = 0$, i.e. $\vec{X}_1 = (x_1, 0, 0), \vec{X}_2 = (x_2, y_2, 0)$ and $\vec{X}_3 = (x_3, y_3, z_3)$. Then, for the latter choice of period lattice vectors, the system of equations (4.2.7) has a solution given by

$$\begin{aligned}
\vec{X}_1 &= \left(\sqrt{g_{11}}, 0, 0\right) \\
\vec{X}_2 &= \left(\frac{g_{12}}{\sqrt{g_{11}}}, \sqrt{g_{22} - \frac{g_{12}^2}{g_{11}}}, 0\right) \\
\vec{X}_3 &= \left(\frac{g_{13}}{\sqrt{g_{11}}}, \frac{1}{\sqrt{g_{22} - \frac{g_{12}^2}{g_{11}}}}\left(g_{23} - \frac{g_{12}g_{13}}{g_{11}}\right), \sqrt{g_{33} - \frac{g_{13}^2}{g_{11}} - \frac{1}{\left(g_{22} - \frac{g_{12}^2}{g_{11}}\right)}\left(g_{23} - \frac{g_{12}g_{13}}{g_{11}}\right)^2}\right).
\end{aligned}$$

Determining phases of nuclear matter and phase transitions in the Skyrme model is a difficult task, and is important if one wants to understand symmetric and asymmetric nuclear matter in high/low density regimes. To study phases of matter at various densities, we consider fixed density variations of the energy functional, i.e. we allow the lattice to vary but keep its volume fixed. Then the volume form vol_g is required to be invariant under variations g_s of the metric, viz.

$$\left.\frac{\mathrm{d}}{\mathrm{d}s}\right|_{s=0} \int_{\mathbb{T}^3} \mathrm{d}^3x\sqrt{g_s} = \frac{1}{2}\int_{\mathbb{T}^3} \mathrm{d}^3x\sqrt{g}g^{ij}\dot{g}_{ij} = 0. \tag{4.2.8}$$

That is, $\dot{g}$ has to be an element of the space of traceless parallel symmetric bilinear forms $\mathscr{E}_0$.

In terms of the energy, we are dealing with a constrained minimization problem: minimize the energy functional for fixed field configuration $\varphi = \varphi|_{\text{fixed}}$ subject to the constraint that $\det(g)$ is constant. The existence and uniqueness of such a metric was proven in Sec. 3.6. In the present chapter, we choose to approach the problem using Lagrange multipliers. Let us define the Lagrangian

$$L(g) = E_\varphi(g) + \lambda\left(\int_{\mathbb{T}^3} \mathrm{d}^3x\sqrt{g} - c\right), \tag{4.2.9}$$

where $\lambda \in \mathbb{R}$ is a Lagrange multiplier and $c \in \mathbb{R}_{>0}$ is a constant. Consider a one-parameter curve g_s in the space of metrics on $\mathbb{T}^3$. Then, for any variation g_s of the metric,

$$\left.\frac{\mathrm{d}L}{\mathrm{d}s}\right|_{s=0} = \left.\frac{\mathrm{d}E_\varphi}{\mathrm{d}s}\right|_{s=0} + \lambda\left.\frac{\mathrm{d}}{\mathrm{d}s}\right|_{s=0}\int_{\mathbb{T}^3} \mathrm{d}^3x\sqrt{g_s} = 0. \tag{4.2.10}$$

We note that

$$\left.\frac{\mathrm{d}E_\varphi(g_s)}{\mathrm{d}s}\right|_{s=0} = \int_{\mathbb{T}^3} \mathrm{d}^3x\sqrt{g}\,\langle S(g),\dot{g}\rangle_g = \int_{\mathbb{T}^3} \mathrm{d}^3x\sqrt{g}\,S_\varphi^{ij}\dot{g}_{ij}, \tag{4.2.11}$$

where S_φ is the (fixed field) stress tensor appearing in (3.4.7). Thus, we can determine the Lagrange multiplier by considering

$$\left.\frac{\mathrm{d}L}{\mathrm{d}s}\right|_{s=0} = \int_{\mathbb{T}^3} \mathrm{d}^3x\sqrt{g}\left(S_\varphi^{ij} + \frac{\lambda}{2}g^{ij}\right)\dot{g}_{ij} = 0 \quad \Rightarrow \quad \lambda = -\frac{2}{3}g_{ij}S_\varphi^{ij}. \tag{4.2.12}$$

Hence, we find that

$$\left.\frac{\mathrm{d}L}{\mathrm{d}s}\right|_{s=0} = \int_{\mathbb{T}^3} \mathrm{d}^3x\sqrt{g}\,\langle S(g) - \frac{1}{3}\,\mathrm{Tr}_g(S_\varphi)\,g,\dot{g}\rangle_g = 0. \tag{4.2.13}$$

Therefore, we modify the stress-energy tensor in (3.4.6) via the metric projection $P_g : \Gamma(\odot^2 T^*\mathbb{T}^3) \to \Gamma(\odot^2 T^*\mathbb{T}^3)$, that is

$$S_\varphi \mapsto \tilde{S}_\varphi \equiv P_g(S_\varphi) = S_\varphi - \frac{1}{3}\,\mathrm{Tr}_g(S_\varphi)\,g \tag{4.2.14}$$

and our convergence criterion becomes $\max(\tilde{S}_\varphi) < \mathrm{tol}$. Likewise, to ensure numerically that $\dot{g}$ is traceless, we need to project out the component of variation vector $\dot{g}$ parallel to the metric g via the mapping $\dot{g} \mapsto P_g(\dot{g})$.

By employing this process at various volumes it enables us to determine an energy-volume curve or, equivalently, an energy-density curve. This is key to obtaining an EoS within our framework, as the EoS is directly related to the $E - V$ curve.

Out of the four crystal configurations, the most of interest to astrophysicists are the α-crystal, chain-crystal and the multi-wall crystal; these resemble non-uniform phases of nuclear matter, known as nuclear "pasta". The iron rich crust of a neutron star could be modeled by $B = 56$ chunks of α-particle crystals, such as those modeled by Feist *et al.* [43], describing the "gnocchi" phase. As we descend deeper towards the outer core, the pressure due to gravity increases and nuclei are squeezed together into long thin tubes of "spaghetti". This spaghetti phase can be modeled using the chain-crystal. Deeper still and the spaghetti flattens into parallel multi-walls, resembling "lasagna", of which the multi-wall crystal is reminiscent of. Of course, for realistic applications the Coulomb interaction must be added. This is because of the fact that different crust phases arise due to a balance between the strong and electrostatic forces. Nevertheless, the Skyrme model has a built-in ability to model such phases.

The multi-wall-crystal is the lowest energy solution at all baryon densities and also yields a lower compression modulus than the other three crystals. This makes it an ideal candidate for nuclear matter and an EoS at high and low densities. With $\varphi_0 = Q_{\text{multi-wall}}\varphi_{1/2}$ as an initial configuration and by considering fixed baryon density variations, as laid out above, the energy-volume curve can be computed and an EoS obtained.

The first main result of this section is the observation that, as it is for the massive $\mathscr{L}_{024}$-Skyrme model, the multi-wall crystal is also the ground state crystalline solution for the generalized $\mathscr{L}_{0246}$-Skyrme model at all densities. In the low density regime the solution clearly exhibits a two-layer structure, extending parallel to the xy-plane with the vacuum ($\sigma = 1$) occupying the regions above and below the multi-wall. This can be seen in Fig. 4.1. Inside the multi-wall center the σ-field is approximately the anti-vacuum ($\sigma \approx -1$). Therefore, the multi-wall crystal is similar to that of a

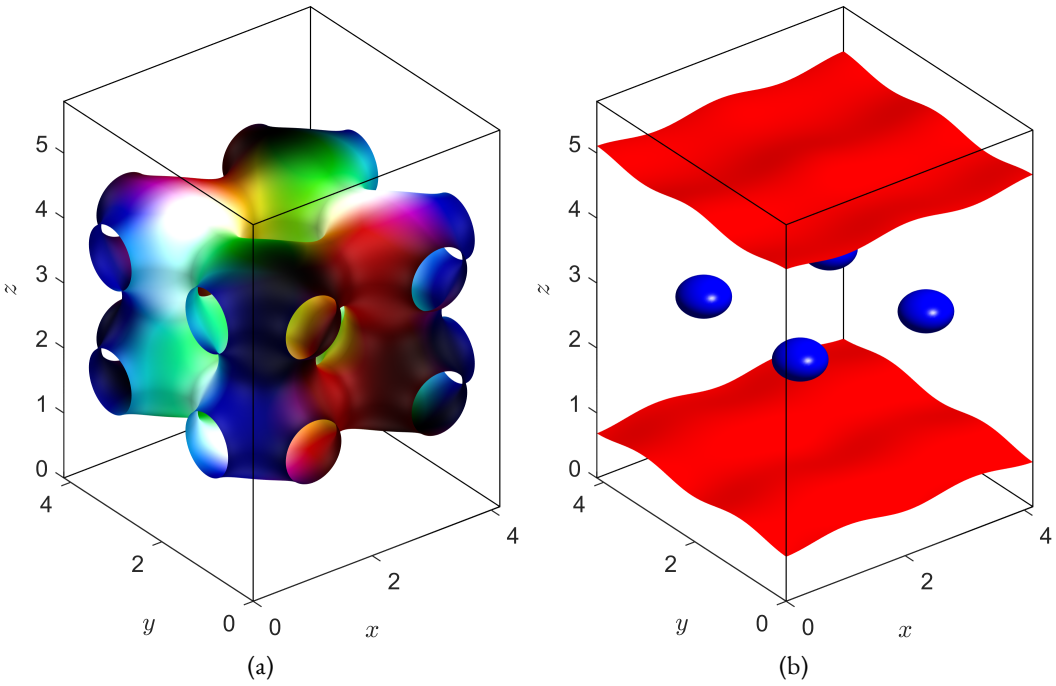

Figure 4.1: $\mathscr{L}_{0246}$-Skyrme multi-wall crystal at a fixed baryon density $n_B < n_0$. The isobaryon density is depicted in (a) and isosurface plots of the σ field, where the vacuum ($\sigma = +0.9$) is colored red and the anti-vacuum ($\sigma = -0.9$) blue, are shown in (b).

domain wall crystal, hence the name convention. As the density increases, the regions occupied by the vacuum reduces and the non-cubic period lattice becomes more cubic, tending asymptotically to the $SC_{1/2}$ crystal in the zero volume limit. These are the true energy minimizers of the generalized $\mathscr{L}_{0246}$-Skyrme model at finite density under assumption that the baryon charge of the unit cell is four, $B_{\text{cell}} = 4$.

In Fig. 4.2 we plot the classical static energy per baryon $E(n_B) = M_B(n_B)/B$ of the multi-wall crystal as a function of the baryon density $n_B = B/V$, with the nuclear saturation density n_0 defined to be the baryon density such that $(\partial M_B)/(\partial n_B)|_{n_B=n_0} = 0$. This EoS is interpreted as one of isospin symmetric nuclear matter since the classical Skyrme model does not distinguish between protons and neutrons.

Expansion of the isospin symmetric energy function $E(n_B)$ around the minimum n_0 gives

$$E(n_B) = E_0 + \frac{1}{2}K_0\frac{(n_B - n_0)^2}{9n_0^2} + \mathcal{O}\left((n_B - n_0)^3\right). \tag{4.2.15}$$

The local minimum, associated to the nuclear saturation point n_0, is identified with the saturation energy $E_0 \equiv M_B(n_0)/B$. The curvature of the energy curve is controlled by the compression modulus K_0 and determines the increase in energy due to compression. For our choice of the coupling constants (4.2.5) the saturation energy per baryon and saturation density are respectively $E_0 = 912$ MeV and $n_0 = 0.160$ fm^{-3}, which almost perfectly corresponds to the physical values of the saturation energy and density [138]. An important observation is that the difference between the energy at nuclear saturation and the classical energy at zero density is much smaller than in

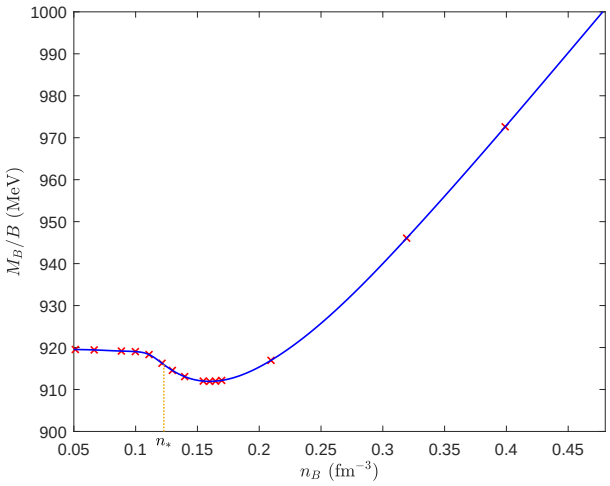

Figure 4.2: The classical static energy per baryon M_B/B as a function of the nuclear density n_B. The nuclear density at which the cusp in the symmetry energy appears is labelled by n_*. This corresponds to the density at which the infinite crystalline multi-wall solution begins transitioning to an isolated multi-wall configuration.

previous works. Indeed, the difference is now roughly $\Delta E \approx 7$ MeV, which is a 0.8% difference with respect to the total energy. Whereas, for a $B = 32$ or $B = 108$ α-crystal the difference is found to be approximately 3% and 1.7%, respectively. This small difference in energy between the nuclear saturation and low-density asymptotic solutions is crucial for the existence of a purely skyrmion generated EoS at all densities.

Unfortunately, the compression modulus still exceeds the experimental value by a factor of $6 \sim 7$. Although, in comparison with studies involving the $SC_{1/2}$ crystal, where $K_0 \sim 1700$ MeV, we do observe an improvement in the (in)compressibility by approximately 200 MeV, the inhomogeneous solution alone cannot solve the compression modulus problem in the Skyrme model. Nevertheless, this negative result is very important as it shows that the purely pionic Skyrme model cannot lead to a physically acceptable compression modulus. Consequently, it seems to be necessary to include other mesonic d.o.f. which may soften the skyrmionic matter at the saturation point.

4.3 Quantum Skyrmion Crystals and the Symmetry Energy

In general, the full symmetry group of the massless $\mathscr{L}_{24}$-Lagrangian is the direct product of the Poincaré group and chiral group: $\tilde{G} = \mathrm{O}(3) \ltimes \mathbb{R}^3 \times \mathrm{SO}(4)_{\text{chiral}}$. However, static energy minimizers break the Poincaré symmetry group $\mathrm{O}(3) \ltimes \mathbb{R}^3$ to the Euclidean subgroup $E_3 = \mathrm{SO}(3) \times \mathbb{R}^3$, corresponding to spatial translations and rotations. The resulting symmetry group of the static energy functional (4.2.2) is thus $G = E_3 \times \mathrm{SO}(4)_{\text{chiral}} \cong E_3 \times \mathrm{SU}(2)_L \times \mathrm{SU}(2)_R$. The action of this group on the Skyrme field is given by

$$\varphi(x) \mapsto A_L \varphi(Rx + X) A_R^\dagger, \quad A_{L/R} \in \mathrm{SU}(2)_{L/R}, \quad R \in \mathrm{SO}(3), \quad X \in \mathbb{R}^3. \tag{4.3.1}$$

For skyrmions on $M = \mathbb{R}^3$, one must impose finite boundary conditions $\varphi(x \to \infty) = \mathrm{Id}_2$. This allows for the compactification of the domain $\mathbb{R}^3 \bigcup \{\infty\} \cong S^3$ and further reduces the symmetry

group G to the subgroup $H = E_3 \times \mathrm{diag}[\mathrm{SU}(2)_L \times \mathrm{SU}(2)_R] \cong E_3 \times \mathrm{SU}(2)_I$, where $\mathrm{SU}(2)_I$ is the isospin internal symmetry group. The corresponding action of the subgroup H on the Skyrme field is given by the transformation (4.3.1) with $A_L = A_R = A \in \mathrm{SU}(2)_I$.

When considering crystals on $M = \mathbb{R}^3/\Lambda$, one must be careful when defining the isospin subgroup $\mathrm{SU}(2)_I$; the vacuum boundary condition is no longer imposed and there is not a natural way to select the diagonal isospin subgroup $\mathrm{SU}(2)_I$, at least if you consider the massless $\mathscr{L}_{24}$-model that is. This problem was addressed by Baskerville [51] in the context of the $\mathrm{SC}_{1/2}$ crystal in the $\mathscr{L}_{24}$-model, wherein she considered full $\mathrm{SO}(4)_{\mathrm{chiral}}$ rotations. She deduced that there are two cubic point groups that can define the $\mathrm{SC}_{1/2}$ crystal, one of which is related to the centres of the half-skyrmions. The cubic point group symmetry corresponding to the half-skyrmion centres is reducible into the trivial 1-dimensional irreducible representation (irrep) and a 3-dimensional irrep. We choose the $\sigma = \varphi^0$ field to transform in the 1-dimensional irrep. Then the isospin group $\mathrm{SU}(2)_I$ can be defined as the group of isorotations of the pion fields $\vec{\pi} = (\varphi^1, \varphi^2, \varphi^3)$, corresponding to transformations in the 3-dimensional irrep. If the pion mass potential term $\mathscr{L}_0$ is included then this is a natural choice of isospin group $\mathrm{SU}(2)_I$.

Rigid Body Quantization of a Crystal Chunk

As a field theory, the Skyrme model is non-renormalizable. One must quantize it semi-classically. It is well-known that the classical dynamics of slowly moving solitons corresponds to geodesic motion on the moduli space of static configurations [139]. Minimal energy configurations in the Skyrme model are unique, for a given baryon number B, up to actions of the symmetry group $H = E_3 \times \mathrm{SU}(2)_I$. The classical configuration space Q of skyrmions is split into connected components, labelled by the baryon number B, $Q = \bigcup_{B\in\mathbb{Z}} Q_B$. The covering space $\tilde{Q}_B$ of each component is a double-cover with a two-to-one map $\pi_Q : \tilde{Q}_B \to Q_B$ [140]. It was argued by Finkelstein and Rubinstein [141] that the wave functions $\Psi \in \mathscr{H}$ must be defined on the covering space of the configuration space $\tilde{Q}$, where $\mathscr{H}$ is a formal Hilbert space such that Ψ is normalizable and square integrable. That is, the wave functions are defined by the map $\Psi : \tilde{Q} \to \mathbb{C}$. We make a simple approximation and require the wave function Ψ to be non-vanishing only on minimal energy configurations and their symmetry orbits. This quantization procedure is known as rigid-body, or zero mode, quantization.

In the zero mode quantization method, a skyrmion is treated as a rigid body that is free to translate and rotate in physical space and also rotate in isospace, with the action defined by (4.3.1). These solutions are all degenerate in energy and this classical degeneracy is removed when one quantizes the theory. We wish to quantize only the isorotational degrees of freedom and work in the zero-momentum frame, ignoring the translational and rotational degrees of freedom. The action of the group of isorotations $\mathrm{SU}(2)_I$ on the Skyrme field φ is defined by the mapping $\varphi(x) \mapsto A\varphi(x)A^\dagger$. Semi-classical quantization is performed by promoting the the collective coordinate $A \in \mathrm{SU}(2)$ to a dynamical degree of freedom $A(t)$ [142]. The dynamical ansatz for the Skyrme field is then given by the transformation

$$\varphi(x) \mapsto \hat{\varphi}(x,t) = A(t)\varphi(x)A^\dagger(t). \tag{4.3.2}$$

We define the isorotational angular velocity $\vec{\omega}$ to be $A^\dagger\dot{A} = \frac{i}{2}\omega_j\tau^j$ such that $\omega_j = -i\,\mathrm{Tr}\left(\tau^j A^\dagger \dot{A}\right)$.

Then, using the dynamical ansatz (4.3.2), consider

$$\begin{aligned}\hat{L}_0 = \hat{\rho}^\dagger \partial_0 \hat{\rho} &= \hat{\rho}^\dagger \partial_0 \left(A(t)\varphi A^\dagger(t)\right) \\ &= \hat{\rho}^\dagger \left(\dot{A}\varphi A^\dagger + A\varphi \dot{A}^\dagger\right) \\ &= A\varphi^\dagger A^\dagger \dot{A}\varphi A^\dagger - \dot{A}A^\dagger \\ &= A\left(\varphi^\dagger [A^\dagger \dot{A}, \varphi]\right) A^\dagger \\ &= A\left(\varphi^\dagger \left[\frac{i}{2}\omega_i \tau^i, \varphi\right]\right) A^\dagger \\ &= A\omega_i \left(\frac{i}{2}\varphi^\dagger [\tau^i, \varphi]\right) A^\dagger \\ &= A\omega_i T_i A^\dagger, \end{aligned} \tag{4.3.3}$$

where $T_i = \frac{i}{2}\varphi^\dagger[\tau^i, \varphi]$ is an $\mathfrak{su}(2)$-valued current. In a similar but simpler fashion, the spatial components of the Maurer-Cartan left current are given by

$$\hat{L}_i = \hat{\rho}^\dagger \partial_i \hat{\rho} = A\varphi^\dagger A^\dagger \partial_i (A\varphi A^\dagger) = A\varphi^\dagger \partial_i \varphi A^\dagger = AL_i A^\dagger. \tag{4.3.4}$$

Then, under the dynamical ansatz (4.3.2), the Maurer-Cartan left current transforms as

$$\hat{L}_\mu = \hat{\rho}^\dagger \partial_\mu \hat{\rho} = \begin{cases} A\omega_i T_i A^\dagger, & \mu = 0 \\ AL_i A^\dagger, & \mu = i = 1,2,3, \end{cases} \tag{4.3.5}$$

In the NLσM formulation, the $\mathfrak{su}(2)$ current T_i is expressed by the vector quaternion

$$T_i = -iT_i^a \tau^a, \quad T_i^j = \delta^{ij}\varphi^k\varphi^k - \varphi^i\varphi^j - \epsilon^{ijk}\varphi^0\varphi^k. \tag{4.3.6}$$

The corresponding contractions are given by

$$T_i^k T_j^k = \delta^{ij}\varphi^k\varphi^k - \varphi^i\varphi^j, \tag{4.3.7a}$$

$$T_i^k L_j^k = -\epsilon^{ikl}\varphi^k \partial_j \varphi^l. \tag{4.3.7b}$$

The dynamical ansatz (4.3.2) induces a rotational kinetic term in the energy functional. Under the dynamical transformation (4.3.2), the Dirichlet energy transforms as

$$\begin{aligned}\mathscr{L}_2 &= \frac{1}{2} g^{\mu\nu} \operatorname{Tr}\left(\hat{L}_\mu \hat{L}_\nu\right) \\ &= \frac{1}{2} g^{00} \operatorname{Tr}\left(\hat{L}_0 \hat{L}_0\right) + g^{0i} \operatorname{Tr}\left(\hat{L}_0 \hat{L}_i\right) + \frac{1}{2} g^{ij} \operatorname{Tr}\left(\hat{L}_i \hat{L}_j\right) \\ &= -\frac{1}{2} \operatorname{Tr}\left(T_i T_j\right) \omega_i \omega_j + \frac{1}{2} g^{ij} \operatorname{Tr}\left(L_i L_j\right), \end{aligned} \tag{4.3.8}$$

where the first term is the Dirichlet energy contribution to the isospin inertia tensor, and the second term is the static Dirichlet energy. Likewise, for the Skyrme term we have

$$\begin{aligned}\mathscr{L}_4 &= \frac{1}{16} g^{\mu\alpha} g^{\nu\beta} \operatorname{Tr}\left([\hat{L}_\mu, \hat{L}_\nu][\hat{L}_\alpha, \hat{L}_\beta]\right) \\ &= \frac{1}{8} g^{00} g^{kl} \operatorname{Tr}\left([\hat{L}_0, \hat{L}_k][\hat{L}_0 \hat{L}_l]\right) + \frac{1}{16} g^{ik} g^{jl} \operatorname{Tr}\left([\hat{L}_i, \hat{L}_j][\hat{L}_k, \hat{L}_l]\right) \end{aligned}$$

$$= -\frac{1}{8}g^{kl}\,\mathrm{Tr}\left([T_i,L_k][T_j,L_l]\right)\omega_i\omega_j + \frac{1}{16}g^{ik}g^{jl}\,\mathrm{Tr}\left([L_i,L_j][L_k,L_l]\right), \tag{4.3.9}$$

where the first term is the Skyrme contribution to the isospin inertia tensor. Finally, the sextic term,

$$\begin{aligned}\mathscr{L}_6 &= -c_6 g^{\mu\nu}\frac{\epsilon^{\mu\alpha\beta\gamma}\epsilon^{\nu\delta\rho\sigma}}{(24\pi^2\sqrt{-g})^2}\,\mathrm{Tr}\big(\hat{L}_\alpha\hat{L}_\beta\hat{L}_\gamma\big)\,\mathrm{Tr}\big(\hat{L}_\delta\hat{L}_\rho\hat{L}_\sigma\big)\\ &= -c_6 g^{00}\frac{\epsilon^{ijk}\epsilon^{abc}}{(24\pi^2\sqrt{-g})^2}\,\mathrm{Tr}\big(L_iL_jL_k\big)\,\mathrm{Tr}(L_aL_bL_c) - c_6 g^{kl}\frac{3^2\epsilon^{kab}\epsilon^{lcd}}{(24\pi^2\sqrt{-g})^2}\,\mathrm{Tr}\big(\hat{L}_0\hat{L}_a\hat{L}_b\big)\,\mathrm{Tr}\big(\hat{L}_0\hat{L}_c\hat{L}_d\big)\\ &= c_6\left(\mathscr{B}^0\right)^2 - c_6 g^{kl}\frac{\epsilon^{kab}\epsilon^{lcd}}{(8\pi^2\sqrt{-g})^2}\,\mathrm{Tr}(T_iL_aL_b)\,\mathrm{Tr}\big(T_jL_cL_d\big)\omega_i\omega_j,\end{aligned} \tag{4.3.10}$$

where we have used the fact that the topological current transforms as

$$\hat{\mathscr{B}}^i = \frac{3}{24\pi^2}\epsilon^{ijk}\,\mathrm{Tr}\big(\hat{L}_0\hat{L}_j\hat{L}_k\big) = \frac{1}{8\pi^2}\epsilon^{ijk}\,\mathrm{Tr}\big(T_lL_jL_k\big)\omega_l. \tag{4.3.11}$$

As the static part of the sextic term is the temporal component, we must take the negative contribution of this. Putting all of this together, we find the effective Lagrangian to be

$$\begin{aligned}\mathscr{L}_{\text{eff}} &= \mathscr{L}_0 + \mathscr{L}_2 + \mathscr{L}_4 - \mathscr{L}_6\\ &= -m^2\,\mathrm{Tr}\left(\mathrm{Id}_2 - \varphi\right) + \frac{1}{2}g^{ij}\,\mathrm{Tr}\left(L_iL_j\right) + \frac{1}{16}g^{ik}g^{jl}\,\mathrm{Tr}\left([L_i,L_j][L_k,L_l]\right) - c_6\left(\mathscr{B}^0\right)^2\\ &\quad + \frac{1}{2}\left\{-\mathrm{Tr}\left(T_iT_j\right) - \frac{1}{4}g^{kl}\,\mathrm{Tr}\left([T_i,L_k][T_j,L_l]\right) + c_6 g^{kl}\frac{\epsilon^{kab}\epsilon^{lcd}}{2(4\pi^2\sqrt{-g})^2}\,\mathrm{Tr}(T_iL_aL_b)\,\mathrm{Tr}\big(T_jL_cL_d\big)\right\}\omega_i\omega_j\\ &= -\mathscr{E}_{\text{stat}} + \frac{1}{2}\omega_i\mathscr{U}_{ij}\omega_j,\end{aligned} \tag{4.3.12}$$

where the isospin inertia tensor contribution from the Skyrme field φ is

$$\mathscr{U}_{ij} = -\mathrm{Tr}\left(T_iT_j\right) - \frac{1}{4}g^{kl}\,\mathrm{Tr}\left([T_i,L_k][T_j,L_l]\right) + c_6 g^{kl}\frac{\epsilon^{kab}\epsilon^{lcd}}{2(4\pi^2\sqrt{-g})^2}\,\mathrm{Tr}(T_iL_aL_b)\,\mathrm{Tr}\big(T_jL_cL_d\big). \tag{4.3.13}$$

The restriction of the induced kinetic energy functional of the model to the isospin orbit of a given static solution defines a left invariant metric on SO(3) called the isospin inertia tensor, which is the symmetric 3 × 3-matrix given by

$$U_{ij} = \int_{\mathbb{T}^3}\mathrm{d}^3x\sqrt{g}\mathscr{U}_{ij}. \tag{4.3.14}$$

Using the NLσM representation (1.1.16), this isospin inertia tensor takes the form (see App. A.1 for calculation)

$$\begin{aligned}U_{ij} = 2\int_{\mathbb{T}^3}\mathrm{d}^3x\sqrt{-g}\,\Big\{&\left(\delta^{ij}\varphi^k\varphi^k - \varphi^i\varphi^j\right) + g^{kl}\left((\delta^{ij}-\varphi^i\varphi^j)\partial_k\varphi^0\partial_l\varphi^0 + (\varphi^m\varphi^m)\partial_k\varphi^i\partial_l\varphi^j\right.\\ &\left.+\varphi^0\varphi^i\partial_k\varphi^0\partial_l\varphi^j + \varphi^0\varphi^j\partial_l\varphi^0\partial_k\varphi^i\right)\\ &+\frac{c_6}{(4\pi^2\sqrt{-g})^2}g_{pq}\epsilon^{pmn}\epsilon^{qkl}\left[(\delta^{ij}\varphi^a\varphi^a - \varphi^i\varphi^j)\left(\partial_m\varphi^\mu\partial_k\varphi^\mu\partial_n\varphi^\nu\partial_l\varphi^\nu - \partial_n\varphi^\mu\partial_k\varphi^\mu\partial_m\varphi^\nu\partial_l\varphi^\nu\right)\right.\\ &+\epsilon^{jac}\varphi^a\partial_m\varphi^c\left(\epsilon^{ibd}\varphi^b\partial_l\varphi^d\partial_n\varphi^\mu\partial_k\varphi^\mu - \epsilon^{ibd}\varphi^b\partial_k\varphi^d\partial_n\varphi^\mu\partial_l\varphi^\mu\right)\\ &\left.\left.+\epsilon^{jac}\varphi^a\partial_n\varphi^c\left(\epsilon^{ibd}\varphi^b\partial_k\varphi^d\partial_m\varphi^\mu\partial_l\varphi^\mu - \epsilon^{ibd}\varphi^b\partial_l\varphi^d\partial_m\varphi^\mu\partial_k\varphi^\mu\right)\right]\right\}.\end{aligned} \tag{4.3.15}$$

Therefore, the effective Lagrangian on this restricted space of configurations is $L_{\text{eff}} = L_{\text{rot}} - M_B$, where M_B is the static mass of the skyrmion defined by (4.2.2) and L_{rot} is the induced isorotational part of the Lagrangian given by

$$L_{\text{rot}} = \frac{1}{2}\omega_i U_{ij}\omega_j. \tag{4.3.16}$$

The rigid-body wavefunctions will be on SU(2) with isospin half-integer if B is odd and integer if B is even. The isorotation angular momentum operator canonically conjugate to $\vec{\omega}$ is the body-fixed isospin angular momentum operator $\vec{K}$, defined by

$$K_i = \frac{\partial L_{\text{rot}}}{\partial \omega_i} = U_{ij}\omega_j. \tag{4.3.17}$$

This is related to the usual space-fixed isospin angular momentum $\vec{I}$ by the relation

$$I_i = -D(A)_{ij}K_j, \tag{4.3.18}$$

where $A \in \text{SU}(2)$ has been recast in the SO(3) form via the map

$$D : \text{SU}(2) \to \text{SO}(3), \quad D(A)_{ij} = \frac{1}{2}\,\text{Tr}\left(\tau^i A \tau^j A^\dagger\right). \tag{4.3.19}$$

These two classical momenta $(\vec{K}, \vec{I})$ are promoted to quantum operators $(\hat{K}, \hat{I})$, both satisfying the $\mathfrak{su}(2)$ commutation relations, and the Casimir invariants satisfy $\hat{I}^2 = \hat{K}^2$. The operator $\hat{I}^2$ has eigenvalue $i(i+1)$ and i_3 the eigenvalue for the operator $\hat{I}_3$. On the double cover of the group of isorotations $\text{SU}(2)_I$, there is a basis of rigid-body wavefunctions $|i, i_3, k_3\rangle$ with $-i \le k_3 \le i$. The rigid-body Hamiltonian takes the general form

$$\mathscr{H} = \frac{\hbar^2}{2}\hat{K}U^{-1}\hat{K}^T + M_B. \tag{4.3.20}$$

We now apply this quantization procedure to a large chunk of crystal, consisting of N_{cell} unit cells. Consider a rigidly iso-spinning crystal chunk with total energy $M_B = N_{\text{cell}}E_{\text{cell}}$ and baryon number $B = N_{\text{cell}}B_{\text{cell}}$. In order to calculate the isospin correction to the energy of the crystal chunk we would need to know the quantum state of the whole crystal chunk. This is obviously a very difficult computation since we want to model neutron stars, which would require us to consider a crystal chunk with many unit cells. However we may impose the following restrictions to solve this problem:

- The total isospin quantum state of the crystal chunk $|\Psi\rangle$ is written as the superposition of each individual unit cell state $|\psi\rangle$. That is $|\Psi\rangle = \otimes_{N_{\text{cell}}} |\psi\rangle$, where $N_{\text{cell}} \to \infty$ in the thermodynamic limit.

- The symmetry of the classical configuration in each unit cell is extended to the whole crystal chunk, so both wavefunctions share the same point symmetry group.

Under these assumptions, we can approximate the isospin inertia tensor of the crystal chunk as $U^N \simeq N_{\text{cell}}U^{\text{cell}}$, where U^{cell} is the isospin inertia tensor of the skyrmion crystal unit cell.

For skyrmion crystals, we can always isorotate them such that the principal axes of inertia are the usual orthogonal axes, which results in the inertia tensor being diagonal, $U_{ij}^{\text{cell}} = 0$ for $i \neq j$. Let us label the eigenvalues $u_i = U_{ii}^{\text{cell}}$, then the quantum Hamiltonian of a crystal chunk takes the form

$$\mathscr{H}^N = \frac{\hbar^2}{2}\left(\frac{\hat{K}_1^2}{U_1^N} + \frac{\hat{K}_2^2}{U_2^N} + \frac{\hat{K}_3^2}{U_3^N}\right) + M_B = \frac{\hbar^2}{2N_{\text{cell}}}\left(\frac{\hat{K}_1^2}{u_1} + \frac{\hat{K}_2^2}{u_2} + \frac{\hat{K}_3^2}{u_3}\right) + N_{\text{cell}}E_{\text{cell}}. \tag{4.3.21}$$

The energy eigenstates of the Hamiltonian (4.3.21) can be classified by i and i_3. To determine bound states with definite energy one must solve the static Schrödinger equation corresponding to this Hamiltonian, $\mathscr{H}^N |\Psi\rangle = E^N |\Psi\rangle$. The Schrödinger equation can be expressed more explicitly within a particular (i, i_3) sector by expanding the quantum state $|\Psi\rangle$ in terms of the total wavefunctions Ψ as [14]

$$|\Psi\rangle = \sum_{k_3=-i}^{+i} \Psi_{k_3}(q)\,|i, i_3, k_3\rangle\,, \qquad \vec{\Psi}(q) = \begin{pmatrix} \Psi_{-i}(q) \\ \vdots \\ \Psi_{+i}(q) \end{pmatrix}, \qquad q \in \tilde{Q}, \tag{4.3.22}$$

and substituting this into the Hamiltonian (4.3.21).

In previous applications of skyrmion crystals to model neutron stars (see, for example, [52, 53, 125, 143, 144]), the $\text{SC}_{1/2}$ crystal was considered. This crystal has an isotropic inertia tensor with eigenvalue $u_i = \lambda$, with λ some constant. However, the multi-wall crystal considered here is anisotropic and the isospin inertia tensor generically has the eigenvalues $u_1 = u_2 < u_3$. Then, we can express the Hamiltonian as

$$\mathscr{H}^N = \frac{\hbar^2 \hat{K}_3^2}{2N_{\text{cell}}}\left(\frac{1}{u_3} - \frac{1}{u_1}\right) + \frac{\hbar^2 \hat{I}^2}{2N_{\text{cell}}u_1} + N_{\text{cell}}E_{\text{cell}}. \tag{4.3.23}$$

Since the Hamiltonian depends on $\hat{K}_3$, it is not sufficient to just fix the value of i_3. We would need to explicitly compute the isospin quantum state via the Finkelstein–Rubinstein constraints. However, the contribution to the energy from this additional term containing $\hat{K}_3$ is determined by the difference between the two inertia tensor eigenvalues, $u_3 - u_1 = \epsilon$. In general, $\epsilon \geq 0$ is relatively small, no more than 18% of u_3 at all densities n_B. Following [117], we now make the approximation $u_1 = u_3(1 - \epsilon)$, with $0 < \epsilon \leq 1$, and expand in perturbation theory. Ignoring the linear correction, this approximation reduces the quantum Hamiltonian to

$$\mathscr{H}^N = \frac{\hbar^2 \hat{I}^2}{2N_{\text{cell}}u_3} + N_{\text{cell}}E_{\text{cell}}. \tag{4.3.24}$$

The Schrödinger equation corresponding to such a rigidly iso-spinning crystal chunk with N_{cell} unit cells can be written as

$$\mathscr{H}^N |\Psi\rangle = \left(M_B + E_{i,i_3}\right)|\Psi\rangle = N_{\text{cell}}\left(E_{\text{cell}} + E_{\text{iso}}\right)|\Psi\rangle\,, \qquad E_{i,i_3} = \frac{\hbar^2 i^2}{2N_{\text{cell}}u_3}, \tag{4.3.25}$$

where the quantum correction to the energy of a unit cell, due to the isospin degrees of freedom, is given by

$$E_{\text{iso}} = \frac{E_{i,i_3}}{N_{\text{cell}}} = \frac{\hbar^2 i^2}{2N_{\text{cell}}^2 u_3}. \tag{4.3.26}$$

It should be noted that in addition to the quantum numbers i, i_3 being density n_B dependent, the inertia tensor is also density dependent, that is $u_i = u_i(n_B)$.

Symmetry Energy and the Cusp Structure

So far we have only considered symmetric nuclear matter, which we have described by using the classical multi-wall skyrmion crystal. In order to study nuclear matter in neutron stars we must consider isospin asymmetric nuclear matter, whereby a small fraction of protons are permitted. Now let us consider asymmetric nuclear matter with baryon number $B = N + Z$, where N is the number of neutrons and Z the number of protons. The asymmetry of such matter is determined by the isospin asymmetry parameter $\delta = (N - Z)/(N + Z) = 1 - 2\gamma$, where γ is the proton fraction. Then the binding energy per baryon number of asymmetric nuclear matter is given by

$$\frac{E}{B}(n_B, \delta) = E_N(n_B) + S_N(n_B)\delta^2 + \mathrm{O}(\delta^3). \tag{4.3.27}$$

The two terms appearing in the asymmetric binding energy (4.3.27) are the binding energy of isospin-symmetric matter E_N and the symmetry energy S_N. In terms of our model, the symmetric binding energy is defined by $E_N = M_B/B$. The symmetry energy S_N dictates how the binding energy changes when going from symmetric ($\delta = 0$) to asymmetric ($\delta \neq 0$) nuclear matter. We can expand the isospin symmetric binding energy E_N and the symmetry energy S_N around the saturation density n_0 for symmetric matter [138],

$$E_N(n_B) = E_0 + \frac{1}{18}K_0\epsilon^2, \tag{4.3.28}$$

$$S_N(n_B) = S_0 + \frac{1}{3}L_{\mathrm{sym}}\epsilon + \frac{1}{18}K_{\mathrm{sym}}\epsilon^2 + \mathrm{O}(\epsilon^3), \tag{4.3.29}$$

where $\epsilon = (n_B - n_0)/n_0$, K_0 is the incompressibility at the saturation point and $S_0 = S_N(n_0)$ is the symmetry energy coefficient at saturation. We remind ourselves that, for our choice of coupling constants (4.2.5), the nuclear saturation point is characterized by the density $n_0 = 0.160\,\mathrm{fm}^{-3}$ and energy (per baryon) $M_B/B = 912$ MeV. The higher-order coefficients, L_{sym} and K_{sym}, appearing in the symmetry energy S_N are defined as

$$L_{\mathrm{sym}} = 3n_0 \left.\frac{\partial S_N}{\partial n_B}\right|_{n_0}, \quad K_{\mathrm{sym}} = 9n_0^2 \left.\frac{\partial^2 S_N}{\partial n_B^2}\right|_{n_0}. \tag{4.3.30}$$

The precise values of these coefficients are not known, but are predicted to be $L_{\mathrm{sym}} = 57.7 \pm 19$ MeV and $K_{\mathrm{sym}} = -107 \pm 88$ MeV [145].

Consider now the $\mathrm{SC}_{1/2}$ crystal, which has unit cell charge $B_{\mathrm{cell}} = 4$. Then there are a finite number of possible quantum states with allowed quantum numbers $i = 0, 1, 2$ [52]. The $i_3 = 0$ case, which corresponds to symmetric nuclear matter, would be the one with the lowest energy since it has no isospin energy compared to the other cases. This is obviously the most symmetric state possible. However, it is known that inside neutron stars there is a huge asymmetry between protons and neutrons. Baskerville [51] investigated the charge neutral case $i_3 = -2$, corresponding to a pure neutron crystal, and computed the quantum isospin corrections to the energy. However, a realistic description of neutron stars would require the presence of protons. Although the concrete value is still unknown, simulations yield values around $\gamma \sim 10^{-2} - 10^{-1}$ [146, 147]. Therefore, following the arguments in [52] we perform a mean-field approximation considering a larger chunk of the multi-wall crystal, enclosing an arbitrary number of unit cells N_{cell}, which is in a generic quantum

state with fixed eigenvalue,

$$i_3 = \frac{(Z-N)}{2} = -\frac{(1-2\gamma)}{2} N_{\text{cell}} B_{\text{cell}}. \tag{4.3.31}$$

Note that in this case the nuclear density of the crystal chunk can be directly interpreted as the nuclear density of the unit cell, since

$$n_B = \frac{B_{\text{crystal}}}{V_{\text{crystal}}} = \frac{N_{\text{cell}} B_{\text{cell}}}{N_{\text{cell}} V_{\text{cell}}} = \frac{B_{\text{cell}}}{V_{\text{cell}}}. \tag{4.3.32}$$

The eigenvalue i_3 is already fixed from the mean-field approximation (4.3.31), and the value of $i = i_3$ is the one which minimizes the isospin energy, since by definition $i^2 \geq i_3^2$. Now we obtain a final expression for the quantum correction (per unit cell) to the energy due to the isospin degrees of freedom,

$$E_{\text{iso}}(n_B) = \frac{\hbar^2}{8u_3(n_B)} B_{\text{cell}}^2 \vartheta^2. \tag{4.3.33}$$

This quantum isospin energy is explicitly related to the proton fraction γ, and so we will need to include leptons if we are to allow the crystal to have a non-zero proton fraction. This is required in order for the system to remain electrically neutral. Thus the proton fraction, and hence the quantum state of the crystal, will be obtained by imposing β-equilibrium for each value of the density.

From the quantum isospin energy (4.3.33), we can determine the nuclear symmetry energy of the multi-wall crystal, which in general plays a crucial role in the structure of neutron-rich nuclei and, of more interest to us, in neutron stars. For general skyrmion crystals the symmetry energy is given by

$$S_N(n_B) = \frac{\hbar^2}{8u_3(n_B)} V_{\text{cell}} n_B, \tag{4.3.34}$$

where the eigenvalue u_3 of the isospin inertia tensor (4.3.14) is implicitly dependent on the nuclear density n_B. We determine the symmetry energy at saturation to be $S_0 = 22.7$ MeV, which is in okay agreement with the experimentally observed value $S_0 \sim 30$ MeV [138]. The resulting symmetry energy curve $S_N(n_B)$ for the multi-wall crystal is plotted in Fig. 4.3. Having obtained the symmetry energy curve we can determine its slope and curvature, which are computed at the nuclear saturation point. We find that they are, respectively, $L_{\text{sym}} = 36.6$ MeV and $K_{\text{sym}} = -15.1$ MeV.

Let us now summarize the results obtained for the multi-wall crystal. First of all, we find that at lower densities the isospin moment of inertia, and specifically its eigenvalue u_3, tends to a constant value. This is an obvious consequence of the inhomogeneous nature of the solution which, in the limit $V_{\text{cell}} \to \infty$, tends to an "isolated" multi-wall configuration on $M = S^1 \times S^1 \times \mathbb{R}$. This simple fact has an important consequence. Namely, it leads to a non-zero value of the symmetry energy at zero density, $S_N(0) = 23.8$ MeV. At a first glance, this seems to be in contradiction with the standard description of nuclear matter where the symmetry energy vanishes at zero density. However, we want to argue that this is a desirable property of the Skyrme model as it indicates a smooth transition between infinite nuclear matter and finite atomic nuclei. Indeed, the asymmetry energy in the Bethe–Weizsäcker SEMF reads

$$E_{\text{asym}} = a_A \frac{(N-Z)^2}{B} = a_A \vartheta^2 B, \tag{4.3.35}$$

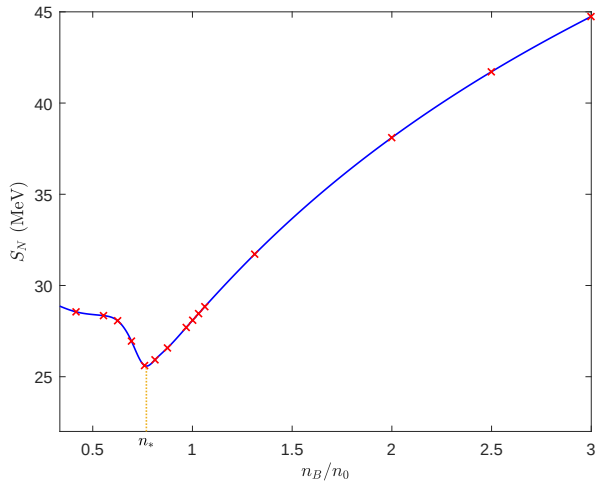

Figure 4.3: The nuclear symmetry energy S_N as a function of the baryon density n_B, exhibiting the cusp structure detailed in the text at $n_* \sim 3n_0/4$.

where $a_A \approx 23.7$ MeV. Thus, our symmetry energy at zero density can be directly identified with a_A with excellent agreement.

We remark that the assumed identification here between the zero density symmetry energy and the asymmetry energy in the Bethe-Weizsäcker formula is not a unique possibility. In fact, in the seminal paper by Natowitz el. al. [148] they computed the symmetry energy of the low density, warm nuclear matter using a quantum-statistical approach. Their results agree amazingly well with values extracted from heavy-ion collisions [149]. The symmetry energy, still taking a non-zero value at zero density, is approximately only one fourth of its value at saturation n_0. It would definitely be very desirable to investigate whether the Skyrme model may lead to similar results or not.

Moving away from zero nuclear density towards $n_* \sim 3n_0/4$, the isospin energy and consequently the symmetry energy slowly decreases, as can be seen in Fig. 4.3. This again is not an unexpected result in the Skyrme model. It was noticed by Kopeliovich *et al.* [150] that the careful analysis of mass splittings of nuclear isotopes leads to the symmetry energy decreasing with increasing baryon number B. Here, we reproduce this result, however, using a completely different setup, i.e. the collective coordinate quantization of the crystal ground state.

Below the nuclear saturation point n_0 at the density $n_* \sim 3n_0/4$, the symmetry energy exhibits a *cusp* structure. This cusp also seems to be a generic feature of the Skyrme model, independent of the choice of values for the coupling parameters (4.2.5) but rather can be interpreted as the point where the multi-wall crystal begins transitioning to an "isolated" multi-wall. On the other hand, its position with respect to the saturation point certainly may be affected by a choice of the model parameters. One can also expect such a cusp to be present where a crystalline configuration transitions to an isolated configuration at zero nuclear density, e.g. for the α and chain crystals. It is interesting to remark that such a cusp, albeit above the saturation density $n_B > n_0$, has been advocated in [151, 152] as an effect of an assumed topological phase transition from the FCC crystal of $B = 1$ hedgehogs to the $SC_{1/2}$ crystal of fractional skyrmions as the nuclear density grows. Although, in reality such a transition does not occur in the Skyrme model as it is found to occur in the thermodynamically unstable regime $n_B < n_0$ [46]. To conclude our findings on

the symmetry energy cusp, we propose that the origin of the cusp can be associated with a phase transition between an *infinite crystalline* state and a somewhat *isolated* state that is *inhomogeneous* and *nucleated*.

4.4 Particle Fractions of npeμ-Matter in β-Equilibrium

For a more realistic description of cold nuclear matter inside neutron stars we need to consider not totally asymmetric nuclear matter. As was shown in the previous section, this can be achieved by allowing a small fraction of protons over neutrons. The presence of protons gives the crystal positive electric charge, so we need to include a background of negatively charged leptons to neutralize the system. To determine the proton fraction γ at a prescribed nuclear density n_B we impose charge neutrality and β-equilibrium conditions, and then we solve the underlying equilibrium equation. Additionally, the presence of protons would require the inclusion of Coulomb interaction within the unit cell and between neighbouring cells. It has been argued [19] that the contribution of this energy diverges in the crystal due to infinitely many interactions between the cells. However, including a background of negatively charged particles in the system suppresses the Coulomb interaction between neighbouring cells and hence has a negligible contribution to the energy [52].

In the neutron star interior, the interaction between leptons and nuclear matter is mediated by the weak force. We can describe the exchange of leptons and nucleons by electron capture and β-decay processes, respectively,

$$p + l \rightarrow n + \nu_l \tag{4.4.1a}$$

$$n \rightarrow p + l + \bar{\nu}_l. \tag{4.4.1b}$$

These processes take place simultaneously at the same rate, assuming that the charge neutrality,

$$n_p = \frac{Z}{V} = n_e + n_\mu, \tag{4.4.2}$$

and the β-equilibrium conditions,

$$\mu_p = \mu_n - \mu_I \quad \Rightarrow \quad \mu_I = \mu_l, \quad l = e, \mu, \tag{4.4.3}$$

are satisfied [153]. Here μ_I is the isospin chemical potential given by

$$\mu_I = \frac{\delta B \hbar^2}{2u_3} = \frac{(1-2\gamma)B\hbar^2}{2u_3}. \tag{4.4.4}$$

Leptons inside a neutron star are treated as a non-interacting, relativistic, highly degenerate Fermi gas. The corresponding chemical potential for such a type of lepton is given by [125]

$$\mu_l = \sqrt{(\hbar k_F)^2 + m_l^2}, \tag{4.4.5}$$

where $k_F = (3\pi^2 n_l)^{1/3}$ is the associated Fermi momentum and m_l the lepton mass. For electrons we take the ultra-relativistic approximation $\mu_e \approx \hbar k_{F,e}$. From the charge neutrality condition (4.4.2), the electron number density is

$$n_e = \frac{\gamma B}{V} - n_\mu. \tag{4.4.6}$$

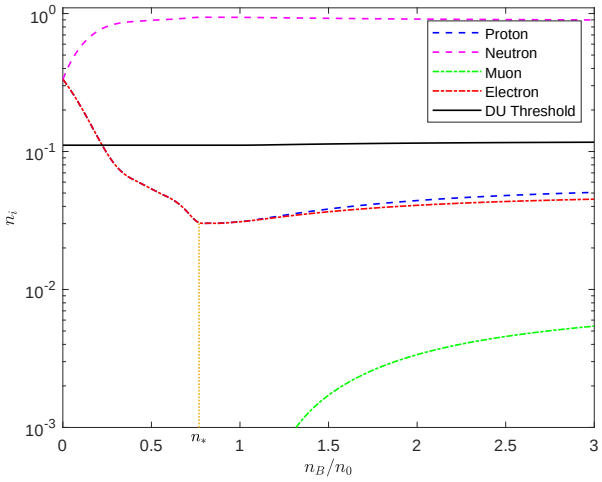

Figure 4.4: Plot of the particle number densities n_i as functions of the baryon density n_B. The particle number densities are normalized such that the total number density is $\sum_i n_i = 1$. The transition between isospin asymmetric infinite matter and symmetric finite matter at the cusp density n_* is now manifest.

The β-equilibrium condition (4.4.3) for electrons yields the following relation

$$\mu_I = \mu_e \quad \Rightarrow \quad \frac{\hbar B(1-2\gamma)}{2u_3} = \left[3\pi^2\left(\frac{\gamma B}{V} - n_\mu\right)\right]^{1/3}, \tag{4.4.7}$$

and for muons gives

$$\mu_I = \mu_\mu \quad \Rightarrow \quad n_\mu = \frac{1}{3\pi^2}\left[\left(\frac{\hbar B(1-2\gamma)}{2u_3}\right)^2 - \left(\frac{m_\mu}{\hbar}\right)^2\right]^{3/2}. \tag{4.4.8}$$

In the low density regime the electron chemical potential will be smaller than the muon mass, $\mu_e < m_\mu$. So we can solve (4.4.7) in the low density regime considering only electrons, by setting $n_\mu = 0$ until $\mu_e \geq m_\mu$. Once the electron chemical potential μ_e reaches the muon mass $m_\mu = 105.66$ MeV at high densities, it will be energetically favourable for muons to appear. Then we solve (4.4.7) and (4.4.8) simultaneously [125], and construct the proton fraction curve $\gamma = \gamma(n_B)$.

In Fig. 4.4 we plot the particle fractions of $npe\mu$ matter in β-equilibrium for the multi-wall crystal. Note that the cusp structure present in the symmetry energy, or equivalently in the isospin energy, results in an appearance of a similar structure in the particle fractions. This reinforces the proposition that the cusp density point n_* is the density at which a phase transition between isospin asymmetric infinite nuclear matter and symmetric finite matter begins. Furthermore, the fact that the symmetry energy S_N tends to a constant value at zero density leads to a similar behavior for the proton, neutron and electron particle fractions. Namely, they take their minimal/maximal value at n_* then they increase/decrease as zero density is approached. This is once again a direct consequence of a non-zero value of the isospin moment of inertia at this limit and, therefore, a generic feature of the Skyrme model. We remark that at zero density $n_B = 0$, which, in the Skyrme model framework, can be interpreted as a limit where we find nuclei in the vacuum, the nuclear matter becomes totally

isospin symmetric with $\gamma_p(0) = 0.5$. This corresponds quite well to the proton fraction in ^{56}Fe, $\gamma_p = 0.46$, which is the element expected to be present in the crust of neutron stars [154]. Further, it appears that there is a phase transition at ($n/n_B = 0.91$, $p = 0.023$MeV fm$^{-}3$). The n_* density occurs in this region of constant pressure, so it could very well be related to the liquid-gas phase transition that is expected to occur in the low density regime of neutron stars [155].

We remark that at the high density, which corresponds to the core of neutron star, the proton fraction is quite small. This agrees with previous computations in the Skyrme model with the $SC_{1/2}$ crystal [52]. Fortunately, inclusion of strange d.o.f. resolves this issue and brings the proton fraction to the widely accepted ~ 0.4 value, see [125]. We expect that the same mechanism applies for the multi-wall crystal. Especially considering this ground state crystalline solution and the $SC_{1/2}$ crystal are basically identical at high density. On the other hand, inclusion of Kaon condensates does not have any impact on the low density regime.

We now summarize our findings and compute the total energy per unit cell in a β-equilibrated multi-wall skyrmion crystal, that is

$$E_{\text{cell}}(\gamma) = \mathcal{M}_B(\gamma) + E_{\text{iso}}(\gamma) + E_e(\gamma) + E_\mu(\gamma), \tag{4.4.9}$$

where the isospin energy for a β-equilibrated crystal is given by

$$E_{\text{iso}}(\gamma) = \frac{\hbar^2 B_{\text{cell}}^2}{8u_3}(1-2\gamma)^2. \tag{4.4.10}$$

The lepton energies are the energies of a relativistic Fermi gas at zero temperature,

$$\begin{aligned} E_l &= \frac{V}{\hbar^3\pi^2}\int_0^{\hbar k_F} k^2\sqrt{k^2+m_l^2}\,\mathrm{d}k \\ &= \frac{Vm_l^4}{8\hbar^3\pi^2}\left[\frac{\hbar k_F}{m_l}\left(1+2\left(\frac{\hbar k_F}{m_l}\right)^2\right)\sqrt{\left(\frac{\hbar k_F}{m_l}\right)^2+1}-\sinh^{-1}\left(\frac{\hbar k_F}{m_l}\right)\right]. \end{aligned} \tag{4.4.11}$$

The crucial observation is that, in the case of the multi-wall skyrmion crystal, the inclusion of the β-equilibrated isospin energy and lepton energies does not completely erase the small minimum in the classical energy $\mathcal{M}_B$. Strictly speaking there is still a very shallow minimum at a density smaller than the saturation density, $n_B = 0.146\,\text{fm}^{-3}$. For smaller densities the total energy grows, until a small maximum is reached. After that the total energy decreases as the nuclear density approaches the zero density limit, $n_B \to 0$. Importantly, the asymptotic value of the total energy per unit cell is smaller than the energy at the minimum. This means that, although the total energy per unit cell still possesses a thermodynamically unstable region, we can take advantage of the Maxwell construction and derive an EoS which is valid at all densities. This is a valid construction and has a minute affect on the EoS since the difference in energy between the asymptotic solution and the minimum is $\Delta E \sim 0.1$ MeV. The formulation of the Maxwell construction is detailed below and the resulting β-equilibrated asymmetric nuclear matter is plotted in Fig. 4.5, alongside the classical isospin symmetric matter and the pure neutron matter.

The pure neutron matter is obtained for the entirely isospin asymmetric case $\eth = 1$ with $I_3 = -2$. Unlike the β-equilibrated matter, the pure neutron matter approaches the asymptotic solution from below. This is due to the non-vanishing of the quantum isospin energy contributions $E_{\text{iso}}(n_B)$

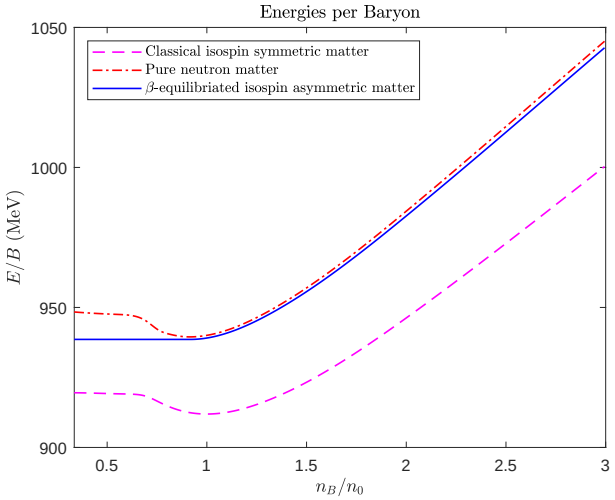

Figure 4.5: Comparison between the isospin symmetric crystal (blue curve) and the β-equilibrated asymmetric crystal with the MC applied (red curve).

in the zero density limit $n_B \to 0$. Consequently, the Maxwell construction cannot be used on the pure neutron matter EoS.

We remark that for the α-crystal the total energy in the zero density limit is greater than the energy at the minimum, so the Maxwell construction is not possible. On the other hand, for $B = 32$ and $B = 108$ crystals constructed from α-particles, such a construction is possible but it extends over a non-physical range of densities and occurs for relatively high values of the pressure. For example, the neutron stars obtained from these crystals would almost be entirely made from the Maxwell construction phase.

The Maxwell construction (MC), or equal area rule, is implemented as follows. We find three points V_1, V_2 and V_{int} on the $E_{\text{cell}}(V_{\text{cell}})$ curve, with $V_1 < V_{\text{int}} < V_2$, that have the same gradient/pressure, i.e. $p(V_i) =: p_{\text{MX}}$. These three points are chosen such that the area enclosed between $p([V_1, V_{\text{int}}])$ and p_{MX} is equal to the area enclosed between $p([V_{\text{int}}, V_2])$ and p_{MX}, where $p([V_1, V_{\text{int}}]) \leq p_{\text{MX}}$ and $p([V_{\text{int}}, V_2]) \geq p_{\text{MX}}$. This ensures that the total energy of the thermodynamic system remains the same while implementing this construction. Then, in the corresponding MC density regime $V_1 < V_{\text{cell}} < V_2$, the total energy function is replaced by a straight line connecting $E(V_1)$ and $E(V_2)$. The resulting total energy per unit cell function can be summarized as

$$E^{\text{MC}}_{\text{cell}}(V_{\text{cell}}) = \begin{cases} E_{\text{cell}}(V_{\text{cell}}) & V \leq V_1 \\ E_{\text{cell}}(V_1) - p_{\text{MX}}(V_{\text{cell}} - V_1) & V_1 \leq V_{\text{cell}} \leq V_2 \\ E_{\text{cell}}(V_{\text{cell}}) & V_{\text{cell}} \geq V_2 \end{cases} . \tag{4.4.12}$$

Now we are in a position to determine the EoS for the multi-wall configuration. The multi-wall crystal EoS for isospin asymmetric nuclear matter can be obtained by defining the energy density ρ and pressure p as, respectively,

$$\rho = \frac{E}{V} = \frac{E_{\text{cell}}}{V_{\text{cell}}} = \frac{n_B}{B} E_{\text{cell}}, \tag{4.4.13}$$

$$p = -\frac{\partial E}{\partial V} = -\frac{\partial E_{\text{cell}}}{\partial V_{\text{cell}}} = \frac{n_B^2}{B} \frac{\partial E_{\text{cell}}}{\partial n_B}. \tag{4.4.14}$$

This EoS $\rho = \rho(p)$, generated purely from the generalized multi-wall skyrmion crystal, is valid at all densities. In our case, the pressure at which the Maxwell construction is applied is quite small, $p_{\mathrm{MX}} = 0.023$ MeV fm^{-3}, which corresponds to an energy difference of ≈ 0.1 MeV over a large density range ($0.91 n_0$ to $0.36 n_0$). The resulting EoS is shown in Fig. 4.7, alongside the EoS without the Maxwell construction applied.

Although the obtained equation of state covers the full range of densities one has to be aware that the multi-wall crystal does not describe the low density regime in its entirety. As we have already mentioned, to get a more realistic description of the crust the electrostatic interaction should be included. This can have an impact on the structure and symmetry of the skyrmions, which could potentially lead to the appearance of other inhomogeneous solutions with different baryon numbers per unit cell.

4.5 Neutron Stars from Quantum Skyrmion Crystals Coupled to Gravity

In order to describe neutrons stars within the Skyrme framework, we need to couple the generalized Skyrme model to gravity. We do this by introducing the Einstein–Hilbert–Skyrme action [126]

$$S = \frac{1}{16\pi G}\int_{\Sigma} \mathrm{d}^4x\sqrt{-g}R + S_{\mathrm{matter}}, \tag{4.5.1}$$

where $G = 1.3238094 \times 10^{-42}$ fm MeV^{-1} is the gravitational constant and R the Ricci scalar. The matter part of the Einstein–Skyrme action, S_{matter}, describes matter in the interior of the neutron star. It is well known that the interior of a neutron star is well described as a perfect fluid of nearly free neutrons and a very degenerate gas of electrons. We exploit this and use a perfect fluid model such that the energy-momentum tensor takes the form

$$T_{\mu\nu} = -\frac{2}{\sqrt{-g}}\frac{\delta S_{\mathrm{matter}}}{g^{\mu\nu}} = \left(\rho + p\right)u_\mu u_\nu + p g_{\mu\nu}, \tag{4.5.2}$$

where the energy density ρ and the pressure p are related by the multi-wall crystal EoS $\rho = \rho(p)$.

The Tolman–Oppenheimer–Volkoff System

Our aim is to calculate the maximum permitted mass and radius for a neutron star described by our system, and obtain the mass-radius curve. Therefore we have to solve the resulting Einstein equations for some particular choice of metric ansatz. The simplest case is that of a static non-rotating neutron star. We use a spherically symmetric ansatz of the spacetime metric, which in Schwarzschild coordinates reads [120]

$$\mathrm{d}s^2 = -A(r)\mathrm{d}t^2 + B(r)\mathrm{d}r^2 + r^2\left(\mathrm{d}\theta^2 + \sin^2\theta\mathrm{d}\phi^2\right) = g_{\mu\nu}\mathrm{d}x^\mu\mathrm{d}x^\nu, \tag{4.5.3}$$

where $x = (t, r, \theta, \phi) \in \Sigma$. The mass and radius of the neutron star can be calculated by inserting this spherical metric ansatz into the Einstein equations

$$G_{\mu\nu} = 8\pi G T_{\mu\nu}, \tag{4.5.4}$$

where $G_{\mu\nu} = R_{\mu\nu} - \frac{1}{2}Rg_{\mu\nu}$ is the Einstein tensor, and solving the standard Tolman–Oppenheimer–Volkoff (TOV) equations.

From the metric ansatz (4.5.3), we can determine the Christoffel symbols

$$\Gamma^{\lambda}_{\mu\nu} = \frac{1}{2}g^{\lambda\sigma}\left(\partial_\mu g_{\nu\sigma} + \partial_\nu g_{\mu\sigma} - \partial_\sigma g_{\mu\nu}\right), \tag{4.5.5}$$

of which the non-zero components are found to be

$$\begin{aligned} &\Gamma^{t}_{tr} = \Gamma^{t}_{rt} = \frac{1}{2A}\frac{\mathrm{d}A}{\mathrm{d}r}, \quad \Gamma^{r}_{tt} = \frac{1}{2B}\frac{\mathrm{d}A}{\mathrm{d}r}, \quad \Gamma^{r}_{rr} = \frac{1}{2B}\frac{\mathrm{d}B}{\mathrm{d}r}, \quad \Gamma^{\phi}_{\theta\phi} = \Gamma^{\phi}_{\phi\theta} = \cot\theta, \\ &\Gamma^{r}_{\theta\theta} = -\frac{r}{B}, \quad \Gamma^{\theta}_{r\theta} = \Gamma^{\theta}_{\theta r} = \Gamma^{\phi}_{\phi r} = \Gamma^{\phi}_{r\phi} = \frac{1}{r}, \quad \Gamma^{r}_{\phi\phi} = -\frac{r\sin^2\theta}{B}, \quad \Gamma^{\theta}_{\phi\phi} = -\sin\theta\cos\theta. \end{aligned} \tag{4.5.6}$$

Thus the Riemann curvature tensor can be obtained using the non-zero Christoffel symbols (4.5.6),

$$R^{\sigma}_{\rho\mu\nu} = \partial_\mu\Gamma^{\sigma}_{\nu\rho} - \partial_\nu\Gamma^{\sigma}_{\mu\rho} + \Gamma^{\lambda}_{\nu\rho}\Gamma^{\sigma}_{\mu\lambda} - \Gamma^{\lambda}_{\mu\rho}\Gamma^{\sigma}_{\nu\lambda}. \tag{4.5.7}$$

The Ricci tensor is given by $R_{\mu\nu} = g^{\rho\sigma}R_{\rho\mu\sigma\nu}$ and the relevant components are found to be given by

$$R_{tt} = -\frac{1}{4B^2}\left[\frac{\mathrm{d}A}{\mathrm{d}r}\frac{\mathrm{d}B}{\mathrm{d}r} + B\left(-\frac{4}{r}\frac{\mathrm{d}A}{\mathrm{d}r} + \frac{1}{A}\left(\frac{\mathrm{d}A}{\mathrm{d}r}\right)^2 - 2\frac{\mathrm{d}^2A}{\mathrm{d}r^2}\right)\right], \tag{4.5.8a}$$

$$R_{rr} = \frac{1}{4A^2Br}\left[A\frac{\mathrm{d}B}{\mathrm{d}r}\left(4A + r\frac{\mathrm{d}A}{\mathrm{d}r}\right) + Br\left(\left(\frac{\mathrm{d}A}{\mathrm{d}r}\right)^2 - 2A\frac{\mathrm{d}^2A}{\mathrm{d}r^2}\right)\right]. \tag{4.5.8b}$$

Now we can compute the Ricci scalar $R = g^{\mu\nu}R_{\mu\nu}$, that is

$$R = \frac{1}{2A^2B^2r^2}\left[Br^2\left(\frac{\mathrm{d}A}{\mathrm{d}r}\right)^2 + 4A^2\left(r\frac{\mathrm{d}B}{\mathrm{d}r} + B^2 - B\right) + Ar\left(r\frac{\mathrm{d}A}{\mathrm{d}r}\frac{\mathrm{d}B}{\mathrm{d}r} - 2B\left(r\frac{\mathrm{d}^2A}{\mathrm{d}r^2} + 2\frac{\mathrm{d}A}{\mathrm{d}r}\right)\right)\right]. \tag{4.5.9}$$

Now we have all the ingredients required to compute the Einstein tensor, $G_{\mu\nu} = R_{\mu\nu} - \frac{1}{2}Rg_{\mu\nu}$. The relevant components of the Einstein tensor are found to be

$$G_{tt} = \frac{A(r)}{B(r)^2r^2}\left[r\frac{\mathrm{d}B(r)}{\mathrm{d}r} + B(r)\left(B(r) - 1\right)\right], \tag{4.5.10a}$$

$$G_{rr} = \frac{1}{A(r)r^2}\left[r\frac{\mathrm{d}A(r)}{\mathrm{d}r} - A(r)\left(B(r) - 1\right)\right]. \tag{4.5.10b}$$

In the static case, and for a diagonal metric (that of which is applicable to us), we have $u_\mu = (\sqrt{-g_{00}}, 0, 0, 0)$ and the non-zero components of the energy-momentum tensor are given by

$$T_{00} = -\rho(p(r))g_{00}, \quad T_{ij} = p(r)g_{ij}. \tag{4.5.11}$$

In particular, for the spherical metric ansatz (4.5.3), the energy-momentum tensor reduces to the four terms:

$$T_{tt} = \rho(p(r))A(r), \tag{4.5.12a}$$

$$T_{rr} = B(r)p(r), \tag{4.5.12b}$$

$$T_{\theta\theta} = r^2 p(r), \tag{4.5.12c}$$
$$T_{\phi\phi} = r^2 p(r) \sin^2\theta. \tag{4.5.12d}$$

We are now in a position to calculate the Einstein equations (4.5.4) by using the energy-momentum tensor (4.5.12) and the Einstein tensor (4.5.10). From this, and the Bianchi identity

$$0 = \nabla_\nu T^{r\nu} = \frac{\partial T^{r\nu}}{\partial x^\nu} + T^{\sigma\nu}\Gamma^r_{\sigma\nu} + T^{r\sigma}\Gamma^\nu_{\sigma\nu}, \tag{4.5.13}$$

we get the following TOV system of ODEs

$$\frac{\mathrm{d}A}{\mathrm{d}r} = A(r)r\left(8\pi G B(r)p(r) - \frac{1-B(r)}{r^2}\right), \tag{4.5.14a}$$
$$\frac{\mathrm{d}B}{\mathrm{d}r} = B(r)r\left(8\pi G B(r)\rho(p(r)) + \frac{1-B(r)}{r^2}\right), \tag{4.5.14b}$$
$$\frac{\mathrm{d}p}{\mathrm{d}r} = -\frac{p(r)+\rho(p(r))}{2A(r)}\frac{\mathrm{d}A}{\mathrm{d}r}. \tag{4.5.14c}$$

The resulting TOV system involves 3 differential equations for A, B and p, which must be solved for a given value of the pressure in the centre of the neutron star ($p(0) = p_0$) until the condition $p(R_{\mathrm{NS}}) = 0$ is achieved. The radial point R_{NS} at which the pressure vanishes defines the radius of the neutron star, and the mass M is obtained from the Schwarzschild metric definition outside the star,

$$B(R_{\mathrm{NS}}) = \frac{1}{1-\frac{2MG}{R_{\mathrm{NS}}}}. \tag{4.5.15}$$

In order for the metric function $B(r)$ to be non-singular at $r = R_{\mathrm{NS}}$, the pressure $p(r)$ must obey $p'(R_{\mathrm{NS}}) = 0$.

The TOV system (4.5.14) is solved via a central shooting method from some initial central pressure p_0 at $r = 0$ until the edge of the star has been reached (corresponding to $p(R_{\mathrm{NS}}) = 0$). The amount of matter contained at $r = 0$ should be zero, which gives the boundary conditions $B(0) = A(0) = 1$. That is, the spacetime metric should approach the Minkowski metric towards the neutron star core. We can simultaneously apply a 4^{th} order Runge–Kutta method to the system of IVPs (4.5.14b), (4.5.14c), for the initial conditions $B(0) = 1$ and $p(0) = p_0$, until the condition $p(R_{\mathrm{NS}}) = 0$ is achieved. This yields the metric function $B(r)$ and the pressure profile $p(r)$ satisfying the necessary boundary conditions. Then the metric function $A(r)$ can be easily obtained by numerically integrating (4.5.14a). The corresponding radius R and the stellar mass $M = M(R_{\mathrm{NS}})$ can be extracted from the Schwarzschild definition (4.5.15). Increasing the central pressure p_0 in succession corresponds to determining a sequence of neutron stars of increasing mass, until the mass limit is reached [153]. The observational mass limit is approximately $2.5M_\odot$ [156], where the solar mass is $M_\odot = 1.116 \times 10^{60}$ MeV.

Neutron Star Properties and the Mass-Radius Curve

Now we solve the TOV equations using the EoS obtained from the isospin asymmetric multi-wall crystal solution in the generalized $\mathscr{L}_{0246}$-Skyrme model. In Fig. 4.6 we present the mass-radius curve for the MC crystal (blue line) together with recent astrophysical observations. It can be seen

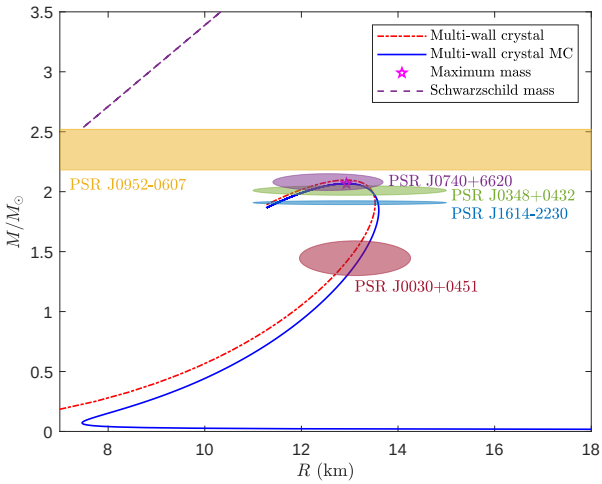

Figure 4.6: Mass-radius curves for neutron stars obtained from the multi-wall crystal EoS with (blue curve) and without (red curve) the Maxwell construction. The maximal mass M_{max} obtained from the MC multi-wall crystal EoS is also shown.

clearly that the obtained mass-radius curve passes through many observational constraints. For our choice of coupling constants (4.2.5), the Skyrme model generates an EoS which supports rather heavy neutron stars, $M > 2M_\odot$. Indeed, the maximum mass is predicted to be $M_{\text{max}} = 2.0971M_\odot$, occurring for a neutron star of radius $R = 13.12$ km. For this solution the central energy density is $\rho(0) = 784\,\text{MeV fm}^{-3}$, while the central pressure is $p(0) = 155.7\,\text{MeV fm}^{-3}$. The associated plots as a function of the maximal neutron star radius is shown in Fig. 4.7. We find that the speed of sound in the core is approximately half of the speed of light, $c_s = 0.491c$. The maximal mass can be further increased if we assume higher value of the sextic term coupling constant λ, at the cost of increasing the corresponding radius.

The main improvement presented by the generalized multi-wall crystal, in comparison to previous studies involving the $\text{SC}_{1/2}$ crystal, is in the low density regime. In previous attempts, except the pure BPS Skyrme case, neutron stars obtained from Skyrme models did not have crusts, i.e. the EoS was only defined up to the nuclear saturation point $n_B \geq n_0$, and not in the low density region $n_B < n_0$. In order to obtain a crust, the $\text{SC}_{1/2}$ crystal EoS can be smoothly joined with an EoS that well describes the low density regime, e.g. the BCPM EoS, as in [54]. In the resulting hybrid EoS, the high density region is still described by the $\text{SC}_{1/2}$ crystal. This typically increases the radius of neutron star by 1-2 km, depending on the mass of the neutron star. However, such a construction is not required here as the EoS from the multi-wall crystal with the Maxwell construction is valid at both high and low densities, naturally giving the neuron star a crust.

4.6 Concluding Remarks

In the present chapter, for the first time, we have obtained a ground state crystalline configuration for the generalized $\mathscr{L}_{0246}$-Skyrme model at finite densities. In contrast to previous studies on the generalized model, it has been carried out without imposing any constraints on the geometry. The

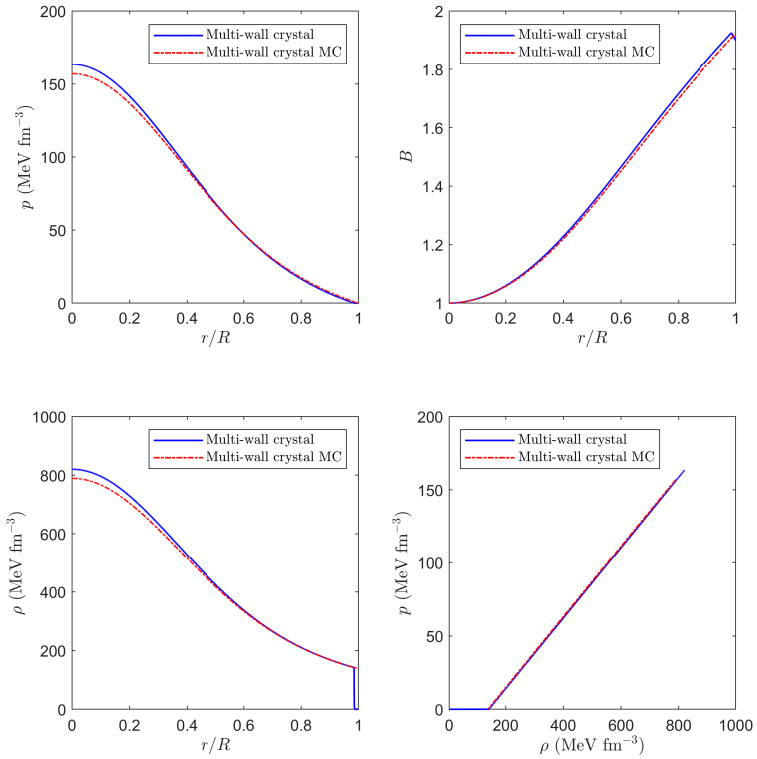

Figure 4.7: Plots at $M_{\max}$ of the pressure p, energy density ρ, metric function $B(r)$ and equations of state $\rho = \rho(p)$. The blue curve is for the crystal EoS with the Maxwell construction applied, removing any negative pressure from the system, whereas the red curve is for the "true" crystal EoS.

only limiting assumption is the amount of the baryon charge hosted by the unit cell, which is $B_{\text{cell}} = 4$. For that, we had to solve a variational problem which involves both the matter Skyrme field φ and the metric g of the unit 3-torus $\mathbb{T}^3$.

For our choice of the values for the coupling constants (4.2.5), we determine the ground state solution in the $\mathscr{L}_{0246}$-model to be the multi-wall crystal, as was recently observed in the previous chapter in the context of the $\mathscr{L}_{024}$-model. At low densities this solution takes the form of an isolated and planar two-wall layer of skyrmionic matter. As the baryon density grows $n_B > n_0$ then there appears to be a restoration of chiral symmetry, and the solution tends to the cubic $\text{SC}_{1/2}$ crystal.

We have used this multi-wall crystal to investigate the three most outstanding issues of the Skyrme model in its application to dense nuclear matter and neutron stars. Namely, (i) the problem of the thermodynamic instability at low densities; (ii) the maximal mass problem; and (iii) the compression modulus problem.

Firstly, in comparison with the $\text{SC}_{1/2}$ crystal or inhomogeneous crystals (e.g. $B = 32$ or $B = 108$ crystals composed of α-particles), the use of the true ground state solution allowed to resolve the issue of thermodynamically instability at low densities. Namely, the classical energy per baryon (of the unit cell) again reveals a minimum identified with the nuclear saturation point, but now

the difference between the energy at this point and at zero density is less than one percent. After inclusion of the quantum corrections to the total energy, due to the isospin d.o.f., and the lepton energy contributions for a β-equilibrated crystal, the total energy E_{cell} of the isospin asymmetric multi-wall crystal as a function of the nuclear density n_B was obtained. This minimum still existed but had reduced significantly and is practically negligible. The energy difference used in the Maxwell construction is so small that it is difficult to tell if the minimum truly exists or if it is just an artifact of our numerical algorithm. Nevertheless, it was still present so we had to use the Maxwell construction, which allowed us to obtain an EoS valid at all densities within the Skyrme model.

We remark that the Maxwell construction was required to avoid a thermodynamically unstable region which formally has negative pressure. Similar regions were found in previous studies where α, $B = 32$ or $B = 108$-crystals were studied. However, it is worth underlining that in these cases the Maxwell construction was impossible (c.f. the α-crystal) or extended to unacceptably large pressure/density regions (e.g. the corresponding neutron stars would possess cores mainly filled up by such regions). In the current work, the pressure at which the Maxwell construction is applied is only $p_{\text{MX}} = 0.022$ MeV fm^{-3} and it extends to densities below the saturation point. Consequently, our neutron stars are mainly governed by the part of EoS above p_{MX}, which is described by the multi-wall crystal EoS.

Of course, it is premature to identify the inhomogeneous low density solution found here with nuclear pasta or lasagna phases in the crust of neutron stars. This is due to the fact that such phases emerge due to a balance between the nuclear and electrostatic forces. However, in our study, the Coulomb interaction has not been taken into account. In particular, we emphasize that, while our crystal qualitatively looks like nuclear pasta, it does not model nuclear pasta. Be that as it may, our result shows that the Skyrme model itself has a tendency to form complicated, geometrically non-trivial and inhomogeneous structures at low density. It should be again underlined that, on the contrary to all previous studies, we did not impose any geometry restrictions on the solutions, e.g. by assuming particular boundary conditions as in [157, 158].

However, already at this stage of research, the multi-wall crystal in the density regime below saturation, $n_B < n_0$, leads to novel and intriguing observations. The first is the symmetry energy's disclosure of its cusp structure below the nuclear saturation density, $n_* \sim 3n_0/4 < n_0$, and, secondly, the finite value of the symmetry energy in the zero density limit, $n_B \to 0$. A cusp in the symmetry energy has previously been advocated for in [151], wherein they attributed the presence of this cusp to a change in topology due to a transition between the FCC_1 crystal of hedgehog skyrmions and the $\text{SC}_{1/2}$ crystal. A key component of their argument relies on this transition occurring in the high density regime $n_B > n_0$, however, this transition is believed to take place in the low density regime $n_B < n_0$ [46]. However, we have argued that these two features are generic of the Skyrme model and should occur for any infinite nuclear matter that undergoes a phase transition to somewhat isolated and finite matter in the zero density limit. This asymptotic transition to finite matter in the zero density limit is essential as the isolated solution will have a finite isospin moment of inertia tensor. A prime example of a crystalline solution in which such a transition occurs is that of the α-crystal, which tends to the isolated α-particle solution as $n_B \to 0$. Therefore, both the presence of the cusp and the non-zero value of the symmetry energy at the vacuum can be attributed as generic properties of the Skyrme model.

In fact, we have observed a further key feature of the symmetry energy. That is, a direct correspondence between the value of the symmetry energy at the vacuum and the asymmetry energy in the Bethe–Weizsäcker SEMF for nuclear binding energies. This strengthens our suggestion that

the Skyrme model can be interpreted as a natural interpolation between infinite isospin asymmetric nuclear matter and finite (almost) symmetric atomic nuclei. This is further supported by the observation that the proton fraction $\gamma_p \to 0.5$ in the zero density limit $n_B \to 0$, which describes almost totally isospin symmetric nuclear matter, and then, for small densities, decreases yielding asymmetric matter. In this pattern one may again recognize finite nuclei. Indeed, the proton number and neutron number are approximately equivalent ($\delta \approx 0$) for smaller atomic nuclei while for larger nuclei there is an asymmetry ($\delta \neq 0$) caused by a surplus of neutrons.

The second big issue is also resolved since the inclusion of the sextic term makes the EoS sufficiently stiff at large densities. Using this EoS we were able to compute the mass-radius curve for the resulting neutron stars. The maximal mass was found to be $M_{\max} = 2.0971 M_{\odot}$, which is a acceptable large mass and the mass-radius curve fits very well to known astrophysical data.

Finally, we shown that the problem of the compression modulus cannot be solved solely by consideration of the newly discovered inhomogeneous ground state crystalline configuration. Although reduced by approximately 200 MeV, the compression modulus is still a few times larger than the experimental value. We underline that this negative result is of high importance for the Skyrme model. It simply shows that the the solitonic model based entirely on the lightest, pionic d.o.f. is not able to correctly describe this quantity. Fundamentally, the compression modulus is related to nuclear binding energies, which is also a problem within the Skyrme model. If a variant of the Skyrme model has low binding energies then, naturally, the compression modulus will closer to its accepted value. Therefore, inclusion of more massive mesons, which are known to soften the EoS at the saturation point, seems to be unavoidable. Interestingly, this coincides with the role playing by ρ mesons in reducing of the binding energies of the Skyrmions.

It should be underlined that, if compared with other effective nuclear models, the generalized Skyrme model has an extremely small number of free parameters. It has only four coupling constants $\{F_\pi, m_\pi, e, \lambda\}$, of which the pion mass m_π and the pion decay constant F_π are, from the onset, fixed to their physical values, or as close to them as possible. The two other parameters e and λ, which, respectively, multiply the quartic (Skyrme) and sextic terms can be treated as free parameters in this model. They can be constrained by fitting the multi-wall crystal to nuclear observables, i.e. they can be chosen such that the symmetric energy $M_B(n_B)$ and nuclear density n_B at saturation n_0 are close to the experimentally determined values.

There are several directions in which our study can be continued. First of all, it is widely known that the lower density phases of nuclear matter are governed by a balance between nuclear and Coulomb forces, which leads to a plethora of geometrically different structures. The fact that the generalized Skyrme model, even without the inclusion of electrostatic interactions, gives rise to the multi-wall crystal (a lasagna like structure) can be viewed as an intrinsic ability of the model to provide such solutions. Other inhomogeneous configurations have been observed in the Skyrme model [157, 158], however they were an effect of the imposed boundary conditions and therefore their applications to nuclear physics remain to be clarified. Undoubtedly, inclusion of the Coulomb interaction seems mandatory, see e.g. [18]. It seems likely that including Coulomb interactions will not only give insight into such geometric phases but could also allow one to avoid use of the Maxwell construction. Thus it could possibly provide a complete description of the crust in neutron star within the Skyrme model framework.

More importantly, the inclusion of other d.o.f., like for example ρ or ω mesons, seems inevitable to resolve the issue of the compressibility at nuclear saturation. This, combined with the inhomogeneous multi-wall crystal detailed in the paper, may possibly lead to the correct value of the

compression modulus.

Five

Skyrmion Crystals Stabilized by ω-Mesons

This chapter is based on work with D. Harland and M. Speight [159].

5.1 Introduction

At its core, the Skyrme model contains the NLσM. This is the lowest-order term in all mesonic effective Lagrangian models and it supports soliton solutions [160]. However, by simple application of Derrick's Theorem, the solitons are not energetically stable as the NLσM is not length scale invariant in three dimensions. Skyrme's proposal was the inclusion of a higher fourth-order term with opposing scaling behaviour to provide the soliton with a scale. There is, however, little phenomenological justification for the addition of the Skyrme term. In particular, it makes the theory non-renormalizable.

Remarkably, it was shown by Adkins and Nappi [161] that the inclusion of the ω meson to the NLσM alone stabilises the solitons, without the need for the Skyrme term. This is achieved by considering ω as a gauge particle associated to $\mathrm{U}(1)_V$ and defining a minimally broken $\mathrm{U}(1)_V$ Lagrangian for spin-1 mesons [162], with explicit breaking of the gauge invariance by introducing a mass term. The abelian nature of the ω-meson means it couples anomalously through the gauged Wess–Zumino (WZ) term [163].

The ω-meson variant of the Skyrme model, initially proposed by Adkins and Nappi, has only been investigated for light nuclei with baryon numbers $B = 1, \ldots, 8$. This is in part due to the complexity of the problem: the temporal component ω_0 is subject to a non-trivial constraint and can be interpreted as a static potential generated by a source proportional to the topological charge density. The technical reason for this is that the static energy is not bounded from below, this renders usual gradient descent based energy minimization algorithms useless. Sutcliffe was the first to consider the model with $B > 1$ [164], using the rational map approximation to construct (approximate) skyrmions with charges 1 to 4. Speight then considered the model in the charge $B = 1$ sector with the addition of an (explicit) chiral symmetry breaking term, successfully reproducing the proton–neutron mass difference [165]. A later breakthrough came when Gudnason and Speight [88] developed a method to solve this constrained energy minimization problem. Therein, they found true static solutions for topological charges 1 through 8, for a range of coupling constants. At high couplings, they observed that the static solutions are qualitatively similar to those of the standard Skyrme model with massless pions. However, at reasonably low couplings, these skyrmions appear quite similar to those of the lightly bound Skyrme model [166, 167], at least for charges 1 to 3, and have realistic classical binding energies.

Thereafter Adkins and Nappi's seminal paper, it was natural to consider generalizations of the non-linear pion theory by replacing the *ad hoc* Skyrme term with explicit interactions with vector mesons. One such approach is based on the so-called hidden local symmetry (HLS) method, where a hidden symmetry of the NLσM is gauged and the corresponding gauge particle acquires mass through the Higgs mechanism [160]. This allows for the incorporation of ρ-mesons, as well as the ω-meson. An alternative option has also been proposed, wherein the ρ-meson was considered instead of the ω-meson [168]. Sutcliffe and Naya [169, 170] explored a slightly more general ρ-Skyrme model than this, which greatly improved on the binding energies. The main difference between coupling to ω-mesons or ρ-mesons is that the ρ-mesons interact with the vector pion current, whereas the ω-mesons interacts with the baryonic current.

The HLS approach has been investigated extensively, especially in the context of dense nuclear matter [171–175]. The ground state configuration of nuclear matter in the Skyrme model was found, independently by Kugler and Shtrikmann [39] and Castillejo *at al.* [40], to be a face-centred cubic crystal of single hedgehog skyrmions. At higher density, this FCC_1 crystal undergoes a phase transition to a simple cubic crystal of half-skyrmions, the $\mathrm{SC}_{1/2}$ crystal. Within the HLS framework, Lee *et al.* [176] incorporated a dilaton field to the massive Skyrme model, which is associated with the scale anomaly of QCD. In their model the dilaton is crucial in realizing the phase transition from the Goldstone mode (spontaneously broken chiral symmetry FCC_1 phase) to the Wigner mode (unbroken chiral symmetry $\mathrm{SC}_{1/2}$ phase) consistently with the vector manifestation (VM) fixed point. This fixed point is characterized by the vanishing of both $\langle\sigma\rangle$ and the in-medium pion decay constant F_π^*, corresponding to the restoration of the spontaneously broken chiral symmetry. Interestingly, the addition of the ω-meson prevents the scale-anomaly dilaton field, and thus the in-medium pion decay constant, from developing a vanishing vacuum expectation value at the VM fixed point [177], resulting in a non-restoration of chiral symmetry. This is reminiscent of pseudo-gap phenomena in condensed matter physics. They also observed that the ω-meson produces not only a strong repulsive force amongst skyrmions, but an intermediate range one as well and causes the skyrmions to become larger in size and more massive.

In all of the above HLS crystal investigations, the Kugler and Shtrikmann Fourier series method was generalized to incorporate vector mesons. However, as we have seen in Chap. 3, the $\mathrm{SC}_{1/2}$ crystal is in fact not the ground state configuration in the Skyrme model with massive pions; a multi-wall solution is. Recall that we obtained four distinct skyrmion crystals: the $\mathrm{SC}_{1/2}$ crystal, an α-particle crystal, a chain crystal, and a multi-wall or crystal.

We are interested in how the ω-meson itself affects the description of these four crystalline solutions and, in particular, if there is a change in the ground state configuration. Further, we predict coefficients in the Bethe–Weizsäcker semi empirical mass formula using ω-skyrmion crystals and the α-particle approximation first considered by Baskerville [17]. Finally, we attempt to address the compression modulus problem within the Skyrme model and determine a more acceptable value of the nuclear matter incompressibility coefficient.

5.2 The ω-Skyrme Model

The ω-meson variant of the Skyrme model is a NLσM coupled to the isoscalar ω vector meson field. It consists of the Skyrme field $\varphi : \Sigma \to \mathrm{SU}(2)$ and the ω vector meson (a 1-form on Σ). Spacetime is given by the $(3+1)$-dimensional Lorentzian manifold $\Sigma = \mathbb{R} \times \mathbb{R}^3$ equipped with

a pseudo-Riemannian metric g that has metric signature $-+++$ and constant coefficients. Our starting point is the ω-Skyrme Lagrangian defined by Adkins & Nappi [161], which is given by

$$\mathscr{L} = \mathscr{L}_\varphi + \mathscr{L}_\omega + \mathscr{L}_{\mathrm{WZ}}, \tag{5.2.1}$$

where $\mathscr{L}_\varphi$ is the NLσM Lagrangian with the explicit chiral symmetry breaking pion mass term,

$$\mathscr{L}_\varphi = -\frac{1}{8\hbar^3}F_\pi^2 m_\pi^2 \operatorname{Tr}\left(\mathrm{Id}_2 - \varphi\right) + \frac{F_\pi^2}{16\hbar}g^{\mu\nu}\operatorname{Tr}\left(L_\mu L_\nu\right). \tag{5.2.2}$$

The minimally broken $\mathrm{U}(1)_V$ Lagrangian for spin-1 mesons is given by the term

$$\mathscr{L}_\omega = \frac{m_\omega^2}{2\hbar^3}g^{\mu\nu}\omega_\mu\omega_\nu + \frac{1}{4\hbar}g^{\mu\alpha}g^{\nu\beta}\omega_{\mu\nu}\omega_{\alpha\beta}, \qquad \omega_{\mu\nu} = \partial_\mu\omega_\nu - \partial_\nu\omega_\mu, \tag{5.2.3}$$

and the gauged Wess-Zumino term is

$$\mathscr{L}_{\mathrm{WZ}} = \beta_\omega g^{\mu\nu}\omega_\mu\mathscr{B}_\nu, \tag{5.2.4}$$

which describes the the coupling of the ω-meson to three pions. The topological charge and baryonic current are, respectively, still defined by (1.1.9).

The main free parameters of this model are the pion decay constant F_π, the pion mass m_π, the ω-meson mass m_ω, and the coupling constant β_ω. As before, $\hbar = 197.3$ MeV fm is the reduced Planck constant, and $L_\mu = \varphi^\dagger\partial_\mu\varphi$ is an $\mathfrak{su}(2)$-valued left current. We will consider different values for the interaction constant β_ω. This coupling constant β_ω can be related to the $\omega \to \pi^+\pi^-\pi^0$ decay rate, which is in reality enhanced by the resonance $\omega \to \rho + \pi$, but is not included in the current theory. The decay rate, calculated using fiducial experimental values, is found to be $\Gamma_{\omega\to 3\pi} = 8.49$ MeV, which gives the upper bound $\beta_\omega \leq 23.9$ [88].

The ω-meson can be integrated out in this theory, reducing the model to an effective field theory of pions only, which is valid in energy regimes lower than the ω-meson mass m_ω. To see this, consider the on-shell condition for the ω-meson (that is, the Euler–Lagrange field equations associated to the Lagrangian $\mathscr{L}_\omega + \mathscr{L}_{\mathrm{WZ}}$ as defined by (5.2.3) and (5.2.4))

$$\frac{\delta(\mathscr{L}_\omega + \mathscr{L}_{\mathrm{WZ}})}{\delta\omega_\mu} = \frac{m_\omega^2}{\hbar^3}\omega^\mu + \beta_\omega\mathscr{B}^\mu - \frac{1}{\hbar}\partial_\nu\omega^{\nu\mu} = 0. \tag{5.2.5}$$

For sufficiently large m_ω, such that $\partial_\nu\omega^{\nu\mu} \ll m_\omega^2$, the on-shell condition can be approximated (by ignoring derivative contributions) as

$$\omega^\mu \simeq -\frac{\beta_\omega\hbar^3}{m_\omega^2}\mathscr{B}^\mu. \tag{5.2.6}$$

Substituting this into the ω-meson Lagrangian yields

$$\mathscr{L}_\omega + \mathscr{L}_{\mathrm{WZ}} \to -\lambda^2\pi^4 g^{\mu\nu}\mathscr{B}_\mu\mathscr{B}_\nu, \tag{5.2.7}$$

where

$$\lambda^2 = \frac{\beta_\omega^2\hbar^3}{2m_\omega^2\pi^4}. \tag{5.2.8}$$

In the large mass limit $m_\omega \to \infty$ with the ratio β_ω/m_ω kept fixed, the ω-Skyrme model reduces to the $\mathscr{L}_{026}$-Skyrme model, described by the Lagrangian

$$\mathscr{L}_{026} = -\frac{1}{8\hbar^3}F_\pi^2 m_\pi^2 \operatorname{Tr}(\mathrm{Id}_2 - \varphi) + \frac{F_\pi^2}{16\hbar} g^{\mu\nu} \operatorname{Tr}\big(L_\mu L_\nu\big) - \lambda^2\pi^4 g^{\mu\nu}\mathscr{B}_\mu\mathscr{B}_\nu. \tag{5.2.9}$$

For convenience, we follow Sutcliffe [164] and rescale the ω meson by $\omega \mapsto \omega F_\pi$, and choose the classical energy scale to be $\tilde{E} = F_\pi^2/m_\omega$ (MeV) and the length scale to be $\tilde{L} = \hbar/m_\omega$ (fm). Then the rescaled ω-Skyrme Lagrangian in dimensionless units is given by

$$\mathscr{L} = -\frac{1}{8}m^2 \operatorname{Tr}(\mathrm{Id}_2 - \varphi) + \frac{1}{16} g^{\mu\nu} \operatorname{Tr}\big(L_\mu L_\nu\big) + \frac{1}{2} g^{\mu\nu}\omega_\mu\omega_\nu + \frac{1}{4} g^{\mu\alpha} g^{\nu\beta}\omega_{\mu\nu}\omega_{\alpha\beta} + c_\omega g^{\mu\nu}\omega_\mu\mathscr{B}_\nu, \tag{5.2.10}$$

where the rescaled pion mass and ω coupling constant are, respectively, $m = m_\pi/m_\omega$ and $c_\omega = m_\omega\beta_\omega/F_\pi$. The energy-momentum tensor (in dimensionless Skyrme units) is given by

$$\begin{aligned} T_{\mu\nu} = &-\frac{1}{8}\operatorname{Tr}\big(L_\mu L_\nu\big) - \omega_\mu\omega_\nu - 2c_\omega\omega_\mu\mathscr{B}_\nu - g^{\alpha\beta}\omega_{\mu\alpha}\omega_{\nu\beta} + g_{\mu\nu}\Big\{-\frac{1}{8}m^2 \operatorname{Tr}(\mathrm{Id}_2 - \varphi) \\ &+\frac{1}{16} g^{\alpha\beta} \operatorname{Tr}\big(L_\alpha L_\beta\big) + \frac{1}{2} g^{\alpha\beta}\omega_\alpha\omega_\beta + \frac{1}{4} g^{\alpha\rho} g^{\beta\sigma}\omega_{\alpha\beta}\omega_{\rho\sigma} + c_\omega g^{\alpha\beta}\omega_\alpha\mathscr{B}_\beta\Big\}. \end{aligned} \tag{5.2.11}$$

The usual energy functional is obtained from the temporal part of the energy-momentum tensor, that is,

$$\mathscr{E}_{\mathrm{stat}} = \frac{1}{8}m^2 \operatorname{Tr}(\mathrm{Id}_2 - \varphi) - \frac{1}{16} g^{ij} \operatorname{Tr}\big(L_i L_j\big) - \frac{1}{2}\omega_0^2 - \frac{1}{2} g^{ij}\omega_{0i}\omega_{0j} - c_\omega\omega_0\mathscr{B}_0. \tag{5.2.12}$$

We wish to study static Skyrme fields $\varphi : \mathbb{R}^3 \to \mathrm{SU}(2)$ and ω-meson fields $\omega : \mathbb{R}^3 \to \mathbb{R}$ that are periodic with respect to some 3-dimensional period lattice

$$\Lambda = \big\{n_1\vec{X}_1 + n_2\vec{X}_2 + n_3\vec{X}_3 : n_i \in \mathbb{Z}\big\}. \tag{5.2.13}$$

As before, we can equivalently interpret the domain of the fields as $\mathbb{R}^3/\Lambda$, and identify this with the unit 3-torus $(\mathbb{T}^3, g)$ via the obvious diffeomorphism

$$F : \mathbb{T}^3 \to \mathbb{R}^3/\Lambda, \qquad (x^1, x^2, x^3) \mapsto x^1\vec{X}_1 + x^2\vec{X}_2 + x^3\vec{X}_3. \tag{5.2.14}$$

The metric g on $\mathbb{T}^3$ is the pullback of the metric d by F, i.e.

$$g = F^* d = g_{ij}\mathrm{d}x^i\mathrm{d}x^j, \qquad g_{ij} = \vec{X}_i \cdot \vec{X}_j. \tag{5.2.15}$$

Varying the metric g_s on $\mathbb{T}^3$ with $g_0 = F^*d$ is equivalent to varying the lattice Λ_s with $\Lambda_0 = \Lambda$. The energy minimized over variations g_s of the domain metric is equivalent to determining the energy minimizing period lattice Λ.

Throughout, it will be convenient to use the NLσM formulation (1.1.16) of the model. We now identify the Skyrme field as the map $\varphi : (\mathbb{T}^3, g) \to S^3$, where g is a flat Riemannian metric. Since we are only interested in static field configurations, only the temporal component of the topological current remains, i.e. $\mathscr{B}^i = 0$. Consequently, only the temporal component ω_0 of the ω-meson survives, since the topological charge density acts as a source term for the ω field. For

notational convenience, we will drop the subscript and denote $\omega \equiv \omega_0$. Then the static energy functional is

$$M_B(\varphi, g) = \int_{\mathbb{T}^3} \mathrm{d}^3x\sqrt{g}\left\{\frac{1}{4}m^2(1-\varphi^0) + \frac{1}{8}g^{ij}\partial_i\varphi^\mu\partial_j\varphi^\mu - \frac{1}{2}g^{ij}\partial_i\omega\partial_j\omega - \frac{1}{2}\omega^2 - c_\omega\omega\mathscr{B}_0\right\}. \tag{5.2.16}$$

This is the energy functional that needs to be minimized with respect to variations of the fields (φ, ω) and the metric g on $\mathbb{T}^3$.

In any Yang–Mills theory, the canonical momentum conjugate to the temporal component of the gauge field is always zero, leading to a constraint of the theory. The Dirac–Bergmann algorithm ensures that the conservation of this constraint in time yields a further constraint [160]. This constraint can then be solved to remove the constrained degree of freedom from the theory; here, that is the temporal component ω. When considering static field configurations, this constraint is identical to the Euler–Lagrange field equations corresponding to temporal ω,

$$\left(-g^{ij}\partial_i\partial_j + 1\right)\omega = -c_\omega\mathscr{B}_0. \tag{5.2.17}$$

This is a linear equation for ω with a source term proportional to the baryon current. The ω-meson is completely determined by the Skyrme field φ and the domain metric g. If we consider the limit where the ω-meson mass m_ω and the coupling constant β_ω becomes large, with their ratio β_ω/m_ω fixed, this leads to the well-known sextic term in the Lagrangian [55].

The static energy can be written more conveniently by taking the inner product of (5.2.17) with ω and integrating by parts to find that

$$\int_{\mathbb{T}^3} \mathrm{d}^3x\sqrt{g}\, c_\omega\omega\mathscr{B}_0 = -\int_{\mathbb{T}^3} \mathrm{d}^3x\sqrt{g}\left(g^{ij}\partial_i\omega\partial_j\omega + \omega^2\right). \tag{5.2.18}$$

Then the energy can be expressed as

$$M_B(\varphi, g) = \int_{\mathbb{T}^3} \mathrm{d}^3x\sqrt{g}\left\{\frac{1}{4}m^2(1-\varphi^0) + \frac{1}{8}g^{ij}\partial_i\varphi^\mu\partial_j\varphi^\mu + \frac{1}{2}g^{ij}\partial_i\omega\partial_j\omega + \frac{1}{2}\omega^2\right\}, \tag{5.2.19}$$

which is bounded below (by 0).

Before moving on, it is interesting to note that the energy (5.2.19) subject the constraint (5.2.17) obeys a topological energy bound. In fact, the bound is valid in the more general setting: the Skyrme field is a map $\varphi : M \to N$ between Riemannian 3-manifolds (M^3, g) and (N^3, h). We have a functional on such maps given by

$$M_B(\varphi, g) = M_B^\varphi(\varphi, g) + M_B^\omega(\varphi, g), \tag{5.2.20}$$

with

$$M_B^\varphi(\varphi, g) = \int_M \left(\frac{1}{8}\left|\mathrm{d}\varphi\right|_g^2 + \frac{1}{4}(V\circ\varphi)\right)\mathrm{vol}_g, \tag{5.2.21}$$

$$M_B^\omega(\varphi, g) = \int_M \left(\frac{1}{2}\left|\mathrm{d}\omega\right|_g^2 + \frac{1}{2}\omega^2\right)\mathrm{vol}_g, \tag{5.2.22}$$

subject to the constraint

$$\left(\Delta_g + 1\right)\omega = -c_\omega *_g \varphi^*\Omega, \tag{5.2.23}$$

where Ω is the normalized volume form on N, i.e

$$\Omega = \frac{\mathrm{vol}_N}{|N|}. \tag{5.2.24}$$

Proposition 15. *For all smooth maps $\varphi : M \to N$ there exists a lower topological energy bound for $M_B(\varphi, g)$, that is,*

$$M_B \geq \frac{B^2 c_\omega^2}{2|M|}. \tag{5.2.25}$$

Proof. Let us define $\mathscr{B} = *\varphi^*\Omega$ such that $\varphi^*\Omega = \mathscr{B}\mathrm{vol}_0$. Then, from the ω-meson constraint (5.2.23), the topological charge can be expressed as

$$B = \int_M \varphi^*\Omega = -\frac{1}{c_\omega}\int_M \left(\Delta_g + 1\right)\omega \,\mathrm{vol}_g = -\frac{1}{c_\omega}\int_M \omega \,\mathrm{vol}_g. \tag{5.2.26}$$

Using the Cauchy–Schwartz inequality, we obtain the following relation

$$B^2 = \frac{1}{c_\omega^2}\left(\int_M \omega \,\mathrm{vol}_g\right)^2 \leq \frac{1}{c_\omega^2}\left(\int_M \omega^2 \,\mathrm{vol}_g\right)\left(\int_M 1 \,\mathrm{vol}_g\right) = \frac{|M|}{c_\omega^2}\int_M \omega^2 \,\mathrm{vol}_g. \tag{5.2.27}$$

With this, we can derive a simple lower topological bound on the static energy (5.2.20), that is,

$$M_B \geq \frac{1}{2}\int_M \omega^2 \,\mathrm{vol}_g \geq \frac{B^2 c_\omega^2}{2|M|} \tag{5.2.28}$$

□

For the particular case of interest, $M = \mathbb{T}^3$, we have

$$M_B \geq E_{\mathrm{bound}} = \frac{B^2 c_\omega^2}{2\sqrt{g}}. \tag{5.2.29}$$

5.3 Stress-Energy Tensor

We now turn to the problem of constructing Skyrme crystals, i.e. minimizing the energy (5.2.19) with respect to variations in φ and g. We do this numerically, using arrested Newton flow. This algorithm works by solving Newton's equations of motion for the energy M_B, written formally as:

$$\frac{\mathrm{d}^2}{\mathrm{d}t^2}(\varphi^\mu, g_{ij}) = -\nabla M_B. \tag{5.3.1}$$

Initial conditions are chosen such that $\frac{\mathrm{d}}{\mathrm{d}t}(\varphi^\mu, g_{ij}) = 0$. These ensure that the flow reduces energy at early times. If at any later time the energy begins to increase, the flow is arrested and the velocities $\frac{\mathrm{d}}{\mathrm{d}t}(\varphi^\mu, g_{ij})$ are set to zero. The flow then resumes from the same position. It is deemed to have converged when ∇M_B is sufficiently small.

We recall that ω appearing in the energy functional (5.2.19) depends on φ and g through the constraint (5.2.17). Thus computing M_B and its gradient entails computing ω at each time step. As in [88], this is accomplished using a conjugate gradient method. The constraint (5.2.17) means that the metric-dependence of the energy is much more complicated than in the standard Skyrme model. As a result, the algorithm described here is slightly different from the algorithm used earlier to find crystals in the standard Skyrme model [100].

The gradient on the right hand side of (5.3.1) is understood using the calculus of variations. We write $\nabla M_B = (\Phi_\mu, S_{ij})$, in which Φ_μ and S_{ij} are defined by

$$\frac{\mathrm{d}}{\mathrm{d}s} M_B(\varphi_s, g_s)\Big|_{s=0} = \int_{\mathbb{T}^3} \mathrm{d}^3x\sqrt{g}\,\left(\Phi_\mu(\varphi,g)\dot{\varphi}^\mu + S_{ij}(\varphi,g)\dot{g}_{kl}g^{jk}g^{li}\right) \tag{5.3.2}$$

for all one-parameter variations φ_s, g_s with $(\phi_0, g_0) = (\phi, g)$ and $\frac{\mathrm{d}}{\mathrm{d}s}(\varphi_s, g_s) = (\dot{\varphi}, \dot{g})$ at $s = 0$. The calculation of Φ_μ and S_{ij} is delicate, because ω appearing in (5.2.19) depends on φ and g implicitly through the constraint (5.2.17). Using results of [88], Φ_μ is given (in the case of flat metrics on $\mathbb{T}^3$) by

$$\Phi_\mu = -\frac{1}{4}(\delta^{\mu\nu} - \varphi^\mu\varphi^\nu)(m^2\delta^{0\nu} + g^{ij}\partial_i\partial_j\varphi^\nu) + \frac{c_\omega}{4\pi^2\sqrt{g}}\epsilon_{ijk}\epsilon_{\mu\nu\rho\sigma}\varphi^\nu\partial_i\omega\partial_j\varphi^\rho\partial_k\varphi^\sigma. \tag{5.3.3}$$

This coincides with the Euler–Lagrange equation of the original unconstrained energy functional (5.2.12). The stress-energy tensor S_{ij} is computed in the following proposition, formulated in the general setting of maps $\varphi : (M, g) \to (N, h)$ between Riemannian 3-manifolds.

Proposition 16. *The stress-energy tensor $S = S_{ij}\mathrm{d}x^i\mathrm{d}x^j$ associated to the energy (5.2.20) is the section of $\Gamma(\odot^2 T^*M)$ given by*

$$S(\varphi, g) = \left(\frac{1}{16}|\mathrm{d}\varphi|_g^2 + \frac{1}{8}(V\circ\varphi) - \frac{1}{4}|\mathrm{d}\omega|_g^2 - \frac{1}{4}\omega^2\right)g - \left(\frac{1}{8}\varphi^*h - \frac{1}{2}\mathrm{d}\omega\otimes\mathrm{d}\omega\right) \tag{5.3.4}$$

Note that in local coordinates the formula (5.3.4) gives

$$S_{ij} = \left(\frac{1}{16}g^{mn}\partial_m\varphi^\mu\partial_n\varphi^\mu + \frac{1}{8}m^2\left(1-\varphi^0\right) - \frac{1}{4}g^{mn}\partial_m\omega\partial_n\omega - \frac{1}{4}\omega^2\right)g_{ij} - \frac{1}{8}\partial_i\varphi^\mu\partial_j\varphi^\mu + \frac{1}{2}\partial_i\omega\partial_j\omega. \tag{5.3.5}$$

This coincides with the stress tensor for the original unconstrained energy functional (5.2.12).

Proof. Let us reintroduce the notation $\langle A, B\rangle_g = A_{ij}B_{kl}g^{ik}g^{jl}$ for the natural inner product of two-tensors $A = A_{ij}\mathrm{d}x^i\mathrm{d}x^j$, $B = B_{kl}\mathrm{d}x^k\mathrm{d}x^l$. On a curve g_s in the space of flat metrics, the variation of the inverse metric is found to be

$$\frac{\mathrm{d}}{\mathrm{d}s}\Big|_{s=0} g^{ij}(s) = -g^{ik}(\delta g)_{kl}g^{lj}, \tag{5.3.6}$$

and the variation of the volume is well-known, which is given by [109, p. 82]

$$\frac{\mathrm{d}}{\mathrm{d}s}\Big|_{s=0} \mathrm{vol}_{g_s} = \frac{1}{2}\langle g, \delta g\rangle_g\,\mathrm{vol}_g. \tag{5.3.7}$$

The first variation of the Dirichlet energy with respect to the metric g is given by, e.g., [110, p. 19]

$$\frac{\mathrm{d}E_2(\varphi, g_s)}{\mathrm{d}s}\Big|_{s=0} = \frac{\mathrm{d}}{\mathrm{d}s}\Big|_{s=0}\left(\frac{1}{8}\int_M |\mathrm{d}\varphi|_{g_s}^2\mathrm{vol}_{g_s}\right) = \int_M \langle\frac{1}{16}|\mathrm{d}\varphi|_g^2 g - \frac{1}{8}\varphi^*h, \delta g\rangle_g\,\mathrm{vol}_g. \tag{5.3.8}$$

The potential function $V\circ\varphi$ has no dependence on the metric g and so the variation of the potential is simply

$$\frac{\mathrm{d}E_0(\varphi, g_s)}{\mathrm{d}s}\Big|_{s=0} = \frac{1}{4}\int_M (V\circ\varphi)\,\frac{\mathrm{d}\mathrm{vol}_{g_s}}{\mathrm{d}s}\Big|_{s=0} = \int_M \langle\frac{1}{8}(V\circ\varphi)g, \delta g\rangle_g\,\mathrm{vol}_g. \tag{5.3.9}$$

This produces the first part of the stress-energy tensor, corresponding to the first variation of the Skyrme energy functional (5.2.21),

$$S^{\varphi}(\varphi, g) = \left(\frac{1}{16}|\mathrm{d}\varphi|_g^2 + \frac{1}{8}(V \circ \varphi)\right) g - \frac{1}{8}\varphi^* h. \tag{5.3.10}$$

Now, let us focus on computing the first variation of the ω-meson energy functional (5.2.22). Using the constraint (5.2.23), the ω-energy functional (5.2.22) can be expressed more conveniently in the form

$$M_B^{\omega}(\varphi, g) = \int_M \left(\frac{1}{2}\left|\mathrm{d}\omega\right|_g^2 + \frac{1}{2}\omega^2\right) \mathrm{vol}_g = -\frac{c_\omega}{2}\int_M \omega\varphi^*\Omega, \tag{5.3.11}$$

where we note that the pullback $\varphi^*\Omega \in \Omega^3(M)$ is g-independent. Then, the first variation of this with respect to the metric g_s is found to be

$$\begin{aligned}\left.\frac{\mathrm{d}M_B^{\omega}(\omega_s, g_s)}{\mathrm{d}s}\right|_{s=0} &= -\frac{c_\omega}{2}\int_M \dot{\omega}\varphi^*\Omega \\ &= -\frac{c_\omega}{2}\left\langle \dot{\omega}, *\varphi^*\Omega\right\rangle_{L^2(g)} \\ &= \frac{1}{2}\left\langle \dot{\omega}, \left(\Delta_g + 1\right)\omega\right\rangle_{L^2(g)} \\ &= \frac{1}{2}\left\langle \left(\Delta_g + 1\right)\dot{\omega}, \omega\right\rangle_{L^2(g)},\end{aligned} \tag{5.3.12}$$

where we have denoted $\dot{\omega} = \left.\frac{\mathrm{d}}{\mathrm{d}s}\right|_{s=0}\omega_s$. This can be simplified as follows. Consider the variation of the Hodge star operator $*_g : \Omega^3(M) \to \Omega^0(M)$,

$$\left.\frac{\mathrm{d}}{\mathrm{d}s}\right|_{s=0} *_{g_s} = -\frac{1}{2}\langle g, \delta g\rangle_g *_g, \tag{5.3.13}$$

and define $\dot{\Delta}_g = \left.\frac{\mathrm{d}}{\mathrm{d}s}\right|_{s=0}\Delta_{g_s}$. Then, varying the ω-meson constraint (5.2.23), and using (5.3.13), yields

$$\begin{aligned}\left.\frac{\mathrm{d}}{\mathrm{d}s}\right|_{s=0}\left\{\left(\Delta_{g_s} + 1\right)\omega_s\right\} &= \left(\Delta_g + 1\right)\dot{\omega} + \dot{\Delta}_g\omega \\ &= \left.\frac{\mathrm{d}}{\mathrm{d}s}\right|_{s=0}\left\{-c_\omega *_{g_s}\varphi^*\Omega\right\} = \frac{c_\omega}{2}\langle g, \delta g\rangle_g *_g \varphi^*\Omega.\end{aligned} \tag{5.3.14}$$

Therefore,

$$\left(\Delta_g + 1\right)\dot{\omega} = -\dot{\Delta}_g\omega + \frac{c_\omega}{2}\langle g, \delta g\rangle_g *_g \varphi^*\Omega \tag{5.3.15}$$

and, hence, the first variation (5.3.12) becomes

$$\left.\frac{\mathrm{d}M_B^{\omega}(\omega_s, g_s)}{\mathrm{d}s}\right|_{s=0} = -\frac{1}{2}\left\langle \dot{\Delta}_g\omega, \omega\right\rangle_{L^2(g)} + \frac{c_\omega}{4}\left\langle *_g\varphi^*\Omega, \omega\right\rangle_{L^2(g)}\langle g, \delta g\rangle_g. \tag{5.3.16}$$

We only need to deal with the first part of (5.3.16) as the second part can be re-expressed via (5.2.23),

$$\frac{c_\omega}{4}\left\langle *_g\varphi^*\Omega, \omega\right\rangle_{L^2(g)} = -\frac{1}{4}\left\langle \omega, \left(\Delta_g + 1\right)\omega\right\rangle_{L^2(g)}. \tag{5.3.17}$$

For any compactly supported function $f : M \to \mathbb{R}$,

$$\int_M f\left(\Delta_{g_s} f\right) \mathrm{vol}_{g_s} = \int_M \langle \mathrm{d}f, \mathrm{d}f \rangle_{g_s} \mathrm{vol}_{g_s} = \int_M g_s^{-1}\left(\mathrm{d}f, \mathrm{d}f\right) \mathrm{vol}_{g_s}. \tag{5.3.18}$$

Varying this gives

$$\begin{aligned} \frac{\mathrm{d}}{\mathrm{d}s}\Big|_{s=0} \left\{ \int_M f\left(\Delta_{g_s} f\right) \mathrm{vol}_{g_s} \right\} &= \int_M \left\{ f\dot{\Delta}_g f + \frac{1}{2} f \Delta_g f \, \langle g, \delta g \rangle_g \right\} \mathrm{vol}_g \\ &= \frac{\mathrm{d}}{\mathrm{d}s}\Big|_{s=0} \left\{ \int_M g_s^{-1}\left(\mathrm{d}f, \mathrm{d}f\right) \mathrm{vol}_{g_s} \right\} \\ &= \int_M \left\{ -\delta g\left(\nabla f, \nabla f\right) + \frac{1}{2} |\mathrm{d}f|_g^2 \, \langle g, \delta g \rangle_g \right\} \mathrm{vol}_g. \end{aligned} \tag{5.3.19}$$

This holds true for all functions f and, in particular, the case of interest $f = \omega$, where ω satisfies the constraint (5.2.23). Thus,

$$\int_M \left(\omega \dot{\Delta}_g \omega\right) \mathrm{vol}_g = \int_M \left\{ -\frac{1}{2}\omega \Delta_g \omega \, \langle g, \delta g \rangle_g - \langle \mathrm{d}\omega \otimes \mathrm{d}\omega, \delta g \rangle_g + \frac{1}{2} |\mathrm{d}\omega|_g^2 \, \langle g, \delta g \rangle_g \right\} \mathrm{vol}_g. \tag{5.3.20}$$

Finally, substituting (5.3.20) into (5.3.16), we obtain the first variation of the ω-energy functional (5.2.22),

$$\frac{\mathrm{d}M_B^{\omega}(\omega_s, g_s)}{\mathrm{d}s}\Big|_{s=0} = \int_M \left\{ \langle \frac{1}{2}\mathrm{d}\omega \otimes \mathrm{d}\omega - \frac{1}{4}|\mathrm{d}\omega|_g^2 g - \frac{1}{4}\omega^2 g, \delta g \rangle_g \right\} \mathrm{vol}_g, \tag{5.3.21}$$

with the corresponding stress-energy tensor given by

$$S^{\omega}(\varphi, g) = \frac{1}{2}\mathrm{d}\omega \otimes \mathrm{d}\omega - \frac{1}{4}\left(|\mathrm{d}\omega|_g^2 + \omega^2\right) g. \tag{5.3.22}$$

Combining the Skyrme and ω stress-energy tensors ((5.3.10) and (5.3.22)), we arrive at the stress-energy tensor (5.3.4) corresponding to the first variation of the energy functional (5.2.20) with respect to the metric g_s, as required. □

To summarize, in the preceding chapters the metric g and Skyrme field φ were varied somewhat independently. Gradient descent based methods were employed to minimize the energy with respect to variations of both the field φ and metric g. Each time step of the minimization scheme for the Skyrme field, the energy with respect to the metric (for fixed field configuration) is completely minimized, thereby continuously determining and updating the optimal metric within the flow. However, this is not possible within the ω-Skyrme model. The ω-meson constraint (5.2.23) prevents the metric and ω-meson from being varied independently. In the current method, only the ω-meson is fully updated each loop, whereas the field and metric minimizations are carried out in tandem.

Let us consider the particular case of interest, $\varphi : \mathbb{T}^3 \to S^3$, and define the new metric independent integrals

$$V^{\pm} = \int_{\mathbb{T}^3} \mathrm{d}^3x \left(\frac{1}{4}m^2\left(1 - \varphi^0\right) \pm \frac{1}{2}\omega^2 \right) = V^{\varphi} \pm V^{\omega}, \tag{5.3.23}$$

$$L_{ij}^{\pm} = \int_{\mathbb{T}^3} \mathrm{d}^3x \left(\frac{1}{8}\partial_i \varphi^{\mu} \partial_j \varphi^{\mu} \pm \frac{1}{2}\partial_i \omega \partial_j \omega \right) = L_{ij}^{\varphi} \pm L_{ij}^{\omega}. \tag{5.3.24}$$

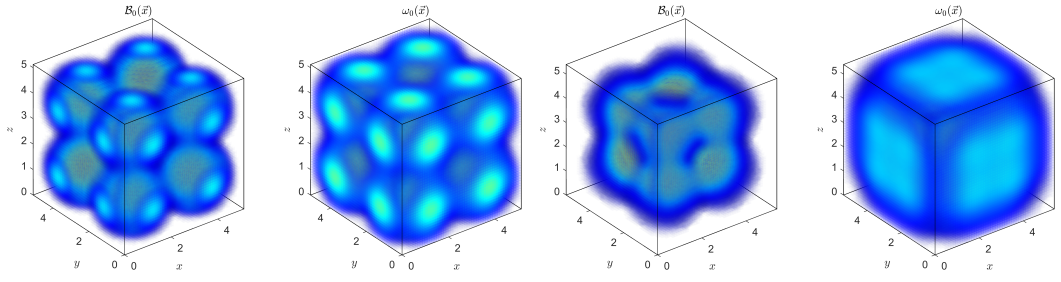

(a) $SC_{1/2}$ crystal (b) α-particle crystal

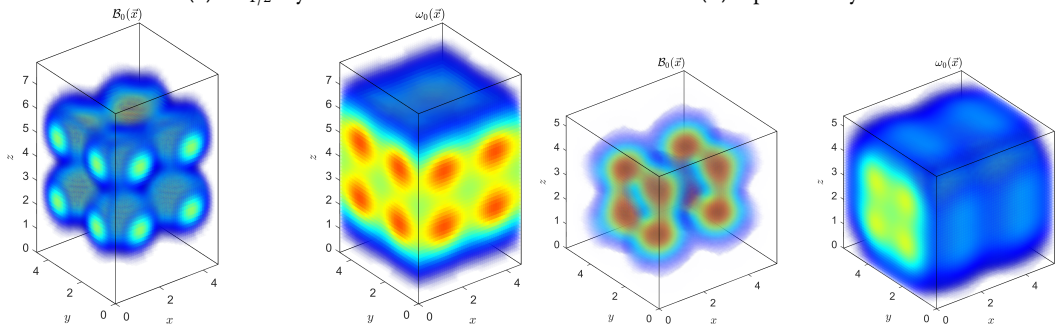

(c) multi-wall crystal (d) chain crystal

Figure 5.1: Baryon density $\mathcal{B}_0(\vec{x})$ and omega density $\omega_0(\vec{x})$ plots of the four crystalline solutions for the coupling constant $c_\omega = 14.34$.

Then the energy functional can be written simply as

$$M_B(\varphi, g) = \sqrt{g}\, g^{ij} L_{ij}^{+} + \sqrt{g}\, V^{+}. \tag{5.3.25}$$

Likewise, the energy gradient with respect to the metric is defined in terms of the metric independent integrals (5.3.23) and (5.3.24) as

$$\frac{\partial M_B}{\partial g_{ij}} = \int_{\mathbb{T}^3} \mathrm{d}^3x \sqrt{g}\, S^{ij} = \frac{1}{2}\sqrt{g}\, g^{ij} V^{-} + \sqrt{g}\left(\frac{1}{2} g^{mn} g^{ij} - g^{im} g^{jn}\right) L_{ij}^{-}, \tag{5.3.26}$$

where the contravariant components of the stress-energy tensor are defined by $S^{ij} = g^{ik} S_{kl} g^{lj}$.

5.4 Skyrmion Crystals Coupled to ω-Mesons

The previous sections have described our numerical algorithm that constructs skyrmion crystals by relaxing a choice of initial configuration $(\varphi_0, \omega_0, g_0)$. As in previous chapters, our initial configurations are based on the $SC_{1/2}$ crystal in the massless $\mathcal{L}_{24}$-Skyrme model with no ω-mesons. The initial Skyrme field and metric are $(\varphi_0, g_0) = (\varphi_{1/2}, g_{1/2})$, where $(\varphi_{1/2}, g_{1/2})$ minimizes the static $\mathcal{L}_{24}$-energy functional. Following Gudnason and Speight [88], we set the initial configuration for the ω-meson to be $\omega_0 = -c_\omega \mathcal{B}_0$. In Chap. 3, we showed that the other three crystals (φ_α, φ_{chain} and $\varphi_{\text{multi-wall}}$) can be constructed from $\varphi_{1/2}$ by applying a chiral SO(4) transformation $Q \in \mathrm{SO}(4)$, with Q defined by (4.2.6).

The energy (5.2.19) and constraint (5.2.17) involve two dimensionless parameters: c_ω and m. We used three different parameter choices that have been proposed in the literature [88, 161, 164].

Crystal	c_ω	F_π (MeV)	m_π (MeV)	m_ω (MeV)	E	E/B (MeV)	E/E_{bound}
$SC_{1/2}$	98.4	124.0	138.0	782.0	145.7761	716.6	3.6683
α	98.4	124.0	138.0	782.0	145.4590	715.0	3.7315
chain	98.4	124.0	138.0	782.0	145.4526	715.0	3.7337
multi-wall	98.4	124.0	138.0	782.0	145.4477	715.0	3.7501
$SC_{1/2}$	34.7	186.0	138.0	782.0	77.8067	860.6	3.8248
α	34.7	186.0	138.0	782.0	77.7126	859.6	3.8699
multi-wall	34.7	186.0	138.0	782.0	77.6870	859.3	3.8954
chain	34.7	186.0	138.0	782.0	77.6758	859.1	3.9137
$SC_{1/2}$	14.34	139.8	43.91	249.5	47.2632	925.6	3.8676
chain	14.34	139.8	43.91	249.5	47.0900	922.2	4.4448
α	14.34	139.8	43.91	249.5	47.0867	922.1	4.5075
multi-wall	14.34	139.8	43.91	249.5	46.8397	917.5	4.9389

Table 5.1: Comparison of the four crystalline solutions for the three different sets of parameters (c_ω = 98.4 [161], c_ω = 34.7 [164] and c_ω = 14.34 [88]).

Adkins and Nappi [161] chose the value $c_\omega = 98.4$ by fitting the mass of the nucleon and the delta resonance. Sutcliffe [164] chose the value $c_\omega = 34.7$ by fitting the pion decay constant F_π and the mass of helium-4 to their experimental values. Finally, Gudnason and Speight [88] chose the value $c_\omega = 14.34$ motivated by a range of considerations and, in particular, it predicted more realistic binding energies. In all calibrations, the parameter $m = m_\pi/m_\omega$ is fixed to its experimental value 0.176. For more details, see Tab. 5.1.

The results of our relaxation algorithm are given in Tab. 5.1. Plots of the baryon density and ω field are shown in Fig. 5.1 for $c_\omega = 14.34$ (pictures for other calibrations are similar). The $SC_{1/2}$ crystal always has a higher energy than the other three, but the α, chain, and multi-wall crystals are very close in energy and their relative ordering seems to depend on c_ω. For $c_\omega = 14.34$ and 98.4 the multi-wall crystal appears to have the lowest energy. For $c_\omega = 34.7$ the chain crystal may have a lower energy, but the numerical values are too close to be confident of this. For comparison, in the Skyrme model with no ω-meson the multi-wall-crystal has lowest energy [100].

As in Chapters 3 and 4, the fundamental domain of the lattice Λ is not cubic for the multi-wall and chain crystals. For the multi-wall crystal the two equal side lengths are shorter than the third side, while for the chain crystal they are longer.

Finally, we note that the energies of the crystals are all greater than the bound (5.2.29) derived in Prop. 16 by a factor of at least 3.5. This is unsurprising, as the derivation of the bound ignores most terms in the energy. The discrepancy seems to be greater for the lowest-energy solutions; this is because the bound (5.2.29) depends on the volume of the lattice fundamental domain, and solutions with lower energy happen to have large volumes. We expect the bound (5.2.29) to be more effective when the size of the lattice fundamental domain is constrained to be small.

5.5 Bethe–Weizsäcker Semi Empirical Mass Formula

In principle, one would like to compare quantized skyrmions to nuclei and their excited states and, in particular, predict correct binding energies using the Bethe–Weizsäcker semi empirical

mass formula (SEMF), or liquid drop model. In this section we use skyrmion crystals to estimate coefficients in the SEMF. This is an approximate formula for the binding energy of a nucleus with baryon number B and takes the form

$$E_b = a_V B - a_S B^{2/3} - a_C \frac{Z(Z-1)}{B^{1/3}} - a_A \delta^2 B + \delta(N,Z), \tag{5.5.1}$$

where Z is the proton number and $N = B - Z$ is the neutron number. We will focus only on the the first two terms, these are associated with the volume and surface area of the nucleus, and they are determined from the classical mass of a nucleus. Therefore, the classical mass M_B of a skyrmion plays an important role in the SEMF, so understanding the phase structure of nuclear matter in the Skyrme model is crucial in estimating these two coefficients. Typical empirically-determined values for their coefficients are $a_V = 15.7 - 16.0$ MeV and $a_S = 17.3 - 18.4$ MeV [178].

Very few attempts have been made at estimating any of the terms using skyrmions. Ma *et al.* [18] have investigated the effect of the Coulomb energy on $\mathcal{L}_{024}$-skyrmions with baryon number $B = 4n$, by applying an α-particle approximation (APA), giving an accurate estimation of the Coulomb coefficient. They find that $a_C = 0.608$ MeV, which is in excellent agreement with the experimentally determined value of $a_C = 0.625$ MeV. We showed in the previous chapter that the asymmetry coefficient a_A can be identified with the symmetry energy $S_N(n_B)$ in the zero density $n_B \to 0$ limit $a_A \sim S_N(0)$. It was found that $S_N(0) = 23.8$ MeV, which agrees extremely well with the experimental value $a_A = 23.7$ MeV. However, the volume a_V and surface a_S coefficients have hitherto remained out of grasp.

Baskerville [17] attempted to address the volume a_V and surface a_S coefficients by building skyrmions from the $SC_{1/2}$ crystal. This was carried out in the massless $\mathcal{L}_{24}$-Skyrme model. Therein, a simple cubic approximation was employed, where the SC unit cell was layered to give $8n^3$ half-skyrmions with a total crystal chunk charge of $B = 4n^3$. The surface and volume energies of a single (cubic) half-skyrmion were estimated and then used to approximate higher charge cubic skyrmions ($B = 4, 32, 108, 256$) using a power-law extrapolation and also an exponential extrapolation. However, this did not reveal promising results. They predicted that $a_V = 136$ MeV and $a_S = 320$ MeV, which are approximately an order of magnitude too large.

As the massive α-particle crystal, in general, has lower energy than the $SC_{1/2}$ crystal, we choose to approach the SEMF using the APA with n^3 α-particles. This gives the correct scaling of both terms, a_V and a_S, with the baryon number B. Within the APA, we are considering a cubic skyrmion built from n^3 $B = 4$ cubic α-particles. The α-particle can be obtained by using the $B = 4$ rational map ansatz as an initial condition [23], with some appropriate profile function $f(r)$ that satisfies the boundary conditions $f(0) = \pi$ and $f(\infty) = 0$, and the O_h-symmetric rational map

$$R(z) = \frac{z^4 + 2\sqrt{3}iz^2 + 1}{z^4 - 2\sqrt{3}iz^2 + 1}. \tag{5.5.2}$$

Using polar coordinates for $\mathbb{R}^3$, $z = \tan(\theta/2)\exp(i\phi)$, with radius r, the rational map ansatz is given by

$$\varphi(r,z) = \exp\left[\frac{if(r)}{1+|R|^2}\begin{pmatrix} 1-|R|^2 & 2\bar{R} \\ 2R & |R|^2-1 \end{pmatrix}\right]. \tag{5.5.3}$$

Higher charge B skyrmions can then be obtained by using the relativized product ansatz

$$\varphi = \frac{\varphi_1\varphi_2 + \varphi_2\varphi_1}{\sqrt{\det(\varphi_1\varphi_2 + \varphi_2\varphi_1)}}. \tag{5.5.4}$$

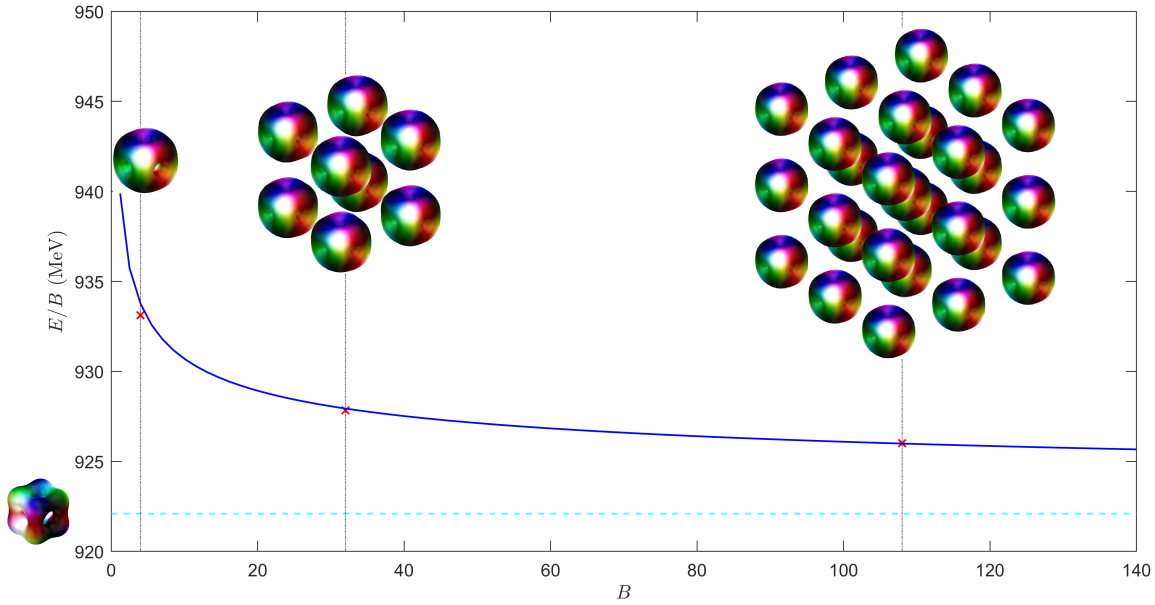

Figure 5.2: Plot of the Bethe–Weizsäcker SEMF from the α-particle approximation for the ω-Skyrme model.

The energy of a $B = 4n^3$ α-particle crystal chunk within the APA can be estimated by decomposing the energy into bulk and surface contributions. The corresponding charge B chunk energy is then approximated by

$$E^B_{\text{chunk}} = \frac{E^\alpha_{\text{cell}}}{B^\alpha_{\text{cell}}} B + E^S_{\text{chunk}}, \tag{5.5.5}$$

where E_{cell} and B_{cell} are the energy and charge of the α-particle crystal unit cell, respectively, and the surface energy of the chunk is

$$E^S_{\text{chunk}} = 6n^2 E^\alpha_{\text{face}} = \frac{3E^\alpha_{\text{face}}}{\sqrt[3]{2}} B^{2/3}. \tag{5.5.6}$$

Therefore, within the APA, the classical binding energy of an isospin symmetric chunk can be expressed as

$$E_b = BM_1 - E^B_{\text{chunk}} = \left(M_1 - \frac{E^\alpha_{\text{cell}}}{B^\alpha_{\text{cell}}} \right) B - \frac{3E^\alpha_{\text{face}}}{\sqrt[3]{2}} B^{2/3}. \tag{5.5.7}$$

Hence, the volume and surface coefficients can be estimated, respectively, by

$$a_V = M_1 - \frac{E^\alpha_{\text{cell}}}{B^\alpha_{\text{cell}}}, \qquad a_S = \frac{3E^\alpha_{\text{face}}}{\sqrt[3]{2}}. \tag{5.5.8}$$

The volume term is relatively straight-forward to compute – we only need to know the energies of the $B = 1$ hedgehog skyrmion and the α-particle crystal. Using the method developed by Gudnason and Speight [88], with coupling constant $c_\omega = 14.34$, we compute $M_1 = 937.7$ MeV. From Tab. 5.1, the α-crystal energy for coupling constant $c_\omega = 14.34$ is given by $E^\alpha_{\text{cell}}/B^\alpha_{\text{cell}} = 922.1$ MeV. Then the volume term is determined to be $a_V = 937.7 - 922.1 = 15.6$ MeV.

Now, computing the surface term, however, is a bit more complicated. It involves estimating the surface energy of a face of the cubic $B = 4$ α-particle. In the context of the baby Skyrme model, a method to determine the surface energy of a crystal chunk was laid out in Chap. 2. Therein, a crystal slab model was developed where crystals were increasingly layered on an infinite cylinder $\mathbb{R} \times S^1$ of width L_{crystal}. This can be generalized to three dimensions such that α-particles are layered on $\mathcal{M} = \mathbb{R} \times S^1 \times S^1$ with cross-sectional area L_α^2, where the volume of the minimal energy cubic α-particle crystal is L_α^3. The domain is still compact without boundary and, so, the baryon number is still well-defined. We define an n-layer crystal slab to be a layered crystal consisting of n α particles stacked vertically as described above. Then, for an n-layer α-crystal slab, the energy can be approximated simply as

$$E_{\text{slab}} = nE^{\alpha}_{\text{cell}} + 2E^{\alpha}_{\text{face}}. \tag{5.5.9}$$

By numerically computing the energies of various n-layer α-slabs with $n \in \{1, 2, 3, 4\}$, the surface energy can be approximated using a least-squares fitting. Using a trust region reflective algorithm, the surface energy of an α-particle face is found to be $E^{\alpha}_{\text{face}} = 7.8$ MeV, which yields $a_S = 18.6$ MeV.

The resulting binding energy per nucleon curve is plotted in Figure 5.2. For comparison, we have also plotted the energy per baryon M_B/B for the three cubic skyrmions with $B = 4n^3$ and $n = 1, 2, 3$ which have been calculated using arrested Newton flow. These are all close to the fitted curve, confirming the validity of the approximate formula (5.5.6). We note the emergence of α-particle clustering, which is expected for light-medium nuclei, and was also observed in the context of the ρ-meson model [169].

Further, let us use the volume $a_V = 15.6$ MeV and surface $a_S = 18.6$ MeV coefficients obtained from our APA and take into consideration the Coulomb coefficient $a_C = 0.608$ MeV predicted by Ma *et al.* [18], also within the APA framework. Then, let us substitute these coefficients into the Bethe–Weizsäcker SEMF (5.5.1) and consider only isospin symmetric nuclear matter, i.e. we ignore the asymmetry term. The results can be compared to experimental data*, where we only consider the subset of data consisting of isospin symmetric nuclei ($N = Z$). These are shown in Fig. 5.3 and it can be seen that the approximation fits the experimental data well.

The caveat with the above result is that, although we have approximated the binding energies per nucleon E_b considerably well, we have used the Coulomb coefficient obtained in the massive $\mathcal{L}_{024}$-Skyrme model. To properly consider the Coulomb effect we would need to quantize the isospin degrees of freedom within the ω-Skyrme model, and construct the isospin density from the vectorial (Noether) current. This would, further, enable us to predict the asymmetry coefficient also, as this is controlled by the isospin moment of inertia tensor.

5.6 Incompressibility of Nuclear Matter

In the previous section we addressed binding energies in finite atomic nuclei using skyrmion crystals. Now we use skyrmion crystals to investigate binding energies in infinitely dense nuclear matter. Consider isospin symmetric nuclear matter at zero temperature with baryon number $B = N + Z$. The (symmetric) energy $E(n_B) \equiv M_B(n_B)/B$ of such matter can be approximated about the nuclear

*Information extracted from the NuDat database, National Nuclear Data Center, https://www.nndc.bnl.gov/nudat/

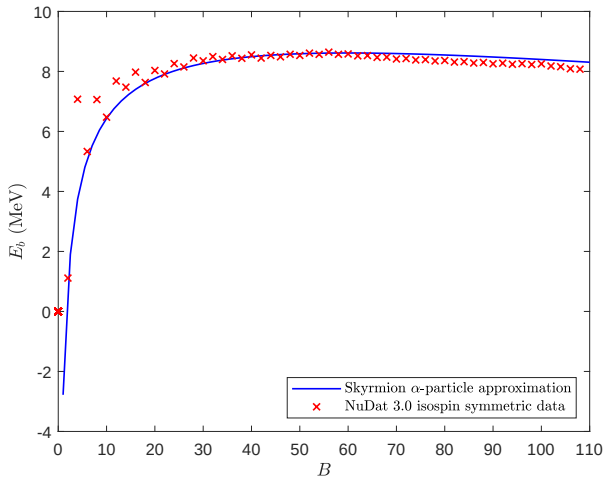

Figure 5.3: The binding energies per nucleon of isospin symmetric nuclei using the Bethe–Weizsäcker semi-empirical mass formula (5.5.1). The experimental data (red crosses) are shown alongside the predicted values within the α-particle approximation (solid blue line).

saturation density n_0 by use of a power series expansion in the baryon density n_B, that is [179]

$$E(n_B) = E_0 + \frac{1}{2}K_0\frac{(n_B - n_0)^2}{9n_0^2} + \mathcal{O}\left((n_B - n_0)^3\right), \tag{5.6.1}$$

where we recall that the first term, associated to the nuclear saturation point n_0, is identified with the saturation energy $E_0 \equiv M_B(n_0)/B$. There is no linear term since symmetric nuclear matter reaches a minimum of the energy at saturation. The next term is the one of interest, it is the nuclear incompressibility coefficient, or compression modulus, K_0, which can be obtained from the expansion (5.6.1),

$$K_0 = 9n_0^2\frac{\partial^2 E}{\partial n_B^2}\bigg|_{n_0}. \tag{5.6.2}$$

This is a fundamental quantity in nuclear physics as it is a measure of nuclear resistance under pressure at the saturation point, and imposes significant constraints on the nuclear matter equation of state.

In order to extract information regarding the incompressibility coefficient, one must investigate the isoscalar giant monopole resonance (ISGMR), or the so-called breathing mode [180], a fundamental problem in nuclear physics, The study of the ISGMR enables one to directly investigate the nuclear incompressibility in *finite* nuclear matter, K_B. This resonance is a collective excitation of the nucleus, in which both protons and neutrons vibrate spherically in phase. It is measured through the low-momentum transfer in inelastic scattering collisions between isoscalar particles (like α particles or deuterons) and medium-heavy nuclei $B \sim 90$ (like ^{90}Zr, $^{112-124}$Sn and $^{106,100-116}$Cd isotopes), and heavier nuclei (such as ^{144}Sm and ^{208}Pb). The energy of this resonance for a given nucleus may be related to its compression modulus K_B [181],

$$E_{\text{ISGMR}} = \hbar\sqrt{\frac{K_B}{M_B\langle r^2\rangle}}, \tag{5.6.3}$$

where $\langle r^2 \rangle$ is the mean square radius of the nucleus and M_B is the mass of the nucleon. In relation to medium-heavy nuclei, this expression is well-defined and the ISGMR is associated to a single peak at the energy $E_{\mathrm{ISGMR}} \sim 80B^{-1/3}$ [182].

The relationship between the finite nucleus incompressibility K_B and the nuclear matter incompressibility K_0 is still an open problem. However, in a similar fashion to the expansion of the liquid drop model (5.5.1), one can consider the so-called leptodermous expansion [180, 182, 183]:

$$K_B = K_0 + K_S B^{-1/3} + K_A \left(\frac{N-Z}{B}\right)^2 + K_C Z^2 B^{-4/3}, \tag{5.6.4}$$

This enables the computation of the finite nucleus incompressibility K_B and, hence, the ISGMR centroid energy E_{ISGMR}. The nuclear matter incompressibility modulus K_0 cannot be directly measured, but it may be extracted from the ISGMR centroid energy E_{ISGMR} by comparing the experimental energies of the ISGMR with the corresponding theoretically calculated values [184–187]. For a recent review on current methods to determine the relationship between K_B and K_0, see, e.g., Garg and Coló [179].

Using the above method, Blaizot [180] showed in 1980 that the experimental data is compatible with a compression modulus value of $K_0 \sim 210 \pm 30$ MeV. If we consider the ratio $c = K_0/K_S \sim -1$ then one obtains the more generally accepted fiducial value of $K_0 \sim 240 \pm 20$ MeV. However, Stone *et al.* [188] observed that fits are significantly improved if c is allowed to vary and they obtain higher values for the compression modulus, $250 < K_0 < 315$ MeV. Many other field theoretic methods have also been employed to predict the compression modulus K_0 using the leptodermous expansion (5.6.4), and are detailed in [178].

Our starting point in determining the compression modulus within the Skyrme model is the $\mathrm{SC}_{1/2}$ crystal in the massless $\mathscr{L}_{24}$-Skyrme model. Consider a variation $\varphi_\lambda : \mathbb{T}^3 \times \mathbb{R} \to S^3$ of the Skyrme field φ such that $\varphi_{\lambda=0} = \varphi$. This has infinitesimal generator $\partial_\lambda \varphi_\lambda|_{\lambda=0} \in \Gamma(\varphi^{-1}TS^3)$, where $\varphi^{-1}TS^3$ is the vector bundle over $\mathbb{T}^3$ with fibre $T_{\varphi(x)}S^3$ over $x \in \mathbb{T}^3$. Explicitly, if we consider the spatial rescaling $x \mapsto e^\lambda x$, then we have a one-parameter family of maps $\varphi_\lambda = \varphi(e^\lambda x)$ such that $\varphi_{\lambda=0} = \varphi$. The rescaled massless $\mathscr{L}_{24}$ static energy functional is then

$$E_\lambda \equiv E_{24}[\varphi_\lambda] = e^\lambda E_2 + e^{-\lambda} E_4. \tag{5.6.5}$$

If the Skyrme field configuration φ is a minimizer of the $\mathscr{L}_{24}$-energy E, then we require

$$\left.\frac{\mathrm{d}}{\mathrm{d}\lambda}\right|_{\lambda=0} E_{24}[\varphi_\lambda] = E_2 - E_4 = 0, \tag{5.6.6}$$

which yields the familiar massless virial constraint $E_2 = E_4$.

The true $\mathscr{L}_{24}$-energy minimizing crystal is the cubic lattice of half-skyrmions ($\mathrm{SC}_{1/2}$ crystal) found independently by Kugler & Shtrikmann [39] and Castillejo *et al.* [40]. Let us denote this minimal energy crystalline solution of the $\mathscr{L}_{24}$-Skyrme model by $\varphi_{1/2} \equiv \varphi(L_{1/2})$, where $L_{1/2}$ corresponds to the side length of the energy minimizing cubic lattice. Under the one-parameter variation $L_{1/2} \mapsto e^\lambda L_{1/2}$, the rescaled $\mathrm{SC}_{1/2}$ crystal configuration $\varphi(e^\lambda L_{1/2})$ approximates the true minimizer at volume $V = e^{3\lambda} L_{1/2}^3$ extremely well for small λ. Then, the compression modulus may be related to the second derivative of the energy with respect to the scaling factor λ,

$$K_0 = \left.\frac{\mathrm{d}^2}{\mathrm{d}\lambda^2}\right|_{\lambda=0} E_{24}[\varphi(e^\lambda L_{1/2})] = E_2[\varphi_{1/2}] + E_4[\varphi_{1/2}] = E_0. \tag{5.6.7}$$

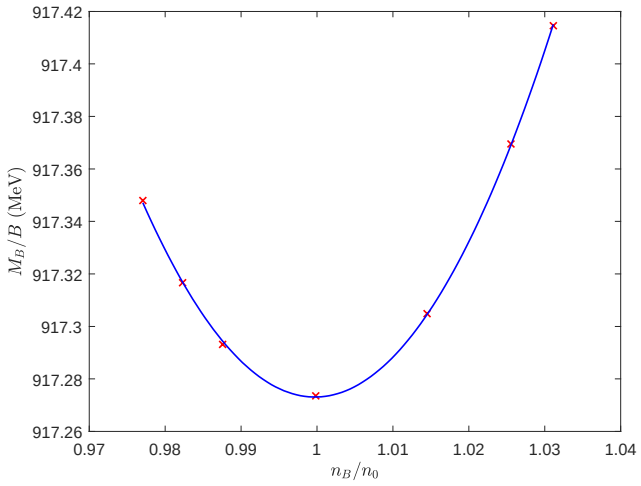

Figure 5.4: The energy per baryon M_B/B of the multi-wall crystal for various baryon densities n_B near saturation n_0. The compression modulus K_0 is determined by fitting a quadratic approximation to various data points about n_0, and is found to be $K_0 = 370$ MeV.

Thus, one obtains the ratio $K_0/E_0 = 1$. However, experimentally, this ratio is approximately $K_0/E_0 \sim 1/4$. Hence, the compression modulus is roughly four times too large in the massless $\mathscr{L}_{24}$-Skyrme model. The other three crystals slightly improves the issue, but still gives compression modulus values $K_0 > E_0/3$.

If we include the pion mass potential then the compression modulus increases further, $K_0 \sim 1350$ MeV in the $\mathscr{L}_{024}$-model. Things appear worse if we include the sextic term as this acts to stiffen the equation of state, leading to neutron stars with larger maximal masses (closer to observed masses), but at the cost of increasing the compression modulus, with coupling constant dependent values of $K_0 \sim 1350 - 2300$ MeV. On the other hand, consider the BPS $\mathscr{L}_{06}$ model, where skyrmion matter behaves as a perfect fluid. This has zero binding energies and so the compression modulus is zero for any potential which provides a non-zero pion mass [137]. So a possible remedy to the compression modulus problem within the Skyrme framework is consideration of a near-BPS Skyrme model [189, 190]. We show here that this is not necessary and inclusion of vector mesons is able to solve the issue.

In general, as we have previously motivated in Sec. 4.2, the multi-wall crystal has a lower compression modulus than the other three crystals. To see this, we must consider the energy at the minimum $M_B(n_0)$ and the zero density energy $M_B(n_B = 0)$. Then the energy difference $\Delta E = M_B(0) - M_B(n_0)$ is minimal for the multi-wall crystal and, so, should provide a more shallow minimum (and, thus, a lower compression modulus). Further, if the model has low binding energies per nucleon then M_1 should be close to $M_B(0)/B$ and the energy difference $\Delta E = M_B(0) - M_B(n_0)$ optimal. So, naturally, a Skyrme model with low binding energies should be able to predict a nuclear matter incompressibility coefficient of the correct order of magnitude. We exploit this knowledge and use the low binding energy ω-Skyrme model with coupling constant $c_\omega = 14.34$ to determine the compression modulus K_0. The resulting data is plotted in Fig. 5.4 and we determine a much more acceptable compression modulus value of $K_0 = 370$ MeV.

Six

Conclusion

In this thesis we have proposed robust methods to determine crystalline configurations in various Skyrme models and investigated their applications to cold dense nuclear matter. We laid out the foundations of the Skyrme model in Chap. 1 and reviewed the current literature on skyrmion crystals. In particular, the $\mathrm{SC}_{1/2}$ and $\mathrm{BCC}_{1/2}$ crystals in the massless $\mathscr{L}_{24}$-Skyrme model, and their corresponding symmetries, were reviewed in detail, with emphasis on the $\mathrm{SC}_{1/2}$ crystal. We then motivated the need for studying skyrmion crystals and posed the question: what happens when the pion mass term is included and the chiral SO(4) symmetry (of which the $\mathrm{SC}_{1/2}$ crystal enjoys) is explicitly broken to a SO(3) isospin symmetry?

However, before pursuing massive (3 + 1)-dimensional skyrmion crystals, we turned our attention to crystals in the (2 + 1)-dimensional baby Skyrme model in Chap. 2. The method developed therein is applicable to an arbitrary choice of potential function $V(\varphi)$, where we chose to focus on two distinct potentials yielding quite different phenomena: the standard and easy plane potentials. Due to the conformal invariance of the Dirichlet term in two dimensions, the problem is much simpler than in the three dimensional case. Having obtained crystal solutions for both potentials on $\mathbb{T}^2 = S^1 \times S^1$, we then exploited this knowledge to construct layered crystal slabs on $\mathbb{R} \times S^1$. From this we extrapolated the surface energy of a crystal chunk and proposed a simple binding energy formula for an arbitrary charge B chunk, consisting of a bulk contribution and a surface term.

For (3 + 1)-dimensional skyrmion crystals we proved, in Chap. 3, the existence of a unique critical metric. Further, we showed that this proof generalizes to fixed density n_B, or volume, variations. This enabled us to investigate phases of nuclear matter and, in particular, obtain an equation of state $\rho = \rho(p)$ valid in all density n_B regimes. Four crystalline configurations, with unit cell charge $B_{\mathrm{cell}} = 4$, were shown to survive perturbation from the massless $\mathscr{L}_{24}$-model to the massive $\mathscr{L}_{024}$-model. These are the $\mathrm{SC}_{1/2}$, α, chain and multi-wall crystals (the latter two being new solutions). The existence of these four distinct crystals were understood semi-analytically by means of the Principle of Symmetric Criticality and the Inverse Function Theorem. It was observed that the multi-wall crystal is the ground state crystalline configuration at all densities n_B, making it the prime candidate for the study of dense inhomogeneous nuclear matter.

In Chap. 4 we utilized the results and numerical method developed in Chap. 3 to investigate crystals in the generalized $\mathscr{L}_{0246}$-Skyrme model. Upon rigid body quantization of the isospin degrees of freedom, we were able to consider isospin asymmetric neutron crystals, which are of relevance in dense nuclear matter such as neutron stars. By allowing a small non-zero proton fraction, an equation of state for β-equilibrated nuclear matter was constructed, with charge neutrality maintained by screening with a constant background of negatively charged leptons. A peculiar

result of this study was the presence of a cusp in the symmetry energy, which we have argued signifies a phase transition from isospin asymmetric infinite nuclear matter to symmetric finite nuclear matter. We reiterate that this phenomena was also observed by Lee *et al.* [151] in the context of the $\mathrm{SC}_{1/2}$ crystal in the massive $\mathscr{L}_{024}$-Skyrme model coupled to a scalar dilaton field. They attributed the cusp to the "topological" phase transition from the $\mathrm{SC}_{1/2}$ crystal (SC lattice of fractional half-skyrmions) to the FCC_1 crystal (FCC lattice of $B = 1$ hedgehogs) [152]. In the zero density limit $n_B \to 0$, two interesting results were also observed/inferred. Firstly, the non-vanishing of the symmetry energy, from which we identified with the asymmetry coefficient $a_A \sim S_N(0)$ in the SEMF. Secondly, nuclear matter becomes symmetric and the proton fraction $\gamma_p \to 0.5$ from below and is close to the proton fraction $\gamma_p = 0.46$ in ^{56}Fe, which is abundant in the crust of a neutron star (where $n_B \sim 0$). Both of these results are due to the non-vanishing of the isospin inertia tensor component $U_{33}(n_B)$ in the zero density limit $n_B \to 0$. Finally, neutron stars were constructed from the β-equilibrated multi-wall equation of state within the TOV framework. The resulting $M - R$ curve fits the recent NICER/LIGO observational data rather well.

It was realized by Baskerville [17] that we could use skyrmion crystals to predict coefficients in the Bethe–Weizsäcker SEMF, namely the volume a_V and surface a_S coefficients. The results they obtained were off by an order of magnitude but the approach they used was not the problem. The real inherent issue was that they considered the massless $\mathscr{L}_{24}$-Skyrme model, which has high binding energies and, so, one would expect the corresponding SEMF coefficients to be too large also. By coupling the Skyrme model to the ω-meson, Gudnason and Speight [88] were able to obtain a Skyrme model with low binding energies. This motivated the study of crystals within the ω-Skyrme model in Chap. 5. The outcome of this chapter was the successful determination of the volume a_V and surface a_S coefficients in the SEMF. Additionally, we were able to extract information regarding the nuclear matter incompressibility coefficient K_0 and address the compression modulus issue.

A

Appendix

A.1 NLSM Formulation

In order to do numerics, we need to employ NLσM notation. To do this, we write the Skyrme field in terms of the pion fields, that is

$$\varphi = \varphi^0 \,\mathrm{Id}_2 + i\varphi^a \tau^a. \tag{A.1.1}$$

This has inverse

$$\varphi^\dagger = \varphi^0 \,\mathrm{Id}_2 - i\varphi^a \tau^a. \tag{A.1.2}$$

Then the Maurer-Cartan form is

$$\begin{aligned} L_i &= \varphi^\dagger \partial_i \varphi \\ &= \left(\varphi^0 \,\mathrm{Id}_2 - i\varphi^a \tau^a\right)\left(\partial_i \varphi^0 \,\mathrm{Id}_2 + i\partial_i \varphi^a \tau^a\right) \\ &= \varphi^0 \partial_i \varphi^0 + \varphi^a \partial_i \varphi^b \tau^a \tau^b - i\varphi^a \partial_i \varphi^0 \tau^a + i\varphi^0 \partial_i \varphi^b \tau^b \\ &= \varphi^0 \partial_i \varphi^0 + \varphi^a \partial_i \varphi^a + i\varphi^a \partial_i \varphi^b \varepsilon_{abc} \tau^c - i\varphi^a \partial_i \varphi^0 \tau^a + i\varphi^0 \partial_i \varphi^b \tau^b \\ &= -i\left(\partial_i \varphi^0 \varphi^a - \partial_i \varphi^a \varphi^0 + \varepsilon_{abc} \partial_i \varphi^b \varphi^c\right) \tau^a. \end{aligned} \tag{A.1.3}$$

Hence, we have that

$$L_i = -iL_i^a \tau^a, \quad L_i^a = \varepsilon_{abc} \partial_i \varphi^b \varphi^c + \partial_i \varphi^0 \varphi^a - \partial_i \varphi^a \varphi^0. \tag{A.1.4}$$

Now, using the relation

$$(\varphi^\mu \partial_i \varphi^\mu)(\varphi^\nu \partial_j \varphi^\nu) = (\varphi^0 \partial_i \varphi^0)(\varphi^0 \partial_j \varphi^0 + \varphi^a \partial_j \varphi^a) + (\varphi^a \partial_i \varphi^a)(\varphi^\mu \partial_j \varphi^\mu) \tag{A.1.5}$$

and the fact that $\varphi^\mu \partial_i \varphi^\mu = 0$, since $\varphi \in S^3$ and $\partial_i \varphi \in TS^3$, we can write

$$(\varphi^0 \partial_i \varphi^0)(\varphi^a \partial_j \varphi^a) + (\varphi^a \partial_i \varphi^a)(\varphi^\mu \partial_j \varphi^\mu) = -(\varphi^0 \partial_i \varphi^0)(\varphi^0 \partial_j \varphi^0). \tag{A.1.6}$$

This, and the identity $\mathrm{Tr}\left(\tau^a\tau^b\right) = 2\delta^{ab}$, enables us to compute the term

$$\begin{aligned}
\mathrm{Tr}\left(L_iL_j\right) &= \left(-iL_i^a\right)\left(-iL_j^b\right)\mathrm{Tr}\left(\tau^a\tau^b\right)\\
&= -L_i^aL_j^b\,\mathrm{Tr}\left(\tau^a\tau^b\right)\\
&= -2L_i^aL_j^a\\
&= -2\left(\varepsilon_{abc}\partial_i\varphi^b\varphi^c + \partial_i\varphi^0\varphi^a - \partial_i\varphi^a\varphi^0\right)\left(\varepsilon_{ade}\partial_j\varphi^d\varphi^e + \partial_j\varphi^0\varphi^a - \partial_j\varphi^a\varphi^0\right)\\
&= -2\Big\{\varepsilon_{abc}\varepsilon_{ade}\varphi^c\varphi^e\partial_i\varphi^b\partial_j\varphi^d + \varepsilon_{abc}\varphi^a\varphi^c\partial_i\varphi^b\partial_j\varphi^0 - \varepsilon_{abc}\varphi^0\varphi^c\partial_i\varphi^b\partial_j\varphi^a\\
&\quad + \varepsilon_{ade}\varphi^a\varphi^e\partial_i\varphi^0\partial_j\varphi^d + \varphi^a\varphi^a\partial_i\varphi^0\partial_j\varphi^0 - \varphi^0\varphi^a\partial_i\varphi^0\partial_j\varphi^a\\
&\quad -\varepsilon_{ade}\varphi^0\varphi^e\partial_i\varphi^a\partial_j\varphi^d - \varphi^0\varphi^a\partial_i\varphi^a\partial_j\varphi^0 + \varphi^0\varphi^0\partial_i\varphi^a\partial_j\varphi^a\Big\}\\
&= -2\Big\{(\partial_i\varphi^b\partial_j\varphi^b)(\varphi^a\varphi^a) - (\varphi^a\partial_i\varphi^a)(\varphi^b\partial_j\varphi^b) - (\varepsilon_{bac}\varphi^a\varphi^c)\partial_i\varphi^b\partial_j\varphi^0\\
&\quad + (\varepsilon_{cba}\partial_i\varphi^b\partial_j\varphi^a)\varphi^c\varphi^0 + (\varepsilon_{dea}\varphi^e\varphi^a)\partial_i\varphi^0\partial_j\varphi^d + (\varphi^a\varphi^a)(\partial_i\varphi^0\partial_j\varphi^0)\\
&\quad - (\varphi^0\partial_i\varphi^0)(\varphi^a\partial_j\varphi^a) - (\varepsilon_{bac}\partial_i\varphi^b\partial_j\varphi^a)\varphi^0\varphi^c - (\varphi^0\partial_j\varphi^0)(\varphi^a\partial_i\varphi^a)\\
&\quad +(\varphi^0\varphi^0)(\partial_i\varphi^a\partial_j\varphi^a)\Big\}\\
&= -2\Big\{(\partial_i\varphi^b\partial_j\varphi^b)(\varphi^a\varphi^a) - (\varphi^a\partial_i\varphi^a)(\varphi^b\partial_j\varphi^b) + (\varphi^a\varphi^a)(\partial_i\varphi^0\partial_j\varphi^0)\\
&\quad +(\varphi^0\varphi^0)(\partial_i\varphi^a\partial_j\varphi^a) - (\varphi^0\partial_i\varphi^0)(\varphi^a\partial_j\varphi^a) - (\varphi^a\partial_i\varphi^a)(\varphi^0\partial_j\varphi^0)\Big\}\\
&= -2\Big\{(\varphi^a\varphi^a)(\partial_i\varphi^\mu\partial_j\varphi^\mu) + (\varphi^0\varphi^0)(\partial_i\varphi^a\partial_j\varphi^a)\\
&\quad -\left[(\varphi^0\partial_i\varphi^0)(\varphi^a\partial_j\varphi^a) + (\varphi^a\partial_i\varphi^a)(\varphi^\mu\partial_j\varphi^\mu)\right]\Big\}\\
&= -2\Big\{(\varphi^a\varphi^a)(\partial_i\varphi^\mu\partial_j\varphi^\mu) + (\varphi^0\varphi^0)(\partial_i\varphi^a\partial_j\varphi^a) + (\varphi^0\partial_i\varphi^0)(\varphi^0\partial_j\varphi^0)\Big\}\\
&= -2\,\partial_i\varphi^\mu\partial_j\varphi^\mu. \qquad \text{(A.1.7)}
\end{aligned}$$

From this we get the following contraction

$$L_i^aL_j^a = \partial_i\varphi^\mu\partial_j\varphi^\mu. \qquad \text{(A.1.8)}$$

Now, let us focus on the $\mathfrak{su}(2)$ current:

$$\begin{aligned}
T_a &= \frac{i}{2}\varphi^\dagger\left[\tau^a,\varphi\right]\\
&= \frac{i}{2}\left(\varphi^0\,\mathrm{Id}_2 - i\varphi^c\tau^c\right)\left[\tau^a,\varphi^0\,\mathrm{Id}_2 + i\varphi^b\tau^b\right]\\
&= \frac{i}{2}\left(\varphi^0\,\mathrm{Id}_2 - i\varphi^c\tau^c\right)\left(i\varphi^b\left[\tau^a,\tau^b\right]\right)\\
&= -\frac{\varphi^b}{2}\left(\varphi^0\,\mathrm{Id}_2 - i\varphi^c\tau^c\right)\left(2i\varepsilon_{abd}\tau^d\right)\\
&= -i\varepsilon_{abd}\varphi^b\left(\varphi^0\,\mathrm{Id}_2 - i\varphi^c\tau^c\right)\tau^d\\
&= -i\varepsilon_{abd}\varphi^b\tau^d\varphi^0 - \varepsilon_{abd}\varphi^b\varphi^c\tau^c\tau^d\\
&= -i\varepsilon_{abd}\varphi^b\tau^d\varphi^0 - \varepsilon_{abd}\varphi^b\varphi^c\left(\delta^{cd}\,\mathrm{Id}_2 + i\varepsilon_{cde}\tau^e\right)\\
&= -i\varepsilon_{abc}\varphi^b\tau^c\varphi^0 - \varepsilon_{abc}\varphi^b\varphi^c - i\varphi^b\varphi^b\tau^a + i\varphi^b\varphi^a\tau^b\\
&= i\varepsilon_{abc}\varphi^0\varphi^c\tau^b - i\varphi^c\varphi^c\delta^{ab}\tau^b + i\varphi^a\varphi^b\tau^b - \varepsilon_{abc}\varphi^b\varphi^c
\end{aligned}$$

$$
\begin{aligned}
&= i\left(\varepsilon_{abc}\varphi^0\varphi^c - \varphi^c\varphi^c\partial^{ab} + \varphi^a\varphi^b\right)\tau^b \\
&= -i\left(\partial^{ab}\varphi^c\varphi^c - \varphi^a\varphi^b - \varepsilon_{abc}\varphi^0\varphi^c\right)\tau^b.
\end{aligned} \tag{A.1.9}
$$

Hence, we find that

$$
T_a = -iT_a^b\tau^b, \quad T_a^b = \partial^{ab}\varphi^c\varphi^c - \varphi^a\varphi^b - \varepsilon_{abc}\varphi^0\varphi^c. \tag{A.1.10}
$$

We are now in a position to compute the following term:

$$
\begin{aligned}
\mathrm{Tr}(T_aT_b) &= (-iT_a^c)\left(-iT_b^d\right)\mathrm{Tr}\left(\tau^c\tau^d\right) \\
&= -T_a^cT_b^d\,\mathrm{Tr}\left(\tau^c\tau^d\right) \\
&= -2T_a^cT_b^c \\
&= -2\left(\partial^{ac}\varphi^d\varphi^d - \varphi^a\varphi^c - \varepsilon_{acd}\varphi^0\varphi^d\right)\left(\partial^{bc}\varphi^e\varphi^e - \varphi^b\varphi^c - \varepsilon_{bce}\varphi^0\varphi^e\right) \\
&= -2\Big\{\partial^{ac}\partial^{bc}\varphi^d\varphi^d\varphi^e\varphi^e - \varphi^a\varphi^b\varphi^d\varphi^d - \varepsilon_{bae}\varphi^0\varphi^d\varphi^d\varphi^e \\
&\quad + \varphi^a\varphi^b\varphi^d\varphi^d + \varphi^a\varphi^b\varphi^c\varphi^c + \varepsilon_{bce}\varphi^0\varphi^a\varphi^c\varphi^e \\
&\quad -\varepsilon_{abc}\varphi^0\varphi^c\varphi^d\varphi^d + \varepsilon_{acd}\varphi^0\varphi^b\varphi^c\varphi^d + \varepsilon_{cda}\varepsilon_{ceb}\varphi^0\varphi^0\varphi^d\varphi^e\Big\} \\
&= -2\Big\{\partial^{ab}\varphi^c\varphi^c\varphi^d\varphi^d - \varphi^a\varphi^b\varphi^c\varphi^c - \varepsilon_{bac}\varphi^0\varphi^c\varphi^d\varphi^d + \varepsilon_{bcd}\varphi^0\varphi^a\varphi^c\varphi^d \\
&\quad -\varepsilon_{abc}\varphi^0\varphi^c\varphi^d\varphi^d + \varepsilon_{acd}\varphi^0\varphi^b\varphi^c\varphi^d + \partial^{ab}\varphi^0\varphi^0\varphi^c\varphi^c - \varphi^0\varphi^0\varphi^a\varphi^b\Big\} \\
&= -2\Big\{\partial^{ab}\varphi^c\varphi^c(\varphi^d\varphi^d + \varphi^0\varphi^0) - \varphi^a\varphi^b(\varphi^c\varphi^c + \varphi^0\varphi^0) - \varphi^0\varphi^c\varphi^d\varphi^d(\varepsilon_{bac} + \varepsilon_{abc}) \\
&\quad +(\varepsilon_{bcd}\varphi^c\varphi^d)\varphi^0\varphi^a + (\varepsilon_{acd}\varphi^c\varphi^d)\varphi^0\varphi^b\varphi^c\varphi^d\Big\} \\
&= -2\left\{\partial^{ab}\varphi^c\varphi^c - \varphi^a\varphi^b\right\}.
\end{aligned} \tag{A.1.11}
$$

This gives the contraction

$$
T_i^aT_j^a = \partial^{ij}\varphi^a\varphi^a - \varphi^i\varphi^j. \tag{A.1.12}
$$

In a similar fashion, consider the following term:

$$
\begin{aligned}
\mathrm{Tr}(T_aL_b) &= (-iT_a^c)\left(-iL_b^d\right)\mathrm{Tr}\left(\tau^c\tau^d\right) \\
&= -T_a^cL_b^d\,\mathrm{Tr}\left(\tau^c\tau^d\right) \\
&= -2T_a^cL_b^c \\
&= -2\left(\partial^{ac}\varphi^d\varphi^d - \varphi^a\varphi^c - \varepsilon_{acd}\varphi^0\varphi^d\right)\left(\varepsilon_{cef}\partial_b\varphi^e\varphi^f + \partial_b\varphi^0\varphi^c - \partial_b\varphi^c\varphi^0\right) \\
&= -2\Big\{(\varphi^d\varphi^d)\varepsilon_{aef}\partial_b\varphi^e\varphi^f + (\varphi^d\varphi^d)\varphi^a\partial_b\varphi^0 - (\varphi^d\varphi^d)\partial_b\varphi^a\varphi^0 \\
&\quad -\varepsilon_{cef}\varphi^a\varphi^c\varphi^f\partial_b\varphi^e - (\varphi^c\varphi^c)\varphi^a\partial_b\varphi^0 + \varphi^0\varphi^a(\varphi^c\partial_b\varphi^c) \\
&\quad -\varepsilon_{cda}\varepsilon_{cef}\varphi^0\varphi^d\varphi^f\partial_b\varphi^e - \varepsilon_{acd}\varphi^0\varphi^c\varphi^d\partial_b\varphi^0 + \varepsilon_{acd}\varphi^0\varphi^0\varphi^d\partial_b\varphi^c\Big\} \\
&= -2\Big\{(\varphi^e\varphi^e)\varepsilon_{acd}\partial_b\varphi^c\varphi^d + (\varphi^d\varphi^d)\varphi^a\partial_b\varphi^0 - \varphi^0(\varphi^d\varphi^d)\partial_b\varphi^a \\
&\quad + (\varepsilon_{ecf}\varphi^c\varphi^f)\varphi^a\partial_b\varphi^e - (\varphi^c\varphi^c)\varphi^a\partial_b\varphi^0 + \varphi^0\varphi^a(\varphi^c\partial_b\varphi^c) \\
&\quad -\varphi^0\varphi^a(\varphi^d\partial_b\varphi^d) + \varphi^0(\varphi^d\varphi^d)\partial_b\varphi^a - (\varepsilon_{acd}\varphi^c\varphi^d)\varphi^0\partial_b\varphi^0 + (\varphi^0\varphi^0)\varepsilon_{acd}\varphi^d\partial_b\varphi^c\Big\} \\
&= -2\left\{(\varphi^e\varphi^e + \varphi^0\varphi^0)\varepsilon_{acd}\partial_b\varphi^c\varphi^d\right\} \\
&= -2\varepsilon_{acd}\partial_b\varphi^c\varphi^d.
\end{aligned} \tag{A.1.13}
$$

So we can write the contraction

$$T_i^c L_b^c = -\varepsilon_{icd}\varphi^c \partial_b \varphi^d. \tag{A.1.14}$$

Using the following relations,

$$\begin{aligned} T_i L_a &= \left(-iT_i^c \tau^c\right)\left(-iL_a^d \tau^d\right) \\ &= -T_i^c L_a^d \tau^c \tau^d \\ &= -T_i^c L_a^d \left(\delta^{cd}\,\mathrm{Id}_2 + i\varepsilon_{cde}\tau^e\right) \\ &= -T_i^c L_a^c\,\mathrm{Id}_2 - i\varepsilon_{cde} T_i^c L_a^d \tau^e \end{aligned} \tag{A.1.15}$$

and

$$L_a T_i = -L_a^c T_i^c\,\mathrm{Id}_2 - i\varepsilon_{cde} L_a^c T_i^d \tau^e, \tag{A.1.16}$$

we can write

$$\begin{aligned} [L_a, T_i] &= L_a T_i - T_i L_a \\ &= \left(T_i^c L_a^c - L_a^c T_i^c\right)\mathrm{Id}_2 + i\varepsilon_{cde}\left(T_i^c L_a^d - L_a^c T_i^d\right)\tau^e \\ &= i\varepsilon_{cde}\left(T_i^c L_a^d - L_a^c T_i^d\right)\tau^e \end{aligned} \tag{A.1.17}$$

and

$$\begin{aligned} [L_b, T_j] &= L_b T_j - T_j L_b \\ &= (T_j^f L_b^f - L_b^f T_j^f)\,\mathrm{Id}_2 + i\varepsilon_{fgh}(T_j^f L_b^g - L_b^f T_j^g)\tau^h \\ &= i\varepsilon_{fgh}(T_j^f L_b^g - L_b^f T_j^g)\tau^h. \end{aligned} \tag{A.1.18}$$

Now, using these relations and the contractions

$$T_i^c T_j^c = \delta^{ij}\varphi^a\varphi^a - \varphi^i\varphi^j, \quad T_i^c L_b^c = -\varepsilon_{icd}\varphi^c\partial_b\varphi^d, \quad L_a^d L_b^d = \partial_a\varphi^\mu\partial_b\varphi^\mu, \quad T_j^d L_a^d = -\varepsilon_{jef}\varphi^e\partial_a\varphi^f,$$

we have that

$$\begin{aligned} \mathrm{Tr}\left([L_a, T_i][L_b, T_j]\right) &= -\varepsilon_{cde}\varepsilon_{fgh}(T_i^c L_a^d - L_a^c T_i^d)(T_j^f L_b^g - L_b^f T_j^g)\,\mathrm{Tr}\left(\tau^e\tau^h\right) \\ &= -2\varepsilon_{ecd}\varepsilon_{efg}(T_i^c L_a^d - L_a^c T_i^d)(T_j^f L_b^g - L_b^f T_j^g) \\ &= -2(T_i^c L_a^d - L_a^c T_i^d)(T_j^c L_b^d - L_b^c T_j^d) + 2(T_i^c L_a^d - L_a^c T_i^d)(T_j^d L_b^c - L_b^d T_j^c) \\ &= -2\left(T_i^c T_j^c L_a^d L_b^d - T_i^c L_b^c L_a^d T_j^d - L_a^c T_j^c T_i^d L_b^d + L_a^c L_b^c T_i^d T_j^d\right) \\ &\quad + 2\left(T_i^c L_b^c L_a^d T_j^d - T_i^c T_j^c L_a^d L_b^d - L_a^c L_b^c T_i^d T_j^d + L_a^c T_j^c T_i^d L_b^d\right) \\ &= -8\left(T_i^c T_j^c L_a^d L_b^d - T_i^c L_b^c T_j^d L_a^d\right) \\ &= -8\left(\delta^{ij}\varphi^c\varphi^c - \varphi^i\varphi^j\right)\partial_a\varphi^\mu\partial_b\varphi^\mu + 8\varepsilon_{icd}\varepsilon_{jef}\varphi^c\varphi^e\partial_b\varphi^d\partial_a\varphi^f. \end{aligned} \tag{A.1.19}$$

Using the identity

$$\varepsilon_{icd}\varepsilon_{jef} = \delta^{ij}(\delta^{ce}\delta^{df} - \delta^{cf}\delta^{de}) - \delta^{ie}(\delta^{cj}\delta^{df} - \delta^{cf}\delta^{jd}) + \delta^{if}(\delta^{cj}\delta^{de} - \delta^{ce}\delta^{dj}) \tag{A.1.20}$$

we can write the second term as

$$\begin{aligned}\varepsilon_{icd}\varepsilon_{jef}\varphi^c\varphi^e\partial_b\varphi^d\partial_a\varphi^f &= \delta^{ij}\left(\varphi^c\varphi^c\partial_a\varphi^d\partial_b\varphi^d - (\varphi^c\partial_a\varphi^c)(\varphi^d\partial_b\varphi^d)\right)\\ &\quad - \varphi^i\left(\varphi^j\partial_a\varphi^c\partial_b\varphi^c - \partial_b\varphi^j(\varphi^c\partial_a\varphi^c)\right) + \partial_a\varphi^i\left(\varphi^j(\varphi^c\partial_b\varphi^c) - (\varphi^c\varphi^c)\partial_b\varphi^j\right).\end{aligned}$$

Writing $\partial_a\varphi^\mu\partial_b\varphi^\mu = \partial_a\varphi^0\partial_b\varphi^0 + \partial_a\varphi^c\partial_b\varphi^c$, and noting that $\varphi^c\partial_a\varphi^c = -\varphi^0\partial_a\varphi^0$, we have that

$$\begin{aligned}\mathrm{Tr}\left([L_a,T_i][L_b,T_j]\right) &= -8\left(\delta^{ij}\varphi^c\varphi^c - \varphi^i\varphi^j\right)\left(\partial_a\varphi^0\partial_b\varphi^0 + \partial_a\varphi^c\partial_b\varphi^c\right)\\ &\quad + 8\left\{\delta^{ij}(\varphi^c\varphi^c)\partial_a\varphi^d\partial_b\varphi^d - \delta^{ij}(\varphi^c\partial_a\varphi^c)(\varphi^d\partial_b\varphi^d)\right.\\ &\quad \left.-\varphi^i\varphi^j(\partial_a\varphi^c\partial_b\varphi^c) + \varphi^i\partial_b\varphi^j(\varphi^c\partial_a\varphi^c) + (\varphi^c\partial_b\varphi^c)\varphi^j\partial_a\varphi^i - (\varphi^c\varphi^c)\partial_a\varphi^i\partial_b\varphi^j\right\}\\ &= -8\left\{\delta^{ij}(\varphi^c\varphi^c)\partial_a\varphi^0\partial_b\varphi^0 + \delta^{ij}(\varphi^c\varphi^c)\partial_a\varphi^d\partial_b\varphi^d - \varphi^i\varphi^j\partial_a\varphi^0\partial_b\varphi^0 - \varphi^i\varphi^j(\partial_a\varphi^c\partial_b\varphi^c)\right\}\\ &\quad + 8\left\{\delta^{ij}(\varphi^c\varphi^c)\partial_a\varphi^d\partial_b\varphi^d - \delta^{ij}(\varphi^c\partial_a\varphi^c)(\varphi^d\partial_b\varphi^d)\right.\\ &\quad \left.-\varphi^i\varphi^j(\partial_a\varphi^c\partial_b\varphi^c) + \varphi^i\partial_b\varphi^j(\varphi^c\partial_a\varphi^c) + (\varphi^c\partial_b\varphi^c)\varphi^j\partial_a\varphi^i - (\varphi^c\varphi^c)\partial_a\varphi^i\partial_b\varphi^j\right\}\\ &= -8\left\{\delta^{ij}(\varphi^c\varphi^c)\partial_a\varphi^0\partial_b\varphi^0 - \varphi^i\varphi^j\partial_a\varphi^0\partial_b\varphi^0 + \delta^{ij}(\varphi^c\partial_a\varphi^c)(\varphi^d\partial_b\varphi^d)\right.\\ &\quad \left.-\varphi^i\partial_b\varphi^j(\varphi^c\partial_a\varphi^c) - (\varphi^c\partial_b\varphi^c)\varphi^j\partial_a\varphi^i + (\varphi^c\varphi^c)\partial_a\varphi^i\partial_b\varphi^j\right\}\\ &= -8\left\{\delta^{ij}(\varphi^c\varphi^c)\partial_a\varphi^0\partial_b\varphi^0 - \varphi^i\varphi^j\partial_a\varphi^0\partial_b\varphi^0 + \delta^{ij}(\varphi^0\partial_a\varphi^0)(\varphi^0\partial_b\varphi^0)\right.\\ &\quad \left.+\varphi^i\partial_b\varphi^j(\varphi^0\partial_a\varphi^0) + (\varphi^0\partial_b\varphi^0)\varphi^j\partial_a\varphi^i + (\varphi^c\varphi^c)\partial_a\varphi^i\partial_b\varphi^j\right\}\\ &= -8\left\{\delta^{ij}(\varphi^c\varphi^c + \varphi^0\varphi^0)\partial_a\varphi^0\partial_b\varphi^0 - \varphi^i\varphi^j\partial_a\varphi^0\partial_b\varphi^0\right.\\ &\quad \left.+\varphi^i\partial_b\varphi^j(\varphi^0\partial_a\varphi^0) + (\varphi^0\partial_b\varphi^0)\varphi^j\partial_a\varphi^i + (\varphi^c\varphi^c)\partial_a\varphi^i\partial_b\varphi^j\right\}\\ &= -8\left\{(\delta^{ij} - \varphi^i\varphi^j)\partial_a\varphi^0\partial_b\varphi^0 + (\varphi^c\varphi^c)\partial_a\varphi^i\partial_b\varphi^j + \varphi^0\varphi^i\partial_a\varphi^0\partial_b\varphi^j + \varphi^0\varphi^j\partial_b\varphi^0\partial_a\varphi^i\right\}.\end{aligned} \tag{A.1.21}$$

A.2 Runge Coloring Scheme

It is conventional to visualize skyrmions by plotting an isosurface of constant energy or baryon density, e.g. $\max\left(\mathscr{B}^0\right)/c$ for some constant c. There is also a rather nice way to graphically encode the pion fields $\vec{\pi}$ onto this isosurface using the Runge color sphere [43], which is detailed as follows. At each point $\vec{x}$ on the isosurface we compute the pion fields $\vec{\pi}(\vec{x})$. Then we introduce a HSV color function at each $\vec{x}$ with the hue H, saturation S and value V defined by

$$0 \le \mathrm{H} \le 1: \quad \mathrm{H}(\vec{x}) = \frac{1}{2} + \frac{1}{2\pi}\arg\left(\pi^1(\vec{x}) + i\pi^2(\vec{x})\right), \tag{A.2.1}$$

$$0 \le \mathrm{S} \le 1: \quad \mathrm{S}(\vec{x}) = \frac{1}{2}\left(\pi^3(\vec{x}) + 1\right), \tag{A.2.2}$$

$$0 \le \mathrm{V} \le 1: \quad \mathrm{V}(\vec{x}) = \mathrm{S}(\vec{x}). \tag{A.2.3}$$

Once the HSV color map is obtained it is then converted to an RGB color map, which is used to color the skyrmion.

If one recasts the SU(2) isospin symmetry (1.1.8) in the SO(3) form via the map

$$D: \mathrm{SU}(2) \to \mathrm{SO}(3), \quad D(A)_{ij} = \frac{1}{2}\mathrm{Tr}\left(\tau^i A\tau^j A^\dagger\right), \tag{A.2.4}$$

then an isospin transformation $A \in \mathrm{SU}(2)$ on the Skyrme field φ acts to continuously cycle the pion fields from one into another, $\pi^i \mapsto D(A)_{ij}\pi^j$. In terms of the Runge coloring, an isospin

transformation rotates the colors on the skyrmion. The Runge coloring scheme is best depicted using the $B = 1$ hedgehog skyrmion and is displayed in Fig. 1.1.

A.3 Non-Linear Conjugate Gradient Descent

Our aim is to solve the unconstrained optimisation problem:

$$\min_{\omega} E(\omega), \quad E(\omega) = \int_M \mathrm{d}^3x\sqrt{-g}\left\{\frac{1}{2}g^{ij}\partial_i\omega\partial_j\omega + \frac{1}{2}\omega^2 + c_\omega\omega\mathscr{B}_0\right\}.$$

We perform a quadratic approximation with $n \in \mathbb{Z}_{\geq 0}$:

$$f_n = \nabla E(\omega_n) = (-g^{ij}\partial_{ij} + 1)\omega_n + c_\omega\mathscr{B}_0, \quad \mathcal{Q} = \nabla^2 E(\omega_n).$$

Evaluating the Hessian $\mathcal{Q}$ is computationally expensive, so one can implement a quasi-Newton method such as the secant method. First, we discretize the ω-energy functional on an N^3-grid such that the energy is $E : \mathbb{R}^N \times \mathbb{R}^N \times \mathbb{R}^N \to \mathbb{R}$ and then apply vectorization to $\omega \in \mathbb{R}^{N^3}$. Then we do a Taylor expansion in a conjugate direction $d \in \mathbb{R}^{N^3}$ with stepsize α,

$$\begin{aligned} E(\omega + \alpha d) &= E(\omega) + \alpha\left[\frac{\mathrm{d}}{\mathrm{d}\alpha}E(\omega + \alpha d)\right]_{\alpha=0} + \frac{\alpha^2}{2}\left[\frac{\mathrm{d}^2}{\mathrm{d}\alpha^2}E(\omega + \alpha d)\right]_{\alpha=0} \\ &= E(\omega) + \alpha E'(\omega)d^T + \frac{\alpha^2}{2}d^T E''(\omega)d \end{aligned}$$

such that we can approximate the first derivative,

$$\frac{\mathrm{d}}{\mathrm{d}\alpha}E(\omega + \alpha d) \approx E'(\omega)d^T + \alpha d^T E''(\omega)d,$$

and the second derivative

$$\begin{aligned} \frac{\mathrm{d}^2}{\mathrm{d}\alpha^2}E(\omega + \alpha d) &\approx \frac{1}{\sigma}\left\{\left[\frac{\mathrm{d}}{\mathrm{d}\alpha}E(\omega + \alpha d)\right]_{\alpha=\sigma} - \left[\frac{\mathrm{d}}{\mathrm{d}\alpha}E(\omega + \alpha d)\right]_{\alpha=0}\right\} \\ &= \frac{1}{\sigma}\left\{E'(\omega + \sigma d)d^T - E'(\omega)d^T\right\}. \end{aligned}$$

Then we can write

$$\frac{\mathrm{d}}{\mathrm{d}\alpha}E(\omega + \alpha d) \approx E'(\omega)d^T + \frac{\alpha}{\sigma}\left\{E'(\omega + \sigma d)d^T - E'(\omega)d^T\right\}.$$

This can be minimised by setting

$$\alpha = -\sigma\frac{E'(\omega)d^T}{E'(\omega + \sigma d)d^T - E'(\omega)d^T}.$$

The NCGD algorithm is detailed as follows. Starting at $\omega_0 = -c_\omega\mathscr{B}_0$ compute $f_0 = \nabla E(\omega_0)$ and set the initial conjugate direction to be the steepest direction $d_0 = -f_0$. Then, while $\max(\nabla E(\omega_n)) > \mathrm{tol}$:

- Start a loop counter $n = 0$.

- Find α_n that minimises $E(\omega_n + \alpha_n d_n)$ by using:
  - The Newton-Raphson method, which requires the computation of the Hessian,

$$\alpha_n = -\frac{f_n^T d_n}{d_n^T \mathbb{Q} d_n} = -\frac{f_n^T d_n}{d_n^T [\nabla^2 E(\omega_n)] d_n}.$$

  - Or performing a line search: use the secant method, with $\sigma_0 \approx 0$,

$$\alpha_n = -\sigma_n \frac{f_n(\omega_n)^T d_n}{f_n(\omega_n + \sigma_n d_n)^T d_n - f_n(\omega_n)^T d_n}, \quad \sigma_{n+1} = -\alpha_n.$$

- Update the position $\omega_{n+1} = \omega_n + \alpha_n d_n$.
- Compute the steepest direction $f_{n+1} = \nabla E(\omega_{n+1})$.
- If $\max(\nabla E(\omega_{n+1})) < \text{tol}$, break.
- Else, update the conjugate direction $d_{n+1} = -f_{n+1} + \beta_n d_n$ where the conjugate stepsize is one of the following:

$$\beta_n^{FR} = \frac{f_{n+1}^T f_{n+1}}{f_n^T f_n}, \qquad \text{(Fletcher-Reeves method)}$$

$$\beta_n^{PRP} = \frac{(f_{n+1} - f_n)^T f_{n+1}}{f_n^T f_n}, \qquad \text{(Polak-Ribiere-Polyak method)}$$

$$\beta_n^{NR} = \frac{f_{n+1}^T [\nabla^2 E(g_n)] d_n}{d_n^T [\nabla^2 E(g_n)] d_n} \qquad \text{(Newton-Raphson method)}$$

$$\beta_n^{HS} = \frac{(f_{n+1} - f_n)^T f_{n+1}}{-(f_{n+1} - f_n)^T d_n}, \qquad \text{(Hestenes-Stiefel method)}$$

$$\beta_n^{DY} = \frac{f_{n+1}^T f_{n+1}}{-(f_{n+1} - f_n)^T d_n}, \qquad \text{(Dai–Yuan method).}$$

Bibliography

[1] G. 't Hooft. "A planar diagram theory for strong interactions". In: *Nucl. Phys. B* 72.3 (1974), pp. 461–473. DOI: 10.1016/0550-3213(74)90154-0.

[2] E. Witten. "Baryons in the 1N expansion". In: *Nucl. Phys. B* 160.1 (1979), pp. 57–115. DOI: 10.1016/0550-3213(79)90232-3.

[3] T. H. R. Skyrme. "A non-linear field theory". In: *Proc. R. Soc. Lond. A* 260 (1961), pp. 127–138. DOI: 10.1098/rspa.1961.0018.

[4] E. Witten. "Global aspects of current algebra". In: *Nucl. Phys. B* 223.2 (1983), pp. 422–432. DOI: 10.1016/0550-3213(83)90063-9.

[5] E. Witten. "Current algebra, baryons, and quark confinement". In: *Nucl. Phys. B* 223.2 (1983), pp. 433–444. DOI: 10.1016/0550-3213(83)90064-0.

[6] G. S. Adkins, C. R. Nappi, and E. Witten. "Static properties of nucleons in the Skyrme model". In: *Nucl.Phys. B* 228.3 (1983), pp. 552–566. DOI: 10.1016/0550-3213(83)90559-X.

[7] E. Braaten and L. Carson. "Deuteron as a Soliton in the Skyrme Model". In: *Phys. Rev. Lett.* 56 (18 1986), pp. 1897–1900. DOI: 10.1103/PhysRevLett.56.1897.

[8] O. V. Manko, N. S. Manton, and S. W. Wood. "Light nuclei as quantized Skyrmions". In: *Phys. Rev. C* 76 (5 2007), p. 055203. DOI: 10.1103/PhysRevC.76.055203.

[9] P. H. C. Lau and N. S. Manton. "States of Carbon-12 in the Skyrme Model". In: *Phys. Rev. Lett.* 113 (23 2014), p. 232503. DOI: 10.1103/PhysRevLett.113.232503.

[10] C. J. Halcrow. "Vibrational quantisation of the $B = 7$ Skyrmion". In: *Nucl. Phys. B* 904 (2016), pp. 106–123. DOI: 10.1016/j.nuclphysb.2016.01.011.

[11] C. J. Halcrow, C. King, and N. S. Manton. "Dynamical α-cluster model of ^{16}O". In: *Phys. Rev. C* 95 (3 2017), p. 031303. DOI: 10.1103/PhysRevC.95.031303.

[12] C. Halcrow, C. King, and N. Manton. "Oxygen-16 spectrum from tetrahedral vibrations and their rotational excitation". In: *Int. J. Mod. Phys. E* 28.04 (2019), p. 1950026. DOI: 10.1142/S0218301319500265.

[13] J. I. Rawlinson. "An alpha particle model for Carbon-12". In: *Nucl. Phys. A* 975 (2018), pp. 122–135. DOI: 10.1016/j.nuclphysa.2018.04.011.

[14] J. I. Rawlinson. "Coriolis terms in Skyrmion quantization". In: *Nucl. Phys. B* 949 (2019), p. 114800. DOI: 10.1016/j.nuclphysb.2019.114800.

[15] L. D. Faddeev. "Some comments on the many-dimensional solitons". In: *Lett. Math. Phys.* 1.4 (1976), pp. 289–293. DOI: 10.1007/BF00398483.

[16] D. Harland. "Topological energy bounds for the Skyrme and Faddeev models with massive pions". In: *Phys. Lett. B* 728 (2014), pp. 518–523. DOI: 10.1016/j.physletb.2013.11.062.

[17] W. Baskerville. "Making nuclei out of the Skyrme crystal". In: *Nucl. Phys. A* 596.3 (1996), pp. 611–630. DOI: 10.1016/0375-9474(95)00432-7.

[18] N. Ma, C. J. Halcrow, and H. Zhang. "Effect of the Coulomb energy on Skyrmions". In: *Phys. Rev. C* 99.4 (2019), p. 044312. DOI: 10.1103/PhysRevC.99.044312.

[19] I. Klebanov. "Nuclear matter in the Skyrme model". In: *Nucl. Phys. B* 262.1 (1985), pp. 133–143. DOI: 10.1016/0550-3213(85)90068-9.

[20] S. B. Gudnason and C. Halcrow. "A Smörgåsbord of Skyrmions". In: *J. High Energ. Phys.* 2022 (2022), p. 117. DOI: 10.1007/JHEP08(2022)117.

[21] E. Braaten, S. Townsend, and L. Carson. "Novel structure of static multisoliton solutions in the Skyrme model". In: *Phys. Lett. B* 235.1 (1990), pp. 147–152. DOI: 10.1016/0370-2693(90)90111-I.

[22] R. A. Battye and P. Sutcliffe. "Symmetric Skyrmions". In: *Phys. Rev. Lett.* 79 (3 1997), pp. 363–366. DOI: 10.1103/PhysRevLett.79.363.

[23] C. J. Houghton, N. S. Manton, and P. Sutcliffe. "Rational maps, monopoles and Skyrmions". In: *Nucl. Phys. B* 510.3 (1998), pp. 507–537. DOI: 10.1016/S0550-3213(97)00619-6.

[24] R. A. Battye and P. Sutcliffe. "Solitonic Fullerene Structures in Light Atomic Nuclei". In: *Phys. Rev. Lett.* 86 (18 2001), pp. 3989–3992. DOI: 10.1103/PhysRevLett.86.3989.

[25] R. A. Battye, C. J. Houghton, and P. M. Sutcliffe. "Icosahedral Skyrmions". In: *J. Math. Phys.* 44.8 (2003), pp. 3543–3554. DOI: 10.1063/1.1584209.

[26] R. A. Battye and P. M. Sutcliffe. "Skyrmions with massive pions". In: *Phys. Rev. C* 73 (5 2006), p. 055205. DOI: 10.1103/PhysRevC.73.055205.

[27] N. S. Manton and B. M. A. G. Piette. "Understanding Skyrmions using rational maps". In: *Progress of mathematics* 201 (2001), pp. 469–479. DOI: 10.1007/978-3-0348-8268-2_27.

[28] N. S. Manton. "Classical Skyrmions - static solutions and dynamics". In: *Math. Meth. Appl. Sci.* 35 (10 2012), pp. 1188–1204. DOI: 10.1002/mma.2512.

[29] D. T. J. Feist. "Interactions of $B = 4$ Skyrmions". In: *J. High Energ. Phys.* 2012 (2 2012), p. 100. DOI: 10.1007/JHEP02(2012)100.

[30] M. F. Atiyah and N. S. Manton. "Skyrmions from instantons". In: *Phys. Lett. B* 222.3 (1989), pp. 438–442. DOI: 10.1016/0370-2693(89)90340-7.

[31] P. Sutcliffe. "Skyrmions, instantons and holography." In: *J. High Energ. Phys.* 2010 (2010), p. 19. DOI: 10.1007/JHEP08(2010)019.

[32] C. Halcrow and T. Winyard. "A consistent two-Skyrmion configuration space from instantons". In: *J. High Energ. Phys.* 2021 (12 2021), p. 039. DOI: 10.1007/JHEP12(2021)039.

[33] T. Sakai and S. Sugimoto. "Low energy hadron physics in holographic QCD". In: *Prog. Theor. Phys.* 113.4 (2005), pp. 843–882. DOI: 10.1143/PTP.113.843.

[34] J. Cork and C. Halcrow. "ADHM skyrmions". In: *Nonlinearity* 35.8 (2022), pp. 3944–3990. DOI: 10.1088/1361-6544/ac72e6.

[35] D. Harland and P. Sutcliffe. "Rational Skyrmions". In: *J. Phys. A: Math. Theor.* 56.42 (2023), p. 425401. DOI: 10.1088/1751-8121/acfbcc.

[36] N. S. Manton and P. M. Sutcliffe. "Skyrme crystal from a twisted instanton on a four-torus". In: *Phys. Lett. B* 342.1 (1995), pp. 196–200. DOI: 10.1016/0370-2693(94)01375-M.

[37] S. Chen, K. Fukushima, and Z. Qiu. "Skyrmions in a magnetic field and π^0 domain wall formation in dense nuclear matter". In: *Phys. Rev. D* 105 (1 2022), p. L011502. DOI: 10.1103/PhysRevD.105.L011502.

[38] A. S. Goldhaber and N. S. Manton. "Maximal symmetry of the Skyrme crystal". In: *Phys. Lett. B* 198.2 (1987), pp. 231–234. DOI: 10.1016/0370-2693(87)91502-4.

[39] M. Kugler and S. Shtrikman. "A new Skyrmion crystal". In: *Phys. Lett. B* 208.3 (1988), pp. 491–494. DOI: 10.1016/0370-2693(88)90653-3.

[40] L. Castillejo, P. S. J. Jones, A. D. Jackson, J. J. M. Verbaarschot, and A. Jackson. "Dense Skyrmion systems". In: *Nucl. Phys. A* 501.4 (1989), pp. 801–812. DOI: 10.1016/0375-9474(89)90161-9.

[41] A. D. Jackson and J. J. M. Verbaarschot. "Phase structure of the Skyrme model". In: *Nucl. Phys. A* 484.3 (1988), pp. 419–431. DOI: 10.1016/0375-9474(88)90302-8.

[42] I. Perapechka and Y. Shnir. "Crystal structures in generalized Skyrme model". In: *Phys. Rev. D* 96 (4 2017), p. 045013. DOI: 10.1103/PhysRevD.96.045013.

[43] D. T. J. Feist, P. H. C. Lau, and N. S. Manton. "Skyrmions up to baryon number 108". In: *Phys. Rev. D* 87 (8 2013), p. 085034. DOI: 10.1103/PhysRevD.87.085034.

[44] R. A. Battye, N. S. Manton, and P. Sutcliffe. "Skyrmions and the α-particle model of nuclei". In: *Proc. R. Soc. A.* 463.2077 (2007), pp. 261–279. DOI: 10.1098/rspa.2006.1767.

[45] J. Silva Lobo. "Deformed Skyrme crystals". In: *J. High Energ. Phys.* 2010 (10 2010), p. 029. DOI: 10.1007/JHEP10(2010)029.

[46] C. Adam, A. G. Martín-Caro, M. Huidobro, R. Vázquez, and A. Wereszczynski. "Dense matter equation of state and phase transitions from a generalized Skyrme model". In: *Phys. Rev. D* 105 (7 2022), p. 074019. DOI: 10.1103/PhysRevD.105.074019.

[47] D. Harland and R. Ward. "Chains of skyrmions". In: *J. High Energ. Phys.* 2008.12 (2008), p. 093. DOI: 10.1088/1126-6708/2008/12/093.

[48] Y. M. Shnir. "Chains of interacting solitons". In: *Symmetry* 284.2 (2021), p. 13. DOI: 10.3390/sym13020284.

[49] R. A. Battye and P. Sutcliffe. "A Skyrme lattice with hexagonal symmetry". In: *Phys. Lett. B* 416.3 (1998), pp. 385–391. DOI: 10.1016/S0370-2693(97)01196-9.

[50] J. Silva Lobo and R. S. Ward. "Skyrmion multi-walls". In: *J. Phys. A: Math. Theor.* 42.48 (2009), p. 482001. DOI: 10.1088/1751-8113/42/48/482001.

[51] W. Baskerville. "Quantisation of global isospin in the Skyrme crystal". In: *Phys. Lett. B* 380.1 (1996), pp. 106–112. DOI: 10.1016/0370-2693(96)00409-1.

[52] C. Adam, A. G. Martín-Caro, M. Huidobro, R. Vázquez, and A. Wereszczynski. "Quantum skyrmion crystals and the symmetry energy of dense matter". In: *Phys. Rev. D* 106 (11 2022), p. 114031. DOI: 10.1103/PhysRevD.106.114031.

[53] C. Adam, A. G. Martín-Caro, M. Huidobro, and A. Wereszczynski. "Skyrme Crystals, Nuclear Matter and Compact Stars". In: *Symmetry* 15.4 (2023), p. 899. DOI: 10.3390/sym15040899.

[54] C. Adam, A. G. Martín-Caro, M. Huidobro, R. Vázquez, and A. Wereszczynski. "A new consistent neutron star equation of state from a generalized Skyrme model". In: *Phys. Lett. B* 811 (2020), p. 135928. DOI: 10.1016/j.physletb.2020.135928.

[55] A. Jackson, A. Jackson, A. Goldhaber, G. Brown, and L. Castillejo. "A modified skyrmion". In: *Phys. Lett. B* 154.2 (1985), pp. 101–106. DOI: 10.1016/0370-2693(85)90566-0.

[56] C. Adam, T. Klähn, C. Naya, J. Sanchez-Guillen, R. Vazquez, and A. Wereszczynski. "Baryon chemical potential and in-medium properties of BPS skyrmions". In: *Phys. Rev. D* 91 (12 2015), p. 125037. DOI: 10.1103/PhysRevD.91.125037.

[57] L. V. Kapitanski and O. A. Ladyzhenskaya. "On the Coleman's principle concerning the stationary points of invariant functionals". In: *Zap. Nauchn. Sem. LOMI* 127 (1983), pp. 84–102.

[58] M. J. Esteban. "A direct variational approach to Skyrme's model for meson fields". In: *Commun. Math. Phys.* 105 (1986), pp. 571–591. DOI: 10.1007/BF01238934.

[59] N. S. Manton and P. Sutcliffe. *Topological Solitons*. Cambridge Monographs on Mathematical Physics. Cambridge University Press, 2004. DOI: 10.1017/CBO9780511617034.

[60] A. Jackson, A. Jackson, and V. Pasquier. "The skyrmion-skyrmion interaction". In: *Nucl. Phys. A* 432.3 (1985), pp. 567–609. DOI: 10.1016/0375-9474(85)90002-8.

[61] J. W. Milnor. *Topology from the Differentiable Viewpoint*. Charlottesville: University Press of Virginia, 1965.

[62] M. Kugler and S. Shtrikman. "Skyrmion crystals and their symmetries". In: *Phys. Rev. D* 40 (10 1989), pp. 3421–3429. DOI: 10.1103/PhysRevD.40.3421.

[63] N. S. Manton. *Skyrmions - A Theory of Nuclei*. London: World Scientific Publishing Europe Ltd., 2022. DOI: 10.1142/q0368.

[64] J. M. Speight. "Solitons on tori and soliton crystals". In: *Comm. Math. Phys.* 332.1 (2014), pp. 355–377. DOI: 10.1007/s00220-014-2104-z.

[65] P. Leask. "Baby Skyrmion crystals". In: *Phys. Rev. D* 105 (2 2022), p. 025010. DOI: 10.1103/PhysRevD.105.025010.

[66] B. Piette, B. Schroers, and W. Zakrzewski. "Dynamics of baby Skyrmions". In: *Nucl. Phys. B* 439.1 (1995), pp. 205–235. DOI: 10.1016/0550-3213(95)00011-G.

[67] X. Z. Yu, Y. Onose, N. Kanazawa, J. H. Park, J. H. Han, Y. Matsui, N. Nagaosa, and Y. Tokura. "Real-space observation of a two-dimensional Skyrmion crystal". In: *Nature* 465 (24 2010), pp. 901–904. DOI: 10.1038/nature09124.

[68] A. A. Kovalev and S. Sandhoefner. "Skyrmions and anti-Skyrmions in quasi-two-dimensional magnets". In: *Frontiers in Physics* 6 (2018), p. 98. DOI: 10.3389/fphy.2018.00098.

[69] S. L. Sondhi, A. Karlhede, S. A. Kivelson, and E. H. Rezayi. "Skyrmions and the crossover from the integer to fractional quantum Hall effect at small Zeeman energies". In: *Phys. Rev. B* 47 (24 1993), pp. 16419–16426. DOI: 10.1103/PhysRevB.47.16419.

[70] V. M. Kuchkin, K. Chichay, B. Barton-Singer, F. N. Rybakov, S. Blügel, B. J. Schroers, and N. S. Kiselev. "Geometry and symmetry in skyrmion dynamics". In: *Phys. Rev. B* 104 (16 2021), p. 165116. DOI: 10.1103/PhysRevB.104.165116.

[71] P. J. Ackerman, T. Boyle, and I. I. Smalyukh. "Squirming motion of baby Skyrmions in nematic fluids". In: *Nat Commun* 8 (2017), pp. 673–686. DOI: 10.1038/s41467-017-00659-5.

[72] I. Hen and M. Karliner. "Hexagonal structure of baby Skyrmion lattices". In: *Phys. Rev. D* 77 (5 2008), p. 054009. DOI: 10.1103/PhysRevD.77.054009.

[73] I. Hen and M. Karliner. "Lattice structure of baby Skyrmions". In: *Theor. Math. Phys.* 160 (1 2009), pp. 933–944. DOI: 10.1007/s11232-009-0083-6.

[74] F. N. Rybakov and N. S. Kiselev. "Chiral magnetic Skyrmions with arbitrary topological charge". In: *Phys. Rev. B* 99 (6 2019), p. 064437. DOI: 10.1103/PhysRevB.99.064437.

[75] A. Bogdanov and A. Hubert. "Thermodynamically stable magnetic vortex states in magnetic crystals". In: *J. Magn. Magn. Mater.* 138.3 (1994), pp. 255–269. DOI: 10.1016/0304-8853(94)90046-9.

[76] W. H. Kleiner, L. M. Roth, and S. H. Autler. "Bulk solution of Ginzburg-Landau equations for type II superconductors: upper critical field region". In: *Phys. Rev.* 133 (5A 1964), A1226–A1227. DOI: 10.1103/PhysRev.133.A1226.

[77] J. Jäykkä and M. Speight. "Easy plane baby Skyrmions". In: *Phys. Rev. D* 82 (12 2010), p. 125030. DOI: 10.1103/PhysRevD.82.125030.

[78] M. Kobayashi and M. Nitta. "Fractional vortex molecules and vortex polygons in a baby Skyrme model". In: *Phys. Rev. D* 87 (12 2013), p. 125013. DOI: 10.1103/PhysRevD.87.125013.

[79] M. Kobayashi and M. Nitta. "Vortex Polygons and Their Stabilities in Bose-Einstein Condensates and Field Theory". In: *J. Low Temp. Phys.* 175 (10 2014), pp. 208–215. DOI: 10.1007/s10909-013-0977-4.

[80] S.-Z. Lin, A. Saxena, and C. D. Batista. "Skyrmion fractionalization and merons in chiral magnets with easy-plane anisotropy". In: *Phys. Rev. B* 91 (22 2015), p. 224407. DOI: 10.1103/PhysRevB.91.224407.

[81] P. Baird and J. C. Wood. *Harmonic Morphisms Between Riemannian Manifolds*. London Mathematical Society monographs. Clarendon Press, 2003. DOI: 10.1093/acprof:oso/9780198503620.001.0001.

[82] J. M. Speight. "Compactons and semi-compactons in the extreme baby Skyrme model". In: *J. Phys. A: Math. Theor.* 43.40 (2010), p. 405201. DOI: 10.1088/1751-8113/43/40/405201.

[83] D. Foster and P. Sutcliffe. "Baby Skyrmions stabilized by vector mesons". In: *Phys. Rev. D* 79 (12 2009), p. 125026. DOI: 10.1103/PhysRevD.79.125026.

[84] P. Salmi and P. Sutcliffe. "Aloof baby Skyrmions". In: *J. Phys. A* 48.3 (2015), p. 035401. DOI: 10.1088/1751-8113/48/3/035401.

[85] I. Hen and M. Karliner. "Rotational symmetry breaking in baby Skyrme models". In: *Nonlinearity* 21.3 (2008), pp. 399–408. DOI: 10.1088/0951-7715/21/3/002.

[86] J. M. Speight and T. Winyard. "Skyrmions and spin waves in frustrated ferromagnets at low applied magnetic field". In: *Phys. Rev. B* 101 (13 2020), p. 134420. DOI: 10.1103/PhysRevB.101.134420.

[87] M. Speight and T. Winyard. "Intervortex forces in competing-order superconductors". In: *Phys. Rev. B* 103 (1 2021), p. 014514. DOI: 10.1103/PhysRevB.103.014514.

[88] S. B. Gudnason and J. M. Speight. "Realistic classical binding energies in the ω-Skyrme model". In: *J. High Energ. Phys.* 2020 (6 2020), p. 184. DOI: 10.1007/JHEP07(2020)184.

[89] R. A. Leese, M. Peyrard, and W. J. Zakrzewski. "Soliton scatterings in some relativistic models in (2+1) dimensions". In: *Nonlinearity* 3.3 (1990), pp. 773–807. DOI: 10.1088/0951-7715/3/3/011.

[90] J. Jäykkä, M. Speight, and P. Sutcliffe. "Broken baby Skyrmions". In: *Proc. R. Soc. A.* 468.2140 (2012), pp. 1085–1104. DOI: 10.1098/rspa.2011.0543.

[91] P. Jennings and T. Winyard. "Broken planar Skyrmions – statics and dynamics". In: *J. High Energ. Phys.* 2014 (1 2014), p. 122. DOI: 10.1007/JHEP01(2014)122.

[92] R. Ward. "Planar Skyrmions at high and low density". In: *Nonlinearity* 17.3 (2004), pp. 1033–1040. DOI: 10.1088/0951-7715/17/3/014.

[93] T. Weidig. "The baby Skyrme models and their multi-skyrmions". In: *Nonlinearity* 12.6 (1999), pp. 1489–1503. DOI: 10.1088/0951-7715/12/6/303.

[94] C. Halcrow. "Quantum soliton scattering manifolds". In: *J. High Energ. Phys.* 2020 (7 2020), p. 182. DOI: 10.1007/JHEP07(2020)182.

[95] S. B. Gudnason, B. Barsanti, and S. Bolognesi. "Near-BPS baby Skyrmions". In: *J. High Energ. Phys.* 2020 (11 2020), p. 62. DOI: 10.1007/JHEP11(2020)062.

[96] D. Harland and R. S. Ward. "Walls and chains of planar Skyrmions". In: *Phys. Rev. D* 77 (4 2008), p. 045009. DOI: 10.1103/PhysRevD.77.045009.

[97] D. Foster. "Baby Skyrmion chains". In: *Nonlinearity* 23.3 (2010), pp. 465–474. DOI: 10.1088/0951-7715/23/3/001.

[98] T. S. Winyard. "The Skyrme Model: Curved Space, Symmetries and Mass". PhD thesis. Durham Theses, 2016, pp. 1–176.

[99] J. Bamberg, G. Cairns, and D. Kilminster. "The crystallographic restriction, permutations, and Goldbach's conjecture". In: *Am. Math. Mon.* 110.3 (2003), pp. 202–209. DOI: 10.2307/3647934.

[100] D. Harland, P. Leask, and M. Speight. "Skyrme crystals with massive pions". In: *J. Math. Phys.* 64 (10 2023), p. 103503. DOI: 10.1063/5.0159674.

[101] D. Auckly and L. Kapitanski. "Holonomy and Skyrme's Model". In: *Commun. Math. Phys.* 240.1-2 (2003), pp. 97–122. DOI: 10.1007/s00220-003-0901-x.

[102] M. Speight, T. Winyard, and E. Babaev. "Symmetries, length scales, magnetic response, and skyrmion chains in nematic superconductors". In: *Phys. Rev. B* 107 (19 2023), p. 195204. DOI: 10.1103/PhysRevB.107.195204.

[103] J. Eells and A. Ratto. *Harmonic Maps and Minimal Immersions with Symmetries (AM-130): Methods of Ordinary Differential Equations Applied to Elliptic Variational Problems*. Princeton: Princeton University Press, 1993. DOI: 10.1515/9781400882502.

[104] C. Adam, J. Sánchez-Guillén, and A. Wereszczyński. "A Skyrme-type proposal for baryonic matter". In: *Phys. Lett. B* 691.2 (2010), pp. 105–110. DOI: 10.1016/j.physletb.2010.06.025.

[105] C. Adam, J. Sánchez-Guillén, and A. Wereszczyński. "BPS Skyrme model and baryons at large N_c". In: *Phys. Rev. D* 82.8 (2010), p. 085015. DOI: 10.1103/PhysRevD.82.085015.

[106] J. Eells and L. Lemaire. *Selected Topics in Harmonic Maps*. CBMS Regional Conference Series in Mathematics. Amer. Math. Soc., 1983. DOI: 10.1090/cbms/050.

[107] C. Adam and A. Wereszczynski. "Topological energy bounds in generalized Skyrme models". In: *Phys. Rev. D* 89 (6 2014), p. 065010. DOI: 10.1103/PhysRevD.89.065010.

[108] J. Eells and J. H. Sampson. "Harmonic mappings of Riemannian manifolds". In: *Am. J. Math.* 86 (1 1964), pp. 109–160. DOI: 10.2307/2373037.

[109] P. Baird and J. Eells. "A conservation law for harmonic maps". In: *Harmonic Maps*. London: World Scientific Publishing Co. Pte. Ltd., 1992. Chap. 9, pp. 131–155. ISBN: 981-02-0704-2. DOI: 10.1142/9789814360197_0009.

[110] F. Hélein. *Harmonic Maps, Conservation Laws and Moving Frames*. 2nd ed. Cambridge Tracts in Mathematics. Cambridge University Press, 2002. DOI: 10.1017/CBO9780511543036.

[111] N. S. Manton. "Scaling identities for solitons beyond Derrick's theorem". In: *J. Math. Phys.* 50 (3 2009), p. 032901. DOI: 10.1063/1.3089582.

[112] P. Fillard, X. Pennec, and N. Ayache. "A Riemannian Framework for Tensor Computing". In: *Int. J. Comput. Vis.* 66 (1 2006), pp. 41–66. DOI: 10.1007/s11263-005-3222-z.

[113] V. Arsigny, P. Fillard, X. Pennec, and N. Ayache. "Geometric Means in a Novel Vector Space Structure on Symmetric Positive-Definite Matrices". In: *SIAM J. Matrix Anal. Appl.* 29 (1 2007), pp. 328–347. DOI: 10.1137/050637996.

[114] M. Speight, T. Winyard, and E. Babaev. "Symmetries, length scales, magnetic response, and skyrmion chains in nematic superconductors". In: *Phys. Rev. B* 107 (19 2023), p. 195204. DOI: 10.1103/PhysRevB.107.195204.

[115] B.-Y. Park, W.-G. Paeng, and V. Vento. "The inhomogeneous phase of dense Skyrme matter". In: *Nucl. Phys. A* 989 (2019), pp. 231–245. DOI: 10.1016/j.nuclphysa.2019.06.010.

[116] D. G. Ravenhall, C. J. Pethick, and J. R. Wilson. "Structure of Matter below Nuclear Saturation Density". In: *Phys. Rev. Lett.* 50 (26 1983), pp. 2066–2069. DOI: 10.1103/PhysRevLett.50.2066.

[117] P. Leask, M. Huidobro, and A. Wereszczynski. "Generalized skyrmion crystals with applications to neutron stars". In: *Phys. Rev. D* 109 (5 2024), p. 056013. DOI: 10.1103/PhysRevD.109.056013.

[118] C. Adam, J. Sanchez-Guillen, R. Vazquez, and A. Wereszczynski. "Adding crust to BPS Skyrme neutron stars". In: *Phys. Rev. D* 102 (2 2020), p. 023019. DOI: 10.1103/PhysRevD.102.023019.

[119] C. Adam, M. Huidobro, R. Vazquez, and A. Wereszczynski. "BPS Skyrme neutron stars in generalized gravity". In: *J. Cosmol. Astropart. Phys* 2020.08 (2020), p. 041. DOI: 10.1088/1475-7516/2020/08/041.

[120] C. Adam, C. Naya, J. Sanchez-Guillen, R. Vazquez, and A. Wereszczynski. "BPS skyrmions as neutron stars". In: *Phys. Lett. B* 742 (2015), pp. 136–142. DOI: 10.1016/j.physletb.2015.01.027.

[121] C. Adam, C. Naya, J. Sanchez-Guillen, R. Vazquez, and A. Wereszczynski. "Neutron stars in the Bogomol'nyi-Prasad-Sommerfield Skyrme model: Mean-field limit versus full field theory". In: *Phys. Rev. C* 92 (2 2015), p. 025802. DOI: 10.1103/PhysRevC.92.025802.

[122] C. Adam, M. Huidobro, R. Vazquez, and A. Wereszczynski. "BPS Skyrme neutron stars in generalized gravity". In: *JCAP* 2020.08 (2020), p. 041. DOI: 10.1088/1475-7516/2020/08/041.

[123] S. Nelmes and B. M. A. G. Piette. "Skyrmion stars and the multilayered rational map ansatz". In: *Phys. Rev. D* 84 (2011), p. 085017. DOI: 10.1103/PhysRevD.84.085017.

[124] S. Nelmes and B. M. A. G. Piette. "Phase transition and anisotropic deformations of neutron star matter". In: *Phys. Rev. D* 85 (12 2012), p. 123004. DOI: 10.1103/PhysRevD.85.123004.

[125] C. Adam, A. G. Martín-Caro, M. Huidobro, A. Wereszczynski, and R. Vázquez. "Kaon condensation in skyrmion matter and compact stars". In: *Phys. Rev. D* 107 (7 2023), p. 074007. DOI: 10.1103/PhysRevD.107.074007.

[126] H. Luckock and I. Moss. "Black holes have skyrmion hair". In: *Phys. Lett. B* 176.3 (1986), pp. 341–345. DOI: 10.1016/0370-2693(86)90175-9.

[127] P. Bizon and T. Chmaj. "Gravitating skyrmions". In: *Phys. Lett. B* 297.1 (1992), pp. 55–62. DOI: 10.1016/0370-2693(92)91069-L.

[128] Y. Shnir. "Black holes with Skyrmion-anti-Skyrmion hairs". In: *Phys. Lett. B* 810 (2020), p. 135847. DOI: 10.1016/j.physletb.2020.135847.

[129] C. Adam, O. Kichakova, Y. Shnir, and A. Wereszczynski. "Hairy black holes in the general Skyrme model". In: *Phys. Rev. D* 94 (2 2016), p. 024060. DOI: 10.1103/PhysRevD.94.024060.

[130] S. B. Gudnason and M. Nitta. "Higher-order Skyrme hair of black holes". In: *J. High Energ. Phys.* 2018 (2018), p. 71. DOI: 10.1007/JHEP05(2018)071.

[131] S. B. Gudnason, M. Nitta, and N. Sawado. "Black hole skyrmion in a generalized Skyrme model". In: *J. High Energ. Phys.* 2016 (2016), p. 55. DOI: 10.1007/JHEP09(2016)055.

[132] G. Dvali and A. Gußmann. "Skyrmion black hole hair: Conservation of baryon number by black holes and observable manifestations". In: *Nucl. Phys. B* 913 (2016), pp. 1001–1036. DOI: 10.1016/j.nuclphysb.2016.10.017.

[133] Y. Brihaye, C. Herdeiro, E. Radu, and D. H. Tchrakian. "Skyrmions, Skyrme stars and black holes with Skyrme hair in five spacetime dimension". In: *J. High Energ. Phys.* 2017 (2017), p. 37. DOI: 10.1007/JHEP11(2017)037.

[134] A. S. Schneider, C. J. Horowitz, J. Hughto, and D. K. Berry. "Nuclear "pasta" formation". In: *Phys. Rev. C* 88 (6 2013), p. 065807. DOI: 10.1103/PhysRevC.88.065807.

[135] A. S. Schneider, D. K. Berry, C. M. Briggs, M. E. Caplan, and C. J. Horowitz. "Nuclear "waffles"". In: *Phys. Rev. C* 90 (5 2014), p. 055805. DOI: 10.1103/PhysRevC.90.055805.

[136] M. E. Caplan and C. J. Horowitz. "Colloquium: Astromaterial science and nuclear pasta". In: *Rev. Mod. Phys.* 89 (4 2017), p. 041002. DOI: 10.1103/RevModPhys.89.041002.

[137] C. Adam, C. Naya, J. Sanchez-Guillen, J. M. Speight, and A. Wereszczynski. "Thermodynamics of the BPS Skyrme model". In: *Phys. Rev. D* 90 (4 2014), p. 045003. DOI: 10.1103/PhysRevD.90.045003.

[138] G. Fiorella Burgio and A. F. Fantina. "Nuclear Equation of state for Compact Stars and Supernovae". In: *Astrophys. Space Sci. Libr.* 457 (2018), pp. 255–335. DOI: 10.1007/978-3-319-97616-7_6.

[139] N. Manton. "A remark on the scattering of BPS monopoles". In: *Phys. Lett. B* 110.1 (1982), pp. 54–56. DOI: 10.1016/0370-2693(82)90950-9.

[140] S. Krusch. "Homotopy of rational maps and the quantization of Skyrmions". In: *Annals of Physics* 304.2 (2003), pp. 103–127. DOI: 10.1016/S0003-4916(03)00014-9.

[141] D. Finkelstein and J. Rubinstein. "Connection between Spin, Statistics, and Kinks". In: *J. Math. Phys.* 9.11 (1968), pp. 1762–1779. DOI: 10.1063/1.1664510.

[142] E. Braaten and L. Carson. "Deuteron as a toroidal Skyrmion". In: *Phys. Rev. D* 38 (11 1988), pp. 3525–3539. DOI: 10.1103/PhysRevD.38.3525.

[143] B.-Y. Park, J.-I. Kim, and M. Rho. "Kaons in dense half-Skyrmion matter". In: *Phys. Rev. C* 81 (3 2010), p. 035203. DOI: 10.1103/PhysRevC.81.035203.

[144] H. Dong, T. T. S. Kuo, H. K. Lee, R. Machleidt, and M. Rho. "Half-Skyrmions and the equation of state for compact-star matter". In: *Phys. Rev. C* 87 (5 2013), p. 054332. DOI: 10.1103/PhysRevC.87.054332.

[145] B.-.-A. Li, B.-.-J. Cai, W.-.-J. Xie, and N.-.-B. Zhang. "Progress in Constraining Nuclear Symmetry Energy Using Neutron Star Observables Since GW170817". In: *Universe* 7.6 (2021). DOI: 10.3390/universe7060182.

[146] J. Piekarewicz and G. T. Sánchez. "Proton fraction in the inner neutron-star crust". In: *Phys. Rev. C* 85 (1 2012), p. 015807. DOI: 10.1103/PhysRevC.85.015807. URL: https://link.aps.org/doi/10.1103/PhysRevC.85.015807.

[147] T. Maruyama, T. Tatsumi, D. N. Voskresensky, T. Tanigawa, and S. Chiba. "Nuclear "pasta" structures and the charge screening effect". In: *Phys. Rev. C* 72 (1 2005), p. 015802. DOI: 10.1103/PhysRevC.72.015802. URL: https://link.aps.org/doi/10.1103/PhysRevC.72.015802.

[148] J. B. Natowitz et al. "Symmetry energy of dilute warm nuclear matter". In: *Phys. Rev. Lett.* 104 (2010), p. 202501. DOI: 10.1103/PhysRevLett.104.202501.

[149] S. Kowalski et al. "Experimental determination of the symmetry energy of a low density nuclear gas". In: *Phys. Rev. C* 75 (2007), p. 014601. DOI: 10.1103/PhysRevC.75.014601.

[150] V. B. Kopeliovich, A. M. Shunderuk, and G. K. Matushko. "Mass splittings of nuclear isotopes in chiral soliton approach". In: *Phys. Atom. Nucl.* 69 (2006), pp. 120–132. DOI: 10.1134/S1063778806010169.

[151] H. K. Lee, B.-Y. Park, and M. Rho. "Half-Skyrmions, tensor forces, and symmetry energy in cold dense matter". In: *Phys. Rev. C* 83 (2 2011), p. 025206. DOI: 10.1103/PhysRevC.83.025206.

[152] H. K. Lee, Y.-L. Ma, W.-G. Paeng, and M. Rho. "Cusp in the symmetry energy, speed of sound in neutron stars and emergent pseudo-conformal symmetry". In: *Mod. Phys. Lett. A* 37.03 (2022), p. 2230003. DOI: 10.1142/S0217732322300038.

[153] N. K. Glendenning. *Compact Stars*. Springer New York, 1997. DOI: 10.1007/978-1-4684-0491-3.

[154] N. Chamel and P. Haensel. "Physics of Neutron Star Crusts". In: *Living Rev. Rel.* 11 (2008), p. 10. DOI: 10.12942/lrr-2008-10.

[155] P. Siemens. "Liquid–gas phase transition in nuclear matter". In: *Nature* 305 (1983), pp. 410–412. DOI: 10.1038/305410a0.

[156] B. P. Abbott et al. "GW190425: Observation of a Compact Binary Coalescence with Total Mass ~ $3.4M_\odot$". In: *Astrophys. J. Lett.* 892.1 (2020), p. L3. DOI: 10.3847/2041-8213/ab75f5.

[157] F. Canfora. "Ordered arrays of Baryonic tubes in the Skyrme model in (3 + 1) dimensions at finite density". In: *Eur. Phys. J. C* 78.11 (2018), p. 929. DOI: 10.1140/epjc/s10052-018-6404-x.

[158] F. Canfora, M. Lagos, and A. Vera. "Crystals of superconducting Baryonic tubes in the low energy limit of QCD at finite density". In: *Eur. Phys. J. C* 80.8 (2020), p. 697. DOI: 10.1140/epjc/s10052-020-8275-1.

[159] D. Harland, P. Leask, and M. Speight. "Skyrmion crystals stabilized by ω-mesons". In: (2024). arXiv: 2404.11287 [hep-th].

[160] H. Forkel, A. Jackson, and C. Weiss. "Skyrmions with vector mesons: Stability and the vector limit". In: *Nucl. Phys. A* 526.3 (1991), pp. 453–478. DOI: 10.1016/0375-9474(91)90429-A.

[161] G. S. Adkins and C. R. Nappi. "Stabilization of chiral solitons via vector mesons". In: *Phys. Lett. B* 137.3 (1984), pp. 251–256. DOI: 10.1016/0370-2693(84)90239-9.

[162] U.-G. Meissner and I. Zahed. "Skyrmions in the Presence of Vector Mesons". In: *Phys. Rev. Lett.* 56 (10 1986), pp. 1035–1038. DOI: 10.1103/PhysRevLett.56.1035.

[163] Ö. Kaymakcalan, S. Rajeev, and J. Schechter. "Non-Abelian anomaly and vector-meson decays". In: *Phys. Rev. D* 30 (3 1984), pp. 594–602. DOI: 10.1103/PhysRevD.30.594.

[164] P. Sutcliffe. "Multi-Skyrmions with vector mesons". In: *Phys. Rev. D* 79 (8 2009), p. 085014. DOI: 10.1103/PhysRevD.79.085014.

[165] J. Speight. "A simple mass-splitting mechanism in the Skyrme model". In: *Phys. Lett. B* 781 (2018), pp. 455–458. DOI: 10.1016/j.physletb.2018.04.026.

[166] M. Gillard, D. Harland, and M. Speight. "Skyrmions with low binding energies". In: *Nucl. Phys. B* 895 (2015), pp. 272–287. DOI: 10.1016/j.nuclphysb.2015.04.005.

[167] M. Gillard, D. Harland, E. Kirk, B. Maybee, and M. Speight. "A point particle model of lightly bound Skyrmions". In: *Nucl. Phys. B* 917 (2017), pp. 286–316. DOI: 10.1016/j.nuclphysb.2017.01.027.

[168] G. S. Adkins. "Rho mesons in the Skyrme model". In: *Phys. Rev. D* 33 (1 1986), pp. 193–197. DOI: 10.1103/PhysRevD.33.193.

[169] C. Naya and P. Sutcliffe. "Skyrmions and clustering in light nuclei". In: *Phys. Rev. Lett.* 121 (23 2018), p. 232002. DOI: 10.1103/PhysRevLett.121.232002.

[170] C. Naya and P. Sutcliffe. "Skyrmions in models with pions and rho mesons". In: *JHEP* 05 (2018), p. 174. DOI: 10.1007/JHEP05(2018)174.

[171] Y.-L. Ma, Y. Oh, G.-S. Yang, M. Harada, H. K. Lee, B.-Y. Park, and M. Rho. "Hidden local symmetry and infinite tower of vector mesons for baryons". In: *Phys. Rev. D* 86 (7 2012), p. 074025. DOI: 10.1103/PhysRevD.86.074025.

[172] Y.-L. Ma, G.-S. Yang, Y. Oh, and M. Harada. "Skyrmions with vector mesons in the hidden local symmetry approach". In: *Phys. Rev. D* 87 (3 2013), p. 034023. DOI: 10.1103/PhysRevD.87.034023.

[173] Y.-L. Ma, M. Harada, H. K. Lee, Y. Oh, B.-Y. Park, and M. Rho. "Dense baryonic matter in the hidden local symmetry approach: Half-skyrmions and nucleon mass". In: *Phys. Rev. D* 88 (1 2013), p. 014016. DOI: 10.1103/PhysRevD.88.014016.

[174] Y.-L. Ma, M. Harada, H. K. Lee, Y. Oh, B.-Y. Park, and M. Rho. "Dense baryonic matter in conformally-compensated hidden local symmetry: Vector manifestation and chiral symmetry restoration". In: *Phys. Rev. D* 90 (3 2014), p. 034015. DOI: 10.1103/PhysRevD.90.034015.

[175] W.-G. Paeng, T. T. S. Kuo, H. K. Lee, and M. Rho. "Scale-invariant hidden local symmetry, topology change, and dense baryonic matter". In: *Phys. Rev. C* 93 (5 2016), p. 055203. DOI: 10.1103/PhysRevC.93.055203.

[176] H.-J. Lee, B.-Y. Park, M. Rho, and V. Vento. "Sliding vacua in dense skyrmion matter". In: *Nucl. Phys. A* 726.1 (2003), pp. 69–92. DOI: 10.1016/S0375-9474(03)01626-9.

[177] B.-Y. Park, M. Rho, and V. Vento. "Vector mesons and dense skyrmion matter". In: *Nucl. Phys. A* 736.1 (2004), pp. 129–145. DOI: 10.1016/j.nuclphysa.2004.01.131.

[178] P.-G. Reinhard, M. Bender, W. Nazarewicz, and T. Vertse. "From finite nuclei to the nuclear liquid drop: Leptodermous expansion based on self-consistent mean-field theory". In: *Phys. Rev. C* 73 (1 2006), p. 014309. DOI: 10.1103/PhysRevC.73.014309. URL: https://link.aps.org/doi/10.1103/PhysRevC.73.014309.

[179] U. Garg and G. Colò. "The compression-mode giant resonances and nuclear incompressibility". In: *Prog. Part. Nucl. Phys.* 101 (2018), pp. 55–95. DOI: 10.1016/j.ppnp.2018.03.001.

[180] J. Blaizot. "Nuclear compressibilities". In: *Physics Reports* 64.4 (1980), pp. 171–248. DOI: 10.1016/0370-1573(80)90001-0.

[181] K. Brueckner, M. Giannoni, and R. Lombard. "Statistical estimate of the breathing mode energy". In: *Phys. Lett. B* 31.3 (1970), pp. 97–98. DOI: 10.1016/0370-2693(70)90119-X.

[182] G. Colò, N. Van Giai, J. Meyer, K. Bennaceur, and P. Bonche. "Microscopic determination of the nuclear incompressibility within the nonrelativistic framework". In: *Phys. Rev. C* 70 (2 2004), p. 024307. DOI: 10.1103/PhysRevC.70.024307.

[183] D. Patel et al. "Giant monopole resonance in even-A Cd isotopes, the asymmetry term in nuclear incompressibility, and the "softness" of Sn and Cd nuclei". In: *Phys. Lett. B* 718.2 (2012), pp. 447–450. DOI: 10.1016/j.physletb.2012.10.056.

[184] V. Tselyaev, J. Speth, S. Krewald, E. Litvinova, S. Kamerdzhiev, N. Lyutorovich, A. Avdeenkov, and F. Grümmer. "Description of the giant monopole resonance in the even-A $^{112-124}$Sn isotopes within a microscopic model including quasiparticle-phonon coupling". In: *Phys. Rev. C* 79 (3 2009), p. 034309. DOI: 10.1103/PhysRevC.79.034309.

[185] D. H. Youngblood, C. M. Rozsa, J. M. Moss, D. R. Brown, and J. D. Bronson. "Isoscalar Breathing-Mode State in ^{144}Sm and ^{208}Pb". In: *Phys. Rev. Lett.* 39 (19 1977), pp. 1188–1191. DOI: 10.1103/PhysRevLett.39.1188.

[186] M. N. Harakeh, K. van der Borg, T. Ishimatsu, H. P. Morsch, A. van der Woude, and F. E. Bertrand. "Direct Evidence for a New Giant Resonance at $80A^{-\frac{1}{3}}$ MeV in the Lead Region". In: *Phys. Rev. Lett.* 38 (13 1977), pp. 676–679. DOI: 10.1103/PhysRevLett.38.676.

[187] N. N. Arsenyev and A. P. Severyukhin. "Isoscalar giant monopole resonance in 40,48Ca". In: *J. Phys.: Conf. Ser.* 2586.1 (2023), p. 012047. DOI: 10.1088/1742-6596/2586/1/012047.

[188] J. R. Stone, N. J. Stone, and S. A. Moszkowski. "Incompressibility in finite nuclei and nuclear matter". In: *Phys. Rev. C* 89 (4 2014), p. 044316. DOI: 10.1103/PhysRevC.89.044316.

[189] J. Speight. "Near BPS skyrmions and restricted harmonic maps". In: *J. Geom. Phys.* 92 (2015), pp. 30–45. DOI: 10.1016/j.geomphys.2015.02.001.

[190] S. B. Gudnason, M. Barsanti, and S. Bolognesi. "Near-BPS Skyrmions". In: *J. High Energ. Phys.* 2022 (11 2022), p. 092. DOI: 10.1007/JHEP11(2022)092.